

# **Prepolymerization and Morphology**

**Study on the factors determining powder morphology  
in catalytic propylene polymerization**

**Jochem T.M. PATER**

## **CIP-gegevens Koninklijke Bibliotheek, Den Haag**

Pater, Joachim Theodorus Maria.

Prepolymerization and Morphology.

Study on the factors determining powder morphology in catalytic propylene polymerization

ISBN 90-365-1662-5

Trefw.: propylene, polymerization, morphology, prepolymerization, videomicroscopy

---

Copyright © 2001 by J.T.M. Pater, Enschede, The Netherlands

No part of this book may be reproduced by any means, nor transmitted, nor translated into machine language without permission from the author

---

Referent: Dr. J.A. Thoen

To the cover design:

The text 'Fatto il polipropilene' on the backside of the cover is reproduced from Moore, E.P., (1996). 'Polypropylene Handbook', Hanser Publishers, Munich, p.9., with permission of the publisher.

The research described in this thesis was performed at the Twente University, Enschede, The Netherlands. The investigations have been funded by The Dow Chemical Company.

# **PREPOLYMERIZATION AND MORPHOLOGY**

## **PROEFSCHRIFT**

ter verkrijging van  
de graad van doctor aan de Universiteit Twente,  
op gezag van de rector magnificus,  
prof. dr. F.A. van Vught,  
volgens besluit van het College voor Promoties  
in het openbaar te verdedigen  
op vrijdag 9 november 2001 te 16.45 uur.

door

**Joachim Theodorus Maria Pater**

geboren op 6 januari 1972  
te Anna Paulowna

Dit proefschrift is goedgekeurd door de promotoren

**Prof. dr. ir. W.P.M. van Swaaij en Prof. dr. -ing. habil. G. Weickert**



*Aan Mariska*



# Contents

<b>Abstract</b>	<b>xi</b>
<b>1. General Introduction</b>	<b>1</b>
1.1 History of catalyzed propylene polymerization	3
1.2 Polypropylene processes, the importance of powder morphology	3
1.3 Pre-polymerization	4
1.4 Pre-polymerization in industrial processes	5
1.5 Outline of this thesis	6
References	7
<b>2. Polymerization of Liquid Propylene with a 4<sup>th</sup> Generation Ziegler-Natta Catalyst - The Influence of Polymerization Temperature and Pre-polymerization on Kinetics - Vapor-Liquid Equilibria of the H<sub>2</sub>-Propylene System</b>	<b>9</b>
2.1 Introduction	11
2.1.1 Pre-polymerization	11
2.1.2 Hydrogen	12
2.2 Experimental	13
2.2.1 Chemicals	13
2.2.2 Experimental set-up	14
2.2.3 Procedures	20
2.2.4 Vapor-Liquid equilibrium measurements of propylene-H <sub>2</sub> system	22
2.3 Results and Discussion	22
2.3.1 Reproducibility	22
2.3.2 Determination of kinetic parameters	23
2.3.3 Influence of temperature on polymerization kinetics	28
2.3.4 Influence of pre-polymerization on polymerization kinetics	31
2.3.5 Influence of evaporation on powder morphology	32
2.3.6 Vapor-Liquid equilibria of propylene-hydrogen system	33
2.4 Conclusions	39
References	41
<b>3. Polymerization of Liquid Propylene with a 4<sup>th</sup> Generation Ziegler-Natta Catalyst - Influence of Temperature, Hydrogen and Monomer Concentration and Prepolymerization Method on Polymerization Kinetics</b>	<b>43</b>
3.1 Introduction	45
3.1.1 Prepolymerization	45
3.1.2 This work	46
3.2 Experimental	47
3.2.1 Chemicals	47
3.2.2 Setup	47
3.2.3 Procedures	48
3.3 Results and Discussion	49
3.3.1 Influence of polymerization temperature	49

3.3.2 The effect of prepolymerization	54
3.3.3. Application of NIPP to an industrial process	58
3.3.4 Influence of hydrogen concentration	61
3.3.5 The effect of monomer concentration	65
3.3.6 Relation between initial reaction rate and deactivation constant	66
3.4 <i>Conclusions</i>	70
<i>References</i>	72
<b>4. Polymerization of Liquid Propylene with a 4<sup>th</sup> Generation Ziegler-Natta Catalyst - Influence of Temperature, Hydrogen, Monomer Concentration and Pre-polymerization Method on Powder Morphology</b>	<b>75</b>
4.1 <i>Introduction</i>	77
4.2 <i>Experimental</i>	79
4.2.1 Chemicals	79
4.2.2 Polymerization methods	79
4.2.3 Powder characterization	81
4.3 <i>Results and Discussion</i>	82
4.3.1 Influence of polymerization temperature	82
4.3.2 The effect of pre-polymerization	84
4.3.3 Influence of hydrogen concentration	87
4.3.4. The effect of the monomer concentration	90
4.4 <i>Conclusions</i>	93
<i>References</i>	95
<b>5. High Precision Pre-polymerization of Propylene at Extremely Low Reaction Rates - Kinetics and Morphology</b>	<b>99</b>
5.1 <i>Introduction</i>	101
5.2 <i>Experimental</i>	103
5.2.1 Chemicals	103
5.2.2 Experimental set-up	103
5.2.3 Polymerization	104
5.2.4 Determination of reaction rate in slurry phase	104
5.2.5 Cross sectional SEM	106
5.3 <i>Results and Discussion</i>	107
5.3.1 Equilibrium propylene and hexane	107
5.3.2 Pre-polymerization kinetics	108
5.3.3 Typical pressure curve	108
5.3.4 Morphology of polymer particles	117
5.4 <i>Conclusions</i>	122
<i>References</i>	124
<b>6. Optical and Infrared Imaging of Growing Polymer Particles in the Homo and Copolymerization of Propylene and Ethylene, using a ZN-Catalyst</b>	<b>127</b>
6.1 <i>Introduction</i>	129
6.1.1 Optical imaging in olefin polymerization reactions	129

6.1.2 Infrared imaging in Chemical Engineering	130
6.1.3 This chapter	130
6.2 <i>Experimental</i>	131
6.2.1 Chemicals	131
6.2.2 Equipment	132
6.2.3 Procedures	133
6.2.4 Determination of single particle polymerization rates	135
6.3 <i>Results – Optical Observations</i>	136
6.3.1 Reproducibility	136
6.3.2 Shape replication and induction period	137
6.3.3. Influence of catalyst preparation	138
6.3.4 Influence of temperature	139
6.3.5 Pre- and Copolymerization	139
6.4 <i>Discussion – Optical Observations</i>	141
6.4.1 The experimental method	141
6.4.2 Tool for catalyst screening	141
6.4.3 The currently used catalyst	142
6.4.4 Comparing gas phase polymerization with bulk polymerization	142
6.4.5 The effect of ethylene addition	144
6.5 <i>Results – Infrared Measurements</i>	144
6.5.1 Particle temperature during polymerization	144
6.6 <i>Discussion - Infrared observations</i>	149
6.6.1 Observation method	149
6.6.2 Curved surfaces	150
6.6.3 Relation between reaction rate and temperature rise	151
6.7 <i>Modeling of particle temperature</i>	151
6.8 <i>Conclusions</i>	155
6.8.1 Optical and infrared application	155
6.8.2 Current catalyst system	155
<i>References</i>	157
<b>Samenvatting</b>	<b>161</b>
<b>Dankwoord</b>	<b>165</b>
<b>Curriculum Vitae</b>	<b>169</b>
<b>List of Publications</b>	<b>171</b>



## Abstract

Due to the developments in catalysis and the use of improved and dedicated catalysts in modern polymerization processes, the variety of different grades of polyolefins produced (and with that the variety of possible applications) has increased rapidly over the past decades. Combined with the low prices of these polymers, this has led to a huge growth rate of the annual worldwide production capacity for polyolefins.

The more modern processes almost always utilize a number of different polymerization reactors in series, often being a combination of one or two liquid phase reactors and one or two gas phase reactors. At the same time, the developments ask for improved control on particle morphology. Improved powder morphology will decrease the presence of fines, it will reduce the chance of wall sheeting in the gas phase reactors and increase the ease of transport and other handling properties of the powder. Next to that, when producing high-impact polypropylene, control on internal particle morphology will allow control of the distribution of the rubbery phase in the homopolymer matrix.

In this work a Ziegler-Natta catalyst of the fourth generation was used, of  $\text{TiCl}_4$  on a  $\text{MgCl}_2$  support, with  $\text{Al}(\text{Eth})_3$  as cocatalyst and di-cyclopentyl di-methoxy silane as external electron donor.

### Experimental tools for morphological research

In the present work two new tools were developed to allow study of the morphological properties of the polymer product. First, the so-called microreactor was built. The 6-ml gas phase polymerization cell is covered by a transparent lid that allows direct observation of the growing polymer particles, during reaction. In the initial application an optical camera was used in combination with a microscope. It was shown that such a system is well suited for screening of catalyst systems. In catalyst screening, factors like particle shape replication, catalyst deactivation and the presence of an inhibition period are of great importance. With this system these characteristics can be studied for different individual particles, which also allows correlation with particle properties like initial particle size. In the second application of the microreactor, an infrared camera was connected to the system, allowing measuring of particle surface temperatures during polymerization. Of course, a direct comparison between particles in this microreactor and particles in a fluidized bed reactor might be daring, due to the stagnancy of the gas phase in the microreactor. However, it is important to be able to know exactly the temperature of the particle during the lab-scale tests. It was shown that particle temperatures can increase up to  $20^\circ\text{C}$  at reaction rates around  $3 \text{ kg}_{\text{PP}}/\text{g}_{\text{cat}} \cdot \text{hr}$ . In contradiction to much published before, the maximum temperatures were reached after some minutes, instead of some seconds or shorter.

The second research tool that has been developed in the present work, was a dilute slurry polymerization reactor that allows polymerization at extremely low reaction

rates. By using this system, we were able to stop the polymerization at a well defined yield-in-prepolymerization to study the particles in different stages of the fragmentation process. After embedding in an epoxy resin, cross-sectional SEM micrographs were made to follow the fragmentation of the support. EDX techniques were used to confirm the origin of the materials distinguished in the micrographs.

#### Catalyst fragmentation

The fragmentation behavior of the presently used catalyst was studied using the very slow slurry prepolymerization. It was shown in the cross-sectional SEM pictures that fragmentation of the catalyst did not proceed layer wise, starting at the outside of the particle as a moving front towards the center of the grain. Instead, a homogeneous breaking of the particle into relatively large fragments was observed, with a subsequent decrease in size of those pieces with continuing fragmentation.

The change in particle morphology coincides with a sharp change in polymerization kinetics in this stage. Reaction rate showed a sharp drop at a fully reproducible yield of pre-polymerization of around  $5 \text{ g}_{\text{PP}}/\text{g}_{\text{cat}}$ , independent from reaction rate and experiment duration. This drop is ascribed to the changes in internal particle morphology in this stage of the polymerization: initially a catalyst particle is built of magnesium dichloride, with small amounts of polymer. With increasing yield, this changes to a polymer particle with a decreasing concentration of catalytic material.

#### Vapor-Liquid equilibrium (VLE) of propylene-hydrogen system

To control the molecular weight of the produced polymer, hydrogen is typically used to decrease molecular weight and therefore it is necessary to know the vapor-liquid equilibrium of the hydrogen propylene system.

A number of equations-of-state (EOS) was tested in their ability to describe experimental data on this equilibrium. It was shown that the Peng-Robinson and Soave-Redlich-Kwong EOS were best able to describe the data, still showing significant differences with the experiments. A temperature dependent binary interaction coefficient was derived for the Peng-Robinson EOS, which resulted in a strongly improved description of the experimental data.

Furthermore, it was shown that the presence of variable amounts of hexane and nitrogen did not significantly influence the equilibrium of the system. This is of importance, as these factors were not perfectly controlled in the polymerization tests.

#### Polymerization kinetics in liquid pool

Because of the high sensitivity of the modern polymerization catalysts to impurities and the very high reaction rates, resulting in huge heat production in a highly flammable liquid, the amount of public work done on kinetics of the bulk polymerization of propylene is very limited. By using a calorimetric method, assuring isothermal conditions and constant heat transfer to the cooling jacket, the temperature difference between reactor content and cooling water can be used as a measure for the



reaction rate. With this method, a full reaction rate versus time curve can be measured in a single polymerization test.

Here, the kinetics of the polymerization in liquid propylene using a commercially available Ziegler-Natta catalyst of the fourth generation was investigated as a function of monomer and hydrogen concentrations, polymerization temperature and the prepolymerization method.

The effect of polymerization temperature on reaction rate and deactivation behavior was described as Arrhenius type of relation. It was shown that the method used for the determination of the monomer concentration at the active site does not significantly change the linearity in the Arrhenius plots, but changes the activation energy that is calculated. Values for  $E_{act}$  ranges from 38 to 91 kJ/mole in the absence of hydrogen and from 60 to 104 in the presence of hydrogen.

At the highest temperatures, between 70 and 80°C, a leveling off of reaction rate was observed: polymerization rate did not increase with increasing temperature. As this effect disappeared after a prepolymerization step, it was ascribed to overheating of the largest catalyst particles.

The effect of hydrogen was studied in detail at 60 and 70°C. It was shown that at low hydrogen concentrations ( $X_{H_2}$  below 0.0025) reaction rates increased rapidly with increasing hydrogen concentration. At higher values, this increase leveled off, leading to a plateau in the reaction rate. The hydrogen influence is ascribed to the existence of dormant sites, due to mis-insertions of the monomer. The large methyl-group is in that case blocking the active site. Hydrogen can transfer the dormant chain from the site, and free it for the start of a new chain.

It was demonstrated that as the monomer concentration was decreased gradually by addition of hexane to the liquid propylene, reaction rates decreased only to a small extent between 500 and 200 g/L. When the concentration decreased to below 200 g/L, a sharp decrease in reaction rate was observed.

Finally, a clear relationship was found between the rate of deactivation in a specific polymerization and the absolute reaction rate in that experiment. As the reaction rate increased, no matter if caused by high hydrogen concentration, temperature or monomer concentration, the deactivation also increased.

### Powder Morphology

The morphology of the powder produced in liquid pool was evaluated qualitatively using SEM microscopy, and quantitatively using bulk density measurements as function of process conditions like monomer concentration, polymerization temperature, prepolymerization method and hydrogen concentration. It is shown that for this catalyst, there is a strong relation between the initial reaction rate and the morphology of the produced polymer powder.

When initial reaction rates are low enough, typically below 35 kg<sub>PP</sub>/g<sub>cat</sub>·hr the bulk density of the product is high, up to 450 g/L, the porosity of the product is low and the

catalyst shows an almost perfect replication of the shape of the catalyst particles. This effect does not depend on the cause of the lowered reaction rate, that might for example be the elimination of hydrogen, a low polymerization temperature or a low monomer concentration.

A gradual change of the shape and structure of the polymer particles was seen, as polymerization temperature changed. At low temperatures, for example 40°C or lower, massive, regularly shaped particles are obtained, showing a particle shape that is a perfect replication of the shape of the catalyst particle. With increasing polymerization temperature, the surface of the particle becomes more irregular, the particle shows higher porosities, resulting in lowering bulk density. At a polymerization temperature of 70°C or higher, the lowest observed bulk density is obtained, around 250 g/L.

It was shown that a short polymerization, for example 10 minutes, at a low temperature, for example 40°C, can permanently change the particle's morphology. After this prepolymerization, the particle will remain regularly shaped, even if it undergoes a long subsequent polymerization at high temperatures. Furthermore, even when using a very short polymerization at a rapidly increasing temperature, the powder morphology shows the characteristics of a powder produced at low temperature, as long as the initial reaction rate is low enough. Starting this so-called non-isothermal prepolymerization at 40°C is fully sufficient to yield a high density powder, even when reactor is heated to 70°C within a few minutes.

This short prepolymerization allows the use of a continuously operated tubular reactor, showing narrow residence time distributions. Such a system even allows an early screening of catalyst activity by means of the tube's axial temperature profiles, and combines that with low costs of a small unit.

# **CHAPTER 1**

## **GENERAL INTRODUCTION**



## 1.1 History of catalyzed propylene polymerization

It was not until the 1940's that only a very limited number of people were getting interested in polymeric materials with higher molecular weights, especially crystalline polymers. By 1950, chemists were familiar with crystalline polyethylene (PE), however crystalline polypropylene (PP) had never been observed. Propylene was being polymerized at that moment, but the product was of low molecular weight, with no regularity in the chain, and often highly branched<sup>[1]</sup>.

In 1950 Karl Ziegler started working on his 'Aufbau' reaction: growing alkyl chains by insertion of ethylene on a Al-C bond of a tri-alkyl aluminum. In the year 1953, Ziegler found that the presence of nickel was slowing down the Aufbau reaction. Soon he started varying with the metal components involved and found that the presence of chromium, and to an even higher extent zirconium, accelerated the insertion, yielding in a small amount of high molecular weight polymer. When titanium was tried the reaction became very rapid. Uncontrolled heating of the polymerization reactor was a result. Reducing polymerization temperature and pressure solved this problem, eliciting from one of Ziegler's co-workers the famous words 'Es geht in Glas!' ('It works in glass').

It is a great pity for Ziegler's group that the tests on the polymerization of propylene were wrongly interpreted as a failure when the high solubility of propylene in the inert hydrocarbon was overlooked. The three assistants that Giulio Natta had sent to Ziegler to learn about these systems reported on the successes, and despite the reportedly negative results on propylene, Natta started to try to polymerize the propylene. In March 1954 he succeeded in producing semi-crystalline PP. As he fully expected this result, he sufficed with a small remark in his notebook shown on the backside of this thesis, saying 'Made polypropylene'.

In 1963 Ziegler and Natta shared the Nobel Prize for chemistry, and already in 1960 there were several commercial PP producers, producing more than 50000 tons of product. In a few years PP changed from a useless material, impossible to be produced in high molecular weight into valuable product with an exploding new market and with numbers of practical applications. A real revolution!

## 1.2 Polypropylene processes, the importance of powder morphology

In the past 40 years the different players in polyolefin markets have developed a number of important industrial processes. Developments in processes came combined with the developments in the catalyst area. Table 1.1<sup>[2,3]</sup> shows these catalyst developments. Usually Ziegler-Natta catalysts are divided in four generations. The first generation of catalysts showed a relatively low activity, poor control over the powder morphology and because of low activities and low isotacticity indices, the product required removal of remaining catalyst and atactic product from the polymer.

The first processes commercialized by Montecatini in Ferrara and by Hercules in New Jersey were based on the use of a hydrocarbon diluent to suspend the crystalline polymer particles and to dissolve the atactic polymer fraction. After polymerization

the product was treated with alcohol to deactivate the catalyst and to allow subsequent washing with water. The polymer powder was separated by filtration, centrifugation, and subsequently dried. Evaporation was used to separate the soluble part of the polymer from the hydrocarbon. These polymerization processes were run semi-continuously: hydrocarbon, catalyst, and other components were loaded, then monomer gas was continuously introduced.

**Tabel 1.1** *Historic development of Ziegler-Natta catalysts*<sup>[2,3]</sup>

Catalyst system	Activity (kg <sub>PP</sub> /g <sub>cat</sub> )	II (-)	Powder morphology	Entailed by morphology
Dilute slurry polymerization in hexane, 70°C, 7 bar, 4 hours				
1st generation TiCl <sub>3</sub> 0.33 AlCl <sub>3</sub> + DEAC	3	92	irregular powder	need of purification and atactic removal
2nd generation TiCl <sub>3</sub> + DEAC	12	96	regular powder	need of purification, no atactic removal
3rd generation TiCl <sub>4</sub> /Ester/MgCl <sub>2</sub> +TEA/Ester	25	94	irregular powder	no purification, need of atactic removal
4th generation TiCl <sub>4</sub> /Diester/MgCl <sub>2</sub> +TEA/Silane	50	97	particles with regular shape, adjustable size and PSD. Designed distribution of different products in each particle	no purification, no atactic removal, no pelletization
5th generation TiCl <sub>4</sub> /Diether/MgCl <sub>2</sub> +TEA	120	98	particles with regular shape, adjustable size and PSD. Designed distribution of different products in each particle	no purification, no atactic removal, no pelletization

### 1.3 Pre-polymerization

Generally, pre-polymerization implies the separation of the catalyst activation stage from the actual polymerization stage. Pre-polymerization is carried out under mild conditions, before the main polymerization takes place. Often, monomer is present already in the early stage of the life of the particle and therefore activation of the catalyst is combined with polymerization. Pre-polymerization is carried out under mild conditions, with lower monomer concentrations and/or lower temperature, to reduce the polymerization rates in this initial stage. The reasons to use a pre-polymerization step before the actual polymerization process can be split in three groups:

- **Thermal effect**

The reason most described in the open literature to use a pre-polymerization step is to avoid thermal runaway on the particle scale during the initial phase of the polymerization. In that stage the growing particle is small and therefore has a small heat-exchanging surface with the bulk phase while the reaction rate is high, as no deactivation has occurred yet and the active site concentration is at a maximum. If monomer concentration and temperature are high at that moment, heat production rate in the particle might be too large with respect to heat removal capacity. Thermal overheating of the particle can occur, resulting in undesired thermal deactivation of the catalyst and even melting of polymer material. This latter factor will affect the powder morphology by formation of agglomerates.

• **fragmentation of support material**

With polymerization, the support material of the catalyst will break up due to internal hydraulic pressure and stresses exerted by the polymer on the support material. When prepolymerizing the catalyst, the support will break up slowly, to form regular, densely packed structures that replicate the original shape of the catalyst particle. Rapid fragmentation can lead to undesired fines. Because of its influence on the fragmentation of the support, pre-polymerization is believed to have a large influence on the powder morphology of the polymer formed in the main process.

• **Influence on polymer properties**

When a non-activated catalyst is introduced in a monomer-containing environment with cocatalyst and electron donor being present, catalyst activation will compete with polymerization in the particle. While the outer active sites of the growing particle are already producing polymer, the inner ones might not yet be fully activated. The produced polymer might form an obstacle to the relatively larger donor and cocatalyst molecules in reaching the potential active sites. Therefore pre-polymerization can lead not only to a more complete activation of the catalyst, but the active sites might also be activated in a more desirable way, leading to for example higher isotacticity indices.

**1.4 Pre-polymerization in industrial processes**

The different important industrial processes used for the catalytic polymerization of  $\alpha$ -olefins deal with the pre-polymerization step in different ways. The use of prepolymerization differs from completely absent to a pre-polymerization with a relatively high reaction rate (in liquid propylene). Table 1.2 shows a number of important processes with a description of the pre-polymerization step.

**Table 1.2** Application of pre-polymerization step in some industrial polypropylene processes.

PROCESS				PRE-POLYMERIZATION		
Process	Developer	Owner	Ann. Cap. <sup>*)</sup> (kton/year)	Prepoly	Medium	C <sub>3</sub> <sup>=</sup> conc (kmole/m <sup>3</sup> )
Spheripol	Montell	Basell	11000	yes, continuous	monomer	10 - 15
Unipol	Union Carbide	Dow	5000	none	-	-
Novolen	BASF	Basell	3800	none	-	-
Hypol	Mitsui Sekka	Grand Polymer	2000	yes, batch	inert HC	-
Innovene-PP	Amoco Chisso	bp	2000	none	-	-
Borstar	Borealis	Borealis	200	yes, continuous	SC C <sub>3</sub>	-

<sup>\*)</sup> The annual world capacities mentioned, are 1998 numbers, mentioned by Potter<sup>[4]</sup>.

As the use of a pre-polymerization step requires an extra reactor, it is a costly procedure. In particular when we think of cost in terms of the polymer yield obtained in it. Of course the main purpose of this reactor is not to produce polymer, but to prevent problems in subsequent process steps, by means of polymer production. The

need to use pre-polymerization strongly depends on the catalyst used and on characteristics of the process.

Some catalysts show an initial inhibition or activation period, which has a moderating influence. When the catalyst used does not show an inhibition period, thus allowing for high initial polymerization rates, and when the monomer concentration is high in the first main polymerization reactor, a pre-polymerization step will be required to prevent thermal runaway at the particle scale. Examples of this case are found in Basell's Spheripol and in Mitsui's propylene bulk process.

But when initial monomer concentrations are much lower in the first main polymerization reactor, for example in the horizontally stirred bed gas phase of the BP or the Dow-UCC gas phase technology, the pre-polymerization step is not applied.

Application of a continuous pre-polymerization step, in a reactor with a CSTR-type behavior introduces the disadvantage of a relatively broad residence time distribution, resulting in either insufficiently prepolymerized catalyst particles or over-prepolymerized particles due to too long residence times. A fraction of the catalyst material will not be fully prepolymerized if its residence time in the pre-polymerization reactor is too short. This can result in catalyst deactivation or formation of undesired fines in the principal reactor. A second option, pre-polymerization in dilute slurry phase in batch operation, introduces extra costs due to its discontinuity and requires separation of the inert hydrocarbon and the prepolymer material.

## **1.5 Outline of this thesis**

Despite the fact that particle morphology is an important item in modern polyolefin processes, little information is available in open literature on the relationship between process conditions and powder morphology. Despite the large quantity of work devoted to modeling polyolefin processes over the past 25 years, particularly in single particle modeling, description of the development of powder morphology has barely been included in these models. Because of the importance of morphology in industrial applications, and also its influence on the transfer of heat and mass from and to the particle, this is a serious deficiency.

The only possibility to start implementation of morphology development in mathematical models is to study the processes determining the morphology development. Fragmentation of the catalyst is the most important issue, but mass transport from bulk to active site, crystallization of the produced polymer and sorption of monomer in the polymeric phase are other determining processes. In the 3-year co-operation between the Dow Chemical company and the IPP Research group of the University of Twente, a large amount of new data and new insights have become available. In addition, new research tools were developed to be able to more precisely study the morphology development, single particle heat and mass transfer and catalyst fragmentation. This thesis describes these developments.



Chapter 2 describes the system and methods that are used in the present work in the polymerization of liquid propylene. It describes procedures followed in experimental tests and it shows calculation methods for extraction of kinetic data from experiments. Literature data and new experimental data on the vapor-liquid-equilibrium of the propylene-hydrogen system are also presented and discussed.

The third chapter shows the influence of temperature, different pre-polymerization steps (pre-polymerization at a fixed temperature or non-isothermal pre-polymerization), hydrogen concentration and monomer concentration on the polymerization kinetics. The same experimental work is analyzed in Chapter 4, with respect to the morphological properties of the polymer powders produced. Here, the link between process conditions like hydrogen and monomer concentration, polymerization temperature, and pre-polymerization method with the powder morphology of the product is shown.

In Chapter 5 the same catalyst system was used for prepolymerization at extremely low reaction rates to be able to influence and to follow the fragmentation process and the morphological developments in the particle at polymer yields between 1 and 50  $\text{g}_{\text{PP}}/\text{g}_{\text{cat}}$ . The particles were subsequently embedded in epoxy resin, cut and photographed using SEM.

In the sixth chapter a newly developed research tool is introduced that allows us to study directly the individual single particle during polymerization. This so-called microreactor is demonstrated using both an optical and an infrared observation system.

Chapters 2 to 6 have all been submitted as individual publications and can be read independently from other chapters. Reiteration of general information in introduction parts of chapters has therefore possibly occurred.

## References

- [1] Moore, E.P., (1996). 'Polypropylene Handbook', Hanser Publishers, Munich Vienna New York.
- [2] Galli, P., (1995). 'Forty Years of Industrial Developments in the Field of Isotactic Polyolefins', *Macromolecular Symposia*, **89**, 13-26.
- [3] Albizzati, E., & Galimberti, M., (1998). 'Catalysts for Olefins Polymerization', *Catalysis Today*, **41**, 159-168.
- [4] Potter, D.J.B., (1998). 'Process Technology Developments flourish', *Chemical Week Supplement*, **9** (30), 14-17.



## **CHAPTER 2**

**POLYMERIZATION OF LIQUID PROPYLENE WITH A  
4TH GENERATION ZIEGLER-NATTA CATALYST**

-

**THE INFLUENCE OF POLYMERIZATION TEMPERATURE  
AND PRE-POLYMERIZATION ON KINETICS**

-

**VAPOR-LIQUID EQUILIBRIA OF THE H<sub>2</sub>-PROPYLENE SYSTEM**

-

## Abstract

*An experimental set-up is presented for the polymerization of liquid propylene. The system is used to carry out main polymerizations with and without a preceding pre-polymerization step. Two types of pre-polymerization are introduced with this system: pre-polymerization at a constant temperature and pre-polymerization at rapidly increasing reactor temperatures. The influence of the polymerization temperature, with and without the pre-polymerization step is shown. It is shown that with the present catalyst system, at high polymerization temperatures, a pre-polymerization step will increase the polymerization rate.*

*Concentration of hydrogen is of huge importance for the molecular weight of the polymeric product made in these reactions. The mentioned polymerization reactor was used in combination with a gas chromatograph to clarify the vapor-liquid equilibrium (VLE) of the propylene-hydrogen system. Measurements are compared to predictions of different equations of state (EOS). It is shown that the Peng-Robinson EOS is best able to describe the VLE for mentioned binary system. A temperature dependent interaction parameter was derived from the fits to measurement. Using this relation for the interaction parameter, the Peng-Robinson equation was even better able to describe the measurements.*

*This chapter has been submitted for publication:  
J.T.M. Pater, G. Weickert, and W.P.M. van Swaij,  
'Polymerization of liquid propylene with a 4<sup>th</sup> generation ZN  
Catalyst - The influence of polymerization temperature and  
pre-polymerization on kinetics and VLE of the H<sub>2</sub>-propylene  
system, AIChE Journal, (2001).*

## 2.1 Introduction

In the past fifteen years, polyolefins (PO) have shown annual growth rates of 7 to 10%. This enormous increase in consumption of these plastics is not only due to the combination of low costs and attractive material properties, but also to the continuous broadening of the properties window of the polyolefins, allowing replacement of other (more expensive) products by PO. On-going developments in catalyst research and process technology competed and pushed each other to new levels. New and improved processes require full control of kinetics, polymer and powder morphology.

### 2.1.1 Pre-polymerization

With the increase of catalyst activity over the past 20 years, the importance of the use of a pre-polymerization step has increased as well, because it allows producers to maintain acceptable powder morphology and to prevent the active catalyst particles from a thermal runaway. Pre-polymerization is defined as a polymerization step under mild polymerization conditions, for example reduced process temperature or monomer concentration. This is done because the catalyst material is at its highest potential activity in terms of polymer produced per unit of particle volume in the initial stage since no deactivation has occurred yet, at the same time the catalyst particle has a small outer surface area. This combination can lead to strong increase of particle temperature and a catalyst deactivation due to overheating. Pre-polymerization can increase the particle surface area without the risk of runaway, due to low reaction rates while allowing us to decrease the rate of polymerization per unit volume. In addition, the pre-polymerization step allows the catalyst support material to fragment in a desirable way, without for example the risk of formation of undesired fines.

One of the most widely known polypropylene processes, that use a pre-polymerization step, is Basell's Spheripol technology. As many other modern processes, it consists of two main polymerization steps: a homopolymerization step in liquid propylene (PPY), and a gas phase copolymerization step in a fluidized bed reactor. As the risk of particle overheating exists in the first reactor because of the high monomer concentrations, especially for larger catalyst particles, a liquid phase pre-polymerization step is often applied. After pre-polymerization, the catalyst particles are fed to the main reactor and will have approximately the same activity per particle as the bare catalyst, but particle size will have increased by a factor of 5-10.

Although the importance of the pre-polymerization step for kinetics and powder morphology is well known, only limited data are available in open literature on these effects. This is mainly due to the difficulties of performing lab scale experiments in liquid pool polymerization, combining difficult nature of the experiments (very high polymerization activities and the relatively high operation pressures) with the sensitivity of the modern catalyst system to even traces of impurities. In the present work we describe a set-up developed for the catalytic polymerization of  $\alpha$ -olefins in gas or liquid phase. With this hardware, a number of experimental procedures were developed to allow a pre-polymerization step in the experiments, to allow powder

sampling during polymerization and to be able to control process parameters like temperature, and gas and liquid composition within narrow boundaries. Next to that, and most important: it is possible to obtain a full reaction rate versus time curve with this method in a single experiment.

### 2.1.2 Hydrogen

An important property of the produced polymer is its molecular weight. Typically the width of the molecular weight distribution of polyolefins is determined by the type of catalyst and the process conditions during polymerization. Ziegler-Natta catalysts lead to a molecular weight distribution (MWD) that is significantly broader than that obtained with the modern metallocene catalysts. The molecular weight and molecular weight distribution of the polymeric material can be described, as mentioned in literature, e.g. by Weickert<sup>[1]</sup>, if we have knowledge of the reaction rate constants of the propagating and terminating reactions, in combination with the concentrations of the different components. Mayo derived a general description of the chain termination probability  $q$  as a function of the different propagating and terminating reaction rates:

$$q = \frac{k_m}{k_p} + \frac{k_{H_2}}{k_p} \cdot \frac{C_{H_2,site}}{C_{PPY,POL}} \quad (-) \quad (\text{eq. 2.1})$$

If all active catalyst sites showing similar behavior, the instantaneous molecular weight distribution can be described by the well-known Schultz-Flory distribution:

$$y_j^d = j \cdot q^2 \cdot e^{-j \cdot q} \quad (-) \quad (\text{eq. 2.2})$$

where  $y_j^d$  is the differential molecular weight distribution as a function of only one parameter, the chain termination probability. However, typical ZN-catalysts show so-called multi-site behavior. The different catalyst sites will each be characterized by a specific set of kinetic parameters (so the different active sites have different  $q$ -values), resulting in a polymer product having a much broader distribution than the one demonstrated in equation 2.2.

In the polymerization of propylene with a conventional Ziegler-Natta catalyst in the presence of hydrogen, chain transfer to hydrogen is the most important chain transfer mechanism. So in modeling MW and MWD as a function of process conditions like temperature and hydrogen pressure, one needs to know  $C_{H_2,site}$ , the hydrogen concentration at the active catalyst center. We propose to obtain this concentration from combination of the propylene concentration in the polymer and the hydrogen concentration in the liquid monomer. Assuming that the sorbed monomer in the amorphous polymer can be considered as a liquid, we propose to calculate  $C_{H_2,site}$  as the product of the molar ratio hydrogen in the liquid propylene ( $L_{H_2}$ ) to the concentration of propylene in the polymer:

$$\frac{C_{H_2,site}}{M_{H_2}} = \frac{L_{H_2} \cdot C_{PPY,POL}}{M_{PPY}} \quad (\text{kmole/m}^3) \quad (\text{eq. 2.3})$$

where monomer sorption in polymeric phase can be described as shown by Meier<sup>[2]</sup>:

$$C_{PPY,POL} = \rho_{liq} \cdot \phi \quad (\text{kg/m}^3) \quad (\text{eq. 2.4})$$

with  $\phi$  being volume fraction of monomer, calculated from Flory-Huggins equation:

$$\ln\left(\frac{P}{P^0}\right) = \ln \phi + (1 - \phi) + \chi \cdot (1 - \phi)^2 \quad (-) \quad (\text{eq. 2.5})$$

where the temperature dependent Flory-Huggins interaction parameter  $\chi$  can be determined experimentally. The mole ratio hydrogen to propylene,  $L_{H_2}$ , mentioned in equation 2.3 is easily calculated from the hydrogen mole fraction in the liquid phase  $X_{H_2}$ .

When now focussing on the system of liquid propylene and hydrogen, the availability of literature data on the vapor liquid equilibria (VLE) is limited. In the 1954, Williams and Katz<sup>[3]</sup> published VLE data on some systems of hydrogen with hydrocarbons. In 1981 Young<sup>[4]</sup> published a valuation of Katz' data. But the ranges of investigated conditions (-73 to 23°C and 17 to 550 bar) only coincide with typical conditions in mentioned polymerizations to a limited extent. At the University of Pittsburgh Mizan et al.<sup>[5]</sup> investigated both dynamic and equilibrium data of the system at different temperatures. They showed that equilibrium in the system is reached rather slowly, and their data is in a good agreement with the data of Williams and Katz at the temperature of 293 K. We will compare literature data with own experimental data, and will describe the data with a suitable equation of state (EOS).

In this paper we show the set-up for carrying out catalytic polymerizations in liquid propylene and demonstrate a method for the determination of the polymerization kinetics. The system was used for the determination of the influence of a pre-polymerization step and the polymerization temperature on polymerization kinetics. Because of the fact that the hydrogen concentration at the active site is an important factor here, the VLE of this system was described using the Peng-Robinson EOS, after fitting these equations to experimental data.

## 2.2 Experimental

### 2.2.1 Chemicals

The propylene used in the experiments was of so-called 'polymer grade' and obtained from Indugas, with a purity >99.5%, with propane as main impurity. The hydrogen and nitrogen used were of >99.999% purity. Table 2.1 shows the different chemicals used, their origin, the purity and the finishing purification steps. The hexane added to the system was of 'Pro Analysi' quality obtained from Merck.

The hydrogen, nitrogen and hexane were further purified by passing them over a reduced BTS copper catalyst and subsequently passing them through three different beds of molecular sieves, with pore sizes of 13, 4 and 3 angstroms respectively. The BTS catalyst was obtained from BASF. The propylene was purified in the same way, additionally it was passed over a bed of oxidized BTS catalyst to remove CO.

**Table 2.1** *The different components used in the polymerization experiments, with their origin, their purity and the final treatment before use.*

Component	Supplier	Purity	Further Processing
TEAL	AkzoNobel	> 96%, AlH <sub>3</sub> <0.07%	none
Nitrogen	PraxAir	> 99.999%, <4 vpm H <sub>2</sub> O, <4 vpm O <sub>2</sub> , <1 vpm CO <sub>2</sub>	3A, 4A, 13X mole sieves, red-ed BTS cat.
Hydrogen	PraxAir	> 99.999%, <5 vpm H <sub>2</sub> O, <1 vpm O <sub>2</sub> , <0.5 vpm CO	3A, 4A, 13X mole sieves, red-ed BTS cat.
Propylene	Prax Air	< 20 wtpm H <sub>2</sub> O, <5 wtpm CO <sub>2</sub> , < 0.5 wtpm CO	3A, 4A, 13X mole sieves, ox-ed + red-ed BTS
Hexane	Merck	>99%, <0.01%H <sub>2</sub> O, <0.05% S compounds	3A, 4A, 13X mole sieves, reduced BTS cat.
D-donor	Dow Chem.		
Mole sieves	Aldrich	N.A.	N.A.
BTS cat	BASF	N.A.	N.A.

### Catalyst system

The catalyst system that was used in the present work was a commercially available Ziegler-Natta catalyst of the fourth generation as defined by Moore<sup>[6]</sup>, with TiCl<sub>4</sub> on a MgCl<sub>2</sub> support. Triethyl aluminum was used as a cocatalyst and the so-called D-donor (di-cyclopentyl di-methoxy silane) was used as external electron donor for regulation of the stereospecificity. Figure 2.1 shows electron microscopy (SEM) pictures of the highly porous catalyst material. It can be seen that the catalyst particles are built from 20 to 30 spherical shaped sub-particles. The particle size distribution of the bare non-activated catalyst is shown in Figure 2.2. The particle size distribution shows an average particle diameter of 24.4 micron.

### 2.2.2 *Experimental set-up*

#### Polymerization reactor

The reactor system used in the present work was a 5-liter stainless steel jacketed batch reactor obtained from Büchi (*Büchi BEP 280*) which is suited for operating pressures up to 40 bar. The batch reactor (indicated with I. in Figure 2.3) is fit out with an overpressure valve and a rupture disk. The autoclave is equipped with a 6-blade turbine stirrer, mounted on a hollow stirrer shaft.



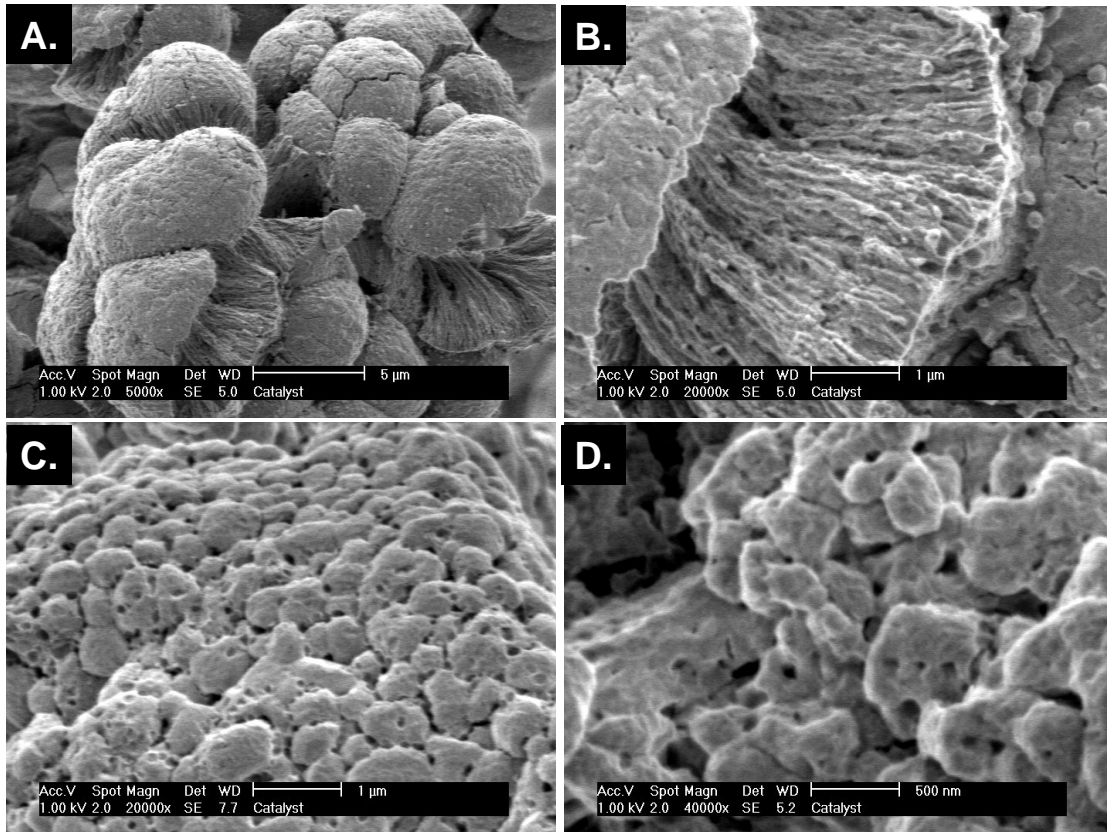


**Figure 2.1** Electron microscopy pictures of the catalyst particles. It is clear that the system is highly porous, with an average pore size of the macro pores around 0.1 micron.

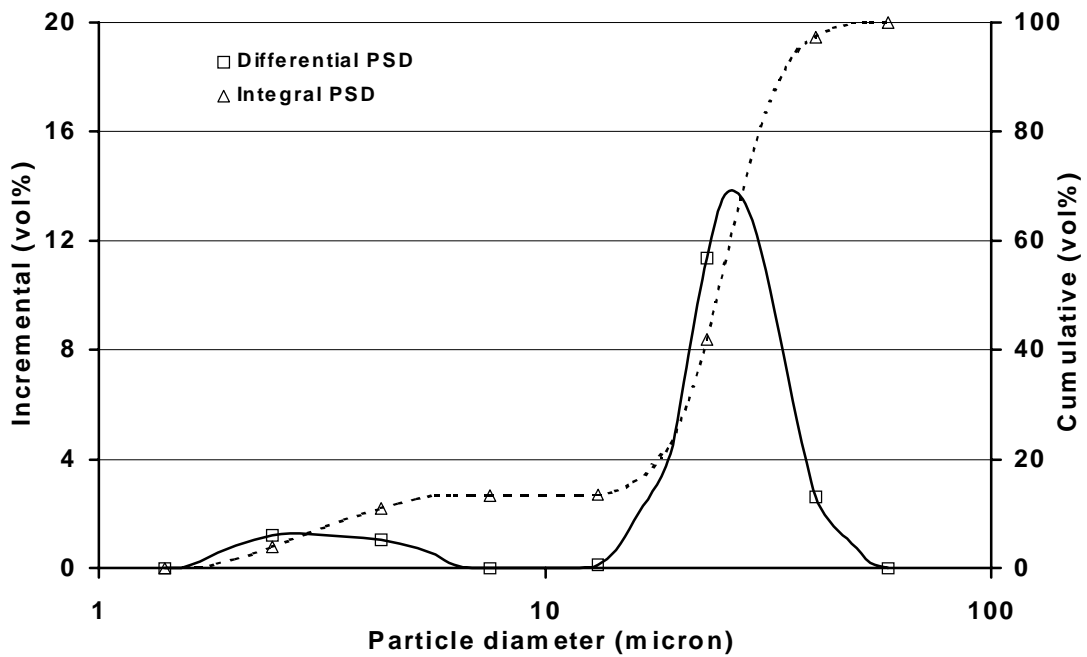


**Figure 2.2** Plot of the particle size distribution of the used catalyst material. The average particle size is about 25 micron.

Small holes at the side of the shaft near the turbine blades and in the reactor gas cap, provide a recirculation of the gas through the liquid phase. Electronic pressure gauges and thermocouples are used to measure reactor pressure and temperature.

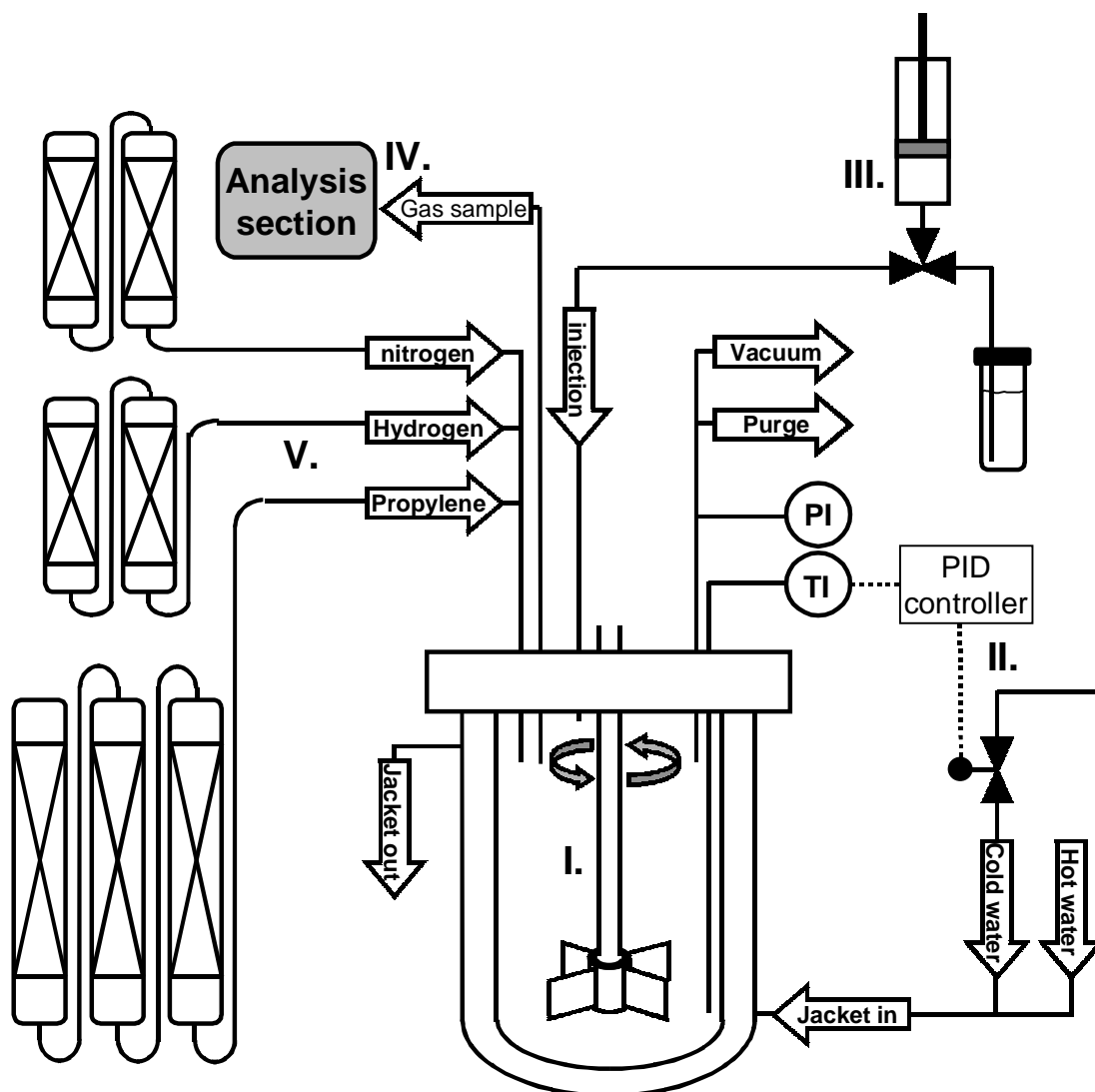


**Figure 2.3** Representation of the polymerization set-up. I. 5-liter autoclave reactor II. PID-temperature control system III. Catalyst injection system IV. Analysis section, using GC and IR-analyzers V. Gas supply system, with gas purification systems.

A cascade PID controller (II in Figure 2.3) was used to control reactor temperature. Water with a temperature of about 5K above the reactor temperature set point was mixed with a varied amount of cold water (temperature about 15-20°C). The amount of cold water added was controlled by the two control loops having reactor temperature and jacket temperature as process variable for the master and slave loop respectively. This temperature control system allowed us to keep the reactor temperature within narrow boundaries of  $\pm 0.2$  K.

For safety reasons the complete set-up was placed in a concrete housing and completely controlled from outside this space. A control PC, running a program that

was developed for this set-up in HPVEE, was connected to a central data acquisition unit (*Hewlett Packard 3852A DACU*). All incoming data from mass flow controllers, thermocouples and pressure gauges is managed by this DACU and sent to the PC. All control actions from PC to mass flow controllers and valves follow the opposite route. Valves are controlled by actuators that are operated with pressurized air, to prevent sparks from electrical switches.

The pneumatic injection system (III) allows introduction of liquids and slurries into the reactor without contamination with impurities, even at high reactor pressures. The needles of the system are continuously flushed with nitrogen to prevent trapping of air when attaching the catalyst vials to the system.

### Reaction rate measurements

The reaction rate of the highly exothermal polymerization reaction was measured by means of a calorimetric method, based on the heat balance of the reactor. Samson et al.<sup>[7]</sup> described the principles of this method, some refinements were applied to the method they used. Here the heat balance of the reactor is represented by:

$$C_w \frac{dT}{dt} = C_1 (\bar{T}_j - T_r) - Q_{BL} + Q_r \quad (\text{J/s}) \quad (\text{eq. 2.6})$$

with the left side of the equation representing the heat accumulation in the system. Under isothermal conditions the left hand term is equal to zero. Measurements of the inlet and outlet cooling water temperatures are taken. As the flow profile in the jacket approaches a plug flow type of pattern, the jacket temperature is approximated by taking the average of these two values:

$$\bar{T}_j = \frac{T_{inlet} + T_{outlet}}{2} \quad (\text{K}) \quad (\text{eq.2.7})$$

In equation 2.6  $C_1$  represents the product of the heat-exchanging surface area and the heat-exchanging coefficient. As these values are hard to determine, but assumed to be constant in time, they are treated as a constant.

In equation 2.6,  $Q_r$  represents the heat produced by reaction and is the product of the enthalpy of reaction  $H_r$ , reaction rate  $R_p$  and the mass of catalyst used  $m_{cat}$ :

$$Q_r = R_p H_r m_{cat} \quad (\text{J/s}) \quad (\text{eq. 2.8})$$

The  $Q_{BL}$  term represents the interaction of the system with the environment, and all other additional heat inputs and outputs, like stirrer dissipation, heat exchange with the heated lid, and so on. Later in this paper we will focus more on the different terms in  $Q_{BL}$ , but because of the fact that this term is shown to be constant over time, both with or without reaction, it is determined without reaction. At isothermal conditions and with  $R_p=0$ , equation 2.6 gives  $Q_{BL}$ :

$$Q_{BL} = [C_1 (\bar{T}_j - T_R)]_{noreaction} \quad (\text{J/s}) \quad (\text{eq. 2.9})$$

This temperature difference can be measured without reaction, and will be referred to as  $\Delta T_{BL}$  and assuming a constant  $C_1$  over time during polymerization, the reaction rate can be expressed as:

$$R_p = C_1 \frac{\Delta T_{BL} - (\bar{T}_j - T_r)}{m_{cat} H_r} \quad (\text{g/g.s}) \quad (\text{eq. 2.10})$$

So the reaction rate  $R_p$  is proportional to the corrected temperature difference between the jacket and the reactor content. Samson<sup>[7]</sup> showed that the curve of this temperature difference coincides with the real reaction rate curve, which was based on GC measurements.

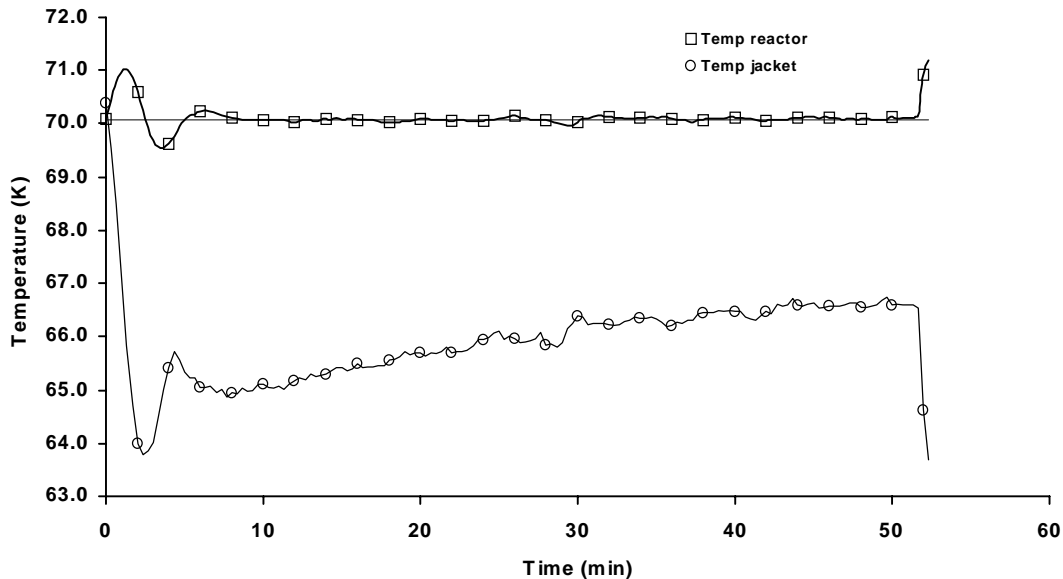


**Figure 2.4** Typical temperature curves for a polymerization test in liquid propylene, at 70°C, in the presence of hydrogen. The jacket temperature is increasing in time, due to catalyst deactivation.

Figure 2.4 shows a typical plot of the reactor and average jacket temperatures during reaction as a function of time. It can be seen that the cascade PID controller keeps the reactor temperature well within narrow boundaries around the reactor temperature ( $\pm 0.2\text{K}$ ). With decreasing catalyst activity, the temperature of the jacket is increasing in time.

When translating this temperature plot to a reaction rate plot, one can see that the reaction rate oscillates in the initial stage due to oscillations of the PID control of the jacket temperature. In this stage, reaction rates indicated by this plot are, of course not real reaction, as the system is not in the isothermal operation yet. So despite the fact that the system allows us to measure polymerization rates with relatively high

accuracy for most of the reaction (certainly long enough to measure kinetic parameters), it is not very suitable for measuring kinetics in the first 3 minutes of the experiment.

### Sampling system

The set-up is equipped with a sampling system that allows the operator to withdraw samples from the reactor, in the present case of slurry of liquid propylene and polymer, during the polymerization run. The bottom valve of the system will open briefly and a sample of about 30 ml is withdrawn without significantly disturbing the calorimetric measurements of reaction rate. After closing the bottom valve, the sample is flashed in the sampling vessel and flushed with nitrogen to remove the monomer. During a run, several samples can be taken, as the minimum interval between two samples is about 10 minutes.

### Gas analysis

A heated pressure reducer valve connected to the gas cap of the reactor, allows us to withdraw gas samples from the high-pressure reactor without the risks of condensation in the sampling lines. Typically 40 Nml of gas is withdrawn from the reactor, and because of the small amount, we can be sure that this is not significantly influencing the composition of the reactor content. The pressure is reduced to a pressure of about 1.5 bar, led through a mass flow controller and fed to a gas analysis section. This section is comprised of infrared analyzers to determine the ratio between the different monomers in case of a copolymerization and a gas chromatograph to measure concentrations of the constant gases like nitrogen and hydrogen (indicated with IV in Figure 2.3).

**Table 2.2** *The recipe and conditions for the preparation of the catalyst.*

Vial 1		
Component	Amount	Description
Al(Ethyl) <sub>3</sub>	270.0 mg	
Hexane	5 ml	Added at RT, to reduce Al(Eth) <sub>3</sub> concentration
D-donor	24.0 mg	Added at RT, contacted with Al(Eth) <sub>3</sub> for 15'
		Injected in liquid propylene
Vial 2		
Component	Amount	Description
Oil	100.0 mg	
Catalyst	10.0 mg	In oil suspended catalyst is weight
Hexane	5 ml	Hexane is added to slurrify the catalyst
		Injected in liquid propylene, after injection Vial 1

### 2.2.3 Procedures

#### Catalyst preparation

The components of the catalyst system are prepared in a *Braun MB 150 B-G-II glovebox*, under a nitrogen atmosphere. Concentrations of oxygen and water are kept below 0.1 PPM level. The catalyst, suspended in mineral oil, is weighed in a vial. The D-donor and aluminum alkyl are weighed in a separate vial diluted in hexane. Time between the contacting of the components - leading to complexation of the dimethoxysilane and the aluminum alkyl at room temperature - and injection of the mixture into the liquid propylene was kept constant at 15 minutes in all the tests. The recipe and conditions for the preparation of the catalyst are shown in Table 2.2.

#### Reactor preparation

To purify the reactor for polymerization one can choose between two methods. Pickling – washing of the reactor with monomer and an aluminum alkyl at elevated temperature – is often used to chemically clean the system. The disadvantage of this method is the non-reproducible amount of aluminum alkyl left behind after dumping of the reactor. A second possibility is to bake the reactor at high temperatures, combined with evacuation and purging with a purified inert gas.

In the present work the reactor was subsequently filled with nitrogen and evacuated during a period of 5 minutes. This was carried out at a wall temperature of 95°C and repeated for at least 5 times. After purifying, the reactor was brought to a pressure of 20 bars with hydrogen and kept there for 10 minutes to check for gas leakage.

#### Polymerization

After purification and evacuation of the reactor system, it was subsequently filled with the prescribed amount of hydrogen and 31.7 mole of propylene (1334 gram or 2.6 L at 20°C). During polymerization, the impeller stirrer was used at 2000 rpm and the reactor was heated to the required temperature. The pre-contacted mixture of aluminum alkyl and D-donor was injected then along with 10 ml of hexane. The vial and injection system are flushed two extra times with 10 ml of hexane. When not using any form of pre-polymerization, the catalyst suspension is subsequently injected and again the vial is washed twice with 10 ml of hexane. During polymerization, the reactor pressure and temperature are recorded, together with temperatures of incoming and outgoing cooling water of the jacket and the temperature of the reactor lid.

To end the experiment, the non-reacted monomer is flashed off by opening the vent valve. The reactor is initially at reaction temperature and will cool down due to this flashing. After flashing, the reactor is flushed several times with nitrogen to remove the last monomer. The powder is then taken from the reactor and dried overnight in a vacuum oven at 80°C. The reactor is washed out with a hydrocarbon, dried with pressurized air and purified by using the method described above.

### Pre-polymerization

In the present work pre-polymerization was carried out by reducing the polymerization temperature. When variations were to be made in the pre-polymerization step, two types of pre-polymerization are distinguished:

- Fixed pre-polymerization. The temperature profile of a so-called fixed pre-polymerization is schematically shown in Figure 2.5a. The reactor is purified, filled with desired amounts of propylene and hydrogen and set to a constant, relatively low temperature, typically 40°C. After a constant reactor temperature is reached, the catalyst components are injected into the reactor as described below and reactor temperature is fixed to the pre-polymerization temperature for a defined period, typically 10 minutes. After this pre-polymerization period, the reactor temperature is raised as quickly as possible to the temperature of the main polymerization. Heating of the system would normally take about 3 minutes.
- Non-isothermal pre-polymerization. The temperature profile of a so-called non-isothermal pre-polymerization is shown schematically in Figure 2.5b. The reactor is purified and filled with the desired amounts of monomer and hydrogen and set to a constant low temperature, typically 20°C. Then the pre-contacted mixture of aluminum alkyl and D-donor is injected into the system and subsequently the temperature of the reactor is raised to a final temperature of the main polymerization, typically 70°C. The non-activated catalyst is injected into the reactor system, at a predefined moment during the heating of the reactor,. This results in a short pre-polymerization step at a variable temperature. Varying the moment of injection of the catalyst can change duration of the pre-polymerization step and reaction rate during pre-polymerization.

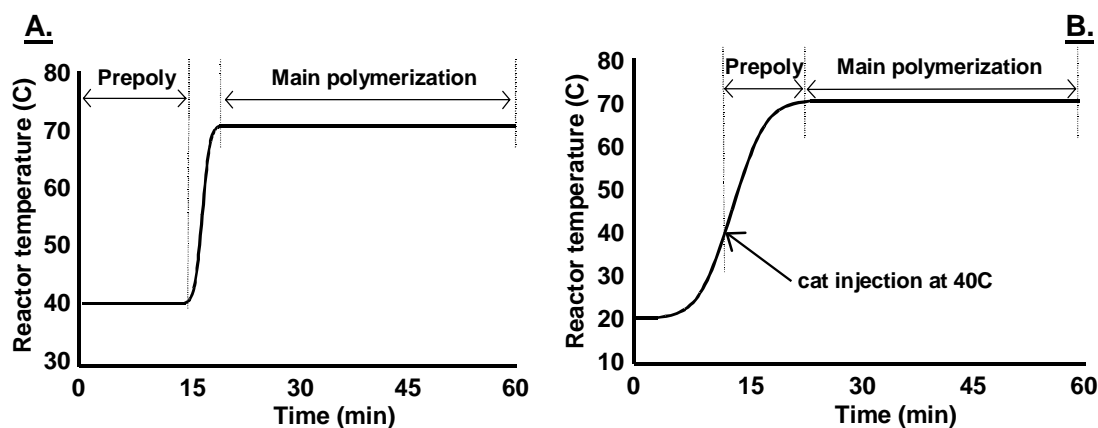


**Figure 2.5** The two different pre-polymerization methods used in the present work. A. The so-called fixed pre-polymerization, for 10 minutes at 40°C. B. The non-isothermal pre-polymerization, with in this case a catalyst injection at 40°C.

#### 2.2.4 Vapor-Liquid equilibrium measurements of propylene- $H_2$ system

##### Set-up for gas analysis

To be able to measure the vapor-liquid equilibria in the hydrogen-propylene system at conditions comparable to those used in polymerization experiments, a *Varian 3300* gas chromatograph (GC) was used in combination with a *Hewlett-Packard 3392A* integrator. The GC was equipped with a 5 foot long HYSEP K column that was kept at  $200^\circ\text{C}$  in combination with a thermal conductivity detector. Nitrogen was used as a carrier gas.

##### Procedure for VLE

In the VLE-measurements the batch reactor was prepared in the same manner as for polymerization. After flushing of the reactor with gaseous propylene, the system was evacuated. A known amount of liquid propylene was fed to the system, typically 31.7 mole. Then by means of mass flow controllers, the prescribed amount of hydrogen was added to the system and the system was subsequently brought to the desired conditions. Again, as with the polymerization tests, the reactor was stirred with the 6-blade turbine impeller at 2000 rpm.

Twenty minutes after reaching the desired process conditions, a small sample flow from the reactor was started, from which a gas sample was injected into the GC column every two minutes. At least 5 samples were analyzed in every batch. The integrator was used for evaluation of the GC-chromatograms. The number of counts in the peaks of the chromatogram was translated to numbers of moles using calibration data obtained with the same system. After analysis of the reactor gas, temperature of the reactor was changed according to the new prescribed conditions and the analysis procedure was repeated.

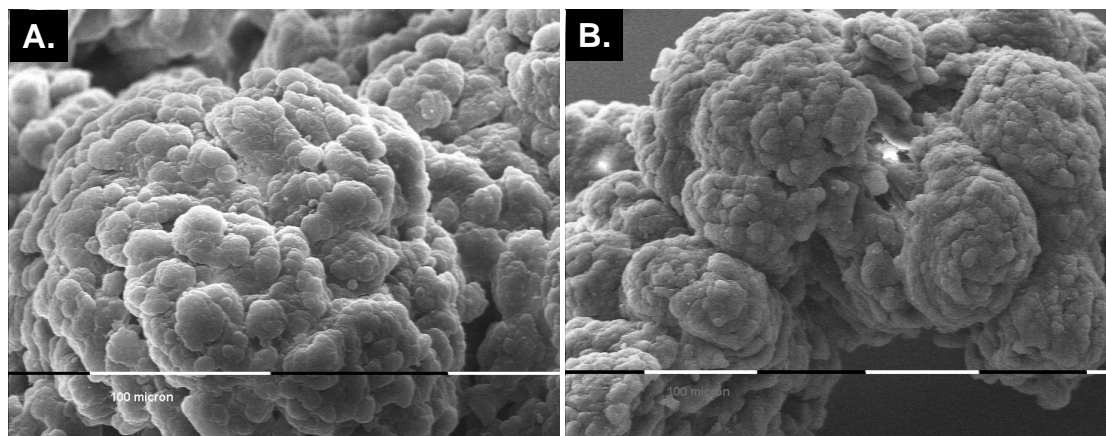


**Figure 2.6** SEM pictures of two powders yielding from different experiments at the same conditions (no pre-polymerization,  $T=70^\circ\text{C}$ , 0.21 mole  $H_2$ , 31 mole PPY).

## 2.3 Results and Discussion

### 2.3.1 Reproducibility

To be able to draw solid conclusions from the experiments, one has to be sure about the reproducibility with respect to powder morphology and the kinetic results of the polymerization reaction. Figure 2.6 shows the SEM pictures of two polymer samples,



obtained in two different experiments at the same conditions. Both powders were produced in the presence of 0.21 mole of hydrogen, without a pre-polymerization step, at 70°C. It can be seen that the reproducibility of the powder morphology is excellent. The same reproducibility is observed in other duplicate polymerization tests.

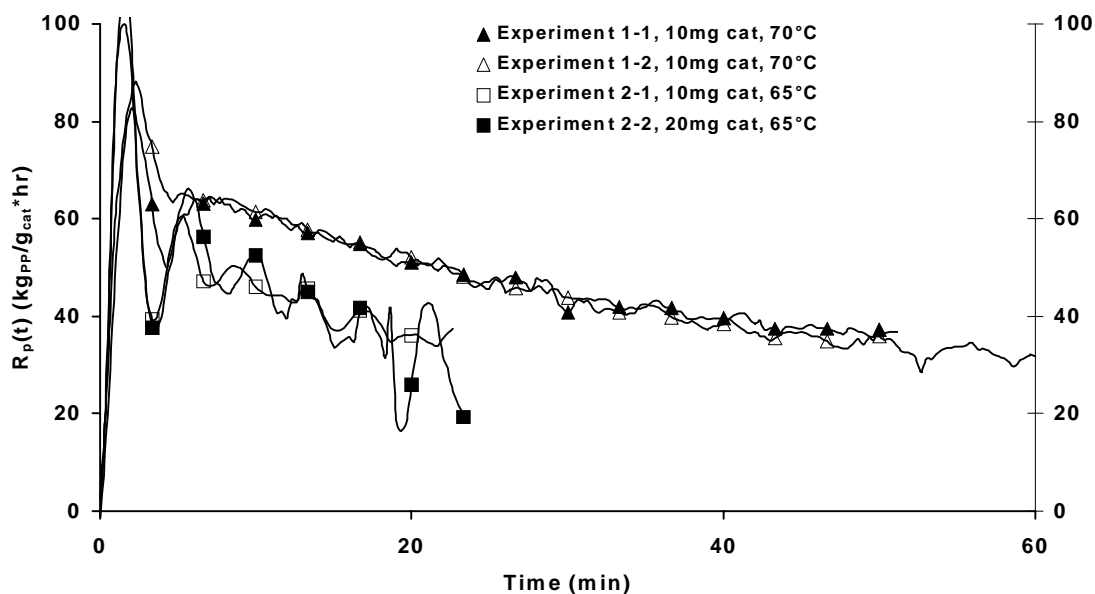


**Figure 2.7** Two duplicated polymerization experiments. Experiments 1-1 and 1-2 do have the same recipe (10 mg of catalyst at 70°C), experiments 2-1 and 2-2 used 20 and 10 mg of catalyst respectively at 65°C.

The measurement of the polymerization rate can also be reproduced to within an acceptable level. Figure 2.7 shows the reaction rate curves of four different experiments. In experiments 1-1 and 1-2 the same recipes and procedures were used. It is clear that reproducibility is very good in this case, reaction rates versus time are fully reproducible.

Because of the fact that the amount of catalyst used in an experiment is not exactly the same in all experiments, the influence of changes is checked. In experiments 2-1 and 2-2 the normal and double amount of catalyst was used respectively. It can be seen that the results of the tests are very similar and thus variations in catalyst amount (in experiments maximum up to 15%) do not influence results.

### 2.3.2 Determination of kinetic parameters

#### Determination of the kinetic parameters $R_{p,0}$ and $k_d$

In the literature, the complicated kinetics of the multi-site Ziegler-Natta catalysts are often dealt with by lumping the kinetic constants of the different types of active sites into one or into a reduced number (for example three sites, like Shimizu et al.<sup>[8]</sup>) of kinetic parameters. For example, assuming the propagation constant is independent of the length of the growing polymer chain, and assuming one overall propagation parameter for all sites reduces the numerous propagation constants to one. The same

is done for the different deactivation processes: when taking all deactivation processes into one lumped empirical deactivation constant, the system is dramatically simplified.

In general, one can describe the rate of polymerization depending on the concentration of active sites  $C^*$ , the concentration of the monomer at these centers  $C_{PPY,site}$ , and the lumped propagation constant  $k_p$ :

$$R_p = k_p \cdot C_{PPY,site}^q \cdot (C^*)^r \quad (\text{kg}_{PP}/\text{g}_{cat} \cdot \text{hr}) \quad (\text{eq 2.11})$$

with  $q$  and  $r$  being the orders of the reaction rate in monomer concentration and concentration of active centers respectively. Due to diverse deactivation processes the number of active sites can decrease in time. Weickert<sup>[9]</sup> proposes a list of possible mechanisms for real and apparent deactivation. When assuming that activation of the catalyst is very fast (instantaneous), the concentration of active sites will be maximum at  $t=0$ . When lumping the rate constants of the various deactivation processes into one single parameter  $k_d$ , the decrease of the number of active sites will then be described by:

$$-\frac{dC^*}{dt} = k_d \cdot (C^*)^p \quad (\text{mole}/\text{g}_{cat} \cdot \text{hr}) \quad (\text{eq 2.12})$$

Of course, the reasons for real or apparent deactivation are numerous and when fitting experimental curves with equations based on eq. 2.12, one might calculate low active sites concentrations even when low reaction rates are caused by other processes.

Equations 2.11 and 2.12 can be combined and integrated for isothermal conditions to a general description for reaction rate depending on time. When assuming first order deactivation and first order dependence of the reaction rate on monomer and active site concentration, this integration leads to:

$$R_p = R_{p,0} \cdot e^{(-k_d \cdot t)} \quad (\text{kg}_{PP}/\text{g}_{cat} \cdot \text{hr}) \quad (\text{eq 2.13})$$

In this equation the complete reaction rate – time curve can be described by two parameters: the initial reaction rate  $R_{p,0}$  (after full activated catalyst, without any deactivation) and the deactivation constant  $k_d$  being independent of polymerization rate.

The two empirical kinetic parameters  $k_d$  and  $k_p$  can be assumed to depend on polymerization temperature according to Arrhenius:

$$k_p = k_{p,0} \cdot e^{\left(\frac{-E_{act,p}}{RT}\right)} \quad (\text{m}^3/\text{hr} \cdot \text{mole}) \quad (\text{eq 2.14})$$

and:

$$k_d = k_{d,0} \cdot e^{\left(\frac{-E_{act,d}}{RT}\right)} \quad (\text{hr}^{-1}) \quad (\text{eq 2.15})$$

After the experiment, the thermal data from reactor and cooling jacket can be translated into a kinetic plot using the method described before. Next, this plot can be fit with the general description of the kinetics from equation 2.13, to quickly extract the basic kinetic parameters  $R_{p,0}$  and  $k_d$ .

By plotting the natural logarithm of the reaction rate as a function of time, a linear fit can be made where the deactivation constant is the slope of the fit, and the natural logarithm of the initial reaction rate is the intercept at the y-axis. This standard and well-known method becomes clear from Figure 2.8.

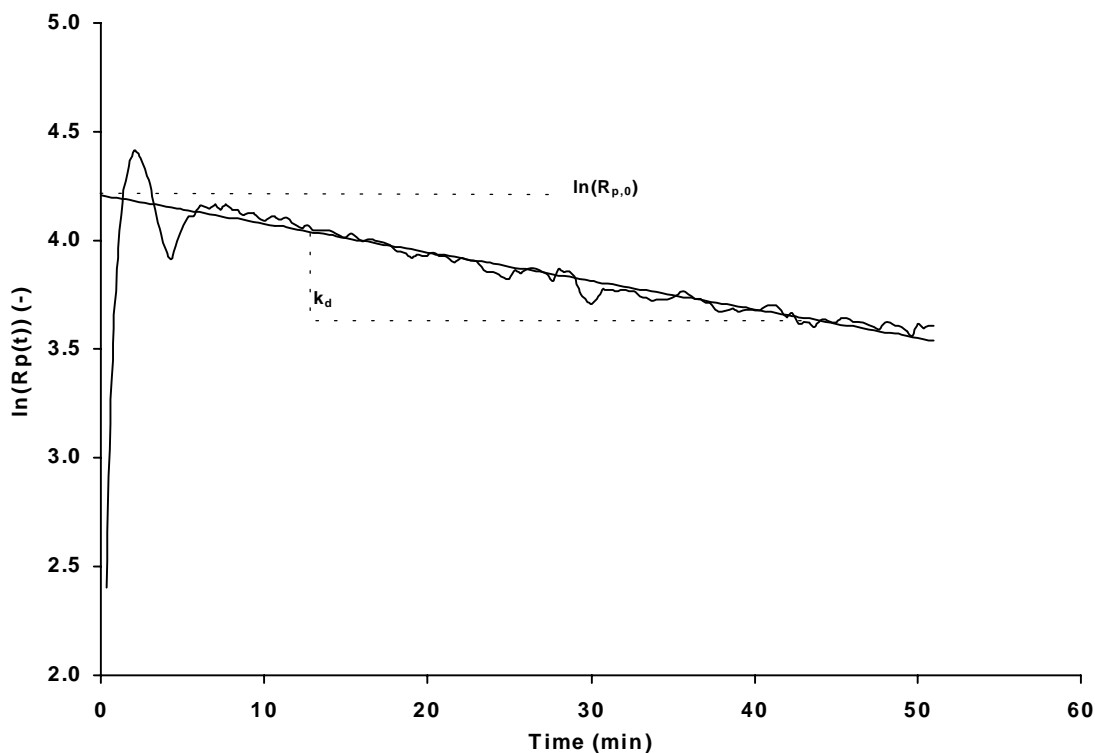


**Figure 2.8** Determination of initial reaction rate  $R_{p,0}$  and the deactivation constant  $k_d$  by plotting the natural logarithm of reaction rate versus time.

#### Influence of 'baseline-correction'

As described in the experimental description, reaction kinetics are determined by evaluation of the temperature difference between the reactor contents and the cooling jacket in the isothermal operation. The method interprets this temperature difference as a linear measure for the amount of heat produced. But when a polymerization experiment at 70°C is considered, one will see that before injection of the catalyst, the jacket temperature exceeds the reactor temperature due to the heat loss to the surroundings. A 'negative' temperature difference is the result and direct interpretation of the temperature difference towards reaction rates, as we proposed

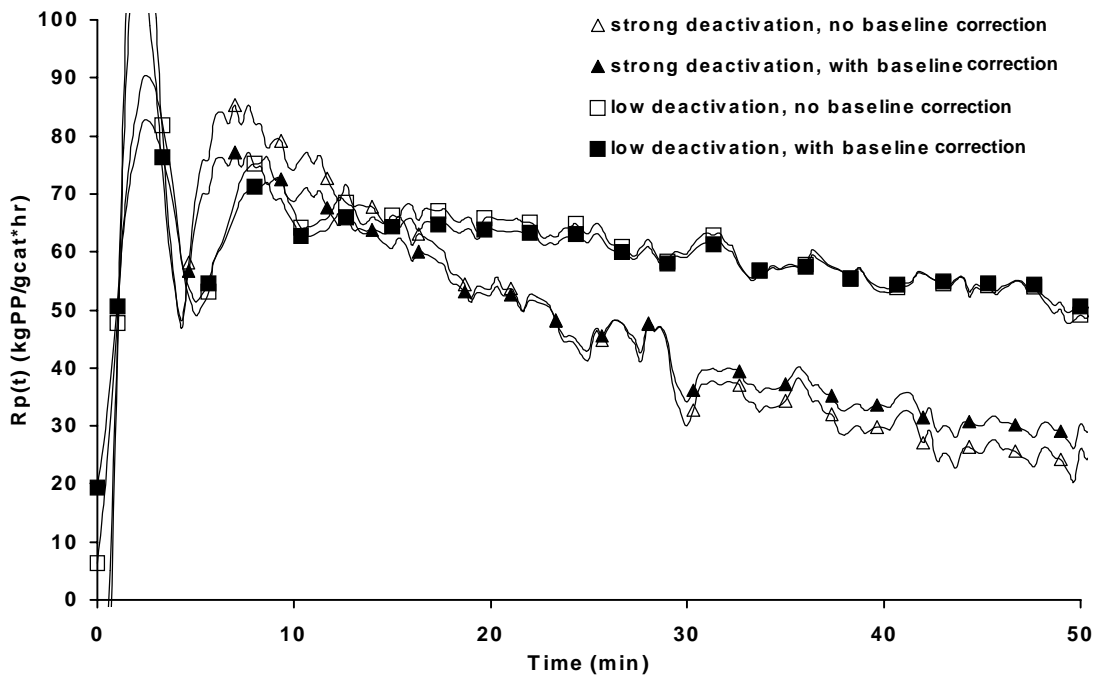


**Figure 2.9** Changes in kinetic profile by neglecting the 'base-line', in experiments with different deactivation.

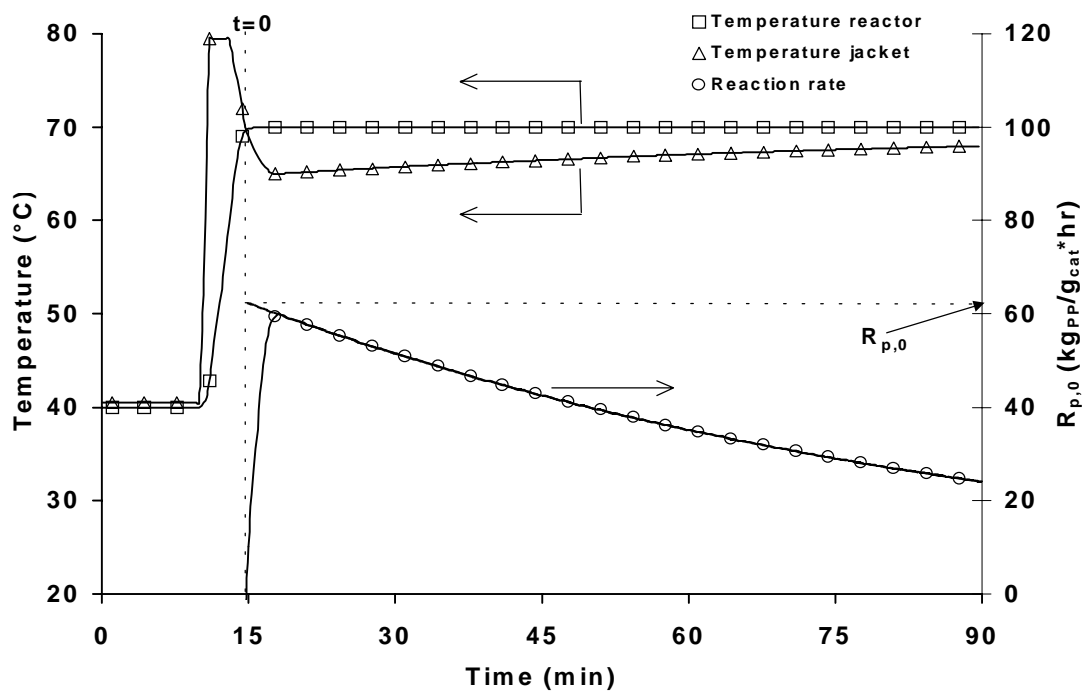


**Figure 2.10** Interpretation of temperature information for an experiment with fixed pre-polymerization step and the difficulty in definition of  $t=0$ .

earlier<sup>[7]</sup> can give problems. Therefore it will be necessary to include the negative temperature difference between reactor and jacket in the case without polymerization in the evaluation. Figure 2.9 shows the effect of neglecting this temperature difference in the calculations. It is clear that the extent of this effect will increase with increasing

deactivation; the effect will be zero when no deactivation occurs. It will also increase with decreasing total heat production rate: at high reaction rates or large amounts of catalyst ( $\Delta T_{BL}/\Delta T_{exp}$  is small), the effect becomes negligible as heat loss to surroundings can be neglected with respect to heat production in polymerization. In the experiments shown in this work, corrections for this baseline effect have been made by adding the baseline temperature difference  $\Delta T_{BL}$  to the temperature difference measured in the experiment,  $T_{exp}$ .

#### Extrapolation of reaction rate: comparison cases with and without pre-polymerization

Determination of the initial reaction rate, the  $R_{p,0}$  value, is done by extrapolation of the reliable values for reaction rate -  $R_p(t > 5 \text{ min})$  - back to  $t=0$ . This will yield reliable values for  $R_{p,0}$  because  $t=0$  is well defined, the catalyst is activated almost instantaneously and catalyst deactivation is negligible in this short initial stage.

In the case where a pre-polymerization step is used, the reactor is prepared at a low temperature, typically 40°C, the alkyl-donor mixture is injected and finally the catalyst is injected. Injection of the catalyst will start the pre-polymerization reaction. Normally reaction rate in the pre-polymerization phase is not determined, but the reaction rate in the main polymerization phase is. Using the method described before, finding a value for the deactivation constant in the main polymerization stage is not a problem. But the problem starts with the definition of  $t_{main}=0$  to find the value for  $R_{p,0,main}$ . Typically the moment  $T_{jacket} < T_{reactor}$  is being defined as  $t_{main}=0$ . But it is clear that one has to be careful when comparing  $R_{p,0}$  values of the cases with and without a pre-polymerization step. Especially in the case of a relatively strong deactivation, the choice for  $t=0$  will significantly influence the  $R_{p,0}$  value. The problem is illustrated in Figure 2.10.

Also, in order to transform the  $\Delta T$ -curve plus the polymer yield into a reaction rate curve, we have to account for the amount of polymer produced during the pre-polymerization step. This amount can be estimated when reaction kinetics without pre-polymerization are well known. With these known kinetics, one can integrate the temperature dependent reaction rate over pre-polymerization time to obtain a reasonable estimation of the amount of polymer produced in this stage. In the pre-polymerization experiments, such calculation was performed.

#### Influence of the heating of reactor lid

The reactor lid is heated by a separate heating system by means of water. The temperature of the lid is kept 2K above the target reactor temperature to reduce condensation of large amounts of monomer on the lid during polymerization. This temperature difference will continuously introduce heat to the reactor, according to:

$$Q_{lid} = (T_{lid} - T_{reactor}) \cdot U_{lid \rightarrow reactor} \cdot A_{lid} \quad (\text{J/s}) \quad (\text{eq 2.16})$$

But of course this is not a problem as all terms in this relation will be constant at isothermal conditions. Therefore the heat input by the lid is constant and is thus included in the ‘baseline correction’ described before.

#### Influence of the heat introduced by the stirrer

In standard correlations that exist for calculation of heat dissipation by agitated tank reactors, the Reynolds number for the tank is correlated with the power number. The Reynolds number for the current system will be around  $6 \cdot 10^4$ , resulting in a correlated power number of about 5 (Perry and Green<sup>[10]</sup>). This means that dissipated heat is about 7 watts:

$$N_{Re} = \frac{D_a^2 N \rho}{\mu} = 6 \cdot 10^4 \Rightarrow N_p = 5 = \frac{g_c P}{\rho N^3 D_a^5} \Rightarrow P = 7 \text{ Watt} \quad (\text{eq. 2.17})$$

In the conversion window within which we are working, the changes in viscosity are very small. Samson<sup>[7]</sup> showed that when going to conversion above 35%, problems occur with maintaining a well-stirred tank with the current agitator, and therefore high conversions are to be avoided. So in the isothermal operation of this system, heat input by the stirrer is constant in time and therefore fully taken into account with the ‘baseline correction’, as described before.

#### 2.3.3 Influence of temperature on polymerization kinetics

A series of experiments was done to investigate the influence of temperature on polymerization kinetics. The recipes used in these polymerization experiments are shown in Table 2.3.

**Table 2.3** The recipes as used in the polymerization experiments of the present work.

Type	Recipe				Pre-polymerization		Main polymerization	
	Cat (mg)	Al/Ti (mg)	Al/Si (mg)	H <sub>2</sub> (mole)	T <sub>prepol</sub> (°C)	Dur (min)	T <sub>main</sub> (°C)	Dur (min)
None	10	270	24	0.22	-	-	70	75
Fixed	10	270	24	0.22	40	10	70	65
NIPP	10	270	24	0.22	various	various	70	± 70

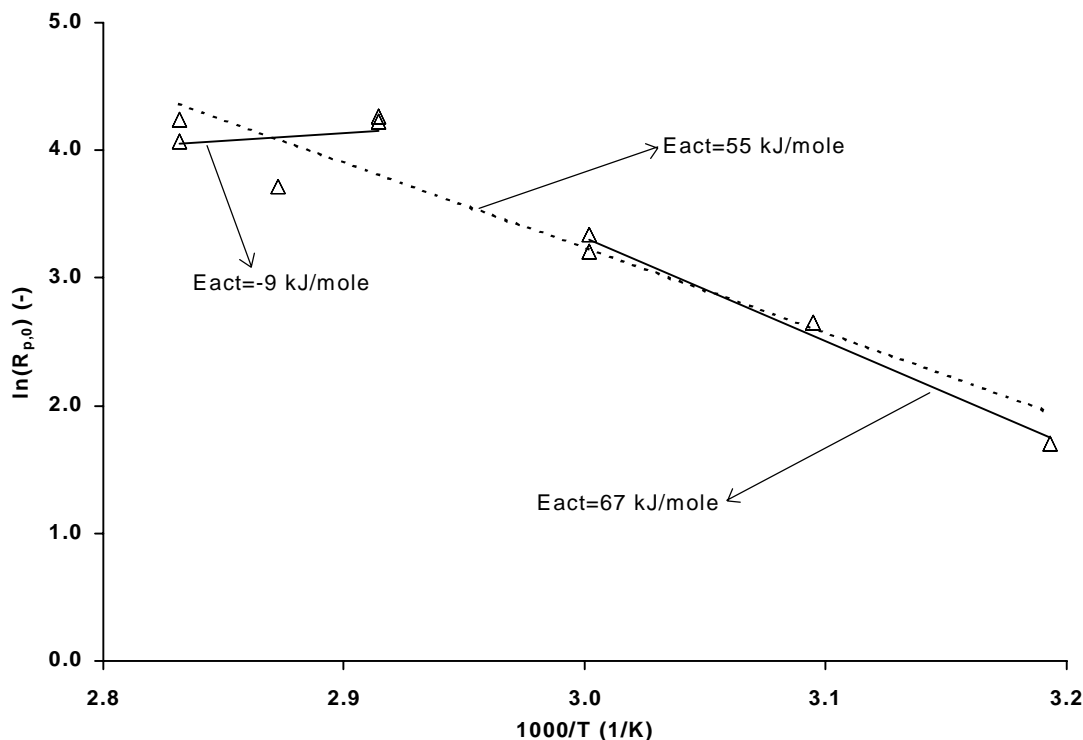


**Figure 2.11** Arrhenius plot for initial reaction rates of experiments without pre-polymerization step. At high temperatures, reaction rate does not increase with increasing temperature.

Figure 2.11 shows the Arrhenius plot of the values of the initial reaction rate at the different temperatures, without applying a pre-polymerization step. Temperatures were varied from 40 to 80°C. It is clear that the polymerization rate strongly decreases with decreasing temperature. But at the higher polymerization temperatures it seems that the temperature influence is significantly decreased. This is visualized by means of the three trend-lines in the plot. The solid trend-lines are linear fits (least squares) to the three highest and three lowest temperatures, i.e. 40-60°C and 70-80°. The dotted line is the fit to all experiments. The respective activation energies calculated from these lines are given in the plot. The fit to the highest values gives even a negative value for  $E_{act}$  which does of course not have a real physical meaning. This indicates that at lower temperatures, the system is not mass transfer limited. Typical activation energies for diffusion coefficients would be significantly lower than the values obtained here. But the leveling-off at higher temperatures is obvious. We can think of different explanations for this effect:

- Mass transfer limitation is playing a role at higher reaction rates. It could be assumed that at higher reaction rates the system becomes mass transfer limited, resulting in much lower activation energies. When considering the different steps in the monomer transport from bulk to active site, being convective transport to particle surface, convective transport through pores throughout the particle and transport by diffusion through the polymer from pore to active site, the diffusion part could become a transport limitation. But the value for  $E_{act}$  determined for the 70 to 80°C interval seems to be close to zero. Reaction rate does not increase with temperature anymore.

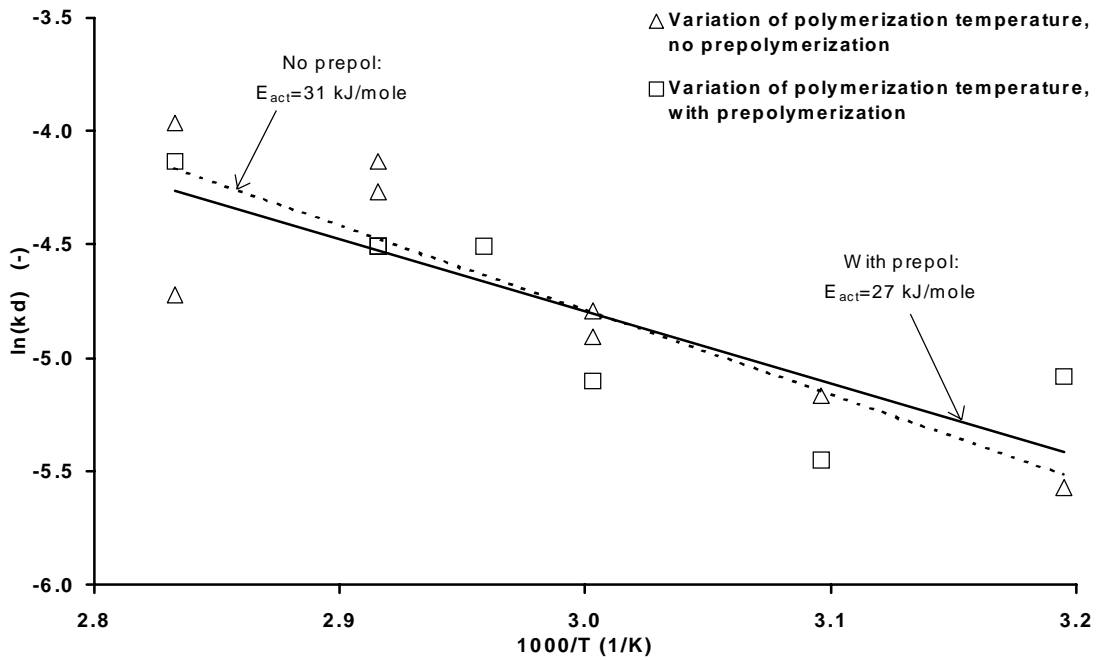


**Figure 2.12** Arrhenius plot for the deactivation constant  $k_d$ . The triangle shaped markers indicate the experiments without a pre-polymerization step, the square shaped markers indicate experiments with a fixed pre-polymerization.

- At high initial reaction rates, the larger catalyst particles deactivate due to overheating. As the particles are not pre-polymerized before injection, the high initial rates can result in overheated particles.

To be able to check both the hypotheses, one should use a pre-polymerization step before the main polymerization. Results of this check are shown below.



The deactivation constants yielding from these experiments were plotted in correlation to polymerization temperature, as shown in Figure 2.12, indicated with the triangle shaped markers. Although correlation between deactivation constant and polymerization temperature is not as obvious as for  $R_{p,0}$ , it is clear that deactivation increases with increasing polymerization temperature. The activation energies that are determined for the lumped deactivation processes are 31 and 27 kJ/mole for without and with pre-polymerization respectively, as indicated with the dotted line in Figure 2.12.

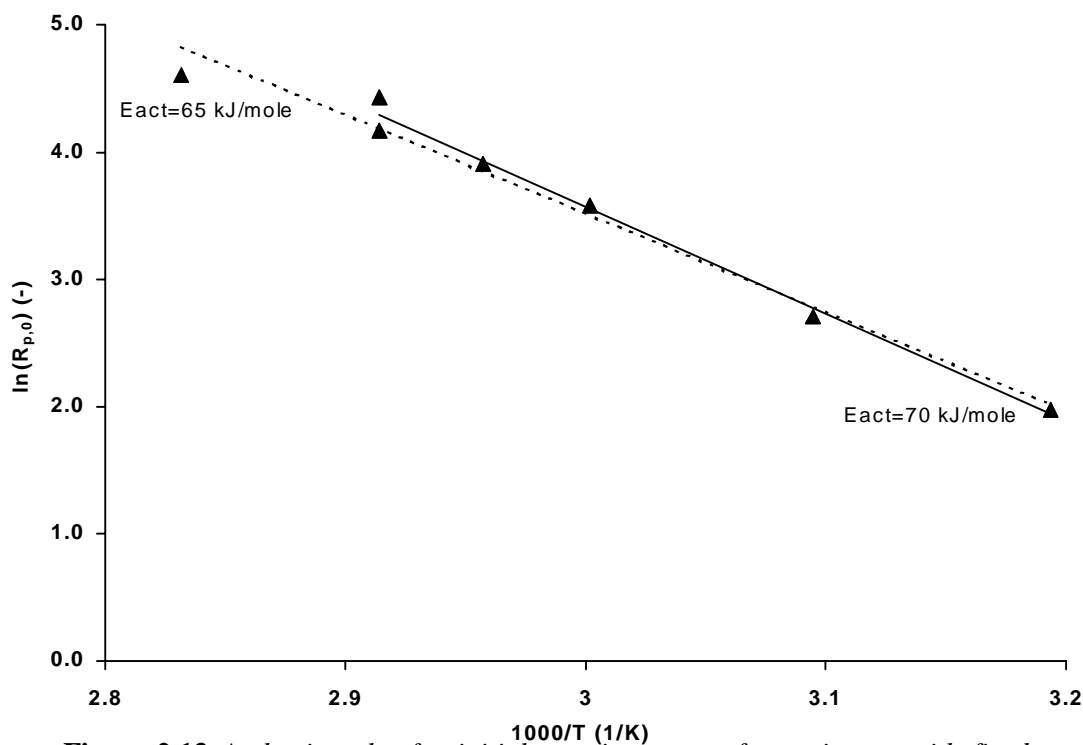


**Figure 2.13** Arrhenius plot for initial reaction rates of experiments with fixed pre-polymerization step. Here, also at high temperature, reaction rate is increasing with increasing polymerization temperature.

#### 2.3.4 Influence of pre-polymerization on polymerization kinetics

A series of experiments were done using the so-called fixed pre-polymerization. In this series, the catalyst was injected in the liquid propylene at a temperature of 40°C. The catalyst was pre-polymerized for 10 minutes, then the temperature was raised to the desired temperature. The results of this series are shown in Figure 2.13. The temperatures used in the Arrhenius plot are the temperatures during the main polymerization. Once again the reaction rate of the main polymerization decreases with decreasing temperature. Again, the dotted trend line is fit to the full temperature range from 40 to 80°C, the solid line leaves out the highest temperature. It is clear that in the case of a pre-polymerization, even at the highest temperatures for main polymerization, the reaction rate keeps increasing with increasing temperature. The

pre-polymerization step seems to solve the issue demonstrated in Figure 2.11. This is a strong indication that the reason for limitation at the highest reaction rate as described before, is a result of thermal runaway on particle scale. A fraction of the catalyst, most probably being the fraction with the largest particles, might deactivate due to overheating when a pre-polymerization step is not applied. Starting the reaction at a lower rate, slowly increasing the outer surface area of the particle, and going to the high reaction rates after that, prevents the particle from runaway.

The deactivation behavior during the experiment is indicated with the square-shaped markers in Figure 2.12. Again, the  $k_d$  values increase with increasing temperature, and again the spread in values is larger than for  $R_{p,0}$  values. The activation energy determined for the lumped deactivation processes is about the same as without pre-polymerization: 27 kJ/mole.

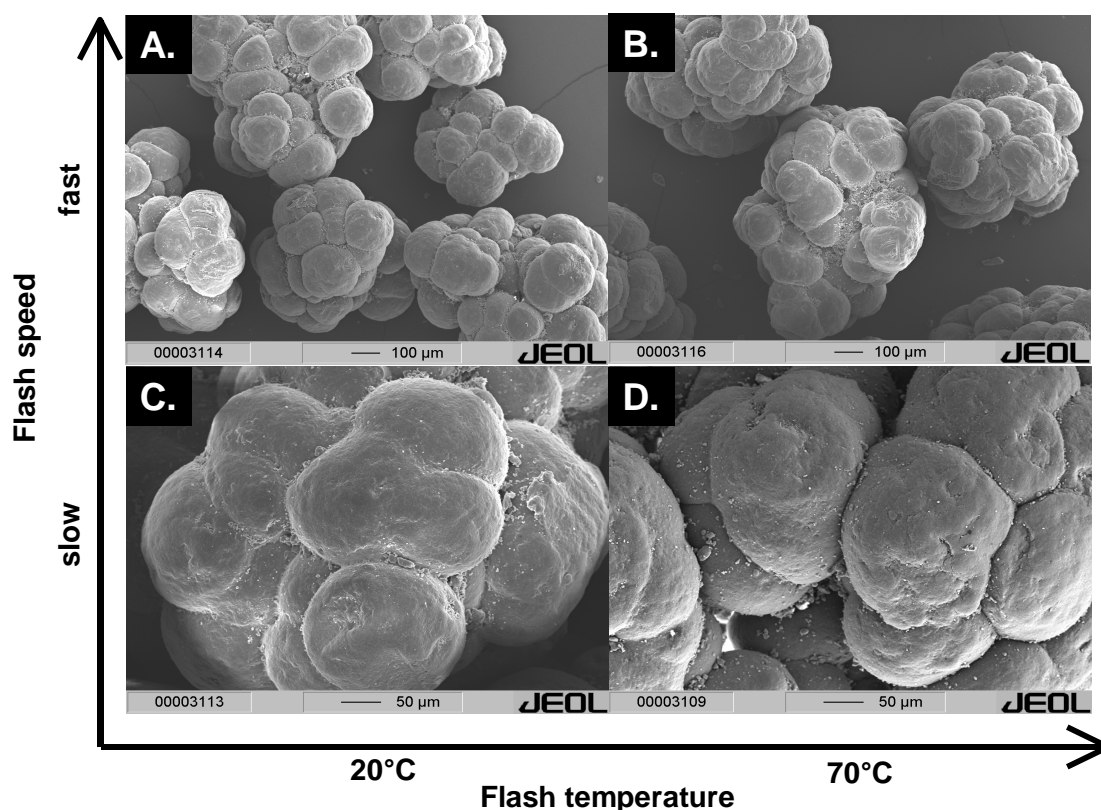


**Figure 2.14** SEM pictures of powders all produced at a standard polymerization experiment, but with varied flashing at end of experiment: A. fast flashing at 20°C, B. fast flashing at 70°C, C. slow flashing at 20°C D. slow flashing at 70°C.

### 2.3.5 Influence of evaporation on powder morphology

When correlating powder properties like the particle size distribution, bulk density and morphology observed by SEM to reaction conditions, one has to be sure that the morphological changes observed due to ending the test and drying the powder can be neglected. As described before, the experiment is usually stopped by flashing the non-reacted monomer. As the speed of flashing will depend on flow restriction in the vent lines and the initial reactor temperature and pressure, we cannot be sure that the

flashing procedure will be fully reproducible in all experiments. To ensure the insignificance of this fact some tests were done to check this influence. Four polymer powders were produced in fully comparable polymerization experiments, but with a different flashing procedure: flashing temperature and speed of the flashing were varied. Two different temperatures were used: 70 and 20°C. In the case of 20°C, the reactor was cooled down first, then the flashing was started. In the case of 'fast-flashing' a small reactor sample was taken by means of the sampling system, and dumped to an open sampling vessel of a much larger volume. In this way, flashing time for the involved particles from reactor pressure to normal pressure is below 1 second. In the case of slow flashing, reactor was vented over a strongly restricted vent line; venting took about 1 hour in this case. The SEM pictures of the four powders produced this way are shown in Figure 2.14. It shows that no influence of the flashing procedure on the powder morphology can be observed. Powder morphology seems to be built before flashing, and is apparently stable enough not to be disturbed by the flashing at the typical yield in these experiments. Therefore the powder morphology observed at the end of a polymerization experiment is fully the result of the experiment and the conditions during that experiment, not the result of its finishing. However, flashing of particles at low pre-polymerization yields, this is of course not ensured.

### 2.3.6 Vapor-Liquid equilibria of propylene-hydrogen system

#### Different equations-of-state

At 5 different temperatures and 3 different hydrogen concentrations the gas composition was measured, of course without polymerization reaction, but in the presence of a, for a polymerization test typical amount of hexane. The results of these equilibrium measurements are shown in Table 2.4.

To be able to describe the experimental data properly, *Hyprotech's HYSYS Plant 2.1* was used for equilibrium calculations. First, four different EOS-systems were used to describe experimental equilibrium data<sup>[11]</sup>, containing hydrogen mole fraction for both the liquid and gas phase of the binary system. The results of this fit are shown in Table 2.5. In this table the deviation between measurement and calculated value is shown to demonstrate the performance of the calculation. Of course, the highest deviation indicates the worst result. It becomes clear that Peng-Robinson and the Soave-Redlich-Kwong are best able to describe the data. In this software package, each EOS is using an own, fixed interaction parameter. To further improve the fit of the data, the optimal interaction parameter was determined for every temperature, from 30 to 80°C, using PR EOS. The following empirical relation describes the temperature dependence of the interaction parameter:

$$IP = 7.524 \cdot 10^{-4} \cdot T^2 - 0.4829 \cdot T + 77.0879 \quad (\text{eq. 2.18})$$

with IP the interaction parameter and T being temperature in Kelvin. Table 2.5 shows the results of the use of the interaction parameters in Peng-Robinson. It is clear that the fit has improved to a large extent. The interaction parameter as described in equation 2.16, used in the Peng-Robinson equation of state gives an accurate relation to describe the H<sub>2</sub>-PPY vapor-liquid system.

**Table 2.4** Results of gas chromatograph measurements on the VLE of the hydrogen-propylene system.

Experimental recipe					Gas Chromatography	
Testno. (-)	PPY (mole)	H <sub>2</sub> (mmole)	C <sub>6</sub> H <sub>14</sub> (mole)	T (K)	(N <sub>H2</sub> / N <sub>PPY</sub> ) <sub>gas</sub> (mole / mole)	Y <sub>H2</sub> (-)
1	31.73	68	0.423	294.1	0.03825	0.03680
2	31.73	68	0.423	313.9	0.02121	0.02080
3	31.73	68	0.423	323.7	0.01504	0.01480
4	31.73	68	0.423	333.8	0.01020	0.01010
5	31.73	68	0.423	343.7	0.00701	0.00700
6	31.73	223.2	0.423	295.4	0.11534	0.10340
7	31.73	223.2	0.423	314.2	0.07025	0.06560
8	31.73	223.2	0.423	323.9	0.05289	0.05020
9	31.73	223.2	0.423	333.9	0.03909	0.03760
10	31.73	223.2	0.423	343.7	0.02845	0.02770
11	31.73	637.9	0.423	293.3	0.34379	0.25580
12	31.73	637.9	0.423	313.3	0.20651	0.17120
13	31.73	637.9	0.423	323.6	0.15869	0.13700
14	31.73	637.9	0.423	333.8	0.12008	0.10720
15	31.73	637.9	0.423	343.8	0.09161	0.08390

**Table 2.5** Results of fitting of set of experimental data<sup>[11]</sup> for X<sub>H2</sub>/Y<sub>H2</sub> data at various temperatures and hydrogen concentrations, using different EOS's. The deviation shows the result for all fits.

Equation of state	Interaction parameter	Deviation
sour-Soive-Redlich-Kwong	Fixed: 0.00000	0.113
Soive-Redlich-Kwong	Fixed: 0.00000	0.179
Peng-Robinson	Fixed: -0.10360	0.115
sour-Peng-Robinson	Fixed: -0.10360	0.115
Peng-Robinson	IP=f(T)	0.033

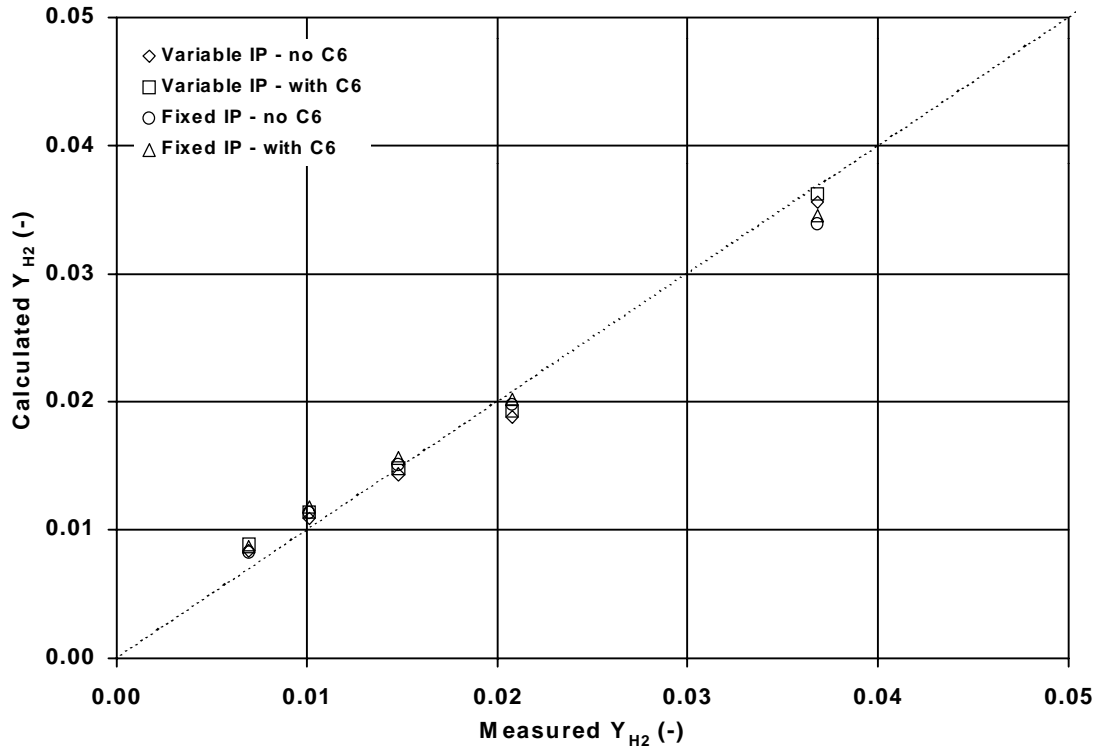


**Figure 2.15** Measured mole fraction of hydrogen in gas phase, versus the calculated mole fraction in gas phase, when adding 0.069 mole of  $H_2$  to the described reactor. Calculation with Peng-Robinson, using different settings.

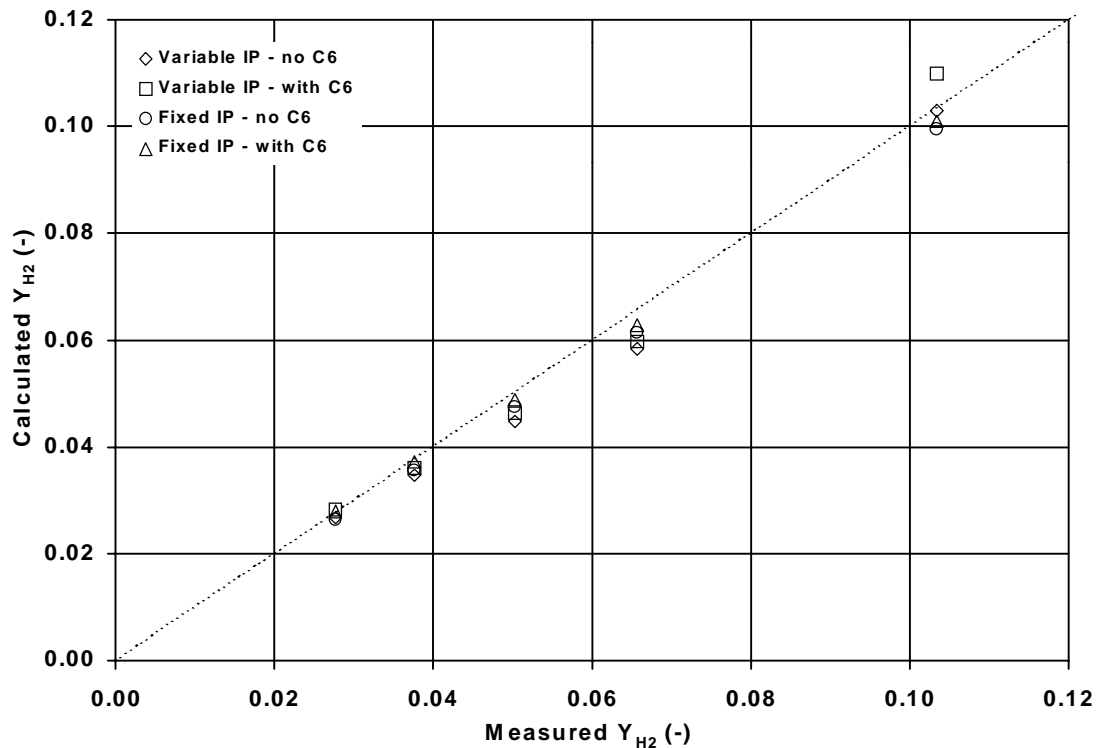


**Figure 2.16** Measured mole fraction of hydrogen in gas phase, versus the calculated mole fraction in gas phase, when adding 0.225 mole of  $H_2$  to the described reactor. Calculation with Peng-Robinson, using different settings.

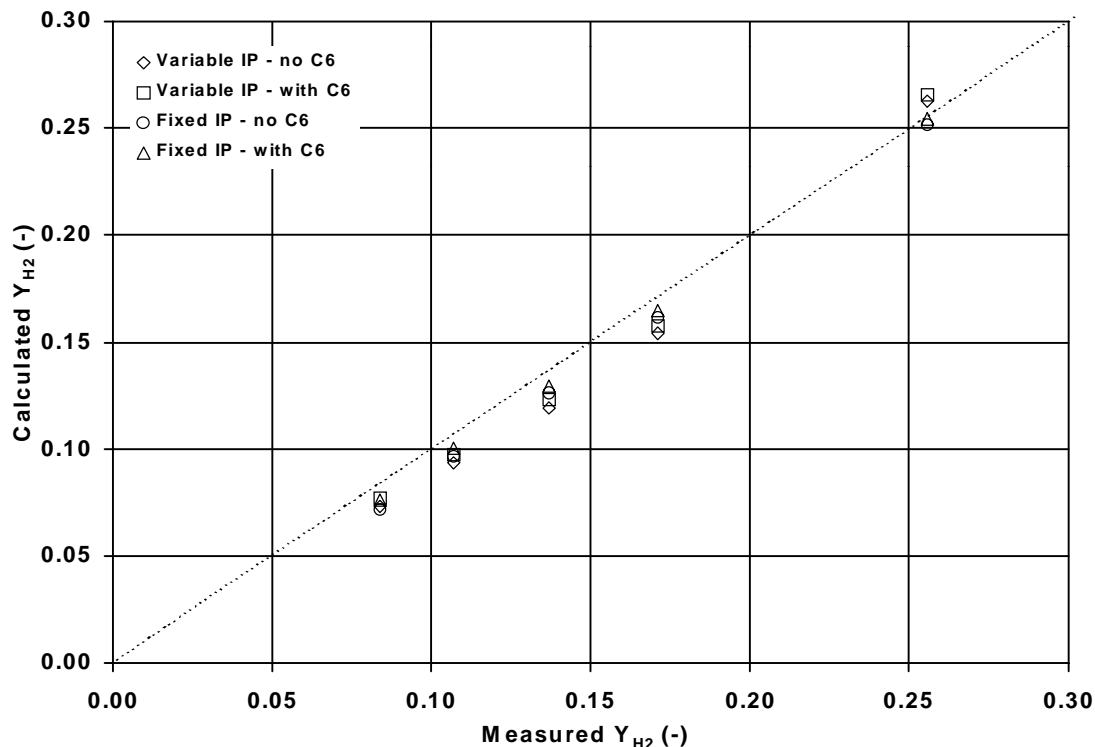


**Figure 2.17** Measured mole fraction of hydrogen in gas phase, versus the calculated mole fraction in gas phase, when adding 0.655 mole of  $H_2$  to the described reactor. Calculation with Peng-Robinson, using different settings.

The now formed system of Peng-Robinson EOS, with the temperature dependent interaction parameter was used to calculate the gas phase composition in the polymerization reactor for the conditions used in the tests of Table 2.4. Figures 2.15 to 2.17 show the results for low, mediate and high hydrogen concentrations in the system respectively. In all cases results calculated with the fixed HYSYS interaction parameter and the results calculated with the temperature dependent interaction parameter were compared for the situation with and without the presence of n-hexane. From these figures it is shown that gas phase hydrogen mole fractions are well predicted with the chosen EOS. Figure 2.18 shows the direct relation between

**Table 2.6** Temperature dependent coefficients for calculation of the relation between compositions of gas phase and liquid phase, to be used in equation 2.19.

Temperature (K)	A (-)	B (-)	Temperature (K)	A (-)	B (-)
303	0.0616	0.01807	343	0.2842	0.11184
313	0.1560	0.01529	353	0.3193	0.19174
333	0.2952	0.05301			

hydrogen mole fraction in gas phase and in liquid phase for typical temperatures used in these polymerizations. These graphs are used to translate GC measurements to hydrogen mole fractions in liquid phase.

The 5 plots in Figure 2.18 can be well described by a second order polynomial function, in the form of:

$$X_{H_2} = AY_{H_2}^2 + BY_{H_2} \quad (\text{eq. 2.19})$$

Table 2.6 shows the values for A and B, best describing the relation between the compositions of gas phase and liquid phase for the 5 temperatures used here.

In the next step, the HYSYS software was used to study the influence of variations in a few parameters that might not have been constant in the polymerization tests.

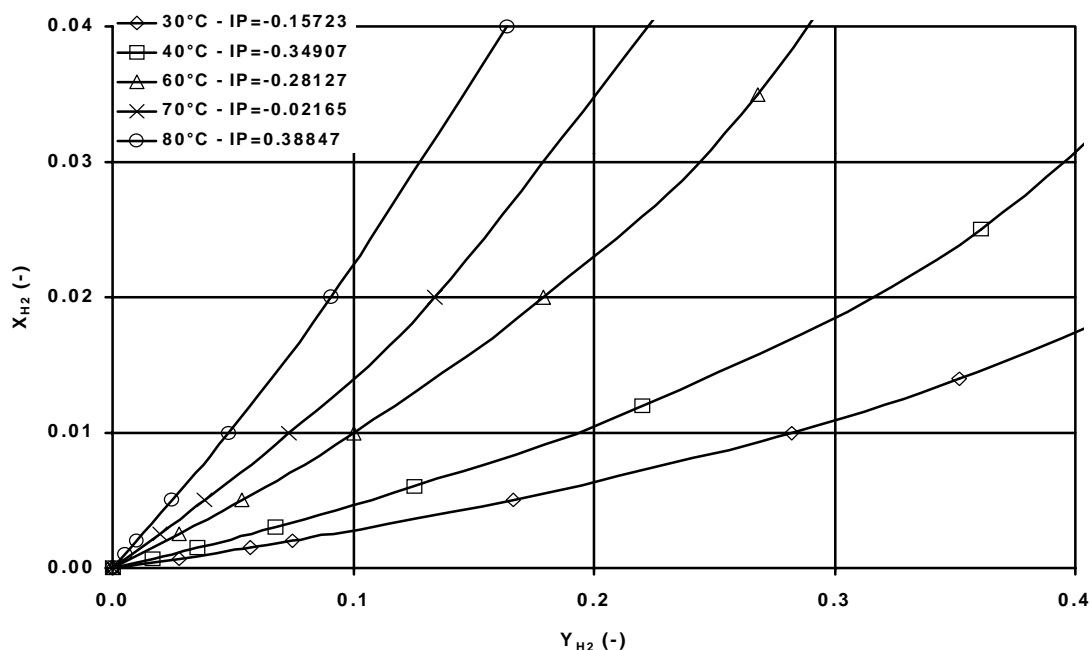


**Figure 2.18** Mole fraction of hydrogen in liquid propylene, as a function of the mole fraction hydrogen in gas phase at different temperature, calculated using Peng-Robinson EOS, with varied interaction parameter.

### Influence of the presence of hexane

As described in part 2, the different catalyst components used in polymerization experiments are injected as slurry in hexane. Typically two vials containing 10 ml of hexane are used, the first containing the alkyl-donor mixture in hexane, the second containing the catalyst in hexane. After injection of the separate liquids, the vial and injection system are always washed twice with 10 ml of fresh hexane. The use of this procedure leads to the introduction of about 60-ml of hexane in the reactor. As this amount is probably not completely constant in all tests, its influence on the gas-liquid equilibrium is investigated by using the calculation described before.

**Table 2.7** Values for  $Y_{H_2}$  and  $X_{H_2}$  at different hexane concentrations and different temperatures, calculated with the Peng-Robinson EOS, using temperature dependent interaction parameter.  $N_2$  is assumed to be absent.

$C_6$ (ml)	Low hydrogen (0.069 mole)						Moderate hydrogen (0.23 mole)						High hydrogen (0.66 mole)					
	30°C		60°C		80°C		30°C		60°C		80°C		30°C		60°C		80°C	
	$Y_{H_2}$	$X_{H_2}$	$Y_{H_2}$	$X_{H_2}$	$Y_{H_2}$	$X_{H_2}$	$Y_{H_2}$	$X_{H_2}$	$Y_{H_2}$	$X_{H_2}$	$Y_{H_2}$	$X_{H_2}$	$Y_{H_2}$	$X_{H_2}$	$Y_{H_2}$	$X_{H_2}$	$Y_{H_2}$	$X_{H_2}$
40	0.0267	0.0007	0.0115	0.0010	0.0066	0.0012	0.0835	0.0022	0.0371	0.0032	0.0217	0.0039	0.2050	0.0063	0.0983	0.0092	0.0595	0.0112
50	0.0268	0.0007	0.0116	0.0010	0.0067	0.0012	0.0837	0.0022	0.0373	0.0032	0.0220	0.0039	0.2054	0.0063	0.0988	0.0092	0.0603	0.0111
60	0.0269	0.0007	0.0116	0.0010	0.0068	0.0012	0.0837	0.0022	0.0375	0.0032	0.0223	0.0038	0.2060	0.0062	0.0994	0.0091	0.0611	0.0110
70	0.0270	0.0007	0.0117	0.0009	0.0069	0.0011	0.0842	0.0022	0.0378	0.0032	0.0226	0.0038	0.2065	0.0062	0.1000	0.0091	0.0619	0.0109

**Table 2.8** Values for  $Y_{H_2}$  and  $X_{H_2}$  at different amounts of  $N_2$  and different temperatures, calculated with the Peng-Robinson EOS using the temperature dependent interaction parameter. For all calculations  $V_{hexane}=60$  ml is used.

$N_2$ (mole)	Low hydrogen (0.069 mole)						Moderate hydrogen (0.23 mole)						High hydrogen (0.66 mole)					
	30°C		60°C		80°C		30°C		60°C		80°C		30°C		60°C		80°C	
	$Y_{H_2}$	$X_{H_2}$	$Y_{H_2}$	$X_{H_2}$	$Y_{H_2}$	$X_{H_2}$	$Y_{H_2}$	$X_{H_2}$	$Y_{H_2}$	$X_{H_2}$	$Y_{H_2}$	$X_{H_2}$	$Y_{H_2}$	$X_{H_2}$	$Y_{H_2}$	$X_{H_2}$	$Y_{H_2}$	$X_{H_2}$
0.00	0.0269	0.0007	0.0116	0.0010	0.0068	0.0012	0.0838	0.0022	0.0375	0.0032	0.0223	0.0038	0.2060	0.0062	0.0994	0.0091	0.0611	0.0112
0.05	0.0264	0.0007	0.0115	0.0010	0.0068	0.0012	0.0824	0.0022	0.0372	0.0032	0.0222	0.0039	0.2037	0.0062	0.0985	0.0091	0.0607	0.0111
0.10	0.0259	0.0007	0.0114	0.0010	0.0067	0.0012	0.0809	0.0022	0.0368	0.0032	0.0220	0.0039	0.1997	0.0062	0.0976	0.0091	0.0603	0.0110
0.15	0.0254	0.0007	0.0113	0.0010	0.0067	0.0011	0.0796	0.0022	0.0365	0.0032	0.0218	0.0039	0.1967	0.0062	0.0967	0.0091	0.0599	0.0109



Table 2.7 shows the results of these calculations. It is clear that there is an influence of the variation in hexane concentration on hydrogen concentrations, but the influence is minor. The percentage in  $Y_{H_2}$  goes up to 4.4% (corresponding change in  $X_{H_2}$  of 3.2%) at the highest temperatures, but this requires deviations in the hexane amount of 30%. As in normal experiments, a maximum variation of 10 ml in the amount of added hexane can be expected, changes in  $H_2$  concentration due to changes in hexane concentration can be neglected. So from this, we can conclude that there is no need to worry about the exact amount of added hexane, as this does not significantly change the parameters important to the polymerization reaction.

#### Influence of the presence of nitrogen

In the preparation of a liquid pool polymerization, liquid monomer is transported from the central storage vessel, through the purification sections, towards the polymerization set-up. Transport of the monomer is done by using an overpressure of nitrogen of about 8 bars (pressure is kept around 18 bar, at a temperature below room temperature). Due to the fact that the nitrogen will dissolve in the propylene, a variable amount of nitrogen is introduced in the polymerization reactor when filling it. As the amount of nitrogen present in the propylene will depend on storage temperature (storage vessel is located outside, so temperature will change with the season) and contact times. As a continuous amount of nitrogen present during polymerization is not guaranteed, the influence of this nitrogen presence is studied using the Peng-Robinson EOS with the temperature dependent interaction parameter. Table 2.8 shows the result of these calculations. Its influence on the hydrogen concentrations is evaluated for four different amounts of nitrogen in the system. It is clear that this influence is very small. Neither  $X_{H_2}$  nor  $Y_{H_2}$  change more than 1% after adding 0.15 mole of nitrogen, the estimated maximum amount of nitrogen that can be present. This is checked by the pressure during the polymerization: from this the amount of nitrogen present in the system can precisely be calculated. Based on the results presented in this table, it can be concluded that there is no need to precisely calculate the amount of nitrogen present in the system during polymerization experiments, as it does not influence the parameters important to the polymerization reaction itself.

## **2.4 Conclusions**

A set-up has been described for the polymerization of liquid propylene using the typical industrial catalyst systems, here a Ziegler-Natta catalyst. In the determination of the polymerization kinetics, a calorimetric method was used based on assumptions of isothermal conditions and a constant heat exchange between reactor content and reactor wall. It was shown in polymerization experiments that the approach previously used by our group could be improved in some details. This is especially important in tests with low heat production, and in experiments showing relatively strong deactivation behavior of the catalyst.

Furthermore, it was experimentally demonstrated that the use of a pre-polymerization step can help to increase the apparent rate of reaction at higher temperatures during the main polymerization stage. This effect is ascribed to the prevention of thermal runaway on particle scale when using this pre-polymerization. The outer surface area of the particle is thus enlarged at relatively low polymerization rate, and only after reaching sufficient surface area reaction rate is increasing at higher polymerization rate.

It has been shown that the Peng-Robinson equation of state gives the best results for describing the binary system of propylene and hydrogen in a vapor-liquid equilibrium. The often-used standard interaction parameter for this system, of  $-0.10360$  did not appear to give the best results, so a temperature dependent interaction parameter was derived. Using this relation, the predictive power of the Peng-Robinson relation was strongly improved.

Applying the PR-EOS, with that temperature dependent IP, equilibrium measurements based on the gas chromatograph analyses carried out using the polymerization reactor were well described. It was also shown that changes in the amount of nitrogen or hexane present in the liquid propylene polymerizations do not change the for polymerization important parameters (like  $X_{H_2}$ ) significantly.

Acknowledgements - The work presented in this paper was carried out in a co-operation with The Dow Chemical Company, Freeport, Texas, USA. The authors wish to thank Dow for both the financial and the intellectual input. The aluminum alkyls used in the work were kindly donated by AkzoNobel, Deventer, The Netherlands.

The work could not have been completed without the experimental work carried out by Eelko Bos, Inge van Putten, Marlies Kopmels, Tom Cellissen and Roxane van Arneman. The importance of their contribution to this work is gratefully acknowledged. Next to that, we would like to thank Louis van der Ham for his assistance in the HYSYS calculations. In addition, the technical assistance of Gert Banis, Fred ter Borg, Karst van Bree and Geert Monnick is highly appreciated.

## Notations

$\Delta H_r$	heat of reaction	(J/mole)
A	Surface area	(m <sup>2</sup> )
C	concentration	(kg/m <sup>3</sup> )
$C_w$	heat capacity	(J/K)
$D_a$	stirrer diameter	(m)
$E_{act}$	activation energy	(J/mole)
$g_c$	gravitational conversion factor	(-)
j	chain length	(-)
k	reaction rate constant	
m	mass	(g)
N	impeller rotational speed	(s <sup>-1</sup> )
$N_p$	Power number	(-)
$N_{Re}$	Reynolds number	(-)
P	Power	(J/s)
p	order of deactivation	(-)
p	pressure	(bar)
$p^0$	normal vapor pressure	(bar)

Q	Dissipated heat	(W)
q	chain transfer probability	(-)
R	gas constant	(J/mole·K)
r	order of reaction rate in $C_m$	(-)
$R_p$	rate of polymerization	(kg/g·hr)
T (or $\bar{T}$ )	temperature (average temperature)	(K)
t	time	(s)
U	Heat transfer coefficient	(J/s·m <sup>3</sup> )
X	Mole fraction in liquid phase	(-)
Y	Mole fraction in gas phase	(-)
$y_j^d$	differential molecular weight distribution	(-)

*Greek*

$\mu$	viscosity	(Pa·s)
$\rho$	density	(kg/m <sup>3</sup> )
$\chi$	Flory-Huggins interaction parameter	(-)
$\phi$	volume fraction	(-)

*Subscripts*

BL	baseline	main	main polymerization stage
cat	catalyst	p	propagation process
d	deactivation process	POL	in the amorphous polymer
gas	gas phase	PPY	propylene
H <sub>2</sub>	Hydrogen	prepol	pre-polymerization stage
jacket	jacket	r, reactor	reactor
lid	reactor lid	site	at the active site
liq	liquid	stirrer	stirrer
m	monomer		

*List of abbreviations*

DACU	Data acquisition and control unit	PPY	Propylene
D-donor	Di-cyclopentyl di-methoxy silane	PR	Peng-Robinson
EOS	Equation of state	RT	Room temperature
GC	Gas chromatograph	SEM	Scanning Electron Microscopy
IP	Interaction parameter	SRK	Soive-Redlich-Kwong
MW	Molecular weight	VLE	Vapor-liquid equilibria
MWD	Molecular weight distribution	ZN	Ziegler-Natta
PO	Polyolefin(s)		

**References**

- [1] Weickert, G. (1996). 'Modellierung von Polymerisationsreaktoren', 16-59, Springer-Verlag, Berlin.
- [2] Meier G.B., Weickert, G., & van Swaaij, W.P.M. (2001). 'Comparison of Gas and Liquid Phase Polymerization of Propylene with a Heterogeneous Metallocene Catalyst', *Journal of Applied Polymer Science*, **81**, 1193-1206.

- [3] Williams, R.B., & Katz D.L. (1954). 'Vapor-Liquid Equilibria in Binary Systems. Hydrogen with Ethylene, Ethane, Propylene, and Propane', *Industrial Engineering Chemistry*, **46**, 2512.
- [4] Young, C.L. (1981). 'Solubility data. Hydrogen-Olefins Systems', *Solubility Data Series*, **5** (6), 400.
- [5] Mizan T.I., Li, J., Morsi, B.I., Chang, M-Y., Maier, E., & Singh, C.P.P., 'Solubilities and Mass Transfer Coefficients of Gasses in Liquid Propylene in a Surface-Aeration Agitated Reactor', *Chemical Engineering Science*, **49**, 821.
- [6] Moore, E.P. (1996). 'Polypropylene Handbook', Hanser Publishers, Munich Vienna New York.
- [7] Samson, J.J.C., Weickert, G., Heerze, A.E., & Westerterp, K.R. (1998). 'Liquid-Phase Polymerization of Propylene with a Highly Active Catalyst', *AIChE Journal*, **44** (6), 1424.
- [8] Shimizu, F., Pater, J.T.M., Weickert, G., & van Swaaij, W.P.M. (2001). 'Three-site Mechanism and Molecular Weight: Time Dependency in Liquid Propylene Batch Polymerization Using a MgCl<sub>2</sub>-supported Ziegler-Natta Catalyst', *Journal of Applied Polymer Science*, **81**, 1035.
- [9] Weickert, G., Roos, P., Meier, G.B., Samson, J.J.C., & Westerterp, K.R. (1996). 'Kinetic study of Gas Phase Polymerization of Ethylene with rac-Me<sub>2</sub>Si[Ind]<sub>2</sub>ZrCl<sub>2</sub> / MAO supported on silica gel', *Proceedings 4<sup>th</sup> meeting Working Party Polymerization Reaction Engineering*, Thessaloniki, Greece.
- [10] Perry, R.H., & Green, D.W. (1998). 'Perry's Chemical Engineers Handbook', 18-12, 7<sup>th</sup> ed., McGraw-Hill, New York.
- [11] Pater, J.T.M. & Weickert, G. (2001). 'Experimental Equilibrium Data on the H<sub>2</sub>-PPY System', internal report IPP Research group, Enschede (NL).

## **CHAPTER 3**

**POLYMERIZATION OF LIQUID PROPYLENE  
WITH A 4<sup>TH</sup> GENERATION ZIEGLER-NATTA CATALYST**

-

**INFLUENCE OF TEMPERATURE, HYDROGEN AND MONOMER  
CONCENTRATION AND PREPOLYMERIZATION METHOD ON  
POLYMERIZATION KINETICS**

-

## Abstract

Liquid propylene was polymerized in a batch autoclave reactor using a 4<sup>th</sup> generation (TiCl<sub>4</sub>-MgCl<sub>2</sub> / (MeO)<sub>2</sub>Si / TEA) Ziegler-Natta catalyst. Calorimetry was used to measure full reaction rate versus time curves in order to obtain data on polymerization kinetics at industrially relevant conditions. The influence of polymerization temperature, the hydrogen and monomer concentration, and the prepolymerization method on reaction kinetics were investigated.

A method for prepolymerization, the so-called non-isothermal prepolymerization, was described. In this short prepolymerization procedure featuring an increasing polymerization temperature, thermal runaway on particle scale was avoided. It was shown that this prepolymerization method can relatively easily be applied to an industrial process, with the introduction of a continuous plug flow reactor, giving a narrow residence time distribution, acceptable yield-in-prepolymerization and a method for monitoring catalyst activity.

Using different methods for calculating the monomer concentration at the active site of the catalyst, the influence of polymerization temperature was determined. It was shown that at high polymerization temperatures, the reaction rate is barely influenced by polymerization temperature, when no prepolymerization is used. This is ascribed to thermal runaway on particle scale of a fraction of the catalyst particles. When a prepolymerization is used, this effect disappears and thermal runaway is avoided.

By replacing part of the liquid propylene by hexane to systematically reduce the monomer concentration ( $C_{m,bulk}$ ) in the bulk, the reaction rate was shown to be remarkably independent of the monomer concentration over a fixed range. Reducing  $C_{m,bulk}$  from 500 to 150 g/L caused the reaction rate to decrease slowly. The rate only began to decrease rapidly for  $C_{m,bulk}$  lower than this value.

The hydrogen concentration was varied over a wide range at 60 and 70°C. For both temperatures it was shown that reaction rates increased rapidly with increasing hydrogen concentration at the low hydrogen concentrations. At higher hydrogen amounts, this effect disappeared and a maximum reaction rate was found.

*A part of this chapter has been submitted for publication:  
J.T.M. Pater, G. Weickert and W.P.M. van Swaaij,  
'Polymerization of Liquid Propylene with a 4<sup>th</sup> Generation  
Ziegler-Natta Catalyst – Influence of Temperature, Hydrogen  
and Monomer Concentration and Prepolymerization Method on  
Polymerization Kinetics, Chemical Engineering Science (2001).*

### 3.1 Introduction

The huge growth of polyolefins (PO) markets worldwide, especially those of polyethylene and polypropylene is well known and well described<sup>[1-6]</sup> in the past years. The most obvious reason for this success is the combination between the low costs and the interesting material properties of PO. With the development of new technologies for polymerization processes and the development of the catalyst systems used, the scope of polyolefins products has rapidly broadened and applications that used to require relatively expensive materials like PVC and ABS can now be satisfied with cheap PO replacements.

Most modern catalyst systems used in industry for polypropylene production at this moment are the higher generation Ziegler-Natta catalysts, meaning the 4<sup>th</sup> generation with dimethoxysilane electron donors and 5<sup>th</sup> generation with the di-ether donors. The polymerization processes often use more than one polymerization reactor, being combination between liquid phase reactors, both liquid monomer or dilute slurry, and gas phase reactors like fluidized bed, vertically stirred bed or horizontally stirred bed, in series. The first reactor in these combinations is, in more than 50% of the cases - measured to worldwide production capacity - a reactor operating with liquid monomer. Liquid pool bulk polymerization typically shows very high reaction rates due to high monomer concentrations.

In open literature a large number of publications are dealing with kinetics of Ziegler-Natta catalyzed polymerization of propylene (for example <sup>[7-12]</sup>). But typical of these publications is the fact that most of them were carried out in a dilute slurry phase polymerization. As polymerization in liquid monomer leads to significantly higher polymerization rates, aspects like mass transport from bulk to particle, heat balance of the particle and the formation of the particle's morphology (fragmentation) will be influenced.

Some groups are indeed working with polymerization in liquid propylene, but typically these bulk polymerizations are used for screening and developing of catalyst systems<sup>[13-16]</sup>. The systems are operated fully batch-wise, and no kinetic information on the reaction other than the final yield is obtained.

The reason why only a limited amount of work on the polymerization of liquid propylene is presented in open literature is obvious: the hardware needed for experiments at very high reaction rates, at relatively high pressures, with highly flammable components is expensive and requires extensive safety-precautions. Nevertheless, such information is required to study the process at industrially relevant conditions.

#### 3.1.1 Prepolymerization

We define the prepolymerization step as a polymerization at mild conditions (relatively low temperature and/or low monomer concentration), typically carried out prior to the main polymerization step. The main polymerization step is, in the modern technologies, normally executed at temperatures of 65 to 80°C, and high monomer concentrations. The prepolymerization step is used to prevent the problems that can

arise at the demanding conditions of the main polymerization with fresh catalyst. We can group the beneficial influence of prepolymerization into three broad effects:

- the relatively slow pre-polymerization allows the particle to reach its critical size, where enough external surface area has been formed to prevent it from experiencing thermal runaway. This reason is mostly discussed in literature.
- the non-activated catalyst is activated in the liquid monomer by the dissolved cocatalyst-donor complex. Because of the fact that the activated sites start to produce polymer directly after activation, polymer production at the outer area of the particle, where activation starts, can disorder activation for the potentially active sites in the center of the particle. In pre-polymerization this effect can be avoided.
- the fragmentation of the catalyst support takes place in the initial stage of the polymerization reaction. An high reaction rate during this stage will influence the fragmentation negatively, and thus the morphology of the product, as we showed earlier<sup>[17]</sup>.

Some results are presented in the literature on the influence of prepolymerization on polymerization kinetics. Most of this experimental work is carried out in dilute slurry phase, meaning at significantly lower reaction rates compared to bulk polymerization. Researchers from the University of Waterloo observed an increase of polymerization rates in the homopolymerization of ethylene after prepolymerization step<sup>[18-19]</sup>, and explained this by proposing that the number of active sites increased during prepolymerization.

When focussing on propylene polymerization, Czaja and Krol<sup>[20-21]</sup> showed some influences of prepolymerization on kinetics of an unsupported  $\text{TiCl}_3$ -based catalyst. They found an increase in activity in the homopolymerization of propylene after a prepolymerization step with propylene. The same effect was observed using a supported 4<sup>th</sup> generation ZN catalyst<sup>[22]</sup>. These results are confirmed by experimental work done by Hutchinson and Ray<sup>[23]</sup>. In these works, the increase in reactivity was ascribed to an increase of the number of active sites due to a more complete fragmentation of the catalyst support. Note that all these experiments were carried out in dilute slurry phase with typical reaction rates in main polymerization up to 2  $\text{kg}_{\text{PP}}/\text{g}_{\text{cat}} \cdot \text{hr}$ .

### 3.1.2 This work

In the present contribution the results of polymerization experiments carried out in liquid propylene, using a 4<sup>th</sup> generation Ziegler-Natta catalyst, so with a dimethoxysilane as the external electron donor. Polymerization temperature, monomer concentration, hydrogen concentration and method of prepolymerization were varied, and the influence of these variations on polymerization kinetics was studied.

Moreover, a formalized model is presented to describe measured data on the polymer's molecular weight distribution. This model uses a normally distributed chain



termination probability to describe the multi-site character of the Ziegler-Natta catalyst. However, only a small amount of GPC data on the samples is presented. The value of the new model is discussed.

## 3.2 Experimental

### 3.2.1 Chemicals

#### Catalyst system

The catalyst system that was used in the present work was a commercially available Ziegler-Natta catalyst of the 4<sup>th</sup> generation as defined by Moore<sup>[1]</sup>, with TiCl<sub>4</sub> on a MgCl<sub>2</sub> support. Triethyl aluminum was used as a cocatalyst and the so-called D-donor (di-cyclopentyl di-methoxy silane) was used as external electron donor for regulation of the stereo specificity.

The particle size distribution of the catalyst (shown in Figure 2.2) is relatively narrow, and shows an average particle size of 24.4 micron. In all polymerization tests, the Al/Ti and Al/Si ratios were kept constant at values of 735 and 45 respectively. The fraction of titanium of the catalyst was 1.54 wt% .

#### Monomer, hydrogen, nitrogen and hexane

The propylene used in the experiments was of so-called ‘polymer grade’ and obtained from Indugas, with a purity >99.5%, with propane as main impurity. The hydrogen and nitrogen used were of >99.999% purity. A detailed description of the origin of the different materials used and the way that they are purified is described in an earlier paper<sup>[24]</sup>. (Table 2.1 summarizes this information.) The hexane added to the system was of ‘Pro Analyti’ quality obtained with Merck.

The hydrogen, nitrogen and hexane were further purified by passing them over a reduced BTS copper catalyst and subsequent passing through three different beds of molecular sieves, with pore sizes of 13, 4 and 3 angstroms respectively. The BTS catalyst was obtained from BASF. The propylene was purified in the same way, after it was passed over a bed of oxidized BTS copper catalyst to remove carbon monoxide.

### 3.2.2 Setup

Polymerization reactions were carried out in a 5-liter stainless steel autoclave reactor. The batch reactor is equipped with a six-blade impeller agitator, typically operated at 2000 rpm, and a small baffle located near the reactor wall. To maintain constant polymerization temperature (temperature in isothermal conditions within  $\pm 0.2\text{K}$ ), the reactor is jacketed, provided with a PID temperature control system. Hot water at about 5 degrees above polymerization temperature is mixed with a varied amount of cold water (around 15°C). This mixture is fed to the reactor jacket. The temperature of the reactor lid is kept 2 degrees above the liquid temperature during polymerization.

Reaction rate is measured using a calorimetric principle. At isothermal bulk conditions and with assuring a constant heat transfer coefficient from reactor to jacket, the temperature difference between reactor and jacket is a measure for the reaction rate. We previously<sup>[24-25]</sup> explained the application of this method more explicitly, as

well as the boundary conditions that apply for the use of this method. The methods results in a complete reaction rate versus time curve of the test.

A pneumatic injection system is used to inject the components of the catalyst system to the liquid propylene, without contacting them to atmosphere, even at high reactor pressures. A pneumatic sampling system can be used to draw samples of the reactor content, during the polymerization reaction.

The complete set-up is located in a concrete box, and operated with pneumatic valves from the outside of the box for safety reasons. The control of the valves, recording of temperatures from thermocouples, recording of the electronic pressure gauges and the control of the mass flow controllers is all done by means of a *Hewlett Packard 3852A Data Acquisition Unit* (DACU). This DACU is connected to the PC that is running the control software (an *HPVEE* based program) for control of valves and mass flow controllers. This PC writes the information to hard disk for later evaluation.

A schematic representation of the reactor set-up is shown in Figure 2.3.

### 3.2.3 Procedures

#### Catalyst preparation

The catalyst was prepared in a *Braun 150 B-G-II glove box* under a nitrogen atmosphere. The desired amounts of TEA and D-donor were prepared as a hexane solution in a vial at room temperature. 15 minutes after adding the components, this mixture was injected into the liquid propylene. In a separate vial, the oil suspended catalyst was weighed in a vial and diluted with some hexane. So, the catalyst was not activated before injection to the polymerization reactor.

#### Reactor preparation

To purify the reactor, it was flushed with nitrogen before every polymerization experiment, at a reactor wall temperature of about 95°C. The reactor was subsequently evacuated for about 5 minutes. This procedure was repeated for at least 5 times. After this flushing procedure, the reactor was tested for leakage with hydrogen at 20 bar. Then the reactor was evacuated and flushed a few times with gaseous propylene to wash out the hydrogen. Then the desired amounts of hydrogen and propylene were fed to the system, typically being 31.6 mole of propylene.

#### Prepolymerization methods

Three different types of experimental procedures with respect to the prepolymerization step are distinguished. In the first case no prepolymerization is used at all. The reactor is prepared at the main polymerization temperature and the two vials are injected at this temperature.

In the second case a fixed prepolymerization for 10 minutes at 40°C was used. Here the reactor was prepared at prepolymerization temperature, the two vials were injected and after 10 minutes the reactor temperature was raised to the main polymerization temperature as quickly as possible. Typically this takes about 3 minutes.

In the last case, a so-called non-isothermal prepolymerization (NIPP) was used. Here the reactor was prepared at 20°C. The TEA/donor containing vial was injected and after injection the reactor temperature was raised to 70°C. During heating, at a predefined temperature, the catalyst was then injected, resulting in a short prepolymerization step at a non constant temperature (increasing from injection temperature to main polymerization temperature).

In this paper we point to these three prepolymerization methods by the terms ‘none’, ‘fixed’ and ‘NIPP’ respectively. In the NIPP-case, it comes with the used injection temperature, or  $T_{inj}$ . Figure 2.5a and 2.5b show schematic representations of the temperature profiles of the fixed and NIPP prepolymerization respectively.

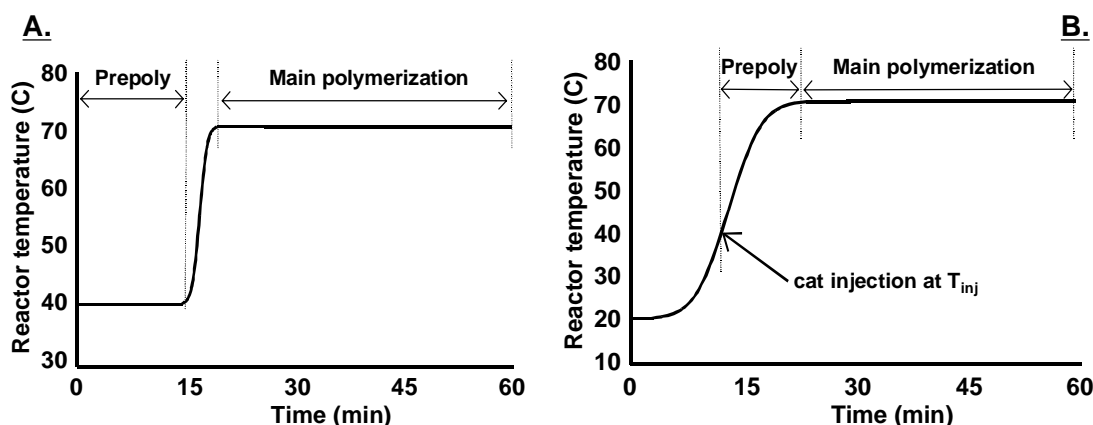


**Figure 2.5.** Temperature profiles for the two prepolymerization methods. A. Fixed prepolymerization for 10 minutes at a prepolymerization temperature of 40°C. B. Non isothermal prepolymerization (NIPP) with catalyst injection during heating of the reactor.

### Polymerization procedure

After the system has reached the desired initial temperature, the TEA/donor/hexane mixture was injected to the reactor. The vial was washed with fresh hexane two times to ensure that all cocatalyst and donor was introduced. Subsequently, about 1 minute after the first injection, the catalyst was injected into the liquid propylene. This vial was also washed twice. Injection of the catalyst started the polymerization reaction. After the prescribed polymerization time, typically being 75 minutes, the reaction was stopped by opening the vent valve, allowing the unreacted monomer to evaporate quickly. After flashing and flushing with nitrogen several times the reactor was opened and the product was dried overnight in an oven at 80°C and weight.

## 3.3 Results and Discussion

### 3.3.1 Influence of polymerization temperature

The influence of the polymerization temperature and of a fixed prepolymerization step on the kinetic parameters  $R_{p,0}$  and  $k_d$  was investigated in a previous paper<sup>[24]</sup>. It was shown that without the prepolymerization step, apparent reaction rates remained independent of temperature, above 70°C. With a fixed prepolymerization step this

effect disappeared and the same activation energy was found for the complete temperature range from 40 to 80°C. In those analyses, the monomer concentration at the active center was not considered.

In literature often a simplified and straight forward method is used to describe the kinetics of the polymerization reaction. For the overview, we will present the equations here too (see equations 3.1 and 3.2), but of course, we are dealing in the present work with a multi-site catalyst system. Nevertheless in this simplified approach, we are treating the system as if it were a single site catalyst, lumping the differences in propagation and deactivation constants for the different sites in single parameters.

When, as we showed earlier<sup>[24]</sup> the rate of polymerization can be described as a first order process in monomer concentration and the deactivation of the catalyst as a first order process in the number of active sites, the following equations are used:

$$R_p = k_p \cdot C_m \cdot C^* \quad \text{and} \quad \frac{dC^*}{dt} = -k_d C^* \quad (\text{eq. 3.1a and b})$$

Combining and integration for isothermal conditions leads then to the following expression that in literature is often used to describe the time dependent rate of polymerization:

$$R_p = R_{p,0} \cdot e^{-k_d \cdot t} \quad (\text{eq. 3.2})$$

using two parameters for the system: the initial reaction rate  $R_{p,0}$  and the deactivation constant  $k_d$ .

When evaluating the temperature dependence of the polymerization, the dependency on temperature in equation 3.1a will mainly be in the propagation rate constant and in the changing monomer concentration with temperature. We propose to use an Arrhenius type of T-dependency for  $k_p$  and  $k_d$ .

Figure 3.1 shows of 5 different experiments the full reaction rate versus time curve. The different tests were carried out at varied polymerization temperatures, from 40 to 80°C. From these curves a fit is made using the described model, and from the fit the values for  $R_{p,0}$  and  $k_d$  (initial reaction rate and deactivation constant) are determined. Earlier we described the used method and the assumptions in more detail<sup>[24]</sup>.

With a changing polymerization temperature, the monomer concentration will also change due to temperature dependency of the bulk monomer concentration and of monomer absorption in the polymer. The simplest way to correct for the changing monomer concentration is to assume the same monomer concentration at the active site as in the bulk. A more sophisticated approach is to use the Flory-Huggins equation to calculate monomer concentrations in the amorphous part of the polymer, as shown in equation 3.3.

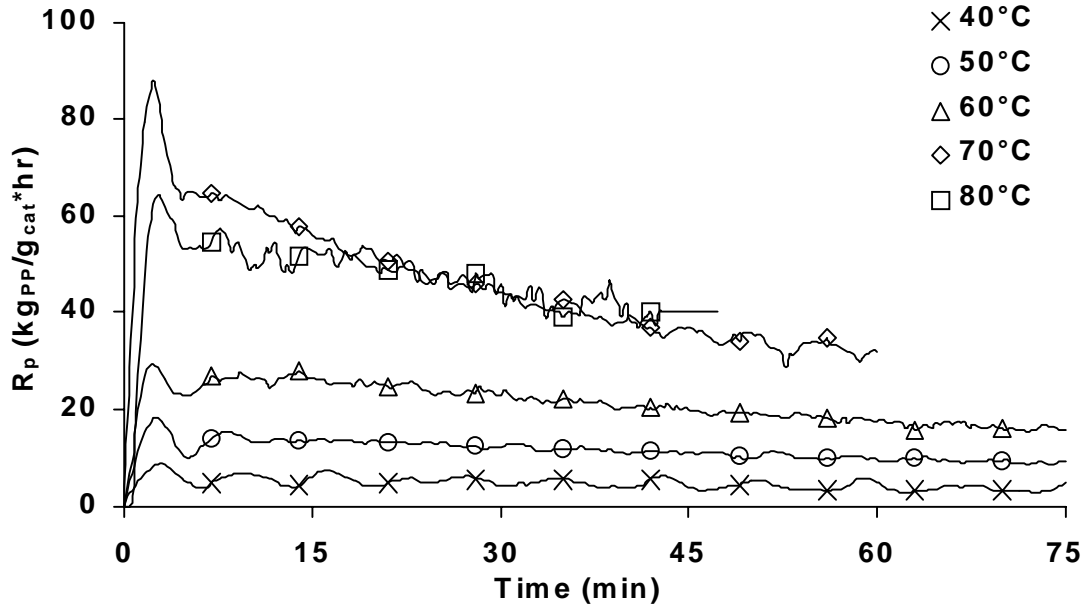


**Figure 3.1.** Reaction rate versus time profiles for 5 polymerization tests at different temperatures from 40 to 80°C.

$$\ln \frac{P}{P^0} = \ln \phi + (1 - \phi) + \chi(1 - \phi)^2 \quad (\text{eq. 3.3})$$

Here,  $P$  is pressure,  $P^0$  the saturation pressure at the temperature in question,  $\chi$  the Flory-Huggins interaction parameter and  $\phi$  the volume fraction of monomer in the polymer. For liquid pool conditions as used here,  $P$  is equal to  $P^0$  and therefore the left hand side of equation 3.3 is equal to zero. Samson<sup>[25]</sup> used this equation to calculate monomer concentrations in the polymer, with an interaction parameter based on literature<sup>[26]</sup> data, Meier<sup>[27]</sup> did the same with an interaction parameter based on data obtained from his own equilibrium measurements. Table 3.1 shows the monomer concentrations in these three cases at different temperatures. Of course, it should be kept in mind that to obtain the concentration data, sorption was measured in dead polymer, which has been dried (and thus ‘fully’ crystallized) before the sorption measurements. Monomer concentrations in the polymer formed in-situ can differ

**Table 3.1.** Monomer concentrations at the active site as a function of temperature, calculated by liquid density, by Meier<sup>[27]</sup> and by Samson<sup>[25]</sup>.

Temperature (°C)	Temperature (K)	$C_{m,dens}$ (kg/m <sup>3</sup> )	$C_{m,Meier}$ (kg/m <sup>3</sup> )	$C_{m,Samson}$ (kg/m <sup>3</sup> )
20	293	512.3	164.4	-
30	303	494.6	185.9	-
40	313	475.6	208.8	200.3
50	323	454.7	233.0	156.5
60	333	431.1	257.9	111.0
70	343	403.3	276.1	70.4
80	353	367.4	300.9	-

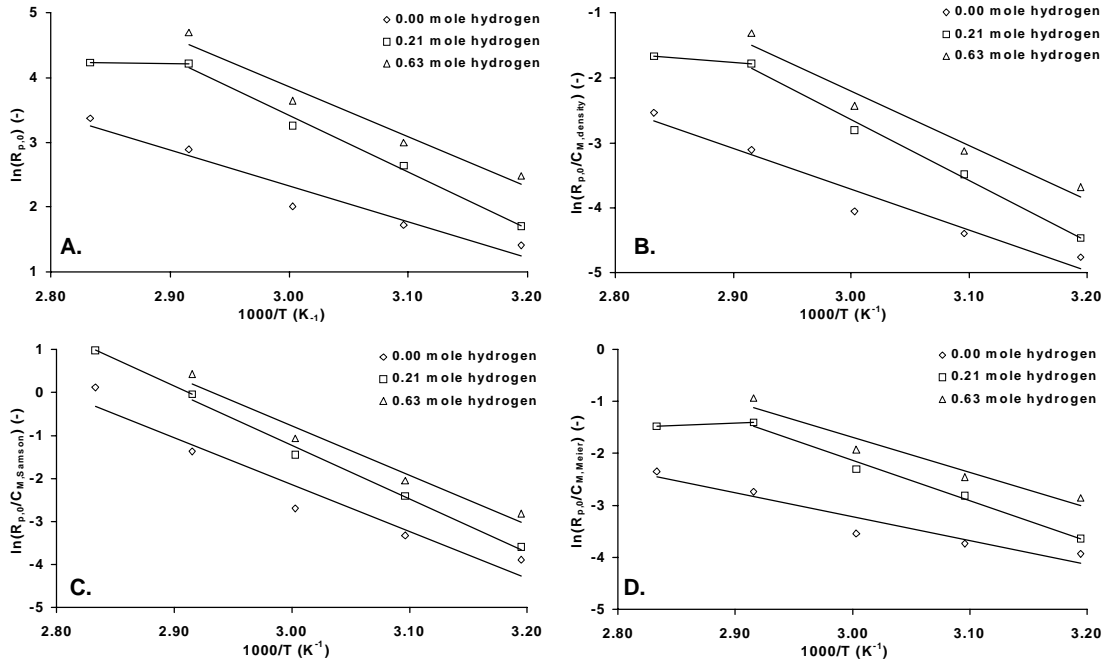


**Figure 3.2.** Arrhenius plots for the initial reaction rates in experiments without a prepolymerization step, for 3 different hydrogen concentrations. A.  $C_m$  is not taken into account B.  $C_m$  calculated from liquid density C.  $C_m$  calculated according to Samson<sup>[25]</sup> D  $C_m$  calculated according to Meier<sup>[27]</sup>.

significantly from the values determined experimentally in thermobalances as the polymer, formed in an environment with these high monomer concentrations, is barely allowed to crystallize.

If we assume a first order dependency of the propagation step on the monomer concentration, the monomer concentration can be included in the Arrhenius plot by dividing the initial reaction rate by the calculated  $C_m$ . The effect of the three different methods to calculate the monomer concentration is shown in Figures 3.2a to 3.2d. In Figure 3.2a, an Arrhenius plot is shown of the initial reaction rates, without taking into account the monomer concentration. In 3.2b this concentration was taken into account, here  $C_m$  was calculated from the density of the liquid monomer, which was calculated using the empirical relation expressed in 3.4<sup>[28]</sup>.

$$\rho = M_{PPY} \cdot \frac{1.5262}{0.2753 \left( 1 + \left( 1 - \frac{T}{364.9} \right)^{0.3055} \right)} \quad (\text{kg/m}^3) \quad (\text{eq. 3.4})$$

where T is expressed in Kelvin and  $M_{PPY}$  represents the molar mass of propylene.

Activation energies for the propagation step, or rather the overall activation energy for the lumped propagation steps, are shown in Table 3.2.

Figure 3.2c and d show the effect of calculating the monomer concentration at the active site as proposed by Samson and by Meier respectively. Of course, the activation energies determined at the different methods for  $C_m$  differ, as the calculation method for  $C_m$  will bring its own temperature dependence.

**Table 3.2.** Activation energies for initial reaction rate and deactivation constant, in the main polymerization, at different hydrogen concentrations and different methods for determination of  $C_m$ , without a prepolymerization.

	$R_{p,0}$ (kJ/mole)	$R_{p,0}/C_{m,Meier}$ (kJ/mole)	$R_{p,0}/C_{m,Samson}$ (kJ/mole)	$R_{p,0}/C_{m,density}$ (kJ/mole)	$k_d$ (kJ/mole)
0.00 mole hydrogen	46.4	38.1	90.9	52.2	-
0.21 mole hydrogen	72.8	64.4	103.8	77.7	37.8
0.63 mole hydrogen	64.5	56.0	95.4	69.3	34.9

In the presence of hydrogen, at really high reaction temperature, a leveling off is observed and the reaction rate barely increases with temperature. Earlier, we ascribed this effect to thermal runaway on particle scale in the initial stage. But in Figure 3.2c we see that the effect has disappeared, due to the low monomer concentration in the polymer for these high temperatures predicted by Samson. To learn if the leveling-off is caused by thermal runaway or by errors in  $C_m$ , tests have to be done with a prepolymerization step. If the effect remains after prepolymerization, Samson seems to be right with  $C_m$  calculations (when linearity of the Arrhenius plot is accepted as an argument).

Now, we will consider the deactivation constant. Figure 3.3 shows the deactivation constants belonging to the same experiments. The information from this Arrhenius plot is summarized in Table 3.2 in the form of activation energies for the deactivation constants for the lumped deactivation processes. Deactivation increases with increasing polymerization temperature. In the presence of hydrogen, the activation energy is around 35 kJ/mole, but in the absence of hydrogen there is no clear trend in temperature dependency of the deactivation.

It is interesting to see that the activation energy determined for deactivation is significantly lower than almost all activation energies for propagation. If this data is valid for a wide temperature window, extrapolation of this information would lead to extremely high reaction rates at high temperatures, without the expected rapid deactivation. Probably additional mechanisms causing the strong deactivation at very high temperatures are not yet observed, at the moderate temperatures used here.

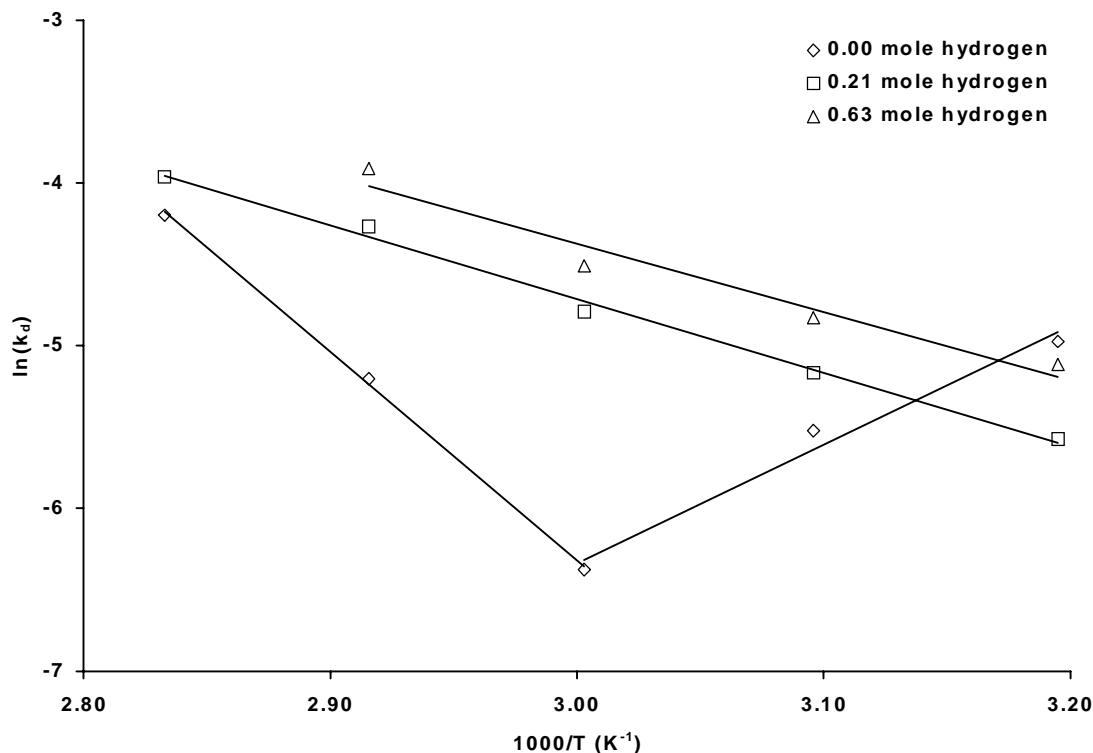


**Figure 3.3.** Arrhenius plot for the deactivation constant at three different hydrogen concentrations, without a prepolymerization step.

### 3.3.2 The effect of prepolymerization

#### Fixed prepolymerization

As already mentioned before<sup>[24]</sup>, the direct comparison of the absolute (initial) reaction rates in cases with and without prepolymerization is not straight forward, as  $R_{p,0}$  will depend on the definition of  $t=0$ . When there is no prepolymerization,  $t=0$  is defined by the moment of catalyst injection. However when we do use a prepolymerization, the definition of  $t=0$  is not straightforward. After prepolymerization, the jacket temperature is increased to heat up the reactor as fast as possible. When coming close to the set point of the reactor temperature, the jacket is of course used for cooling. Here,  $t=0$  after prepolymerization is arbitrarily defined as the moment that temperature of the cooling water is lower than temperature of the reactor. Of course, definition of  $t=0$  does not influence values for the deactivation constant  $k_d$  as derived from our method.

Figures 3.4a to 3.4d show the Arrhenius plots of the initial reaction for the cases with a fixed prepolymerization step (10 minutes at 40°C). In a manner analogous to Figures 3.2a to 3.2d, the monomer concentration used to calculate the Arrhenius plot differs in 3.4a to 3.4d. In these plots, the temperature used at the x-axis is the temperature in the main polymerization. The activation energies calculated from these figures are summarized in Table 3.3. Figure 3.5 shows the values for deactivation in the experiments with a prepolymerization step at 40°C; the resulting activation energies calculated from these plots are shown in the last column of Table 3.3.



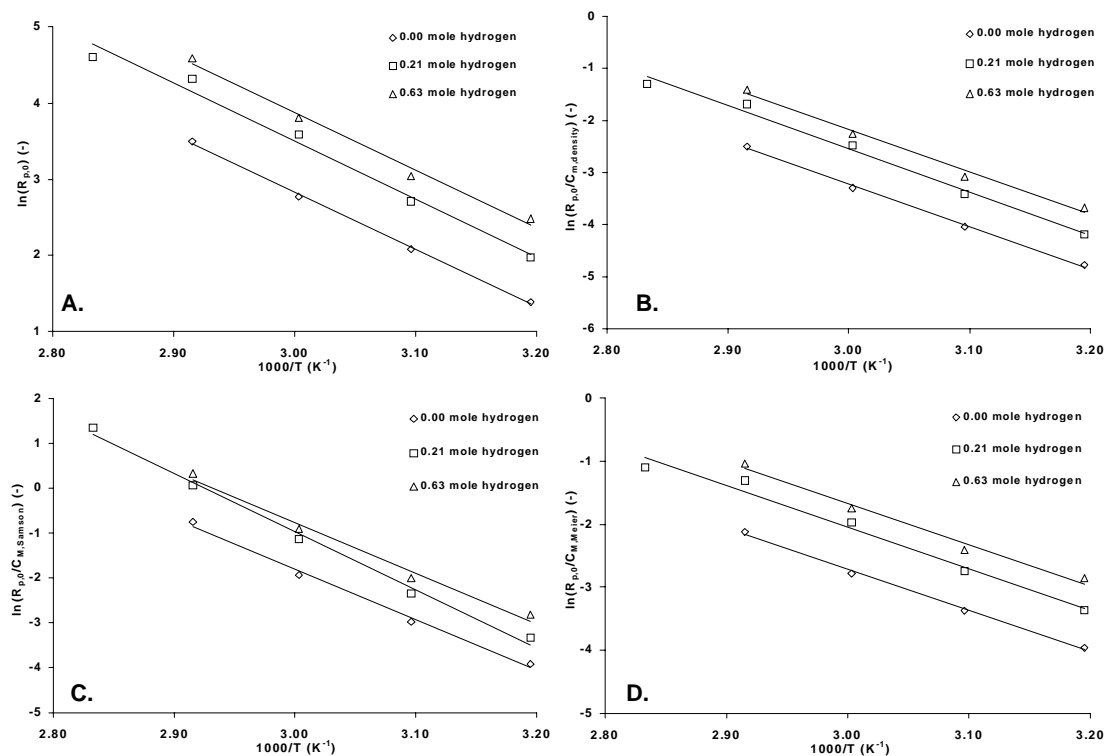


**Figure 3.4.** Arrhenius plots for the initial reaction rates in experiments with a fixed prepolymerization step, for 3 different hydrogen concentrations. A.  $C_m$  is not taken into account B.  $C_m$  calculated from liquid density C.  $C_m$  calculated according to Samson<sup>[25]</sup> D  $C_m$  calculated according to Meier<sup>[27]</sup>.

In the figures of 3.4, the leveling off of reaction rate at the highest temperatures was not observed, not even when the liquid density is used as estimation for the monomer concentration. From this we conclude that thermal runaway on particle scale as shown in Figure 3.2 causes the leveling off, as we already mentioned before<sup>[24]</sup>. The runaway damages a part of the catalyst; this is avoided when a pre-polymerization is used. Unfortunately with the current setup it is not possible to measure kinetics at 80°C at high hydrogen concentrations due to total pressure exceeding the maximum working

**Table 3.3.** Activation energies for initial reaction rate and deactivation constant, in the main polymerization, at different hydrogen concentrations and different methods for determination of  $C_m$ , after a fixed prepolymerization.

	$R_{p,0}$ (kJ/mole)	$R_{p,0}/C_{M,density}$ (kJ/mole)	$R_{p,0}/C_{M,Samson}$ (kJ/mole)	$R_{p,0}/C_{M,Meier}$ (kJ/mole)	$k_d$ (kJ/mole)
0.00 mole hydrogen	62.6	68.3	93.6	54.2	32.1
0.21 mole hydrogen	70.5	75.4	101.4	62.1	42.9
0.63 mole hydrogen	62.9	67.8	93.8	54.5	23.8

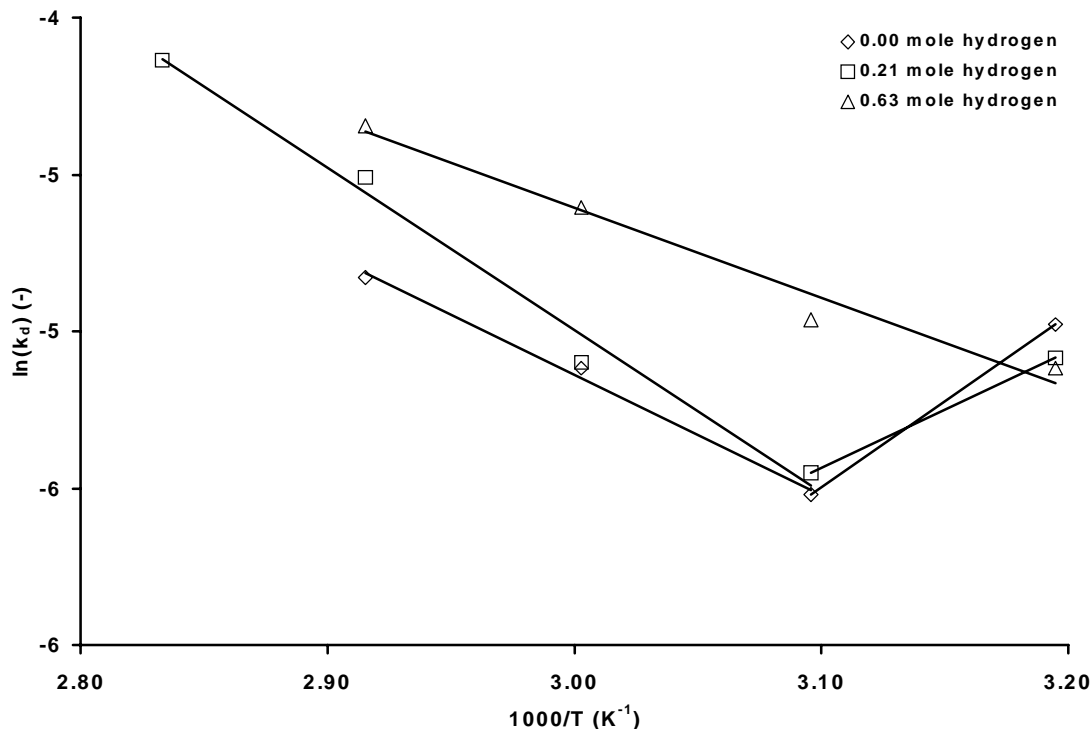


**Figure 3.5.** Arrhenius plot for the deactivation constant at three different hydrogen concentrations, with a fixed prepolymerization step.

pressure of the system.

#### Non-isothermal prepolymerization

Another prepolymerization method that was used is the so-called non-isothermal prepolymerization where catalyst is injected during the heating trajectory, resulting in a short prepolymerization (maximum 3 minutes) at a rapidly increasing temperature. In a separate study<sup>[17]</sup> we showed that a NIPP prepolymerization step starting at 40°C, was fully sufficient to ensure the right powder morphology of the end product. Table 3.4 shows the results of the polymerization kinetics, when using a NIPP prepolymerization. The experiments with a fixed prepolymerization are added for comparison. From this table it can be seen that the short prepolymerization during three minutes shows very similar polymerization kinetics in the main polymerization, compared to the fixed prepolymerization.

**Table 3.4.** Influence of a short, non-isothermal prepolymerization step on initial reaction rate in main polymerization and deactivation behavior of the catalyst at three different hydrogen concentrations.

H <sub>2</sub> (mole)	NIPP T <sub>inj</sub> =50		NIPP T <sub>inj</sub> =60		NIPP T <sub>inj</sub> =70		Fixed prepol	
	R <sub>p,0</sub> (kg <sub>PP</sub> /g <sub>cat</sub> *hr)	k <sub>d</sub> (min <sup>-1</sup> )	R <sub>p,0</sub> (kg <sub>PP</sub> /g <sub>cat</sub> *hr)	k <sub>d</sub> (min <sup>-1</sup> )	R <sub>p,0</sub> (kg <sub>PP</sub> /g <sub>cat</sub> *hr)	k <sub>d</sub> (min <sup>-1</sup> )	R <sub>p,0</sub> (kg <sub>PP</sub> /g <sub>cat</sub> *hr)	k <sub>d</sub> (min <sup>-1</sup> )
0.00	34	0.009	27	0.008	30	0.006	33	0.008
0.21	77	0.009	70	0.010	68	0.015	75	0.011
0.63	81	0.014	85	0.014	76	0.016	87	0.013

Fresh catalyst, if introduced into the liquid pool, may get overheated. This will depend on the liquid pool temperature, reaction rate of the particle and the heat transfer rate. The latter two factors will depend on particle size. With a very simple model we calculated the heat transfer rates required to keep the particle within 10K from the liquid bulk temperature. The heat transfer was modeled using the following expression:

$$Q = h \cdot A_p \cdot (T_p - T_{\text{bulk}}) \quad (\text{J}) \quad (\text{eq. 3.5})$$

The Nusselt number that is required for sufficient heat transfer is expressed as:

$$\text{Nu}_{\text{req}} = \frac{h \cdot d_p}{\lambda_{\text{bulk}}} \quad (-) \quad (\text{eq. 3.6})$$

with  $h$  being the heat transfer coefficient,  $A_p$  and  $d_p$  the particle's surface area and diameter,  $T_p$  and  $T_{\text{bulk}}$  the temperatures of particle and bulk and  $\lambda_{\text{bulk}}$  the thermal conductivity of the bulk.

When assuming that the relation between the Nusselt number, the Reynolds number and the Prandl number can be described similar to:

$$\text{Nu} = 2 + A \cdot (\text{Re}^a \cdot \text{Pr}^b) + B \cdot (\text{Re}^c \cdot \text{Pr}^d) \quad (-) \quad (\text{eq. 3.7})$$

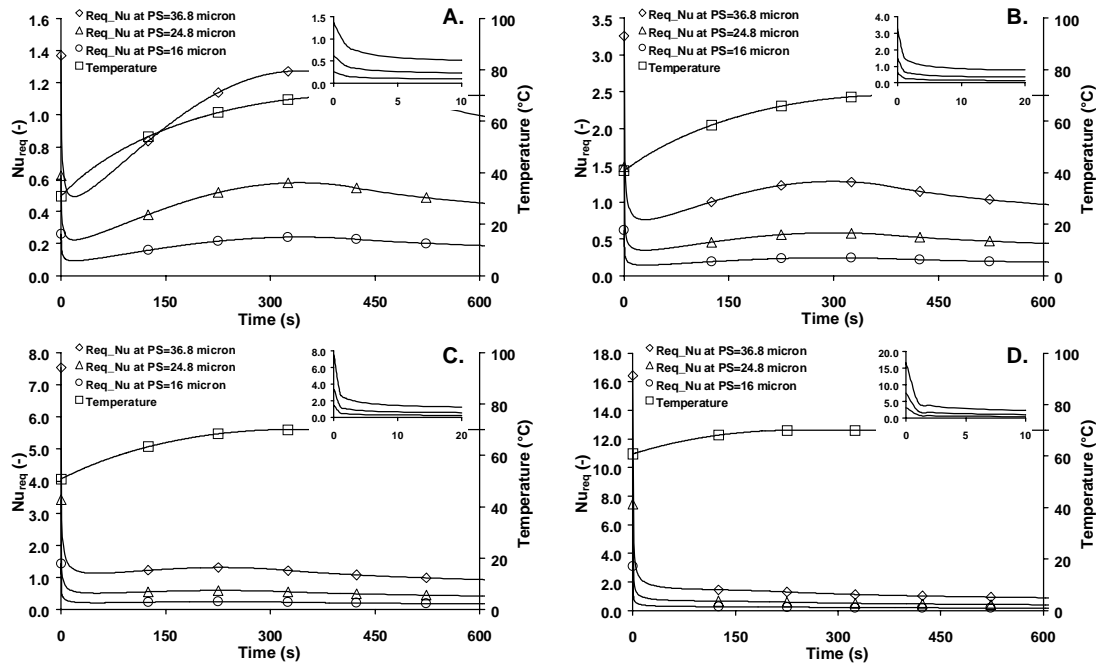


**Figure 3.6.** Calculated required Nusselt numbers during the non-isothermal prepolymerization, with catalyst injection at 30°C, 40°C, 50°C and 60°C respectively. Calculations are based on the kinetics measured in this work, the temperature profiles plotted in the figures are experimentally obtained profiles. The inserted pictures show the initial stage in more detail.

and we consider the particle as floating inside the liquid monomer (without a slip velocity between particle and bulk) the lowest value for Nusselt becomes 2. In any case the catalyst will not overheat:  $Nu_{req} < 2$ .

As said, a maximum temperature difference between particle and bulk of 10K is assumed, basically meaning that formation of gas bubbles in the particles is not expected at a  $\Delta T < 10K$ . The results of these calculations are sensitive to this value that has been chosen arbitrarily. At lower values, overheating will be more probable.

Figure 3.6 shows for four different injection temperatures, 30°C, 40°C, 50°C and 60°C respectively for 3.6a to 3.6d, the required Nusselt numbers to remove the produced reaction heat. Four lines are plotted in each figure: the experimentally obtained temperature profile in the reactor and three lines each representing a different fraction of the PSD of the catalyst. The three lines are calculated for particle sizes of 16, 25 and 37 microns, representing  $X_{15}$ ,  $X_{50}$  and  $X_{95}$  in the PSD. The calculations are based on the kinetics presented above and a thermal conductivity of the bulk of 0.092 W/m·K was used. Possible retarded catalyst activation and catalyst deactivation are neglected.

In Figure 3.6a it can be seen that even the largest particles give  $Nu_{req}$  values at the largest of 1.4. But already at  $T_{inj}=40^\circ C$ , we see that a part of the catalyst population risks thermal overheating, as  $Nu_{req}$  goes up to 3.3 in the initial stage. At 50°C even particle with the average particle size of the used catalyst (25 micron), show values for  $Nu_{req}$  above 3. From these calculations it becomes clear that the NIPP can be used to prevent particles from overheating, as long as the injection temperature of the catalyst is low enough.

Apart from the influence of the NIPP pre-polymerization on the polymerization kinetics, there is important influence on the morphology of the polymer powder. We previously described this influence extensively<sup>[17]</sup>.

### 3.3.3. Application of NIPP to an industrial process

The non isothermal pre-polymerization could be applied in industrial polymerization processes as a continuous prepolymerization reactor. At present, typically two types of prepolymerization are industrially applied:

- batch-wise prepolymerization at low monomer concentrations in dilute slurry. This is an expensive and time consuming procedure
- continuous prepolymerization in stirred tank or loop-reactor. This implies a relatively broad residence time distribution (RTD), which is not desired.

For a catalyst behaving like the one used in the present work, a short prepolymerization would be satisfactory with respect to the influence on kinetics and on powder morphology. In that case a tubular prepolymerization reactor, providing short and controllable residence times with a narrow RTD could be used. As catalyst amounts are limited, even in large industrial plants, the polymerization system can remain relatively small and thus inexpensive. Besides, the temperature behavior of the

prepolymerization tube reactor could be used for monitoring catalyst activity when switching to other catalyst batches or another monomer feed.

As an example, such a non-isothermal prepolymerization reactor having realistic industrial scale dimensions, was simulated. This is a rough calculation to show the possibilities of the method.

A 250 kton/year plant was considered, using a catalyst that reaches a final catalyst efficiency of  $40 \text{ kg}_{\text{PP}}/\text{g}_{\text{cat}}$ . When assuming 8000 operating hours per year, the catalyst flow to be pre-polymerized will be  $13 \text{ g}_{\text{cat}}/\text{minute}$ . In the calculations, the Reynolds number characterizing the monomer flow through the tube is demanded above 2300 and flow velocities in the tube need to be above particle settling rate.

Zacca<sup>[29]</sup> showed the minimum needed yield of prepolymerization (YOP) for liquid pool main polymerization to be around  $120 \text{ g/g}$  for an average catalyst particle size of 67 micron. In that calculation a reaction rate in liquid pool of  $20 \text{ kg/g} \cdot \text{hr}$  was assumed. In the present situation, the initial reaction rates are significantly higher, but the catalyst particles are smaller. For the present case, a yield in prepolymerization of about  $150 \text{ g/g}$  is needed to avoid particle overheating at the highest reaction rates in the initial stage in main polymerization.

One of the main advantages of the use of a tubular reactor for a non-isothermal prepolymerization is the possibility of activity monitoring, by means of the axial temperature profile that develops. By using a jacketed reactor it would be possible to force a temperature profile, but for monitoring purposes an adiabatic operated tube would be optimal. This adiabatic operation is studied in this example. Figure 3.7 shows the results of reactor calculations, where the inlet temperature was set to  $30^\circ\text{C}$  and the outlet temperature to  $70^\circ\text{C}$ , as this would be a typical temperature for the succeeding main liquid pool reactor.

The parameters used in the calculations are shown in Table 3.5. When adjusting the length and the residence time of the reactor in such a way that the  $T_{\text{in}}$ ,  $T_{\text{out}}$  and YOP agree with the mentioned values, the lengths of reactors with internal diameters of 3, 4 and 5cm are 66, 37 and 24 meters respectively, all with a residence time of 35 seconds. Here the monomer throughput varies with reactor dimensions and residence time, in the most extreme case 1.3 liters of propylene per second are fed to the prepolymerizer. Figures 3.7a and b show the profiles for the reactors with diameters of 3 and 4 cm respectively. It is clear that the axial temperature profile can very well be

**Table 3.5** *Parameters as used in the tube-shaped non isothermal pre-polymerization reactor calculations.*

Plant capacity	250	kt/yr	Density polymer	800	kg/m <sup>3</sup>
Final CE	40	kg/g	Heat of polymerization	104	kJ/mole
Hrs/year	8000	hrs/yr	Viscosity of propylene	0.0004	kg/m.s
			$C_p$ propylene	3290	J/kg.K
Tinlet	30	°C			
Toutlet	70	°C	YOP	150	g/g

used to monitor polymerization rates in a very early stage, but from these plots the weak point in this application also becomes clear. The temperature increase in the last part of the system is relatively fast, leading to possible problems in the control of the system. Sudden temporary decreases in monomer flow to the pre-polymerizer can easily bring the tube reactor to runaway conditions.

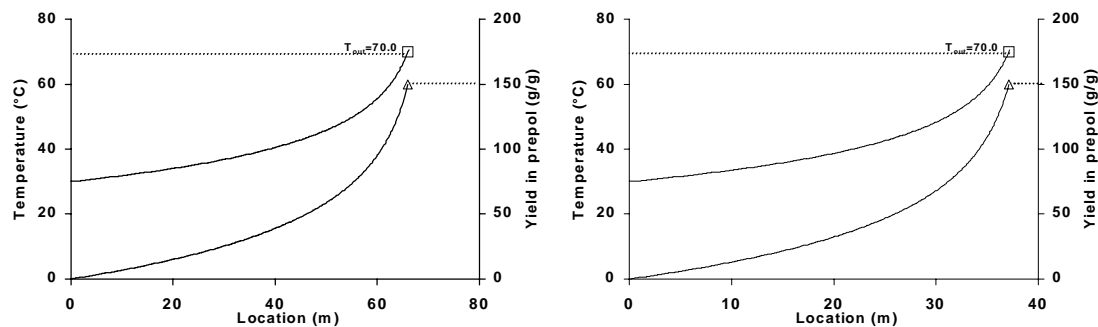


**Figure 3.7** Axial temperature and polymerization yield profiles as example for a NIPP tube reactor. The reactor is operated adiabatically,  $T_{inj}$  and  $T_{out}$  are set to 30 and 70°C respectively. A) Reactor with internal diameter of 3 cm, resulting in RT of 35 s and length of 66 m. B) Reactor with internal diameter of 4 cm, resulting in RT of 35 s and length of 37 m

The catalyst described by Zacca, showing lower activities in the main polymerization reactor, needs according to his calculations a YOP of 120 g/g, requiring a reactor length of 42 m and a residence time of 28 seconds at a reactor diameter of 3 cm.

The rough calculations shown here, demonstrate the power of these polymerization reactors, showing a narrow residence time distribution, relatively cheap installation costs and a monitoring possibility for the catalyst activity. More detailed reactor simulations would be necessary to come to a more complete insight in the reactor behavior.

### 3.3.4 Influence of hydrogen concentration

The hydrogen supply was varied over a relatively wide range. In this work, the amount of hydrogen added to the reactor is given, instead of the gas phase or liquid phase concentrations, as this will depend on the reactor temperature. For example, when changing the temperature during an experiment, as is done in an experiment with prepolymerization, different hydrogen concentrations will exist during the same batch experiment. Table 3.6 shows the relation of the added amount of hydrogen to the concentrations for gas- and liquid phase for the different reactor temperatures, calculated with the Peng-Robinson equation of state (EOS), using a temperature dependent binary interaction coefficient as we proposed earlier<sup>[24]</sup>. The binary interaction coefficient was obtained from fitting to experimental vapor-liquid equilibrium data.

**Table 3.6.** Relation between the amount of hydrogen added to the system and the concentrations in gas- and liquid phase (indicated with mole fractions  $X_{H_2}$  and  $Y_{H_2}$ ).

$T_{system}$	0.21 mole H <sub>2</sub> added		0.63 mole H <sub>2</sub> added	
	$Y_{H_2}$	$X_{H_2}$	$Y_{H_2}$	$X_{H_2}$
30°C	0.0837	0.0022	0.2060	0.0062
40°C	0.0652	0.0025	0.1639	0.0072
50°C	0.0498	0.0029	0.1284	0.0081
60°C	0.0375	0.0032	0.0994	0.0091
70°C	0.0283	0.0035	0.0770	0.0100
80°C	0.0223	0.0038	0.0611	0.0110

In Figures 3.2 to 3.5, the effect of hydrogen has already been presented. It shows as expected, the presence of hydrogen increases the polymerization rate significantly at all polymerization temperatures. In addition to the increased polymerization rate, it is also clear that the deactivation constant increases in the presence of hydrogen. As it is well known that the consumption of hydrogen in these polymerizations is negligible, we can be sure that this observed increase in the deactivation rate is not caused by a decreasing hydrogen concentration.

To get a more detailed image of the effect of the hydrogen concentration, Figure 3.8 shows the initial reaction rates as a function of the added amount of hydrogen at 60 and 70°C. The results agree with general data in literature on the hydrogen influence on highly active Ziegler-Natta catalysts. In the absence of hydrogen the catalyst shows a low activity, which increases with hydrogen concentration. At higher concentrations this influence levels off, and initial reaction rate reaches a maximum value. When fitting the reaction rates to the empirical relation of equation 3.8, the two lines plotted in Figure 3.8 are obtained (solid line for 70°C and dotted line for 60°C).

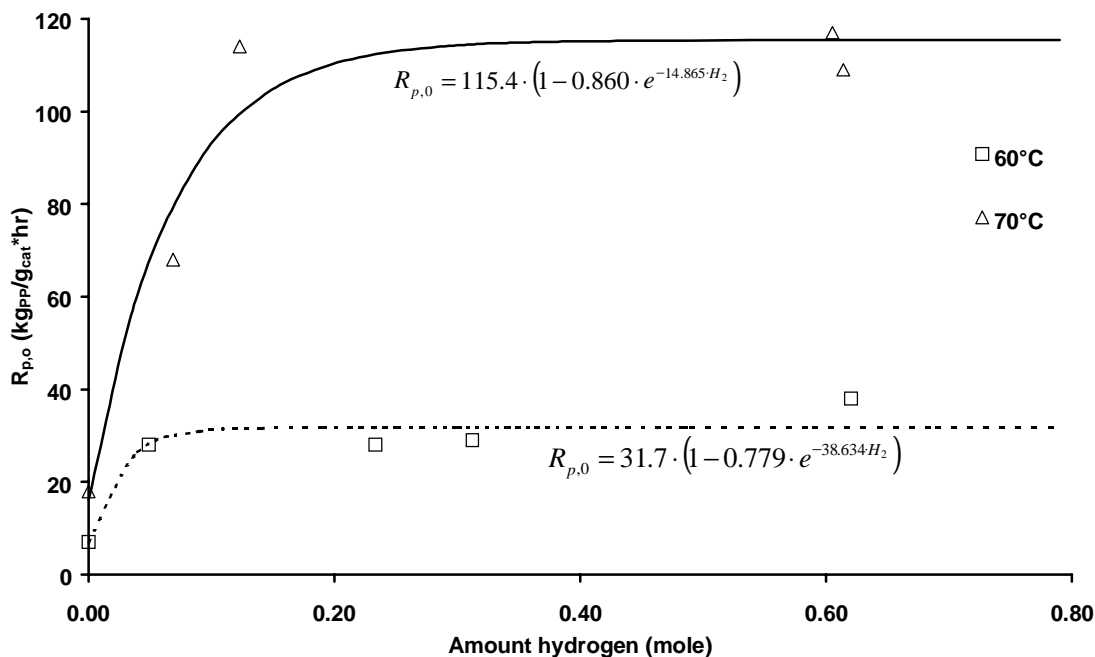


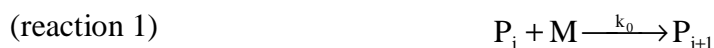
**Figure 3.8.** Influence of hydrogen concentration on the initial reaction rate at 60 and 70°C.

$$R_{p,0} = A \cdot (1 - B \cdot e^{-C \cdot H_2}) \quad (\text{kg}_{\text{PP}}/\text{g}_{\text{cat}} \cdot \text{hr}) \quad (\text{eq. 3.8})$$

The maximum reaction rates ( $A$  in eq. 3.8) for 60 and  $70^\circ\text{C}$  are 32 and 115  $\text{kg}/\text{g}_{\text{cat}} \cdot \text{hr}$  respectively. The ratio between the reaction rates without hydrogen and with enough hydrogen to reach the plateau level (so being  $(R_{p,0,\text{min}}/R_{p,0,\text{max}})$ ) differs somewhat for the both temperatures: 0.22 and 0.14 for 60 and  $70^\circ\text{C}$  respectively. Of course this result is relatively sensitive to the low reaction rates measured without hydrogen.

The general relation between the hydrogen concentration and the reaction rate is observed for all temperatures, of course at lower reaction rates for lower temperatures. This hydrogen acceleration and the ‘saturation’ -effect of the hydrogen at higher concentration are ascribed to the blocking and de-blocking of active centers by mis-inserted monomer units. After 2-1 insertion the site is temporarily not active, due to steric hindrance by the methyl group of the monomer. The hydrogen will act as chain transfer agent on these dormant sites, and free the site for further reaction. At high hydrogen concentrations, the concentration of temporarily blocked sites is very low. Because of the multi-site character of these catalysts, the sensitivity of the different sites to mis-insertions might be different. With this respect the fact that  $(R_{p,0,\text{min}}/R_{p,0,\text{max}})$  differs for 60 and  $70^\circ\text{C}$ , is interesting.

In the description of the mechanism with respect to the formation of dormant sites, the following representation is proposed:







In the first reaction a monomer unit (M) reacts with the active site that contains a polymer chain with length j (P<sub>j</sub>) to form an active site containing a polymer chain with length j+1 (P<sub>j+1</sub>). In addition to this normal propagation reaction, the second reaction represents a so-called mis-insertion where a dormant site (D) is formed. The third reaction represents the reactivation of a dormant site with hydrogen to a dead polymer (M<sub>j</sub>) and an empty active site (P<sub>0</sub>) and the fourth reaction shows reactivation of the dormant site with monomer. Of course this mechanism is not complete, but it is assumed that reactions involved with the (de-)formation of dormant sites are included. When all potential active sites are represented as C\*, the rate of polymerization can be described by:

$$R_p = k_p \cdot (C^* - D) \cdot M \quad (\text{eq. 3.9})$$

When assuming a quasi-steady state for the concentration of dormant sites, the following expression for that concentration can be derived:

$$\frac{d[D]}{dt} = 0 = k_1 \cdot P \cdot M - k_2 \cdot D \cdot H_2 - k_3 \cdot D \cdot M \quad (\text{eq. 3.10})$$

$$D = \frac{k_1 \cdot P \cdot M}{k_2 \cdot H_2 + k_3 \cdot M} \quad (\text{eq.3.11})$$

Combining 3.11 with P=(C\* -D), gives the following expression for the dormant sites:

$$D = \frac{C^*}{1 + \frac{k_1}{k_3}} \quad (\text{eq. 3.12})$$

For the maximum reaction rate (at high hydrogen concentration) and minimum reaction rate (in absence of hydrogen) equations 3.9 and 3.12 can be combined giving the expression for the ratio between these two extreme cases:

$$\frac{R_{p,\min}}{R_{p,\max}} = \frac{k_1/k_3}{1 + k_1/k_3} = \frac{K}{1 + K} \quad (\text{eq. 3.13})$$

with  $K=k_1/k_3$ . The factor K is a measure of the sensitivity of the system to the hydrogen concentration, depending on the reaction rate constant of the dormant site

forming and dormant site removing reactions. These kinetic expressions can be related to the empirical description mentioned earlier in equation 3.8. For 60 and 70°C we come to values of 0.163 and 0.282 respectively for K, which results in a temperature dependency of the hydrogen sensitivity of the presently used catalyst of  $E_{act}=52$  kJ/mole, when expressed as an Arrhenius type of temperature dependency.

The deactivation behavior of the catalyst at the various hydrogen concentrations is shown in Figure 3.9. As said, the deactivation shows to be stronger at higher hydrogen concentrations. As the profile of deactivation constant versus hydrogen concentration is the same as that of the initial reaction rate it is possible also to describe  $k_d$  analogously to equation 3.8, as is shown with the solid and dotted line for 70 and 60°C respectively in Figure 3.9.

In fact, it is interesting to see that  $k_d$  and  $R_{p,0}$  seem to be so closely related to each other. This relation is further discussed for all presented experiments below, but from this hydrogen dependency one could conclude that dormant sites are not sensitive (or less sensitive) to deactivation than the waked sites. Depending on the process leading to deactivation, this could very well be the case. Below we will discuss this matter further.

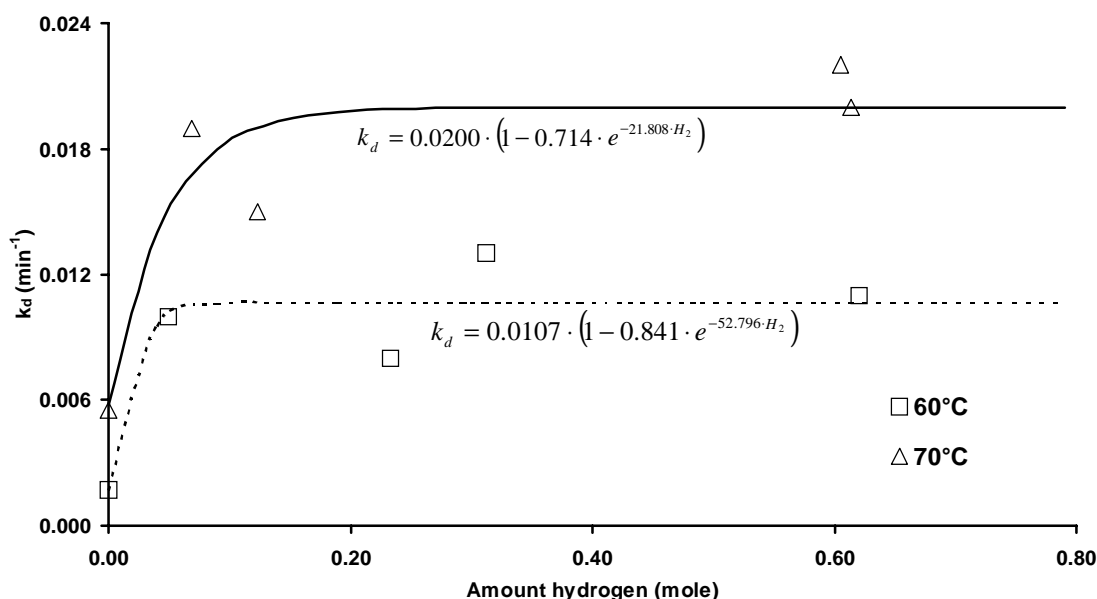


**Figure 3.9.** Influence of hydrogen on the deactivation behavior of the catalyst system at 60 and 70°C.

### 3.3.5 The effect of monomer concentration

In a series of experiments, the concentration of the monomer was reduced by the addition of a varied amount of hexane. To keep the liquid volume constant, the amount of propylene was reduced and the amount of hexane was increased. In this way,  $C_m$  was reduced from 500 g/L in pure propylene to below 100 g/L (dilute slurry polymerization). The initial reaction rates are plotted in Figure 3.10. It can be seen that reaction rate decreases with decreasing monomer concentration, but the decrease is obvious not linear as implied by equation 3.1a, with the assumption of first order dependence. The initial reaction rate remains almost constant as we begin to lower monomer concentration, then drops more and more rapidly as the monomer concentration falls below 180 g/L. One explanation for this behavior could be a reaction rate that is not first order in monomer concentration, at elevated monomer concentrations. If a saturation effect intervenes in the propagation step (that is proved to be of first order at lower  $C_m$  values), it could explain an order in monomer concentration far below one.

But when assuming this first order dependency, other reasons for this behavior can be proposed. An option is the existence of a difference between the monomer concentrations at the active site and the one in the bulk. A few aspects of the addition of hexane are playing a role here.

Hexane is transported with the monomer into the particle, during reaction. The hexane molecule is relatively large and can therefore be hindered in diffusing out of the particle against the flow of the incoming monomer. (Simple diffusion calculations show that at reaction rates between 50 and 70  $\text{kg}_{\text{PP}}/\text{g}_{\text{cat}} \cdot \text{hr}$  hexane will barely be able to

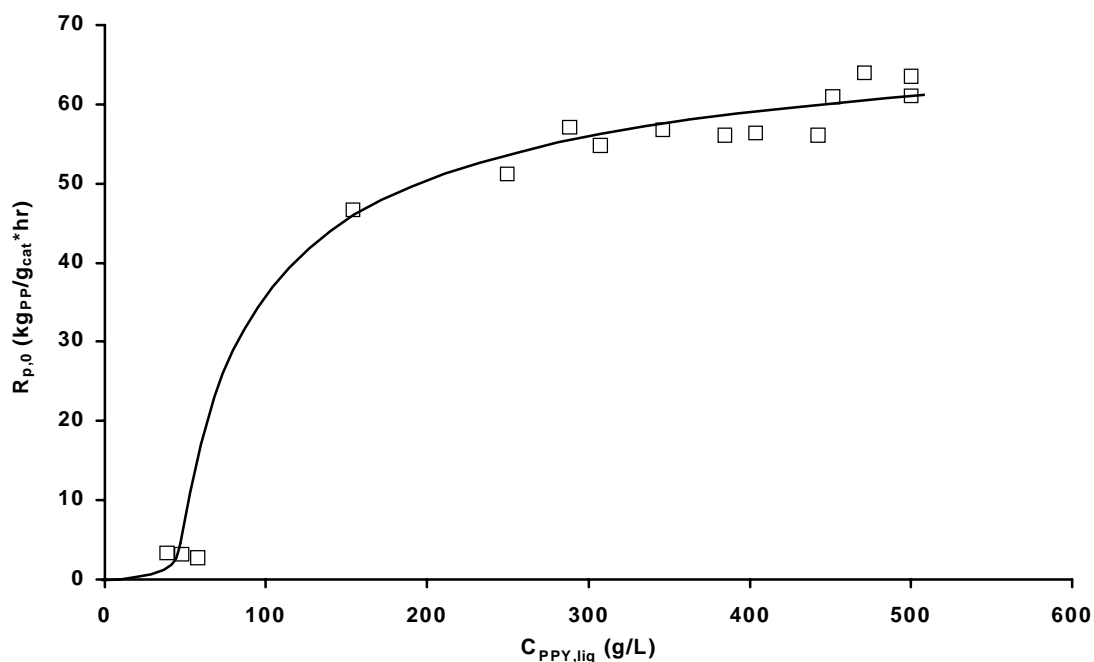


**Figure 3.10** Influence of monomer concentration in the liquid bulk on the initial reaction rate.

diffuse against the convective flow). As the hexane is inert to the polymerization reaction this can lead to enrichment of the hexane in the particle with respect to the bulk hexane concentration. Similar cases for gas phase polymerization and possible resulting enrichment of inert and low-reactive gases like nitrogen, propane and hydrogen (only at high reaction rates) have been discussed in literature before.

Next to the changing monomer concentration, the properties of the polymer are also changing. The hexane will dissolve in the polymer and the swollen polymer possibly has different properties (for example better monomer diffusivity, lowered rate of crystallization) than the non-swollen polymer.

Also because of the fact that there is essentially no information available on hexane concentration in the polymer and its influence on in-situ crystallization behavior of the polymer, it is difficult to conclude on the reasons for the influence of the monomer concentration. Besides, it is an open question whether or not the macroscopic equilibrium data for the multi-component system can be applied to a microscopic area around the active sites that differs so significantly from its surrounding bulk. The results shown in Figure 3.10 clearly show that a direct comparison between polymerization reactions at different process conditions, is a complicated matter and numerous aspects are influencing the relation between polymerization rate and monomer concentration.

### *3.3.6 Relation between initial reaction rate and deactivation constant*

In the simple kinetic model used here, the deactivation is expressed as a first order process in the concentration of active sites. This means that deactivation is assumed to be independent of the propagation rate constant. The values for  $k_d$  are plotted in Figure 3.11 as a function of  $R_{p,0}$  for all experiments performed until this point. In this figure the variation in reaction rate (plotted on the x-axis) was reached by changes in temperature, in hydrogen and monomer and in prepolymerization method. It is remarkable that the series that differ so significantly in process conditions, show all the same correlation between initial reaction rate and deactivation constant. This would suggest that the deactivation of the catalyst should be described as a function of the propagation rate, rather than of active site concentration. We already described the consequences for the kinetic model before<sup>[30]</sup>, and are currently working on a more detailed explanation.

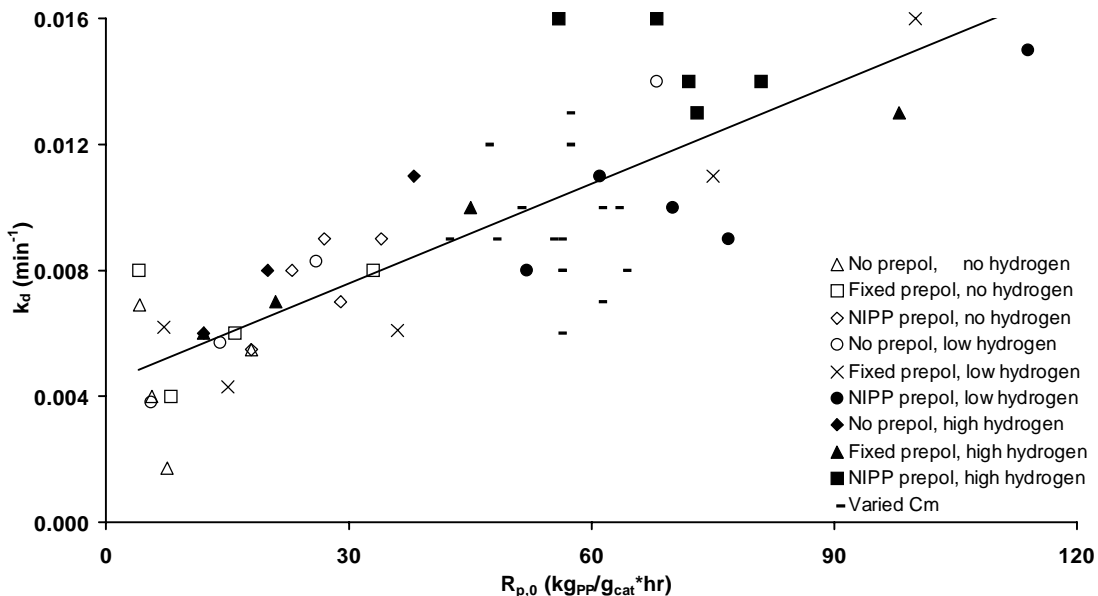


**Figure 3.11** Relation between the deactivation behavior of the catalyst and the initial reaction rate, at a wide variety of hydrogen and monomer concentrations, prepolymerization methods and polymerization temperatures.

### 3.3.7 Molecular weight distribution

It is well known that the magnesium chloride supported ZN-catalysts show multi-site behavior. The reasons for the different kinetics of the various sites are multiple and not well identified. The different origins of various physical locations on the support material and possible divergent circumstances for the components during preparation will lead to a spread in the type of the active sites. In nature, a lot of these types of processes show a normal distribution in the properties. Here, we described the molecular weight distribution (MWD) of the produced polymer, by assuming that the large number of active sites show a normal distribution in the chain termination probability  $q$ .

In the calculations, we use the well-accepted assumption that every site is producing polymer with an instantaneous MWD that is described by a Schultz-Flory distribution:

$$y_j^d = j \cdot q^2 \cdot e^{-jq} \quad (-) \quad (\text{eg. 3.16})$$

where  $y_j^d$  represents the MWD of chains with length  $j$ , depending on only one parameter being the chain termination probability  $q$ . Here, we assume the number of active sites in the catalyst having a specific  $q$ -value to be distributed normally. When the propagation rate constants  $k_p$  of the different sites are the same, the overall molecular weight distribution of the polymer product, can be calculated for specific values of the average  $q$ -value and the broadness of the distribution indicated with its standard deviation.

A few of the powders produced in experiments shown before were analyzed by using GPC. By fitting the calculated GPC curve with the measured distribution by minimizing the sum of the square of the differences between calculated and measured

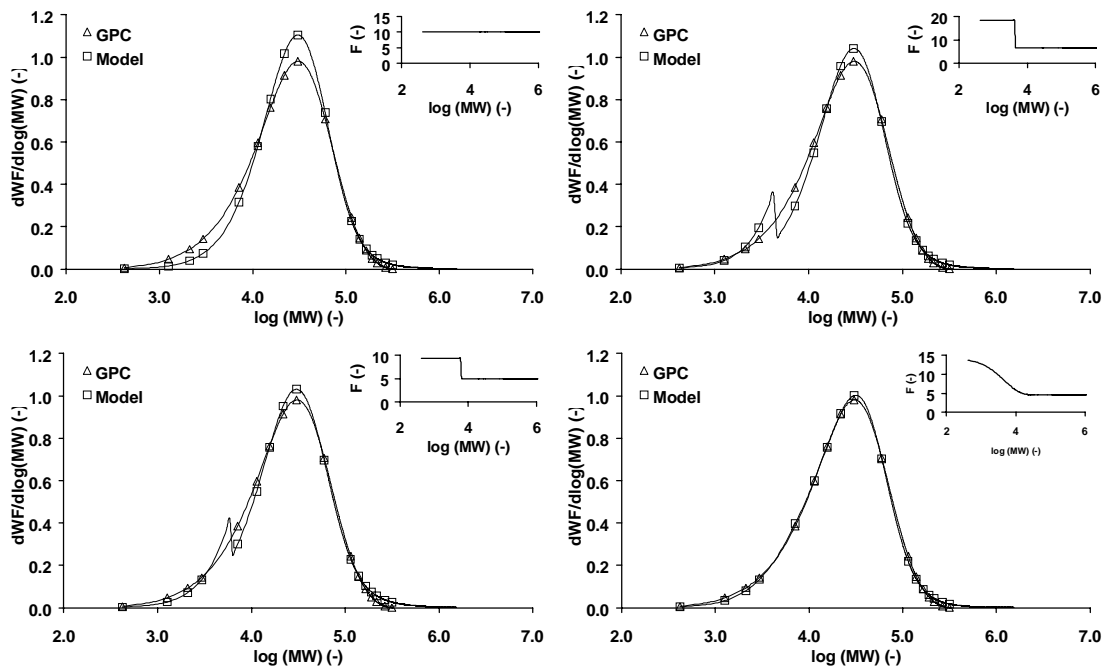


**Figure 3.12** Fitting of experimental GPC curve with a modeled MWD, based on a normal distributed chain termination probability. A. All sites have equal propagation rate B. Two levels for propagation rate defined C. Three levels for propagation rate defined D. Propagation rate described as continues function of chain length.

values, the distribution is reduced to the two parameters: the average  $q$  and  $\sigma^2$ . Figure 3.12a shows the result of such a fit.

It can be seen that the fit is reasonably good, but it shows a deviation at the low-molecular weight side. When one assumes that this deviation is not caused by the deviation from the normal distribution for the different sites, but by differences in the propagation rate constant of the different sites, we can think of a formalized approach of this low molecular weight side deviation. Of course it should be kept in mind that introduction of new fit-parameters will probably improve the fitting possibilities, but will reduce the predictive power of the model.

- We can implement different levels of the propagation constant. Because of the low average chain length at the active site that produces a low molecular weight, one could imagine this site shows a higher  $k_p$  value than the site that produces a high MW. Figure 3.12b shows a fit carried out with introduction of a stepped  $k_p$ -value, the plot in the upper right corner shows the factor that is applied to the propagation rate constant. Figure 3.12c shows the same fit, with the introduction of an extra step in  $k_p$ . In the fitting procedure, first the average  $q$ -value in the normal distributed was determined, then the  $k_p$ -correction was fit without changing the average value of the N-distribution. It can be seen that in both cases a large jump in the distribution exists on the low MW side and further optimization does not lead to reduction of this jump. The two-step system converges during fitting to a single step variation in  $k_p$ .

- Because we showed that the step-approach is not satisfactory, a continuously changing rate constant was introduced. The correction factor for the propagation rate was defined as a function of the average chain length produced by that specific site. Here, we used a function of the structure:

$$F = A \cdot (1 + e^{-x \cdot B}) \quad (-) \quad (\text{eq. 3.17})$$

with  $x$  being an indication for the average chain length produced by the site and the  $F$  a scaling factor on the propagation rate of the site producing polymer with chain length  $x$ . The result of this fit is shown in Figure 3.12d. Now, the results are much better, with this changing effect the measured GPC curve can be well fitted with the model equations.

So, the best result is obtained here with the continuous function from equation 3.17. With this simple fitting method it seems to be possible to describe a full molecular weight distribution, without the use of a large number of parameters. Of course, it is important to be able to correlate the fit parameters to process conditions. The model shown in Figure 3.12d was used to fit two different GPC curves, of two different experiments in presence and in absence of hydrogen. The results of this fitting are shown in Table 3.7. It is clear that the hydrogen, as expected, significantly influences the average chain termination probability. The width of the molecular weight distribution also seems to be increased as the hydrogen concentration increases. We can also see that the first model parameter  $A$  remains constant, but that the necessary correction on the propagation rate constant to obtain a satisfying fit, expressed by the parameter  $B$ , is also different for the two tests.

It is clear that we need to carry out more GPC measurements on the powders that we produced in the different polymerization tests to be able to fully correlate the process conditions like temperature, monomer and hydrogen concentration and maybe even prepolymerization conditions to the resulting MWD and parameters describing the MWD.

**Table 3.7.** Indicative result of the fitting between the measured MWD and the calculated MWD by means of the  $N$ -distributed  $q$ -value, for two different hydrogen concentrations.

Experiment		Fitting results			
Exp	$X_{H_2}$	$N_{average}$	$N_{sigma^2}$	A	B
1	0.0000	0.2155	0.2612	11.0	0.00127
2	0.0101	1.5512	0.6727	10.8	0.00707

### 3.4 Conclusions

The kinetics of a liquid pool polymerization of propylene using a 4<sup>th</sup> generation Ziegler-Natta catalyst were studied under conditions similar to those used in industry. In particular the influence of changing temperature, hydrogen and monomer concentration and the method for prepolymerization were investigated. The observed activation energies of the polymerization experiments were strongly dependent on the method used for calculation of the monomer concentration at the active site, as each of these methods uses its own temperature dependency. In all cases, the observed activation energies are relatively high, and polymerization rates seem not to be limited by the intra-particle monomer mass transfer.

With the catalyst used here, at high initial reaction rates, a prepolymerization is needed to ensure prevention of thermal runaway on particle scale, for the largest catalyst particles. Even a short prepolymerization step seems to be sufficient to overcome this problem.

When the monomer concentration was varied by the addition of hexane to the liquid propylene, the initial reaction rates remain fairly constant at a high level for a broad propylene concentration range, and rapidly falls at lower concentrations. As an explanation for this effect the differences in monomer concentration between bulk and active site are mentioned.

The hydrogen concentration was varied over a wide range at 60 and 70°C. For both temperatures it was shown that reaction rates increased rapidly with increasing hydrogen concentration at the low hydrogen concentrations. At higher hydrogen amounts, this effect disappeared and a maximum reaction rate was found.

A normally distributed chain termination probability was assumed for the multi-site catalyst to model the measured molecular weight distribution of a few polymer samples. With this method it is possible to describe the GPC curves, but the description is significantly improved by introduction of a propagation rate constant that depends on the chain length produced by the specific sites.

Acknowledgements - The work presented in this paper was carried out in co-operation with The Dow Chemical Company, Freeport (TX), USA. The authors wish to thank Dow for both the financial and the intellectual input. The aluminum alkyls used in the work were kindly donated by AkzoNobel, Deventer, The Netherlands.

The work could not have been completed without the experimental work carried out by Eelko Bos, Marlies Koppels, Tom Cellissen and Roxane van Arneman. The importance of their contribution is highly acknowledged. In addition, the technical assistance of Gert Banis, Fred ter Borg, Karst van Bree and Geert Monnik is highly appreciated.



## Notations

A	surface area	(m <sup>2</sup> )
C*	concentration of active sites	(mole/g)
C <sub>m</sub>	concentration of monomer	(kg/m <sup>3</sup> )
D	concentration of dormant sites	(mole/g)
D <sub>r</sub>	internal reactor diameter	(m)
E <sub>act</sub>	activation energy	(kJ/mole)
h	heat transfer coefficient	(W/m <sup>2</sup> · K)
k	reaction rate constant	
k <sub>d</sub>	deactivation constant	(min <sup>-1</sup> )
k <sub>p</sub>	propagation rate constant	(m <sup>3</sup> /mole· hr)
M	molar mass	(g/mole)
P	pressure	(bar)
q	chain termination probability	(-)
Q	transferred heat	(J)
R <sub>p</sub>	rate of polymerization	(kg/g· hr)
t	time	(s)
T	temperature	(K)
U	heat transfer coefficient	(W/m <sup>2</sup> · K)
X	mole fraction in liquid phase	(-)
Y	mole fraction in gas phase	(-)
y <sub>j</sub> <sup>d</sup>	differential molecular weight distribution	(-)
<i>Greek</i>		
σ <sup>2</sup>	standard deviation	(-)
φ	monomer volume fraction	(-)
χ	Flory-Huggins interaction parameter	(-)
λ	thermal conductivity	(W/m· K)

## Subscripts

0	initial condition	max	maximum
cat	catalyst	min	minimum
H <sub>2</sub>	hydrogen	PP	polypropylene
inj	injection	PPY	propylene
m	monomer	req	required

## List of abbreviations

ABS	Acrylonitrile-Butadiene-Styrene	PO	polyolefins
D-donor	dicyclopentyl dimethoxy silane	PVC	polyvinyl chloride
GPC	Gel Permeation Chromatography	TEA	triethylaluminum
MW	molecular weight	YOP	yield of prepolymerization
MWD	molecular weight distribution	ZN	Ziegler-Natta
NIPP	non-isothermal prepolymerization		

## References

- [1] Moore, E.P. (1996). 'Polypropylene Handbook – Polymerization, Characterization, Properties, Processing and Application', Hanser Publishers: Munich.
- [2] Moore, E.P. (1998). 'Rebirth of Polypropylene: Supported Catalysts', Hanser Publishers.
- [3] Potter, D.J.B., & Tattum, L. (1998). 'Polypropylene – The boom continues', *Chemical Week*, Suppl. S- Sept. 30, 4-11.
- [4] Balsam, M., Barghoorn, P., & Stebani, U. (1999). 'Trends in Applied Macromolecular Chemistry', *Die Angewandte Makromolekulare Chemie*, **267**, 1-9.
- [5] Ghosh, M.K., & Maiti, S. (1999). 'Polyolefins Technology – A Comprehensive Review', *Journal of Polymer Materials*, **16**, 113-134.
- [6] Galli, P., (1995). 'Forty Years of Industrial Developments in the Field of Isotactic Polyolefins', *Macromolecular Symposia*, **89**, 13-26.
- [7] Soares, J.B.P., & Hamielec, A.E., (1996). 'Kinetics of Propylene Polymerization with a Non-Supported Heterogeneous Ziegler-Natta Catalyst – Effect of Hydrogen on Rate of Polymerization, Stereoregularity and MWD', *Polymer*, **37**(20), 4607-4614.
- [8] Ferreira, M.L., & Damiani, D.E., (1999). 'Effect of Different Donors on Kinetics of ZN Catalysts and Molecular Weight of the Obtained Polypropylene', *Journal of Molecular Catalysis A: Chemistry*, **150**, 53-69.
- [9] Kim, I., Choi, H.K., Kim, J.H., & Woo, S.I., (1994). 'Kinetics Study of Slurry-Phase Propylene Polymerization with Highly active Mg(Oet)<sub>2</sub>/Benzoyl Chloride/TiCl<sub>4</sub> Catalyst', *Journal of Applied Polymer Science*, **52**, 1739-1750.
- [10] Han-Adebekun, G.C., & Ray, W.H., (1997). 'Polymerization of Olefins Through Heterogeneous Catalysis. XVII. Experimental study and Model Interpretation of Some Aspects of Olefin Polymerization over a TiCl<sub>4</sub>/MgCl<sub>2</sub> Catalyst', *Journal of Applied Polymer Science*, **65**, 1037-1052.
- [11] Kahraman, R., Erdogan, M., & Bilgic, T. J., (1996). 'Polymerization of Propylene using a Prepolymerized High-Active Ziegler-Natta Catalyst. I. Kinetic Studies', *Journal of Applied Polymer Science*, **60**, 333-342.

- [12] Rishina, L.A., Vizen, E.I., Sosnovskaja, L.N., & Dyachkovsky, F.S., (1994). 'Study of the Effect of Hydrogen in Propylene Polymerization with the  $MgCl_2$ -supported Ziegler-Natta Catalyst – Part I. Kinetics of Polymerization', *European Polymerization Journal*, **30**(11), 1309-1313.
- [13] Nedorezova, P.M., Galashina, N.M., Tsvetkova, V.I., Sukhova, T.A., Saratovskikh, S.L., Babkina, O.N., & Dyachkovskii, F.S., (1996). 'Isospecific Polymerization of  $\alpha$ -olefins in the Presence of Metallocene Complex Catalysts Fixed on Graphite', *European Polymerization Journal*, **32**(9), 1161-1165.
- [14] Naga, N., & Mizunuma, K., (1998). 'Stereochemical Control in Propylene Polymerization with Non-Bridged Metallocene Dichloride/MAO', *Polymer*, **39**(13), 2703-2708.
- [15] Spaleck, W., Küber, F., Bachmann, B., Fritze, C., & Winter A., (1998). 'New Bridged Zirconocenes for Olefin Polymerization: Binuclear and Hybrid Structures', *Journal of Molecular Catalysis A: Chemical*, **128**, 279-287.
- [16] Kemp, R.A., Brown, D.S., Lattmann, M., & Li, J., (1999). 'Calixarenes as a New Class of External Electron Donors in Ziegler-Natta Polypropylene Catalysts', *Journal of Molecular Catalysis A: Chemical*, **149**, 125-133.
- [17] Pater, J.T.M., Weickert, G., & Swaaij van, W.P.M., (2001). 'Polymerization of Liquid Propylene with a 4<sup>th</sup> Generation Ziegler-Natta Catalyst, Influence of Temperature, Hydrogen and Monomer Concentration and Prepolymerization Method on Powder Morphology', *submitted to Journal of Applied Polymer Science*.
- [18] Soares, J.B.P., & Hamielec, A.E., (1996). 'Effect of Hydrogen and of Catalyst Prepolymerization with Propylene on the Polymerization Kinetics of ethylene with a non-supported heterogeneous Ziegler-Natta Catalyst', *Polymer*, **37**(20), 4599-4605.
- [19] Chu, K-J., Soares, J.B.P., Penlides, A., & Ihm, S-K., (2000). 'Effect of Prepolymerization and Hydrogen Pressure on the Microstructure of Ethylene/1-hexene Copolymers made with  $MgCl_2$ -supported  $TiCl_3$  Catalysts', *European Polymerization Journal*, **36**, 3-11.
- [20] Czaja, K., & Krol, B., (1997). 'The effect of Prepolymerization of a titanium catalyst on its deactivation in propylene polymerization', *Polimery* 1997, **42**(10), 620-624.

- [21] Czaja, K., & Krol, B., (1999). 'Nature of Activating Effect of Two-Step Polymerization of Propylene', *Journal of Applied Polymer Science*, **71**, 353-359.
- [22] Czaja, K., & Krol, B., (1998). 'Two-step Polymerization of Propylene over MgCl<sub>2</sub>-supported titanium Catalyst', *Macromolecular Chemistry and Physics*, **199**, 451-455.
- [23] Hutchinson, R.A., & Ray, W.H. J., (1991). 'Polymerization of Olefins Through Heterogeneous Catalysis. IX. Experimental Study of Propylene Polymerization over a High Activity MgCl<sub>2</sub>-Supported Ti Catalyst', *Journal of Applied Polymer Science*, **43**, 1271-1285.
- [24] Pater, J.T.M., Weickert, G., & Swaaij van, W.P.M., (2001). 'Polymerization of Liquid Propylene with a 4<sup>th</sup> Generation Ziegler-Natta Catalyst, The Influence of Polymerization Temperature and Prepolymerization on Kinetics and Vapor-Liquid Equilibria of the H<sub>2</sub>-Propylene System', *submitted to AIChE Journal*.
- [25] Samson, J.J.C., Weickert, G., Heerze, A.E., & Westerterp, K.R., (1998). 'Liquid-Phase Polymerization of Propylene with a Highly Active Catalyst', *AIChE Journal*, 44(6), 1424-1437.
- [26] Barton, A.F.M., (1990). *CRC Handbook of Polymer-Liquid Interaction Parameters and Solubility Parameters*, CRC Press, Boca Raton FL, 284.
- [27] Meier, G.B., Weickert, G., & Swaaij van, W.P.M., (2001). 'Comparison of Gas- and Liquid-Phase Polymerization of Propylene with Heterogeneous Metallocene Catalyst', *Journal of Applied Polymer Science*, **81**, 1193-1206.
- [28] AIChE, & DIPPR, (1999). *Physical and Thermodynamic Properties of Pure Chemicals, Part 1*, Greyden Press, Columbus, OH.
- [29] Zacca, J.J., & Debling, J.A., (2001). 'Particle Population Overheating Phenomena in Olefin Polymerization Reactors', *Chemical Engineering Science*, **56**, 4029-4042.
- [30] Roos, P., Meier, G.B., Samson, J.J.C., Weickert, G., & Westerterp, K.R., (1997). 'Gas Phase Polymerization of Ethylene with a Silica Supported Metallocene Catalyst: Influence of Temperature on Deactivation', *Macromolecular Rapid Communications*, **18**, 319-324.

## **CHAPTER 4**

### **POLYMERIZATION OF LIQUID PROPYLENE WITH A 4<sup>TH</sup> GENERATION ZIEGLER-NATTA CATALYST**

-

### **INFLUENCE OF TEMPERATURE, HYDROGEN, MONOMER CONCENTRATION AND PRE-POLYMERIZATION METHOD ON POWDER MORPHOLOGY**

-

## Abstract

*Liquid propylene was polymerized in a 5-liter autoclave batch reactor using a commercially available  $\text{TiCl}_4 / \text{MgCl}_2 / \text{Al}(\text{Ethyl})_3 / \text{DCPDMS}$  4<sup>th</sup> generation Ziegler-Natta catalyst. The powders from these polymerizations were characterized using laser diffraction particle size analysis, scanning electron microscopy and bulk density measurements. These characteristics were analyzed as a function of the process conditions, including hydrogen and monomer concentration, polymerization temperature and the prepolymerization method.*

*It was shown that polymerization temperature influences the powder morphology to a large extent. At low polymerization temperatures, high-density particles were obtained, showing regular particle surfaces and low porosities. With increasing polymerization temperature, the morphology was gradually transformed into a more open structure, with irregular surfaces and poor replication of the shape of the catalyst particle.*

*When using a prepolymerization step for 10 minutes at a relatively low temperature the morphology obtained was determined by this prepolymerization step and was independent from conditions in the main polymerization. The morphology obtained was the same as that observed after a full polymerization at low temperature. Even when using a short polymerization at an increasing temperature, the morphology was strongly influenced by the initial conditions.*

*The effect of variation in hydrogen concentration supported the conclusion that the initial polymerization rate determines the powder morphology. In the absence of hydrogen, high bulk densities and regularly shaped particles were obtained, even at high temperatures and without prepolymerization. With increasing hydrogen concentration, the reaction rates increased rapidly, and with that the morphology also changed.*

*This chapter has been submitted for publication:*

*J.T.M. Pater, G. Weickert, W.P.M. van Swaaij, 'Polymerization of Liquid Propylene with a 4<sup>th</sup> Generation ZN-catalyst – Influence of Temperature, Hydrogen, Monomer Concentration and Pre-polymerization Method on Powder Morphology', Journal of Applied Polymer Science, (2001).*

## 4.1 Introduction

Since the first successful attempts to produce isotactic polypropylene in the laboratories of Natta, a number of new catalyst systems have been developed. When naming the  $\text{TiCl}_3/\text{AlEt}_2\text{Cl}$  catalyst a 'first generation', four more generations of Ziegler-Natta catalysts have been developed until today, and development is still going on. Parallel to this continuous evolution of the ZN catalyst, the metallocenes – sometimes called the sixth generation catalyst – have been developed and implemented in industrial processes. But despite some clear advantages of these new metal-organic components, and in contrast with almost all predictions made in the last two decades on the future of metallocenes, the vast majority of the world's polypropylene production is based on ZN catalysis, typically the third and fourth generation catalysts. Two important reasons for this are the relatively high costs of metallocenes due high amounts of methyl aluminumoxanes required, and the leaching problems with metallocenes.

These new designs of the conventional catalyst systems are used in all the different industrial processes for polypropylene. Because of the fact that the modern processes typically involve a cascade of polymerization reactors, varying from the bulk – gas phase combination in Basell's Spheripol to the series of gas phase compartments in BP's PP-Innovene (formerly known as Amoco process), the powder morphology of the polymer product is of great importance. First, the particle shape determines its hydrodynamic behavior in the reactors, especially in the fluidized bed gas phase systems. Secondly, the distribution of the rubbery components in the production of high impact polypropylene in the i-PP matrix is, to a large extent, determined by the morphology of catalyst and polymer powders. Finally, the absence of fines prevents reactor fouling and the absence of coarse particles eliminates undesirable fluidization and agglomeration effects.

Of course, an optimal polymer particle morphology is one of the important goals in catalyst development. In addition, influencing and controlling the development of powder morphology is also an issue in the polymerization process itself, as process conditions in the industrial scale plants determine reaction rates in the initial stage of the life of the particle, and also for example physical stress on the particle due to stirrer-action can change this morphology.

Control of particle morphology is based on the fact that the polymer tends to replicate the shape of the catalyst particle on which it is produced. To be able to understand the process of shape replication, one should understand the growth mechanism of the particle. It is well accepted that growth of the particle shows the following characteristics, in Ziegler-Natta catalyzed olefin polymerizations:

- In the initial stage of the polymerization, the catalyst particle breaks up into a large number of smaller catalyst fragments. During the polymerization the size of these fragments is decreases due to further fragmentation.

- The entangled polymer produced keeps the different fragments together and forms the continuous phase in the growing particle very soon after the start of fragmentation<sup>[1]</sup>.
- After full fragmentation, the small fragments are well distributed over the growing particle. Polymer production occurs on all the catalyst fragments.

With these characteristics, particle growth is believed to show replication of the shape of the catalyst particle. However, it is shown<sup>[2-5]</sup> that there are some requirements with respect to catalyst structure and reaction conditions to show uniform catalyst fragmentation. The catalyst needs to be highly porous to allow monomer to flow into the center of the particle, and to ensure a large number of possible crack positions. The catalyst structure must have a mechanical strength high enough to withstand handling, but low enough to break in polymerization conditions. Of course, active sites should be well distributed over the catalyst to ensure an even distribution of polymer production over the catalyst<sup>[6]</sup>. Furthermore, assuming one wants a homogeneous polymer everywhere inside the particle produced, then polymerization conditions should be chosen in such a way that mass transfer limitations are not likely to occur, to ensure even polymerization across the particle. This is well demonstrated in the 'Reactor Granule Technology' of Himont/Montecatini where the spherical polymer granule is formed with high porosity to allow copolymerization for polyolefin alloys<sup>[7]</sup>.

The growth model of these particles has been modeled by a large number of scientists over the past years, where the Multi Grain Model (MGM) is the most well known<sup>[8-12]</sup>. It should be realized that in the MGM model, fragmentation is assumed to be complete at time zero and catalyst fragments are assumed to be equal in size. The group of Chiovetta has worked intensively in the early 90's on implementation of the fragmentation step in single particle models. Their aim was to demonstrate its effect on the transfer of heat and mass to and from the particle<sup>[13-17]</sup>, rather than describing its effect on morphology development.

Until now it has not been possible to develop models that are able to describe and predict particle morphology as a function of reaction conditions and recipe. The reason for this is that the fragmentation of the catalyst is a very complex process, depending on a large number of variables like local initial polymerization rates and crystallization of the polymer product. We think that in order to be able to develop such models, one needs full understanding of the different processes that play a role in the development of the internal and external shape of the particle. This is possible with the combination of model development with experimental data of real polymerizations. In the recent past some groups attempted to clarify the particle growth mechanisms, for example Noristi et al.<sup>[18]</sup>, Kakugo et al.<sup>[19-20]</sup>, and Ferrero<sup>[21]</sup>. These studies are hard to generalize, as the behavior of the system will also depend on the type of the catalyst used and the type of polymer formed. For example, Han-



Adebekun et al. studied the effect of reaction conditions on polymer particle morphology, and showed that the influence of temperature and comonomer composition on particle morphology were sintering effects due to polymer melting<sup>[22-23]</sup>. Only by systematically varying reaction conditions and recipes, in boundaries far wider than the industrial relevant operation window and by analyzing the powders yielding from these tests, can the basic mechanisms creating particle morphology be revealed.

In this work we will study powders from the polymerization of liquid propylene using a highly active Ziegler-Natta catalyst. The relations between process conditions like polymerization temperature, the application of a pre-polymerization step, the monomer concentration, the hydrogen concentration and the morphology of the produced powder will be discussed.

## 4.2 Experimental

### 4.2.1 Chemicals

#### Catalyst system

The catalyst system used here was a commercially available Ziegler-Natta catalyst of the fourth generation as defined by Moore<sup>[24]</sup>, with TiCl<sub>4</sub> on a MgCl<sub>2</sub> support. Triethyl aluminum was used as a cocatalyst and the so-called D-donor (di-cyclopentyl dimethoxy silane) was used as external electron donor for regulation of the stereospecificity. Figure 2.1 shows electron microscopy pictures of the highly porous catalyst material. In these pictures it can be seen that the catalyst particles are built from 20 to 30 spherical shaped sub-particles. The particle size distribution of the catalyst is shown in Figure 2.2., it shows an average particle size of 24.4 micron. The titanium concentration at the catalyst was 1.54 wt% .

In all polymerization tests, the Al/Ti and Al/Si ratios were kept constant at values of 735 and 45 respectively and typically 10 mg of catalyst was used.

#### Monomer, hydrogen, nitrogen and hexane

The propylene used in the experiments was of so-called 'polymer grade' and obtained from Indugas, with a purity >99.5%, with propane as main impurity. The hydrogen and nitrogen used were of >99.999% purity. Table 2.1 shows the different chemicals used, their origin, the purity and the finishing purification steps. The hexane added to the system was of 'Pro Analysi' quality obtained with Merck.

The hydrogen, nitrogen and hexane were extra purified by leading them over a reduced BTS copper catalyst and subsequent passing through three different beds of molecular sieves, with pore sizes of 13, 4 and 3 angstrom respectively. The BTS catalyst was obtained from BASF. The propylene was purified in the same way, after it was led through a bed of oxidized BTS copper catalyst to remove carbon monoxide.

### 4.2.2 Polymerization methods

The procedure and hardware used in the polymerization experiments presented here, was described by us recently<sup>[25-26]</sup> in more detail. Reactions were carried out in a 5-

liter stainless steel *Büchi BEP 280* reactor with a 6-blade impeller type stirrer at 2000 rpm. Cooling water in the jacket was used to maintain isothermal conditions during the experiment. The reactor set-up is schematically shown in Figure 2.3.

#### Catalyst preparation

The catalyst was prepared in a *Braun 150 B-G-II glove box* under a nitrogen atmosphere. The oil suspended catalyst was weighed in a vial and diluted with some hexane. In another vial the desired amounts of TEA and D-donor were precontacted at room temperature, diluted in hexane. The catalyst was not activated before injection to the polymerization reactor.

#### Reactor preparation

To purify the reactor, it was flushed with nitrogen before every polymerization experiment, at a reactor wall temperature of about 95°C. The reactor was subsequently evacuated for about 5 minutes. This procedure was repeated at least 5 times. After this flushing procedure, the reactor was tested for leakage with hydrogen at 20 bar. Then the reactor was evacuated and flushed a few times with gaseous propylene to wash out the hydrogen. Then the desired amounts of hydrogen and propylene were fed to the system, typically being 31.6 mole of propylene.

#### Polymerization procedure

After the system had reached the desired initial temperature, the TEA/donor/hexane mixture was injected to the reactor. The vial was washed with fresh hexane two times to ensure that all cocatalyst and donor was introduced. Subsequently, about 1 minute after the first injection, the catalyst was injected into the liquid propylene. This vial was also washed twice. Injection of the catalyst started the polymerization reaction. After the prescribed polymerization time, typically being 75 minutes, the reaction was stopped by opening the vent valve, allowing the not reacted monomer to evaporate quickly. After flashing and flushing with nitrogen several times the reactor was opened and the product was dried overnight in a vacuum oven at 80°C.

#### Pre-polymerization method

Three different types of experimental procedures with respect to the pre-polymerization step are distinguished. In the first case no pre-polymerization is used at all. The reactor is prepared at the main polymerization temperature and the content of the two vials is injected at this temperature.

In the second case a fixed pre-polymerization during 10 minutes at 40°C was used. Here the reactor was prepared at pre-polymerization temperature, the components were injected and after 10 minutes the reactor temperature was raised to the main polymerization temperature as quickly as possible. Typically this takes about 3 minutes.

In the last case, a so-called non-isothermal pre-polymerization (NIPP) was used. Here the reactor was prepared at 20°C. The TEA/donor was injected and after injection the

reactor temperature was raised to 70°C. During heating, the catalyst was injected at a predefined temperature, resulting in a short pre-polymerization step at a varying temperature (increasing from injection temperature to main polymerization temperature).

In this paper we will refer to these three pre-polymerization methods by the terms 'none', 'fixed' and 'NIPP' respectively. In the NIPP-case, it comes with the used injection temperature, or  $T_{inj}$ .

#### *4.2.3 Powder characterization*

##### Bulk density

The bulk density was determined using a standardized method of weighing a known loosely packed polypropylene powder. The test method is according to the Japanese Industrial Standard (JIS) K6721. The set-up consists of a supported funnel, placed above a receiver. An amount of about 120 ml powder is pored through the funnel into the receiver. This receiver is a cylinder with a precisely known volume of about 100 ml. Excess of powder is carefully removed and the filled cylinder is weighed. The bulk density is indicated in gram polymer per liter volume.

##### Particle size analysis

The particle size distribution of the polymer was measured by laser diffraction. About 5 grams of polymer was analyzed by a *SympaTec HELOS Laser Diffraction* in combination with a *Rodos T4* powder disperser. *Windox* software calculated the complete particle size distribution using the Fraunhofer High Reliability Laser Diffraction calculation and provided values for  $x_{50}$ ,  $x_{10}$  and  $x_{90}$  as well as mean particle size values.

##### Surfacial SEM pictures

Scanning Electron Microscopy (SEM) was used to visualize details on the surface of the produced polymer particles. The PP powders were mounted on aluminum stubs via double-sided conductive carbon tape and sputter coated with gold to make them conductive. Secondary electron images were taken at represented regions of the specimens via a *Philips 505 SEM* operating at a working distance of 12 mm. The magnifications and accelerating voltage used in the imaging are shown in the pictures.

##### Cross sectional SEM pictures

Some powders produced in slurry pre-polymerization were analyzed using SEM imaging on a cross sectional area after cutting of particles. These investigations were done using a Philips environmental scanning electron microscope XL-30 ESEM FEG (Philips, Eindhoven, The Netherlands) equipped with energy dispersive x-ray spectrometer (EDX) for local and area distribution analyses of elements. Secondary electron imaging of the sample surfaces was performed in high vacuum mode using acceleration voltages of 1 kV, whereas qualitative EDX analysis was carried out in wet-mode at accelerating voltages of 5 kV, 10 kV and 20 kV, respectively. In both

cases no additional coating of the sample surface was done because charging is not an issue for the chosen imaging conditions. For an acceleration voltage of 1 kV, the penetration of the incident electron beam is on the order of a few tens nanometers for the investigated materials. Therefore, in addition to standard high acceleration voltage scanning electron microscopy, SE images acquired at 1 kV acceleration voltage show surface features in more detail, even at high magnification, whereas the wet mode renders EDX analysis without coating of non- conductive samples unnecessary. To obtain cross sectional pictures of the polymer particles, the samples were embedded in epoxy resin and fractured at room temperature.

### 4.3 Results and Discussion

#### 4.3.1 Influence of polymerization temperature

A number of polymerization tests were carried out at various temperatures. The recipes and procedures used are shown in Table 4.1. Temperatures were varied from 40 to 80°C and the catalyst used was not pre-activated. This means that, directly after

**Table 4.1** Typical recipes used in the polymerization tests in this work. Typically 10 mg of catalyst was used. Al/Ti=735 , Al/Si=45.

Experiment type	Hydrogen	Prepolymerization		Main polymerization	
	Amount (mole)	T <sub>prepol</sub> (°C)	Duration (min)	T <sub>main</sub> (°C)	Duration (min)
No prepol	var: 0-0.069-0.21-0.66	-	-	40-50-60-70-80	75
Fixed prepol	var: 0-0.069-0.21-0.66	40	10	40-50-60-70-80	75
NIPP prepol	var: 0-0.069-0.21-0.66	40-50-60	short	70	75

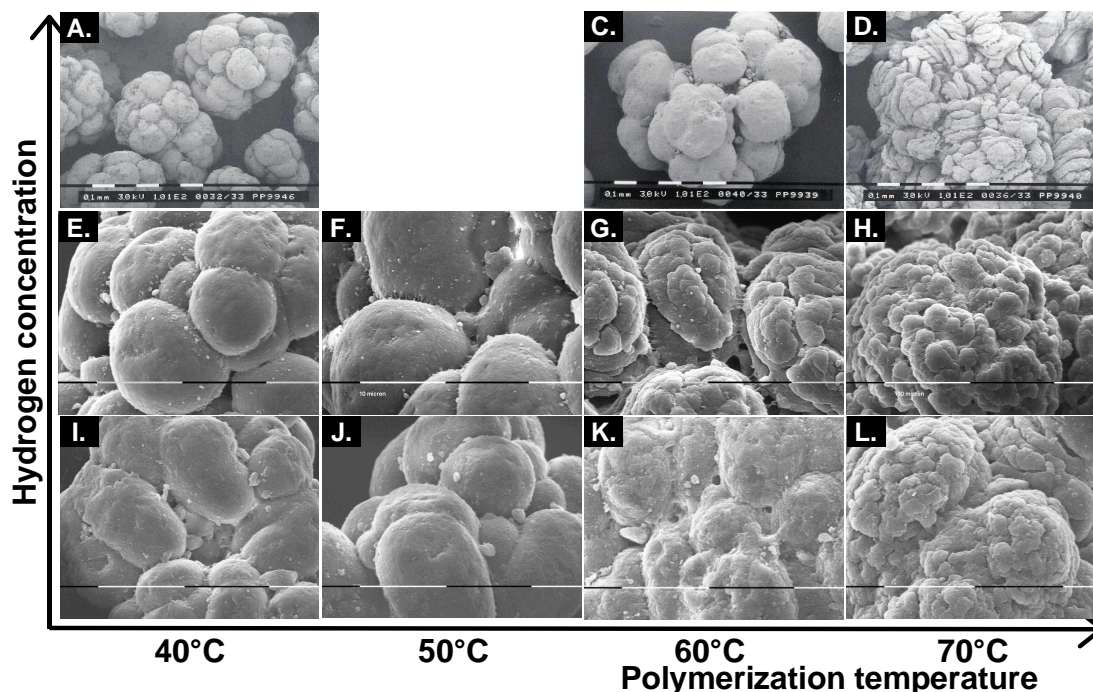


**Figure 4.1** SEM pictures of powders produced without a pre-polymerization step, at different polymerization temperatures and different hydrogen concentrations. (white bar indicates 100 microns, in F. it indicates 10 microns).

injection of the catalyst into the liquid monomer, the dissolved donor-alkyl complex in the reactor activates the catalyst under polymerization conditions. Figures 4.1e to 4.1h show SEM pictures of polymer samples produced at 4 different polymerization temperatures (40, 50, 60 and 70°C) in the presence of hydrogen.

It is immediately clear that the morphology of the particle has a strong relation to the temperature of the polymerization. The particle shapes follow a clear trend from dense, low porosity particles with smooth surface structures, towards the open, irregular shaped particles with low densities produced at high temperatures. The powder morphology shows a continuous gradual change of structure. This is also supported by porosity and bulk density measurements. The series indicated with a square shaped marker in Figure 4.2 shows these values for the powders in Figure 4.1e to 4.1h (produced at 40, 50, 60 and 70°C, with 0.21 mole hydrogen). With increasing polymerization temperature, bulk densities of the produced powders are rapidly decreasing from the maximum value of about 450 g/liter, to the lowest values around 350 g/liter. Theoretically the maximum bulk density of spherical polymer particles of identical size, with a crystallinity of about 60% would be 500 g/l, but these values are often not reached, as the particles are not perfectly spherical.

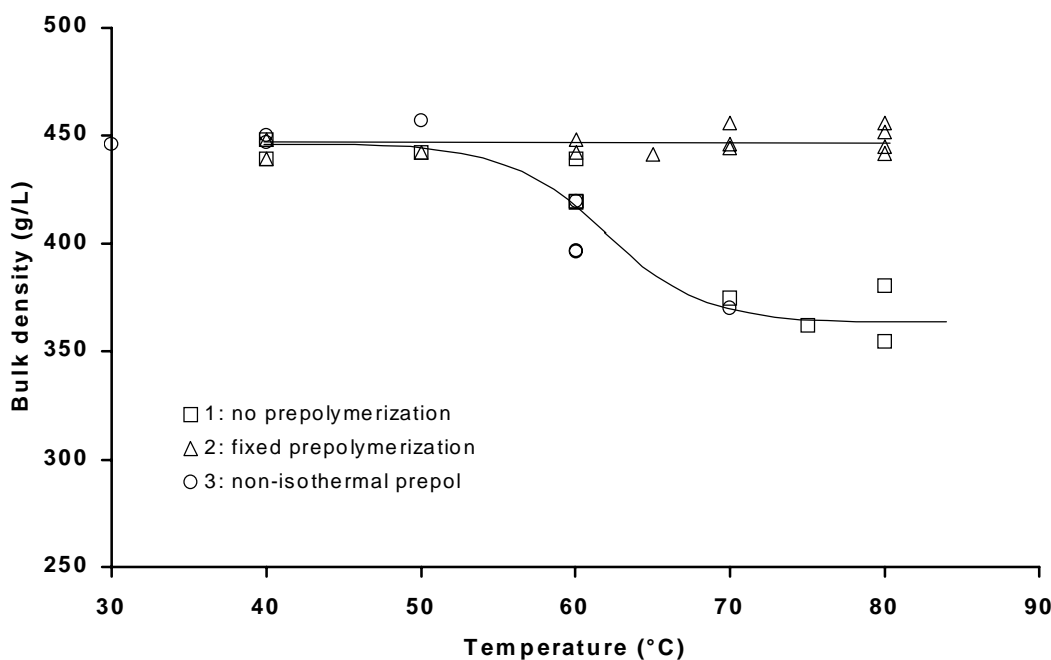


**Figure 4.2** Bulk density as a function of polymerization temperature for series of experiments without, with a fixed and with a non-isothermal pre-polymerization step. In case of NIPP the temperature at the x-axis corresponds to  $T_{inj}$

There are different explanations for the influence of polymerization temperature:

- Local boiling. The change in temperature causes a change in reaction rate in the particle. At higher polymerization rates it is possible that the particle overheats due to insufficient heat transfer. This overheating can lead to the sudden formation

of a gas bubble. The force of the gas expansion can cause the surface to form a more open structure.

- Rate of fragmentation. A higher temperature causes a higher reaction rate in the particle. As fragmentation of the support material is caused by a build-up of internal pressure of polymer on the pore wall, too rapid increase in this pressure could force the support to fragment in an uncontrolled way, resulting in powders as shown in Figure 4.1h.
- Softening of the polymer. The higher temperature causes a change in the physical properties of the polymer itself. At high pressures, high temperatures and to some extent the swelling with monomer, the polymeric material will be more soften and more sensitive to changes in shape, caused by shear stresses working on the polymer.

Of course, one can also think about a combination of one or more effects described above. To systematically investigate the effects, a similar series of polymerization tests was done, at different polymerization temperatures, but after a constant pre-polymerization step.

#### 4.3.2 The effect of pre-polymerization

A series similar to the temperature series was done, but with the use of a so-called fixed pre-polymerization step. The unactivated catalyst was injected into liquid monomer at a temperature of 40°C. The pre-polymerization step was continued for 10 minutes and then the reactor temperature was raised to the final, main polymerization temperature, which was varied from 40 to 70°C.

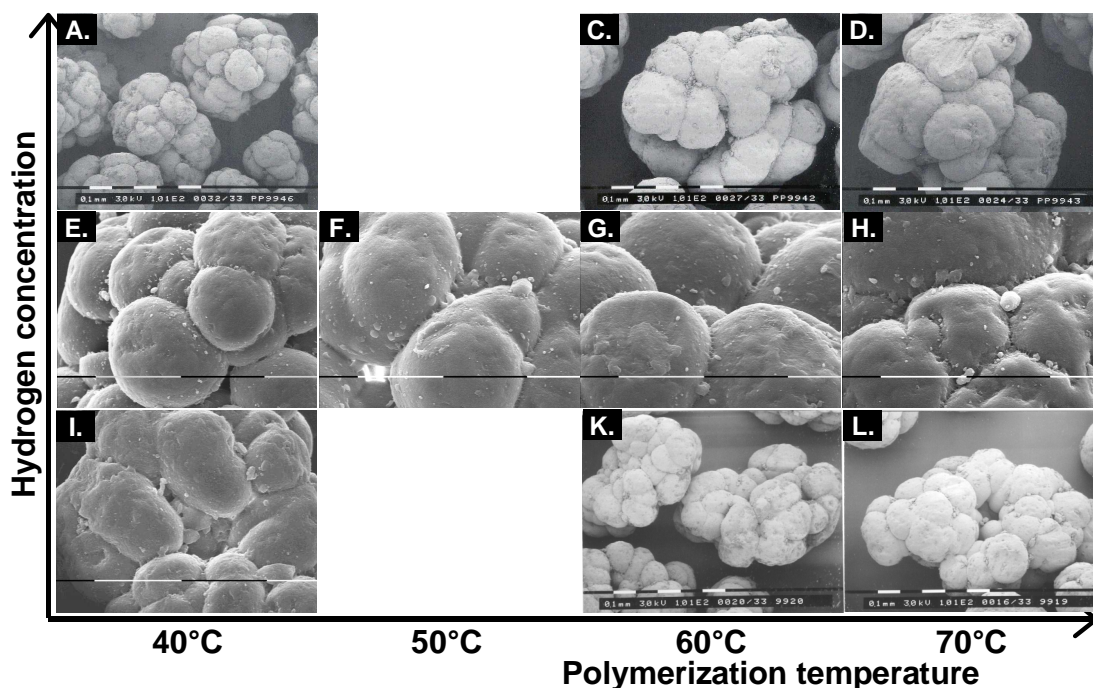


**Figure 4.3** SEM pictures of powders produced with a fixed pre-polymerization step of 10 minutes at 40°C, at various main polymerization temperatures and hydrogen concentrations. (In all pictures, the white bar indicates 100 microns)

Figures 4.3e to 4.3h show the SEM pictures of the 4 polymer samples taken from those tests. The difference with the case without pre-polymerization is remarkable. All particles are very similar, and powder morphology does not seem to be influenced by main polymerization temperature at all. All powders show the same morphology as the one shown in Figure 4.1e, produced without a pre-polymerization step at 40°C. When comparing the particle shape to the shape of the catalyst particles, one can conclude that shape replication is very well.

The observations in SEM are fully supported by the results of porosity and bulk density measurements, as shown in Figure 4.2. The triangle shaped markers indicate the temperature series including a fixed pre-polymerization step as described above. The bulk density of the powders remains a completely stable value of 450 g/l, for all polymer samples. The main polymerization temperature is not influencing this at all.

We previously showed<sup>[25]</sup> that the final stage of the polymerization, i.e. reduction of reactor temperature, flashing of the unreacted monomer and drying of the powder, in no way influences the particle morphology. From this, we can conclude that the morphology of the particles is determined in the initial stage of the polymerization process.

The first explanation that we mentioned above for the changing morphology is not obvious. If the sudden formation of gas bubbles were causing the open particle structure one would expect 'two cases in morphology'. In the first case the gas bubbles were formed and the particle was opened up. In the other case thermal runaway did not occur, therefore no bubbles were formed and thus particles were regularly shaped. What can be seen is a gradual change in morphology and thus the first mentioned explanation is not acceptable.

To investigate further these phenomena, the so-called non-isothermal pre-polymerization step was applied. The reactor was prepared at 20°C, the donor-alkyl mixture was injected and the reactor temperature was increased. During heating up of the reactor, the unactivated catalyst was injected at a predefined temperature, leading to a short pre-polymerization at an increasing temperature. Temperature during the main polymerization was 70°C in all cases. Injection temperature of the catalyst was varied from 30 to 70°C.

Figures 4.4d to 4.4f show the SEM images of the powders yielding from experiments including a non-isothermal pre-polymerization step. It can be seen that the morphology of the powder produced with the longest pre-polymerization (starting at the lowest temperature, being 30°C) shows a particle shape very similar to the particles produced with a fixed pre-polymerization. But when increasing the injection temperature, and with that shortening the pre-polymerization period and increasing the initial reaction rate that the particle experiences, the structure of the particle's surface opens up and comes to a situation close to a non pre-polymerized particle.

This shows that not only the reaction conditions during the main polymerization determine the morphology of the final powder, but also that it is really the process



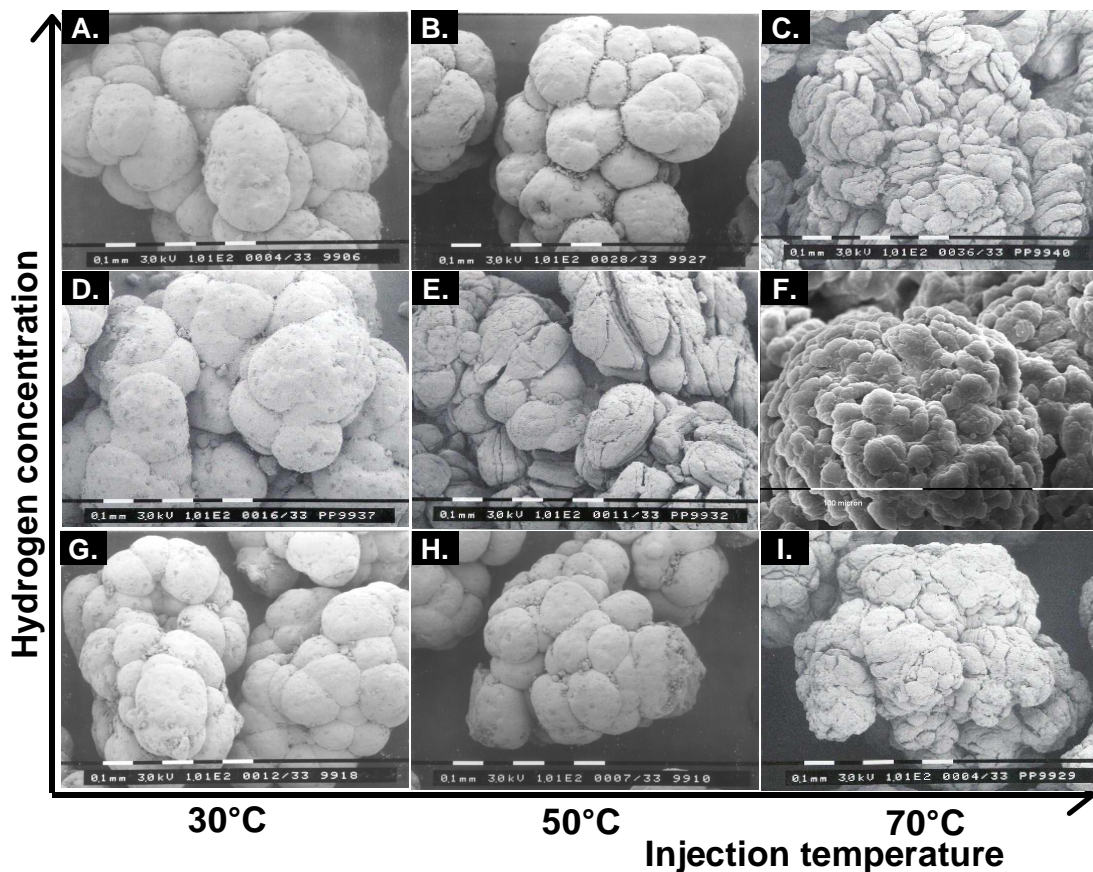


**Figure 4.4** SEM pictures of powders produced with a NIPP pre-polymerization step, at different catalyst injection temperatures and different hydrogen concentrations. (In all pictures the white bar indicates 100 microns).

conditions in the first stage of the reaction, that determine how the particle forms and what it will look like. Again, this is supported by the measurements of the bulk density. The circular markers in the plot of Figure 4.2 show the bulk densities of the powders yielding from the non-isothermal pre-polymerization experiments. It is clear that the experiments with longer pre-polymerizations, starting at lower initial temperatures, show higher bulk densities.

**Table 4.2** Vapor and liquid concentrations of hydrogen in the  $H_2$ -PPY system at different temperatures and different added amounts of hydrogen<sup>[10]</sup>.

Hydrogen (moles)	30°C		60°C		80°C	
	$Y_{H_2}$	$X_{H_2}$	$Y_{H_2}$	$X_{H_2}$	$Y_{H_2}$	$X_{H_2}$
0.00	0.0000	0.0000	0.0000	0.0000	0.0000	0.0000
0.069	0.0269	0.0007	0.0116	0.0010	0.0068	0.0012
0.23	0.0837	0.0022	0.0375	0.0032	0.0223	0.0038
0.66	0.2060	0.0062	0.0994	0.0091	0.0611	0.0110



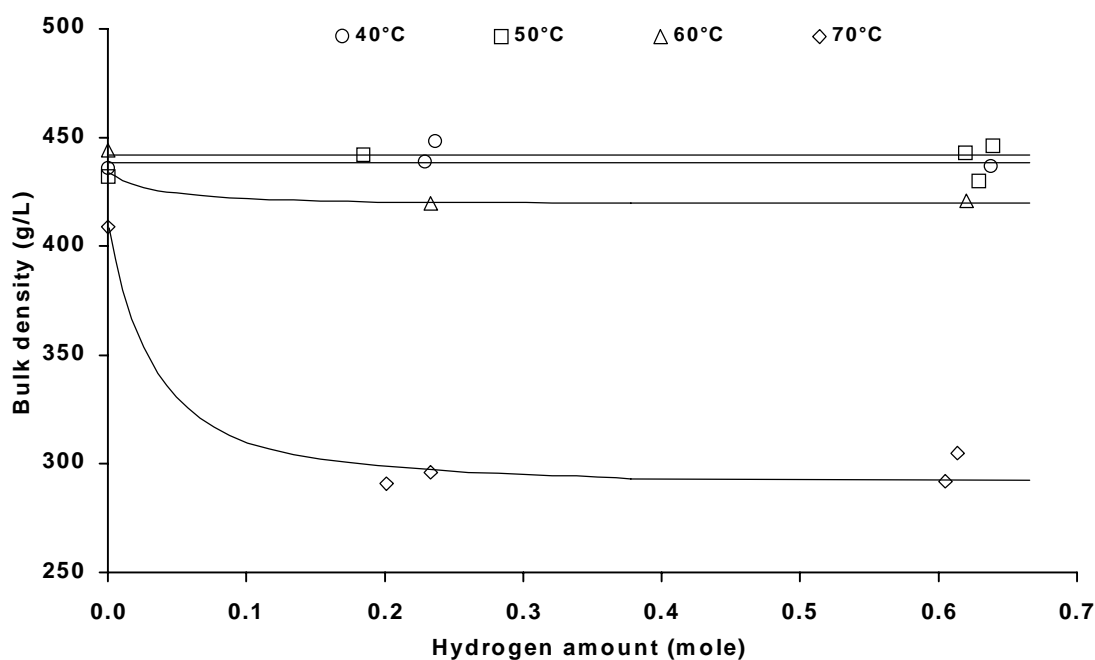
### 4.3.3 Influence of hydrogen concentration

Many studies have been carried out to try to understand the influence of hydrogen on the kinetics and molecular weight in olefin polymerization with Ziegler-Natta catalysts. But it is interesting to see what the addition of hydrogen changes in the morphology of the powder that is produced. Does the influence of the hydrogen on the molecular weight and polymerization rate affect the processes that determine the powder morphology?

The hydrogen concentration during polymerization was varied over a wide range, at different temperatures. This variation was introduced by varying the amount of added hydrogen in the batch experiments targeting at hydrogen amounts of 0, 0.21 and 0.63 moles. In a previous paper we described the vapor-liquid equilibria of the hydrogen-propylene system in more detail. Table 4.2 shows the gas and liquid concentrations at different temperatures at the various hydrogen amounts.

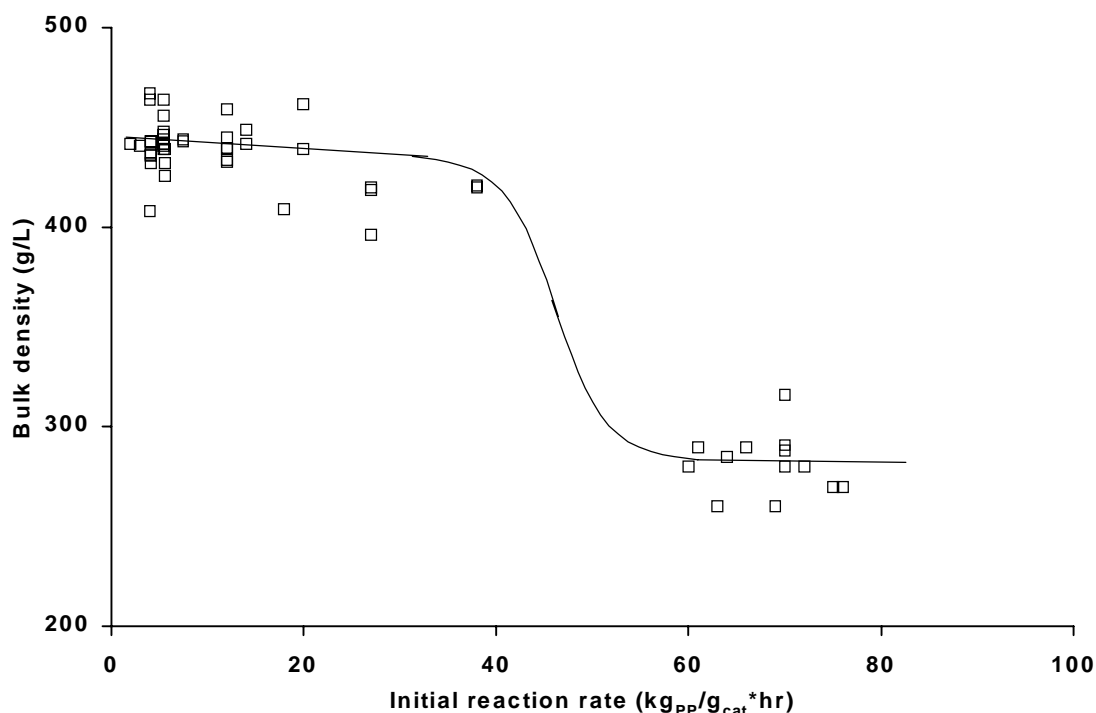
The variations in hydrogen concentration were performed for all three types of pre-polymerization (none, fixed and NIPP). The powders resulting from these experiments are also shown in Figures 4.1, 4.3 and 4.4 for cases without, with fixed and with NIPP pre-polymerization respectively, and Figure 4.5 shows the BD values for the series without a pre-polymerization step.

Figure 4.3 shows the almost perfect replication of shape for all particles. When a fixed pre-polymerization step was used, the replication of shape for all particles was almost perfect, bulk densities are high and porosities are low. When comparing Figures 4.3d, 4.3h and 4.3l we see that changes in the H<sub>2</sub> concentration do not influence the particle morphology, at least not at the scale observed here with SEM and BD-measurements.



**Figure 4.5** Bulk density of the resulting powders, as a function of the hydrogen concentration in the polymerization experiment for series of different polymerization temperatures. In none of the plotted tests a pre-polymerization was used.

But when no pre-polymerization step is used, as shown in Figure 4.1, the hydrogen concentration clearly effects the morphology of the powder. Powders produced in the absence of hydrogen seem to show the same effect as the powder in the presence of some hydrogen: with increasing polymerization temperature, the surface of the particles is becoming more irregular, and the sub-structures from which the particles are built become smaller. But this effect seems to start at higher temperatures than when hydrogen is present. At 60°C, the experiment with hydrogen included shows significant changes in particle shape (shown in Figure 4.1g), whereas in the absence of hydrogen this effect only starts at 70°C. The same is shown evident larger amounts of hydrogen are used. The addition of more hydrogen does not significantly influencing the particle morphology. With these effects, the impression rises that the morphology of the particles is to a large extent determined by reaction rate, rather than by some specific reaction conditions. Including the results of the experiments with the NIPP pre-polymerization step, we can refine this observation to: ‘the particle morphology is determined to a large extent by the initial reaction rate that the particle experiences in its polymerizing life.’



**Figure 4.6** Bulk density of the polymer powder as a function of the initial reaction rate. All types of experiments (no, fixed and NIPP pre-polymerization) are included here.

Figure 4.6 shows the correlation between the bulk density and the initial reaction rate that the particle experiences. The reaction rates in the initial stage presented here are extrapolated rates from the reaction rates in the complete experiment and are taken from the kinetic work that we published before<sup>[27]</sup>. In the case of a non-isothermal

prepolymerization, the reaction rate used in this graph is the reaction rate at the temperature of the system at the moment of injection (based on the kinetics [27]).

In this figure the experiments, without, with fixed and with non-isothermal prepolymerization are included. It seems to be clear that initial reaction rate is indeed the key-factor in determination of the powder morphology. When initial reaction rates are low, bulk densities are always high, and close to the maximum reached value of 450 g/L. With increasing initial reaction rate, the bulk density decreases, towards the lowest observed values of about 250 g/L at initial reaction rates above 60  $\text{kg}_{\text{PP}}/\text{g}_{\text{cat}} \cdot \text{hr}$ .

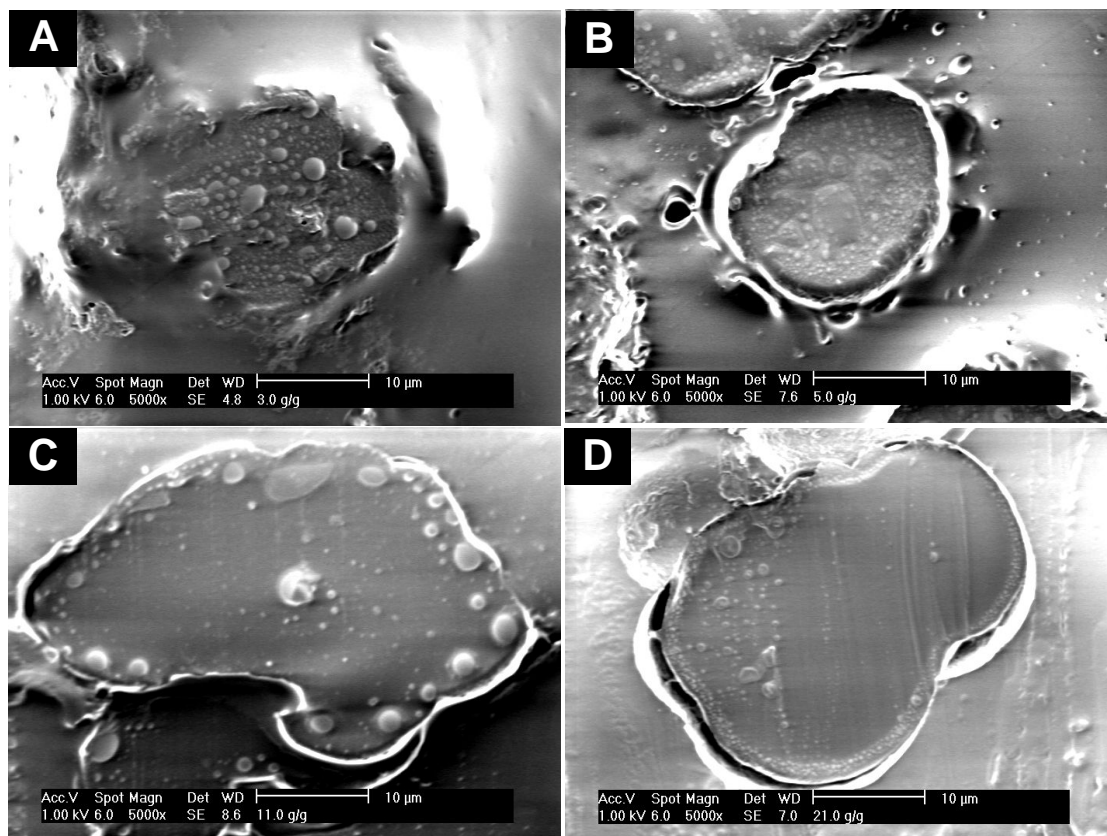


**Figure 4.7** A to D: SEM pictures of a cross-sectional cut of prepolymer particles, produced at very low polymerization rates, with the following values for degree of pre-polymerization: A. 3, B. 5, C. 11, D. 21

The most likely explanation that the influence of the initial reaction rate on the morphology of the final polymer particles is caused by the influence of the reaction rate on the fragmentation of the catalyst support. Figures 4.7a to 4.7d (taken from<sup>[1]</sup>) show the development of the internal particle structure of a polymer particle produced with the same catalyst, at very low reaction rates (between 1 and 5  $\text{g}_{\text{PP}}/\text{g}_{\text{cat}} \cdot \text{hr}$ ). In these pictures the continuous dark colored phase is the polymeric material and the heterogeneous, light colored phase is the catalyst support material, as was concluded from EDX measurements. It can be seen that in the initial stage, polymerization starts throughout the complete particle. Polymer formed in the center of the particle will cause the catalyst support to crack also in the center of the particle and not only at the outside of the particle, as has been assumed. Figure 4.7a shows a nice distribution of

support material over the radius of the particle. With increasing degree of pre-polymerization, the fragments get smaller and smaller, until they disappear below the resolution of the electron microscope used here.

When the reaction rates are higher in the initial stage of the polymerization, the ‘phase transition’ of the particle from catalyst-with-polymer to polymer-with-catalyst is changed as rate of polymer formation and rate of catalyst fragmentation are changed. At higher initial reaction rates the particle is not able to start fragmentation of the support evenly over the complete particle. When this fragmentation is uneven throughout the particle, the shape of the original catalyst particle will not fully replicate, leading to the shape as shown in for example Figure 4.1h.

To prove this, one should be able to carry out polymerizations with this same catalyst in liquid propylene at various polymerization temperatures, and stop it at very low yields. Table 4.3 shows typical reaction times for polymerizations at 40 and 70°C resulting in powders with yields in pre-polymerization between 3 and 50 g<sub>PP</sub>/g<sub>cat</sub>. As these extremely short residence times can not easily be reached in a batch tank reactor, one should use for example stopped-flow type of method to start and stop the polymerization within a few tenths of a second. Powders from such tests would give new information on the difference in fragmentation between different rates of polymerization.

**Table 4.3** Typical polymerization times necessary for reaching the given yield in pre-polymerization, for the presently used catalyst at 40 and 70°C.

Temperature (°C)	R <sub>p,0</sub> (kg <sub>PP</sub> /g <sub>cat</sub> *hr)	Typical polymerization time (s)				
		CE=3	CE=5	CE=11	CE=21	CE=50
40	5	2.2	3.6	7.9	15	36
70	70	0.15	0.26	0.57	1.1	2.6

#### 4.3.4. The effect of the monomer concentration

If the morphology is indeed determined to a large extent by the (initial) rate of polymerization, then one should expect that the effect of reducing the monomer concentration would be similar to the effect of reducing the polymerization temperature. To check this effect, a series of experiments was done at reduced monomer concentrations, without a prepolymerization step. This reduction was provided by replacement of a variable part of the liquid monomer by hexane. By using hexane instead of propylene, the total liquid volume was kept in the same range as the liquid volume in the pure propylene case. So here, the polymerization conditions were gradually changed from bulk liquid pool polymerization towards dilute slurry polymerization in hexane. Of course one has to keep in mind that, in addition to monomer concentration in bulk, more factors are changed by the addition of the hexane. At higher reaction rates and lower catalyst porosity, the presence of inert components can lead to enrichment of this component in the particle. Because of the relatively high molecular weight of hexane this becomes even more important. Also,

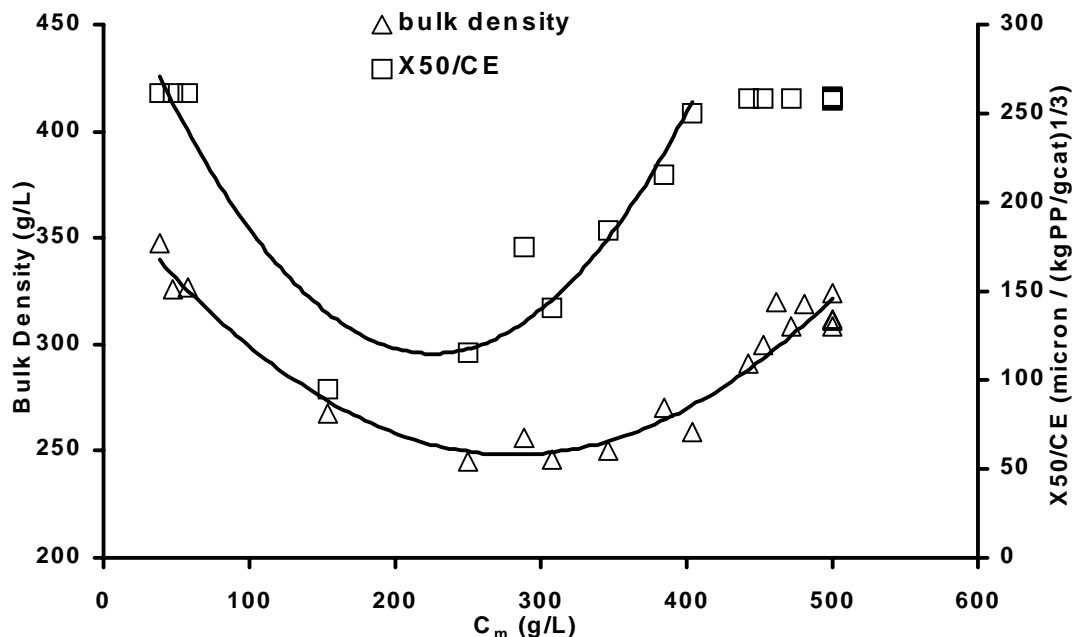


**Figure 4.8** Bulk density of final powder as a function of monomer concentration in main polymerization. Concentration of propylene was reduced by addition of hexane to the liquid monomer.

the hexane will be sorbed in the polymer leading to swelling and influencing crystallization of the polymer.

As the reduction of the monomer concentration is expected to decrease reaction rate and a decreased initial reaction rate, has been shown to correlate directly with a more regular powder morphology, a reduction of the monomer concentration should enlarge bulk densities and improve the replication of the shape of the catalyst particles. Figure 4.8 shows the bulk densities of the powders yielding from this series. It is clear that the bulk density shows a minimum around 300 g/l and goes up again at lower concentrations. The SEM pictures of these powders give more insight in this unexpected result. Figure 4.9a to 4.9f show a series of pictures from the highest to the low monomer concentrations. In the pictures it is clear that all particles look similar, but the particles seem to break up in smaller particles. Figure 4.9f for example, at a  $C_m$  of 48 g/L shows clearly bimodality in the particle size distribution. The sample consists of two types of particles: the particles that are not yet broken and the smaller particles yielding from breaking of the particles.

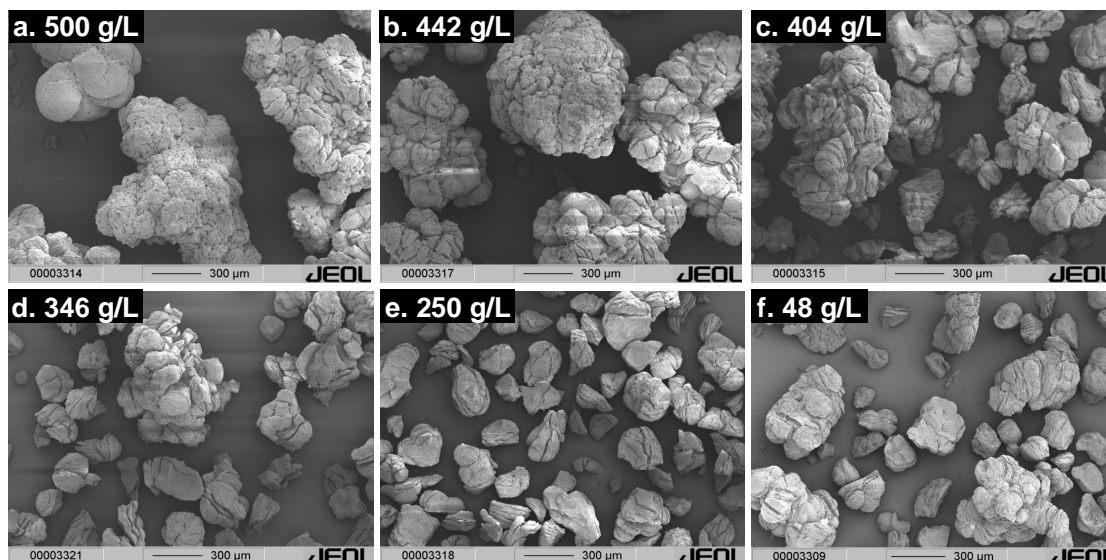


**Figure 4.9** SEM pictures of polymer powders yielding from experiments at various monomer concentrations (monomer concentration was reduced by addition of hexane to liquid monomer).

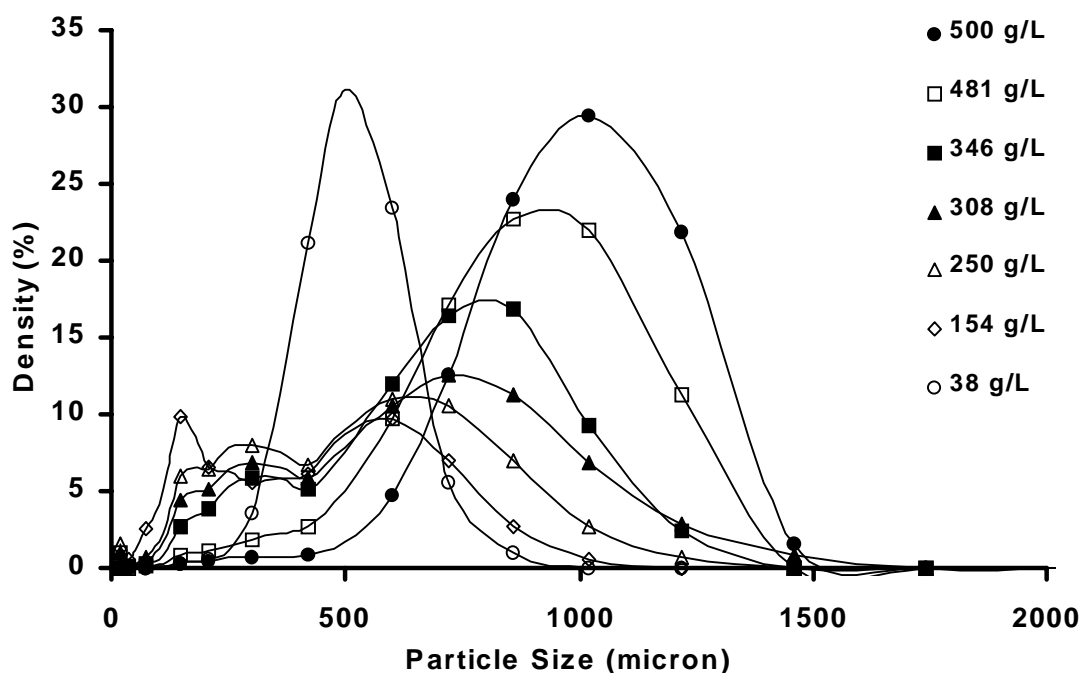


**Figure 4.10** Particle Size Distribution (PSD) curves for powders produced at varied monomer concentration. Bimodality appears at lower values for  $C_m$ . At the lowest  $C_m$  values, this effect has disappeared.

In a previous study<sup>[27]</sup> (chapter 3 of these thesis), we examined the relation between the monomer concentration and the observed reaction rates. It was shown there that the reaction rate did not, as would be expected from the usual kinetic models, decrease linearly with decreasing monomer concentration. Rather, contrarily to what one would expect from equation 4.1, it was more or less constant when  $C_m$  decreased from 500, down to a value of about 200 g/L.

$$R_p = k_p \cdot (C_m)^n \cdot C^* \quad (\text{eq.4-1})$$

Decreasing monomer concentration any further, below this concentration, caused a sudden drop of reaction rate.

The apparent bimodality of the particle size distribution seen in the SEM pictures, is fully supported by particle size measurements shown in Figure 4.10. It is clear that with reducing monomer concentration the relatively narrow PSD develops to lower particle sizes and at a certain moment towards bimodality. At really low  $C_m$ , the bimodality disappears and a low PS remains. Of course the low reaction rates at low monomer concentrations also contribute to the change in PS, therefore the ratio between the average particle size and the catalyst efficiency (expressed in  $\text{kg}_{\text{PP}}/\text{g}_{\text{cat}}$ ),  $X_{50}/\text{CE}$  is added to the plot in Figure 4.8, indicated with the square shaped markers. As expected, it follows the same trend as the bulk density.

A further proof for the fact that the morphology of the particles is indeed determined in the initial stage of the polymerization is given in the SEM pictures of Figure 4.11. This figure shows powder after a pre-polymerization step in liquid propylene and a subsequent polymerization at  $70^\circ\text{C}$  at lowered monomer concentration ( $C_m = 420 \text{ g/L}$ ). The powder shows a perfect replication of the particle's shape and shows very regular, smooth particle surface. This is a proof that the typical structures formed in the dilute polymerization are annulled by the pre-polymerization in liquid propylene at lowered temperature and the main polymerization in hexane diluted monomer does not lead to typical structures coming with this dilution.

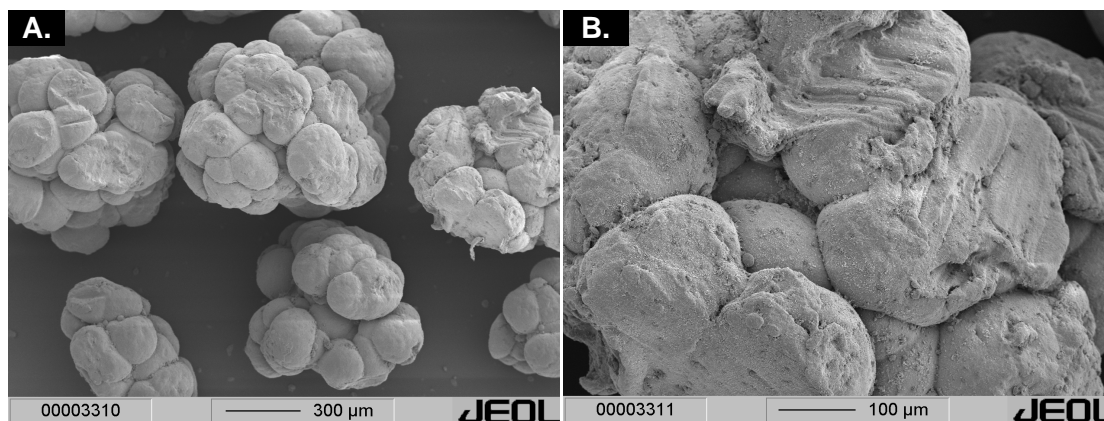


**Figure 4.11** SEM pictures of powder produced at reduced monomer concentration ( $C_m=420 \text{ g/L}$ ) after a pre-polymerization step in liquid monomer of  $40^\circ\text{C}$  for 10 minutes. ( Picture B is enlargement of part of picture A.)

#### 4.4 Conclusions

Many factors determine the morphology of the polymer powder. Most of them are expected to influence morphogenesis directly, but the way and type of this effect is often not understood. As the fragmentation of the catalyst support plays an important

role in the formation of the particle shape, especially the nature of the polymerization reaction, and in the initial (fragmentation) stage is important.

Next to that, the state of the polymer formed, influenced by temperature, swelling with monomer and polymer properties like tacticity and molecular weight can determine the particle's structure.

In the present work it has been shown experimentally that the initial reaction rate is the crucial factor in the development of the shape of the polymer particle. The influence of other parameters like temperature, pressure, hydrogen concentration can be traced back to their influence on the initial rate. When this rate is high, the particle will not be able to replicate the shape of the catalyst particle, will form irregularly shaped surface structures, will show high porosities and will show low values for bulk density. A short pre-polymerization, lasting no longer than 1 minute at an increasing polymerization temperature - or polymerization rate - is often sufficient to effect that the particle will show a high density and that the shape of the particle will be very regular while a perfect reproduction of the catalyst particle is realized.

Finally, it can be concluded that to understand the fragmentation process and the other processes playing a role in the development of the particle morphology, also at higher reaction rates (e.g. without prepolymerization), one should solve the experimental problem of following polymerizations at high polymerization rates.

Acknowledgements - The work presented in this paper was carried out in co-operation with The Dow Chemical Company, Freeport (TX), USA. The authors wish to thank Dow for both the financial and the intellectual input. The aluminum alkyls used in the work were kindly donated by AkzoNobel, Deventer, The Netherlands.

Imaging of the cross sectional areas of cut particles was done in a Dutch Polymer Institute co-operation with Joachim Loos of the Technical University of Eindhoven, The Netherlands.

The work could not have been completed without the experimental work carried out by Eelko Bos, Marlies Kopmels, Tom Cellissen and Roxane van Arneman. The importance of their contribution to this work is highly acknowledged. In addition, the technical assistance of Gert Banis, Fred ter Borg, Karst van Bree and Geert Monnik is highly appreciated.



## Notations

$C^*$	Concentration of active sites	mole/g
$C_m$	Concentration of monomer	g/L
$k_p$	Propagation rate constant	L/mole·hr
$n$	Order of propagation	-
$P$	Pressure	bar
$R_p$	Reaction rate of polymerization	kg <sub>PP</sub> /g <sub>cat</sub> ·hr
$T$	Temperature	K
$X$	Mole fraction in liquid phase	-
$Y$	Mole fraction in gas phase	-

### Subscripts:

0	Initial, at time = 0
main	Related to main polymerization step
ppy	Related to propylene
prepol	Related to pre-polymerization step
H <sub>2</sub>	Related to the hydrogen
inj	Related to injection

### List of abbreviations

BD	Bulk density	PPY	Propylene
CE	Catalyst efficiency	PS	Particle size
D-donor	Di-cyclopentyl di-methoxy silane	PSD	Particle size distribution
EDX	Energy dispersive x-ray	SEM	Scanning Electron Microscopy
NIPP	Non-isothermal pre-polymerization	TEA	Tri ethyl aluminum
PP	Polypropylene	ZN	Ziegler-Natta

## References

- [1] Pater, J.T.M., Weickert, G., Loos, J. & van Swaaij, W.P.M. (2001). 'High Precision Pre-polymerization of Propylene at Extremely Low Reaction Rates – Kinetics and Morphology'. *Chemical Engineering Science*, **56**, 4107-4120.
- [2] Galli, P., Barbe, P.C., & Noristi, L. (1984). 'High Yield Catalysts in Olefin Polymerization'. *Die Angewandte Makromolekulare Chemie*, **120**, 73-90.
- [3] Galli, P., Luciani, L. & Cecchin, G. (1981). 'Advances in the Polymerization of Polyolefins with Coordination Catalysts', *Die Angewandte Makromolekulare Chemie*, **94**, 63-89.
- [4] Galli, P. & Haylock, J.C. (1991). 'Continuing Initiator System Developments Provide a new Horizon for Polyolefin Quality and Properties', *Progress in Polymer Science*, **16**, 443-462.
- [5] Galli, P. & Haylock, J.C. (1992). 'Advances in Ziegler-Natta Polymerization – Unique Polyolefin Copolymers, alloys and Blends Made Directly in the Reactor', *Makromolekulare Chemie - Macromolecular Symposia*, **63**, 19-54.

- [6] Sasaki, T., Ebara, T. & Johoji, H. (1993). *Pol. Adv. Techn.*, **4**, 406.
- [7] Albizzati, E. & Galimberti, M. (1998). 'Catalysts for Olefin Polymerization', *Catalysis Today*, **41**, 159-168.
- [8] Floyd, S., Heiskanen, T., Taylor, T.W., Mann, G.E. & Ray, W.H. (1987). 'Polymerization of Olefins Through Heterogeneous Catalysis. VI. Effect of Particle Heat and Mass Transfer on Polymerization Behavior and Polymer Properties', *Journal of Applied Polymer Science*, **33**, 1021-1065.
- [9] Nagel, E.J., Kirillov, V.A., & Ray, W.H. (1980). 'Prediction of Molecular Weight Distribution for High Density Polyolefins', *Industrial Engineering Chemistry*, **19**, 372-379.
- [10] Floyd, S., Choi, K.Y., Taylor, T.W. & Ray, W.H. (1986). 'Polymerization of Olefins through Heterogeneous Catalysis. IV. Modeling of Heat and Mass Transfer Resistance in the Polymer Particle Boundary Layer', *Journal of Applied Polymer science*, **32**, 2231-2265.
- [11] Floyd, S., Choi, K.Y., Taylor, T.W. & Ray, W.H. (1986). 'Polymerization of Olefins through Heterogeneous Catalysis. III. Polymer Particle Modeling with an Analysis of Intraparticle Heat and Mass Transfer Effects', *Journal of Applied Polymer Science*, **32**, 2935-2960.
- [12] Hutchinson, R.A., Chen, C.M. & Ray, W.H. (1992). 'Polymerization of Olefins through Heterogeneous Catalysis. 10. Modeling of Particle Growth and Morphology', *Journal of Applied Polymer Science*, **44**, 1389.
- [13] Ferrero, M.A., & Chiovetta, M.G. (1987a). 'Catalyst Fragmentation during Propylene Polymerization: Part I. The Effects of Grain Size and Structure', *Polymerization Engineering Science*, **27**, 1436-1447.
- [14] Ferrero, M.A., & Chiovetta, M.G. (1987b). 'Catalyst Fragmentation during Propylene Polymerization: Part II. Microparticle Diffusion and Reaction Effects', *Polymerization Engineering Science*, **27**, 1448-1460.
- [15] Ferrero, M.A., & Chiovetta, M.G. (1991a). 'Effects of Catalyst Fragmentation during Propylene Polymerization. IV. Comparison between Gas Phase and Bulk Polymerization Processes', *Polymerization Engineering Science*, **31**, 904-911.
- [16] Ferrero, M.A., & Chiovetta, M.G. (1991b). 'Catalyst Fragmentation during Propylene Polymerization. III. Bulk Polymerization Process Simulation'. *Polymerization Engineering Science*, **31** (12), 886-903
- [17] Ferrero, M.A., Koffi, E., Sommer, R. & Conner, W.C. (1992). 'Characterization of the Changes in the Initial Morphology for MgCl<sub>2</sub>-supported Ziegler-Natta Polymerization Catalysts', *Journal of Polymer Science: Part A Polymer Chemistry*, **30**, 2131
- [18] Noristi, L., Marchetti, E., Baruzzi, G. & Sgarzi, P. (1994). 'Investigation of the Particle Growth Mechanism in Propylene Polymerization with MgCl<sub>2</sub>-

- Supported Ziegler-Natta Catalysts'. *Journal of Polymer Science: Part A Polymer Chemistry*, **32**, 3047-3059.
- [19] Kakugo, M., Sadatoshi, H., Sakai, J., & Yokoyama, M. (1989). 'Growth of Polypropylene Particles in heterogeneous Ziegler-Natta Polymerization'. *Macromolecules*, **22**, 3172-3177.
- [20] Kakugo, M., Sadatoshi, H., Yokoyama, M., & Kojima K. (1989). 'Transmission Electron Microscopic Observation of Nascent Polypropylene Particles using a new Staining Method', *Macromolecules*, **22**, 547-551.
- [21] Ferrero, M.A., Sommer, R., Spanne, P., Jones, K.W., & Conner, W.C. (1993). 'X-Ray Microtomography Studies of nascent Polyolefin Particles Polymerized over Magnesium Chloride-supported Catalysts', *Journal of Polymer Science: Part A Polymer Chemistry*, **31**, 2507-2512.
- [22] Han-Adebekun, G.C., Hamba, M. & Ray, W.H. (1997). 'Kinetic Study of Gas Phase Olefin Polymerization with a  $\text{TiCl}_4/\text{MgCl}_2$  Catalyst. I. Effect of Polymerization Conditions', *Journal of Polymer Science: Part A Polymer Chemistry*, **35** (10), 2063-2074.
- [23] Han-Adebekun, G.C. (1996). Ph.D. thesis, Department of Chemical Engineering, University of Wisconsin, Madison, WI.
- [24] Moore, E.P. (1996). 'Polypropylene Handbook', Hanser Publishers, Munich Vienna New York.
- [25] Pater, J.T.M., Weickert, G. & van Swaaij, W.P.M. (2001). 'Polymerization of Liquid Propylene with a 4<sup>th</sup> Generation Ziegler-Natta Catalyst - A system for pre-polymerization and VLE of the  $\text{H}_2$ -propylene system', *submitted to American Institute for Chemical Engineers Journal*.
- [26] Shimizu, F., Pater, J.T.M., Weickert, G. & van Swaaij, W.P.M. (2001). 'Three-Site Mechanism and Molecular Weight: Time Dependency in Liquid Propylene Batch Polymerization Using a  $\text{MgCl}_2$ -Supported Ziegler-Natta Catalyst', *Journal of Applied Polymer Science*, **81**, 1035.
- [27] Pater, J.T.M., Weickert, G., & van Swaaij, W.P.M. (2001). Liquid Pool II paper, *Submitted to Journal of Polymer Science: Part A Polymer Chemistry*.



## **CHAPTER 5**

### **HIGH PRECISION PRE-POLYMERIZATION OF PROPYLENE AT EXTREMELY LOW REACTION RATES**

-  
**KINETICS AND MORPHOLOGY**  
-

## **Abstract**

*A one-liter slurry phase polymerization reactor was set-up to carry out catalytic polymerizations of propylene at low reaction rates. The catalyst system used in this work was a fourth generation Ziegler-Natta catalyst, with tri-ethyl aluminum as cocatalyst and di-cyclo pentyl di-methoxy silane as external electron donor. The low reaction rates allowed us to systematically study the formed particles. Polymer powder was produced with a yield of pre-polymerization (YPP) varying from 0.3 grams of polypropylene (PP) per gram catalyst to 50 grams PP per gram catalyst.*

*Because of the well-defined polymerization conditions, the intra- and inter-particle morphologies can be studied in order to investigate the fragmentation of the catalyst. Cross-sectional SEM pictures show a decreasing size of fragments with increasing YPP. The fragmentation does not proceed as sometimes described in literature in layers, starting from the outer layer and advancing to the center of the particle. Rather the fragments are initially well distributed throughout the particle. At higher values for YPP - above 2 to 4 grams PP per gram the size of the fragments continues to decrease with increasing YPP, but the fragments 'drift' to the outer portions of the particles.*

*In addition to the morphological aspects, a precise study of the 'early-stage'-polymerization kinetics was carried out using measurements of monomer pressure as a function of time. Up to a YPP of about 2 to 4 gram PP per gram catalyst, the reaction rate decreases strongly with increasing YPP, but above this value, reaction rate remains constant with increasing YPP. This effect is ascribed to a phase transition in the growing particle. Initially the catalyst forms the continuous phase, within which the polymer is distributed. After the phase transition, the polymer forms the continuous phase in which catalyst fragments are distributed. This change causes a change in monomer concentration at the active sites, resulting in lower reaction rates.*

*This chapter has been published:*

*J.T.M. Pater, G. Weickert, J. Loos, W.P.M. van Swaaij, 'High Precision Pre-polymerization of Propylene at Extremely Low Reaction Rates, Kinetics and Morphology', Chemical Engineering Science, 56, 4107-4120, (2001).*

## 5.1 Introduction

Over the past 40 years the market for polyolefins, polyethylene and polypropylene in particular, has grown tremendously. It is also projected that this market will continue to grow as the product properties of the different materials are broadening rapidly due to new developments in both the field of catalysis and the production processes, while production costs remain relatively low.

Still, despite high expectations for large-scale introduction of metallocene catalysts, the vast majority of polypropylene is made using conventional Ziegler-Natta catalysts. These traditional catalysts currently account for about 98% of all polypropylene produced worldwide. When using titanium based catalysts supported on magnesium chloride, a pre-polymerization step is often used. Pre-polymerization is essentially a polymerization step performed under mild conditions and at low reaction rates. The low reaction rates allow the particle to fully activate, help to prevent thermal runaway, and provide a controlled fragmentation of the catalyst resulting in improved particle morphology. As the major high impact polypropylene processes often make use of different polymerization reactors in series, a good particle morphology – meaning a spherical shape, a controlled porosity and a narrow particle size distribution – is essential for the performance of the gas phase copolymerization reactors and distribution of the rubbery part throughout the homopolymer matrix. Control of particle morphology, and tools to influence this particle structure are very important. It is believed that the fragmentation of the catalyst is a decisive step in the determination of the final particle morphology, and that it can be used to control particle structure.

Due to the extreme sensitivity of modern catalyst systems to impurities, and due to the intrinsically high polymerization activities, reliable and reproducible experimental results are hard to obtain in bench- or pilot-scale set-ups. Nevertheless, we must be able to produce the catalyst/polymer samples in a strictly controlled manner, to understand the underlying causal processes in fragmentation behavior and to the study of the influence of the relevant variables.

Ferrero and Chiovetta<sup>[1-5]</sup> and Lawrence and Chiovetta<sup>[6]</sup> performed a series of simulations in order to understand the importance of the fragmentation stage. They proposed a model for fragmentation that assumes that the process proceeds layer by layer, starting at the surface of the particle and continuing towards the core of the catalyst macroparticle. This is illustrated in Figure 5.1. In this representation, the reaction starts at the outer surface of the particle, and the polymerization front "walks" through the particle since it is assumed that polymer is produced only in the fragmented layers. This behavior leads to the conclusion that the influence of fragmentation on heat and mass transport processes is significant.

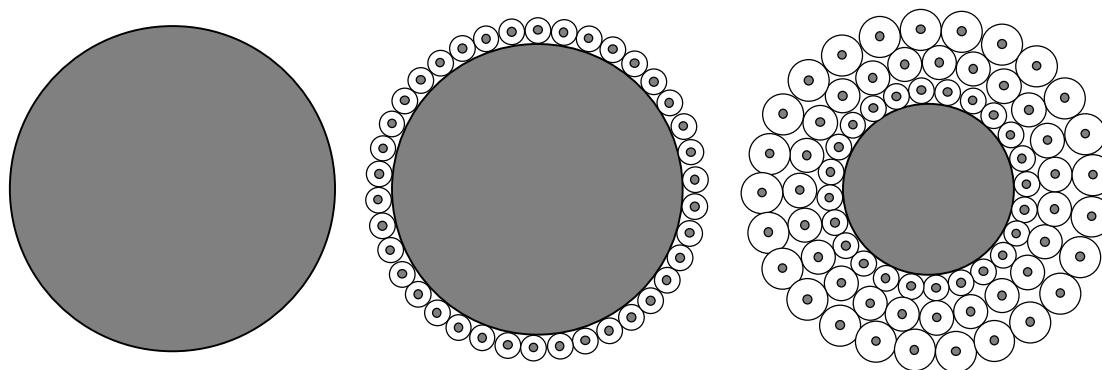


**Figure 5.1** Schematic representation of the fragmentation model as proposed by Ferrero and Chiovetta<sup>[1-5]</sup>. The catalyst fragments layer wise, starting at the surface towards the center of the particle.

Of course, when doing experimental work on this problem, one has to keep in mind that the type of the catalyst, and specifically the nature of the support material is of utmost importance in the fragmentation behavior of the catalyst. Papers published in the area of nascent morphology<sup>[7-9]</sup> of polymer particles and catalyst fragmentation clearly show the importance of the nature of the catalyst support material. It is demonstrated<sup>[10]</sup> for example that a silica supported chromium catalyst shows a different fragmentation behavior compared to a magnesium chloride supported catalyst, most likely due to different internal coherent forces in the support material.

For Ziegler-Natta catalysts Cecchin et al.<sup>[11]</sup> propose a morphology of the polymer powder in three levels. Catalyst grains show a dual morphological structure of microparticles (catalyst crystallites) and larger agglomerates of crystallites (subparticles). This structure is reproduced in the polymer: the microparticles grow to microglobules, but these microglobules maintain clustered in subglobules. With proceeding polymerization, fragmentation proceeds, and catalyst material tends to be convected to the surface of the subglobules.

Apart from the nature of the support, one can imagine that the reaction rate of the polymerization can also influence the fragmentation behavior. When fractured by a blow of a hammer or within a bench-vice, a pebble will show a complete different fragmentation behavior<sup>[12]</sup>. Such differences will occur in the various supported catalyst particles. The speed of polymer formation inside the pores of the support, and the corresponding internal stress built-up rate will change the way the catalyst fragments. In most previous studies on the development of the particle morphology reaction rates are not mentioned at all. Usually a sample is only characterized by the original properties of the catalyst and the polymer yield per unit of catalyst weight.

In the present work we show a method that allows measurements of reaction kinetics in the earliest stage of the polymerization very accurately. The experiments are stopped at well-defined yields – or yield of pre-polymerization (YPP), expressed in grams of polymer per gram catalyst (support included) – and the polymer samples are analyzed and characterized. The reaction rates used here are extremely low, thereby enabling us to see the fragmentation behavior of the catalyst particles at low rates.



## 5.2 Experimental

### 5.2.1 Chemicals

The catalyst used in this work is a commercially available fourth generation<sup>[13]</sup>  $\text{TiCl}_4$  Ziegler-Natta catalyst on a  $\text{MgCl}_2$  support. Tri-ethyl aluminum, kindly donated by Witco GmbH, was used as the cocatalyst, and di-cyclo pentyl di-methoxy silane (the so-called D-donor) was used as the electron donor. The catalyst components are prepared in a glove box under nitrogen. 'Pro Analyti' quality hexane (Merck) was used to suspend the catalyst. Propylene was obtained from Indugas with a purity >99.5%, with propane as main impurity. The hydrogen and nitrogen used were of >99.999% purity.

The hydrogen, nitrogen and hexane were extra purified by passing them over a reduced BTS copper catalyst and subsequent passing through three different beds of molecular sieves, with pore sizes of 13, 4 and 3 angstrom respectively. The BTS catalyst was obtained from BASF. The propylene was purified in the same way, after which it was passed through a bed of oxidized BTS copper catalyst to remove carbon monoxide.

### 5.2.2 Experimental set-up

A schema of the experimental set-up used in this work is represented in figure 5.2.

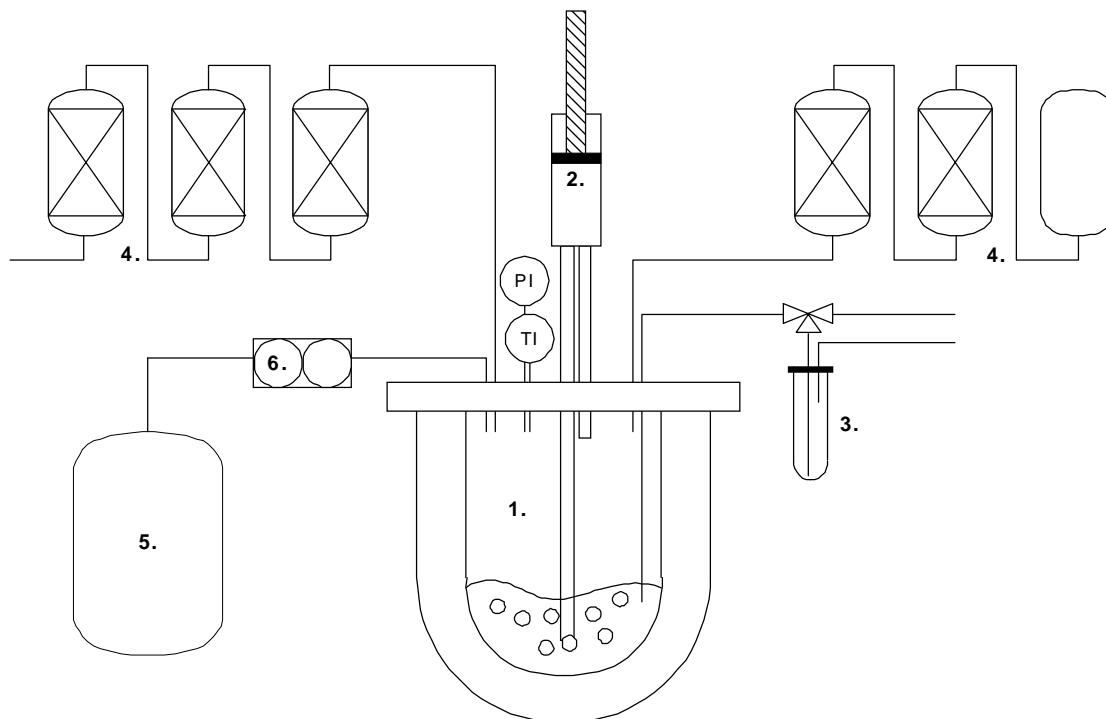


**Figure 5.2** Experimental set-up represented schematically used in this work. 1. Slurry phase bubble reactor, 2. Gas recirculation membrane pump, 3. Catalyst introduction system, 4. Gas and hexane purification columns, 5. Monomer vessel, 6. Mass flow controller for monomer injection.

The polymerization experiments were carried out in the 1-liter glass reactor (1). 150 ml of hexane was used in the experiments to suspend the catalyst-polymer particles. A membrane gas circulation pump (2) was used to stir the slurry. This provides effective mixing, but with much lower local shear stresses than would be observed with a standard magnetic bar stirrer. The injection system (3) allows the components of the catalyst system to be introduced into the reactor without exposing them to contact with the atmosphere. Reaction gases are all purified again before use in the experiment by molecular sieves and copper catalysts (4). The polymerization is started by injecting pulses of monomer from the monomer reservoir (5), through the mass flow controller (6) to the reactor.

### *5.2.3 Polymerization*

The glass reactor is heated overnight at 120°C. Then, just before performing a polymerization, it is connected to the rest of the experimental system, and cleaned by subjecting it to a vacuum for 5 minutes and flushing it with nitrogen at a temperature of 90°C. After cleaning, the reactor is tested for gas leakage and filled with the hexane.

The different components of the catalyst system are prepared in the glovebox under nitrogen. The catalyst, suspended in a mineral oil, is weighed in a vial and diluted with hexane. The aluminum alkyl and the d-donor are weighed in separate vials, and both diluted with hexane. After the reactor has been filled with 100 ml of hexane, the alkyl and the donor are introduced. The components are contacted in the reactor for 20 minutes at room temperature. At the end of the contact time, the catalyst is introduced. The liquid volume after introduction of the catalyst is 150 ml. Once the catalyst has been contacted for 15 minutes with the diluted cocatalyst and electron donor, the monomer is injected and the polymerization reaction starts.

Injection of a pulse of monomer leads to an increase of the reactor pressure. Once the pressure comes to equilibrium, pressure measurements can be used to monitor the reaction rate, as described below. Reactor temperature and pressure data are saved to the hard disk of the data acquisition unit every five seconds, together with jacket inlet and outlet temperatures.

After an experiment, that is typically comprised of 3 or more monomer injections, the resulting polymer powder is removed from the slurry reactor and reintroduced into the glovebox. The material is then washed several times with fresh hexane to remove aluminum alkyl and donor, deactivated by introduction of small amounts of air to the suspension and subsequently dried by slow evaporation of the hexane.

### *5.2.4 Determination of reaction rate in slurry phase*

Monitoring of pressure and temperatures begins directly after the catalyst has been added to the system. Before injection of the monomer, the total pressure in the reactor

consists of two contributions: the vapor pressure of the hexane and the inert nitrogen present in the system. With information on temperature these two terms can be determined, using the well-known law of Raoult's:

$$P_{\text{Hex}} = x_{\text{Hex}} \cdot P_{\text{Hex}}^0 \quad (\text{eq. 5.1})$$

where  $P_{\text{Hex}}^0$  is the partial pressure of pure hexane at the specific temperature  $T$  and  $P_{\text{Hex}}$  the actual partial pressure of hexane at mole fraction  $x_{\text{Hex}}$ . When a pulse of monomer is added to the reactor, the pressure increases. After equilibrium is reached, the total reactor pressure consists of three contributions: vapor pressure of hexane and partial pressures of nitrogen and propylene. The vapor pressure of the propylene is calculated using Henry's law, as the propylene is only present at very low mole fractions:

$$P_{\text{PPY}} = x_{\text{PPY}} \cdot H \quad (\text{eq. 5.2})$$

with  $P_{\text{PPY}}$  being the partial pressure of the propylene at mole fraction  $x_{\text{PPY}}$ , and  $H$  as the Henry's Law coefficient. Therefore, the total reactor pressure  $P_{\text{R}}$  can be defined with equation 5.3 and 5.4, before and after monomer addition, respectively. The moment of monomer injection is said to be  $t=0$ .

$$t = 0 \quad P_{\text{R}} = P_{\text{N}_2} + P_{\text{Hex}}^0 \quad (\text{eq. 5.3})$$

$$t > 0 \quad P_{\text{R}} = P_{\text{N}_2} + (1 - x_{\text{PPY}}) \cdot P_{\text{Hex}}^0 + x_{\text{PPY}} \cdot H \quad (\text{eq. 5.4})$$

Because equilibrium between gas- and liquid phase is reached quickly, with information on the solubility of propylene in hexane, these three terms can be determined fairly accurately, and therefore the amount of unreacted propylene is known at every moment in time. The reaction rate is thus defined:

$$R_p(t) = \frac{[m_{\text{PPY}}(t) - m_{\text{PPY}}(t + \Delta t)]}{m_{\text{catalyst}} \cdot \Delta t} \quad (\text{eq. 5.5})$$

with  $m_{\text{PPY}}$  and  $m_{\text{catalyst}}$  being the mass of unreacted propylene present in the system and the mass of the catalyst respectively. Because of the fact that this differential method is sensitive to small variations in the pressure registration, results can be improved by smoothing the measured pressure curve, using a fitting tool. Figure 5.3 shows both the raw pressure curve and the smoothed version. It can be seen that when the noise disappears, results from calculations will gain accuracy, even at small pressure differences below 0.1 bar.

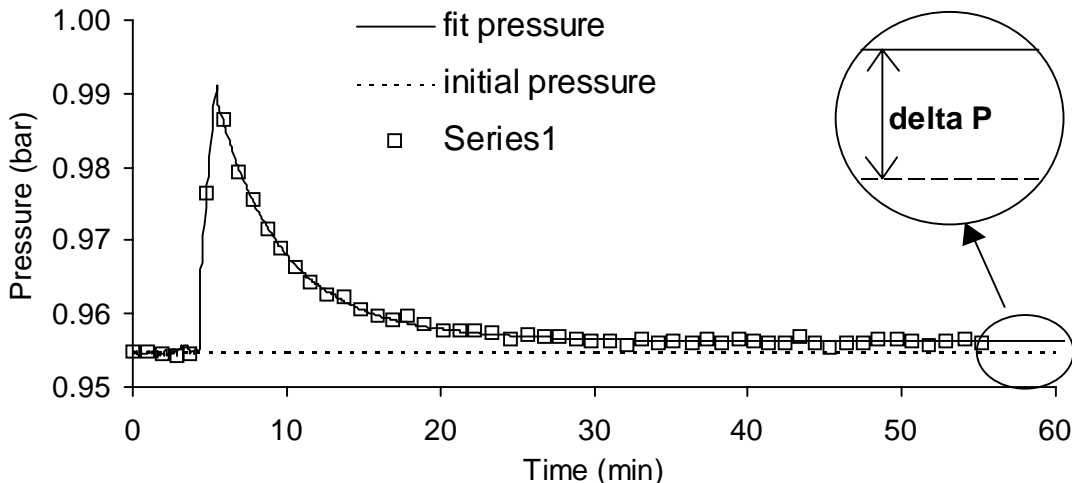


**Figure 5.3** Typical pressure curve versus time for a dose of monomer, with measured data, smoothed pressure curve and initial pressure level.

### 5.2.5 Cross sectional SEM

The morphologies of the samples were investigated using a Philips environmental scanning electron microscope XL-30 ESEM FEG (Philips, Eindhoven, The Netherlands) equipped with energy dispersive x-ray spectrometer (EDX) for local and area distribution analyses of elements. Secondary electron (SE) imaging of the samples surfaces was performed in high vacuum mode using acceleration voltages of 1 kV, whereas qualitative EDX analysis were carried out in wet-mode at accelerating voltages of 5 kV, 10 kV and 20 kV, respectively. For both cases no additional coating of the sample surface was done because charging is not an issue for the chosen imaging conditions. For an acceleration voltage of 1 kV, the penetration of the incident electron beam is in the order of a few tens of nanometers for the materials in question, therefore, in addition to standard high acceleration voltage scanning electron microscopy, SE images acquired at 1 kV acceleration voltage show surface features in more details, even at high magnification, whereas wet mode renders EDX analysis without coating of non- conductive samples unnecessary.

Samples were embedded in epoxy resin and cut at room temperature to obtain cross sectional pictures of the polymer particles.

## 5.3 Results and Discussion

### 5.3.1 Equilibrium propylene and hexane

It is assumed that the gas and liquid phases are in equilibrium during the polymerization. Equilibrium data of the hexane-nitrogen-propylene system are needed in order to calculate the amount of propylene present in the reactor from the reactor pressure. Measurements were performed without catalyst components using equations 1, 3 and 4. Figure 5.4 shows that the equilibrium can be well described by Henry's.

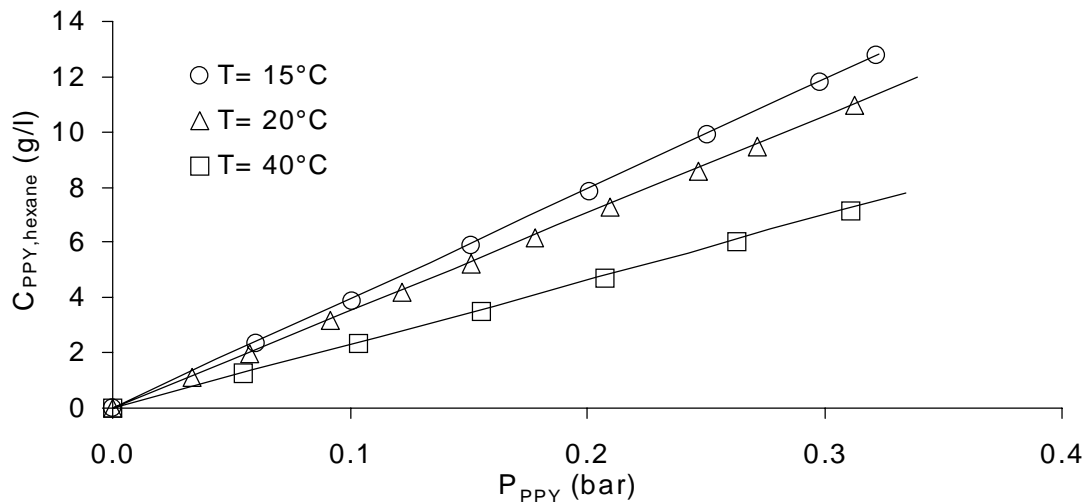


**Figure 5.4** Solubility of propylene in hexane at various temperatures. The markers were obtained from measurements, the lines resulted from HYSYS-calculations, with the Peng-Robinson EOS.

HYSYS calculations, also shown in this figure, show excellent agreement with these measurements. The Henry's-law coefficient describing the equilibrium was determined at different temperatures, and it was shown that the temperature dependence of this coefficient can be modeled linearly over the narrow range of temperatures of interest in this work:

$$H = 0.221 \cdot T - 55.32 \quad (\text{eq. 5.6})$$

This relation was then used to translate data on reactor pressure to amounts of monomer by using equations 5.1 to 5.4.

### 5.3.2 Pre-polymerization kinetics

As mentioned before, the kinetic data presented here are the result of different monomer injections within the same experiments. In the initial stage after monomer injection, the pressure decrease is used to calculate the reaction rate in that stage of the experiment. As pressure becomes extremely small in the final stage of the pulse, calculations are no longer reliable.

**Table 5.1** Overview experiments presented in this work.

Exp. [-]	Temperature [°C]	Duration [min]	Catalyst [mg]	Al/Ti [mole/mole]	Al/Si [mole/mole]	#pulses [-]	PPY [mg]	YPP [g/g]
1	20	140	151.1	11.9	3.4	4	921	6.10
2	20	120	150.3	11.9	3.3	3	691	4.60
3	20	140	151.4	11.7	3.4	4	921	6.08
4	20	180	150.1	11.8	3.2	6	1500	9.99
5	20	130	600.3	11.8	3.4	2	192	0.32
6	20	130	300.4	11.8	3.4	2	219	0.73
7	20	100	88.0	10.4	3.3	3	397	4.51
8	20	165	151.5	11.9	3.3	8	1050	6.93
9	20	75	150.2	11.8	3.3	1	301	2.00
10	20	150	152.0	11.6	3.2	3	744	4.89
11	20	150	150.1	11.8	3.3	4	1701	11.33
12	20	240	150.0	11.8	3.4	5	3136	20.91
13	20	75	151.0	11.9	3.4	1	454	3.01
14	20	120	150.8	11.8	3.4	8	935	6.20

Although a total of approximately 40 experiments were performed in this study, we will only present the results of the 14 most illustrative runs here for reasons of clarity. Nevertheless, it should be pointed out here that the results presented below are representative of all the experiments. The recipes and experimental conditions used in these tests are shown in Table 5.1. It can be seen from this table that the amount of monomer used per injection, and the amount of catalyst used in each experiment vary over a relatively wide range. This was done in order to obtain a large variation in the final values of YPP and reaction times. However, the Al/Ti and Al/Si ratios were kept constant at 12 and 3.4 mole/mole respectively in all experiments.

### 5.3.3 Typical pressure curve

A typical curve is shown in Figure 5.3 for the reactor pressure over time. It can be seen that the pressure rises with monomer injection, and then drops due to consumption of the monomer. On the right hand side of this same figure, it can be seen that the final pressure does not return to the initial pressure before injection. This is due to two factors:

- Formation of the polymer. The solid polymer material will occupy reactor volume and will cause a pressure increase with increasing yield. This will give an increase in pressure of about 30 Pa per injection.

- Injection of inert gases with monomer. The injected propylene contains about 0.5% propane and some various amount of solved nitrogen due to transport of the liquid propylene with nitrogen at elevated pressures. This will cause a momentary increase of reactor pressure with monomer injection. This will give an increase in pressure of about 25 Pa per injection.

Corrections in the pressure measurements were made for these two factors, and are taken into account in the kinetic data presented here. The polymer volume will increase with YPP and with time, and the pressure increase due to inert gases occurs directly after each monomer injection.

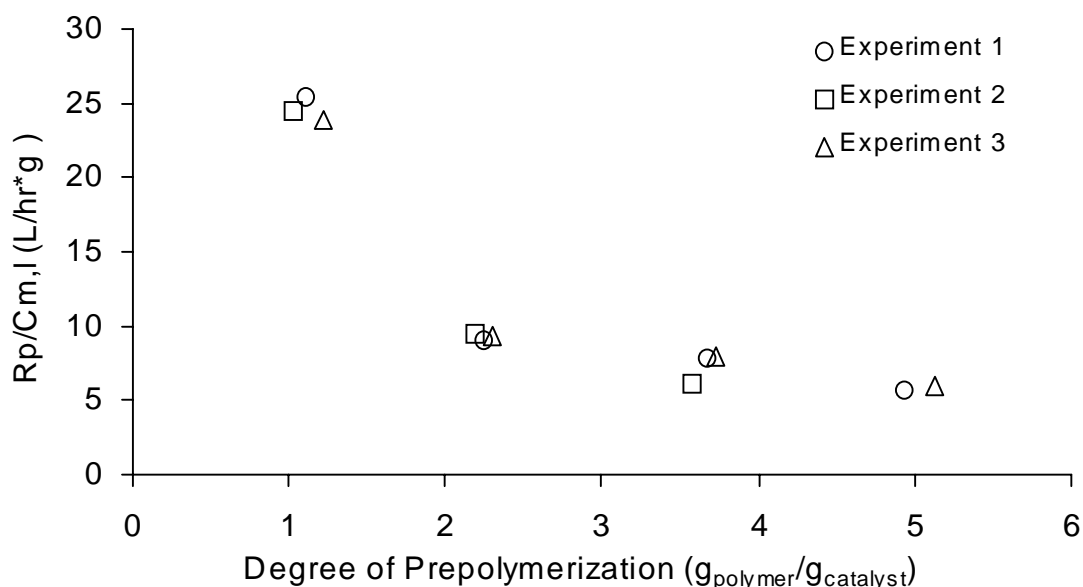


**Figure 5.5** An indication for the reproducibility of the kinetic results. The four experiments were exactly the same in method and recipe.

### Reproducibility

The reproducibility of the polymerization kinetics was examined by performing three experiments with the same procedure and recipe (experiments 1,2 and 3 in Table 5.1). Figure 5.5 shows the kinetic results calculated from these experiments. The reaction rate, corrected for the monomer concentration in the bulk was plotted versus YPP. It can be seen that the results are highly reproducible, despite the extremely low reaction rates. The reaction rate decreases with increasing YPP, and appears to be of first order with respect to monomer concentration. A calculated standard deviation of the data from the first monomer pulse gives 0.76. The maximum deviation in Figure 5.5 is 6%. The reason for plotting the reaction rate versus the YPP values, instead of plotting it versus time, are described below.

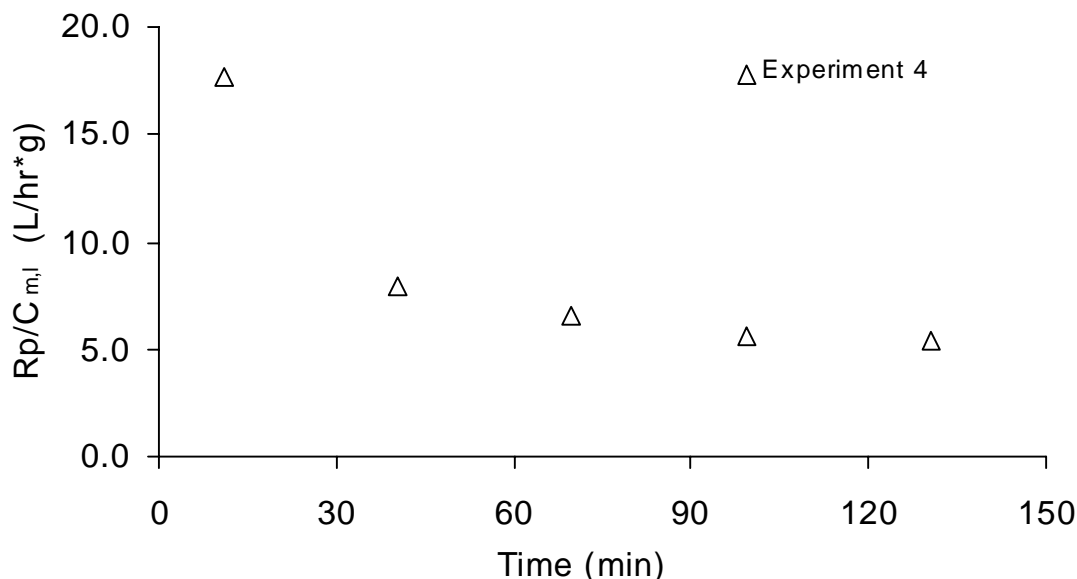


**Figure 5.6** Typical time dependence of the reaction rate corrected for monomer concentration during pre-polymerization experiment.

#### Relation reaction rate and time

Figure 5.6 shows the development of the reaction rate corrected for the monomer concentration related to reaction time. It is clear that the reaction rate decreases strongly in the course of an experiment. There can be a number of different causes for this behavior, of which chemical deactivation of the active sites, caused for example by over-reduction of titanium sites by the aluminum alkyl, might be one. If a chemical process was causing the decreasing reaction rate one would expect a clear relation between this deactivation and reaction time. In the literature, a simplified model is often used to describe the kinetics of these polymerization reactions, e.g. Meier<sup>[14]</sup> or Samson et al.<sup>[15]</sup>. In the model used in these two papers, the propagation rates of the different active sites are lumped into a single propagation parameter and the different deactivation mechanisms are lumped into a single deactivation parameter. The reaction rate is represented as:

$$R_p = k_p \cdot C_m^n \cdot C^* \quad \text{or} \quad \frac{R_p}{C^*} = k_p \cdot C_m^n \quad (\text{eq. 5.7a and b})$$

with an Arrhenius temperature dependence of the propagation constant:

$$k_p = k_{p,0} \cdot e^{(E_{a,p}/RT)} \quad (\text{eq. 5.8})$$

where  $k_p$  is the propagation rate constant,  $E_{a,p}$  is the activation energy for the lumped propagation reactions,  $T$  is the temperature,  $C_m$  represents the concentration of the monomer at the active site and  $C^*$  is the concentration of the active centers. In many studies, the reaction rate has been confirmed to follow a first-order dependence with



respect to the monomer concentration. The decay of the catalyst is described by a decreasing number of active centers with time, according to the following mathematical equation that has only an empirical meaning:

$$-\frac{dC^*}{dt} = k_d (C^*)^q \quad (\text{eq. 5.9})$$

with an Arrhenius type of temperature dependence of the deactivation constant  $k_d$ :

$$k_d = k_{d,0} \cdot e^{(E_{a,d}/RT)} \quad (\text{eq. 5.10})$$

where,  $q$  is the order of deactivation,  $E_{a,d}$  is the activation energy for the lumped deactivation reactions. Combination of equations 5.7 and 5.9 leads to:

$$-\frac{dC^*}{dt} = k_d \left( \frac{R_p}{k_p \cdot C_m^n} \right)^q \quad (\text{eq. 5.11})$$

After integration assuming isothermal conditions and first order deactivation ( $q=1$ ), the expression for the reaction rate as function of time is given by:

$$R_p = R_{p,0} \cdot e^{-k_d t} \quad (\text{eq. 5.12})$$

with

$$R_{p,0} = k_{p,0} \cdot e^{-E_{a,d}/RT} \cdot C_0^* \cdot C_m \quad (\text{eq. 5.13})$$

with  $C_0^*$  being the initial concentration of active sites.

In the experiments shown here, the monomer concentration is not constant over time. When assuming a first order dependence of reaction rate in monomer concentration (i.e.  $n = 1$ ) the kinetics - being the product of  $k_p$  and  $C^*$  - can be evaluated by using  $R_p/C_m$  in the kinetic plots, as shown in equation 5.7b.

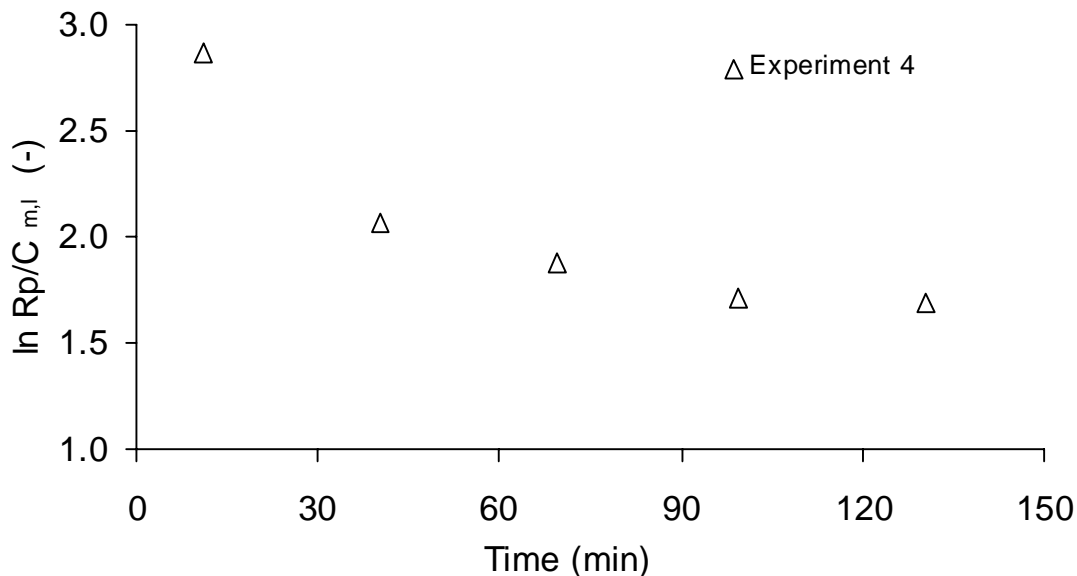


**Figure 5.7** Assuming a first order deactivation behavior in time, the relation between the natural logarithm of reaction rate and time should be linear, which it is not.

If the deactivation of the catalyst observed in these experiments could be described with the model presented above, a linear relation should exist between the natural logarithm of the reaction rate corrected for the monomer concentration and time. However, it is shown in Figure 5.7 that no such linearity exists. The decrease of corrected reaction rate with time is relatively strong in the initial stage, but levels off and finally becomes zero. A time defined process, such as a chemical reaction does not seem to be the main reason for the decreasing reaction rate.

In this work, a number of experiments were carried out using different quantities of catalyst and varying sizes of the monomer pulses to the system. Figure 5.8 shows a graph of the corrected rates versus experimental time for 3 such experiments. It can be seen here that the decay in reaction rate is not determined by reaction time. A factor of at least 5 exists between reaction rates observed at catalyst amount of 90 mg, compared to a catalyst amount of 300 mg, despite the fact that the reaction rate is expressed per amount of catalyst.

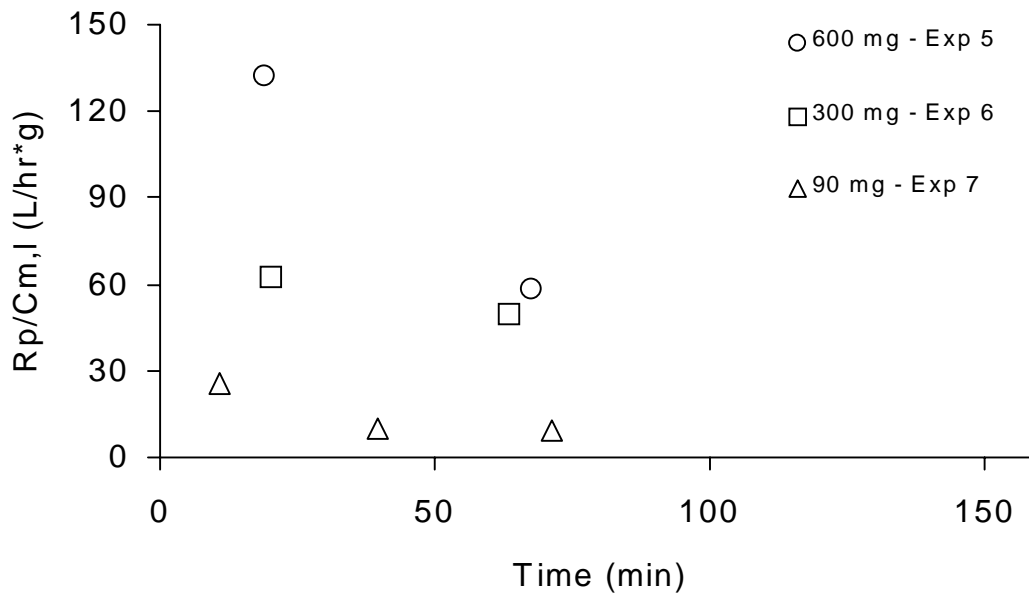


**Figure 5.8** Reaction rate corrected for monomer concentration versus the time of pre-polymerization for three different amounts of catalyst.

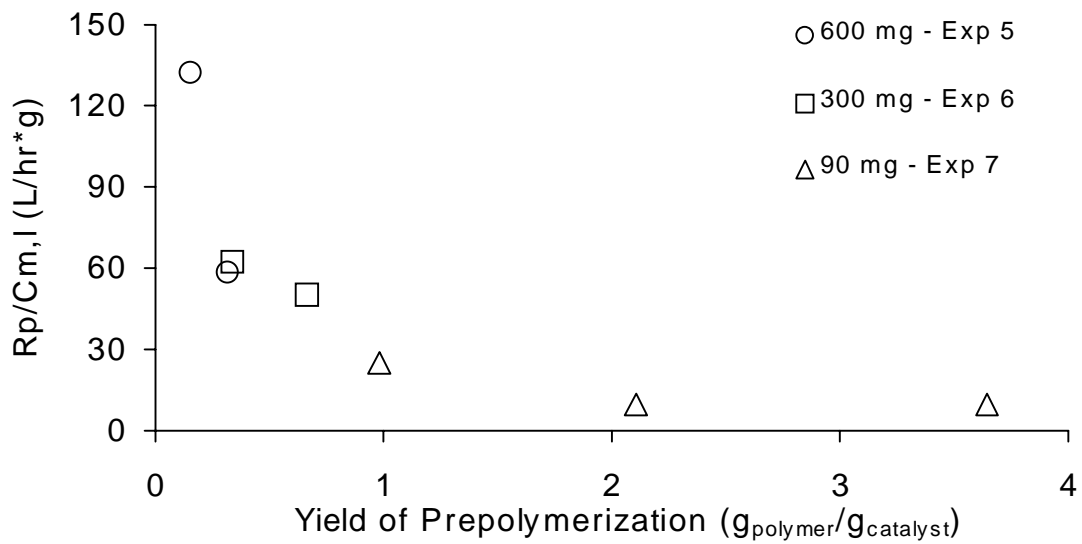


**Figure 5.9** Reaction rate corrected for monomer concentration versus the yield of pre-polymerization for three different amounts of catalyst.

### Relation reaction rate and yield of pre-polymerization (YPP)

If the same experiments are plotted in relation to the yield of pre-polymerization, as done in Figure 5.9, we can see that the three experiments show exactly the same behavior. Recall that the experiments shown in this figure have very different reaction time – YPP behaviors. Figure 5.10 shows the increase of the YPP values versus time for the different experiments. Despite these differences, the experiments show a similar deactivation behavior, suggesting that the decay in reaction rate depends on the amount of polymer produced in the catalyst particle, not on the reaction time.

Complicating the explanation of the experimental observations is the fact that when

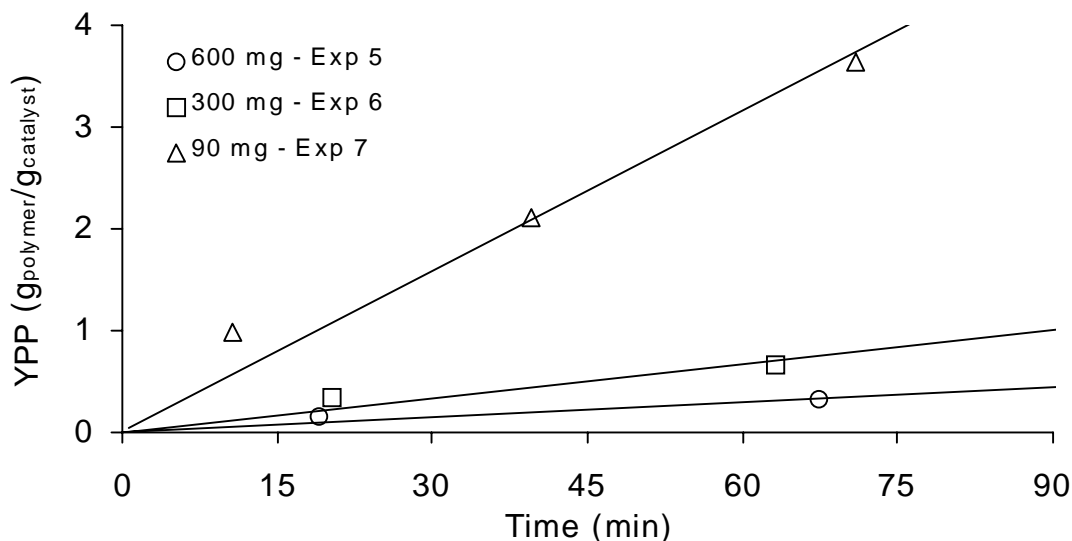


**Figure 5.10** Relation between yield of pre-polymerization and time for the different experiments. The overall reaction rate for an experiment, including a number of monomer injections - so the slope of the lines - was varied over a wide range in these experiments.

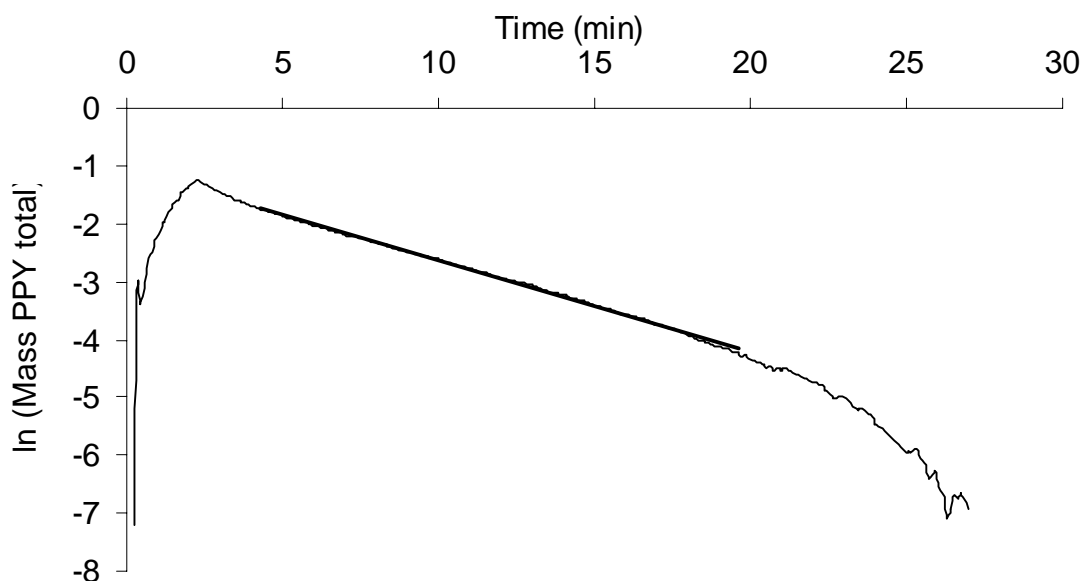


**Figure 5.11** The natural logarithm of the amount of monomer plotted versus time. The linear behavior up to more than 90% conversion does not agree with the decreasing reaction rates with increasing YPP values.

plotting the monomer-corrected reaction rates of a single injection versus time, a constant slope is obtained.

Despite the fact that the YPP value is increasing, the reaction rate does not decrease during this single peak, but rather decreases over the course of different peaks. This effect can be illustrated when the integral method for kinetic evaluation is used, instead of the differential method. The natural logarithm of the amount of propylene present in the system is plotted versus time in Figure 5.11. It can be seen that after stopping the injection and coming to equilibrium, a linear relation is obtained. At very low reaction rates (i.e. where more than 90% of the monomer initially present has then been consumed), the linearity disappears. In the linear stage, the reaction rate does not decrease with increasing YPP. A possible explanation for this would be the presence of fast reacting impurities in the propylene, resulting in reduced activity after every injection. But as the reaction rate becomes constant at higher YPP values, and no longer decreases upon injection of fresh monomer, this cannot be the case.

Two different mechanisms were proposed to explain the decreasing reaction rate with increasing YPP. It is generally accepted that the catalyst as used here is sensitive to 2,1-insertions of propylene, resulting in a dormant state of the active sites. As the initial propagation frequency in these experiments is on the order of 0.1 to 10 monomer molecules per second, one could imagine that the decay of catalyst activity with increasing yield in the early stage of the polymerization reaction could be the result of an increasing number of active sites blocked by 2,1-inserted monomer. In the initial stage of the experiment, the number of dormant sites increases with increasing YPP, but at higher YPP values, all the sites that are sensitive to 2,1-insertions are dormant and the activity of the overall-catalyst reaches a constant level. If this mechanism is the reason for the strong catalyst decay in the initial stage, the phenomenon should disappear, or should at least be significantly diminished, in the presence of a chain transfer agent like hydrogen. The hypothesis was tested in an experiment in the presence of hydrogen. In this experiment the hydrogen concentration was about 10 volume percent in gas phase, and thus well within the range where hydrogen concentration normally does not affect the reaction rate. The result of this run, experiment 14, is shown in Figure 5.12. It is clear that the activity in the presence of hydrogen is significantly higher than in the absence of the hydrogen, but both curves seem to show the same initial reaction rate. With hydrogen present, the decay seems to be less strong and therefore come to a higher final value. It is therefore possible that the number of dormant sites increases with increasing YPP in the absence of hydrogen, and that this effect is prevented in experiment 14. However, even in presence of hydrogen the effect of the decreasing activity with increasing YPP, especially for YPP values below 2 to 4 g/g is similar. Therefore, another explanation for these observations must be found.

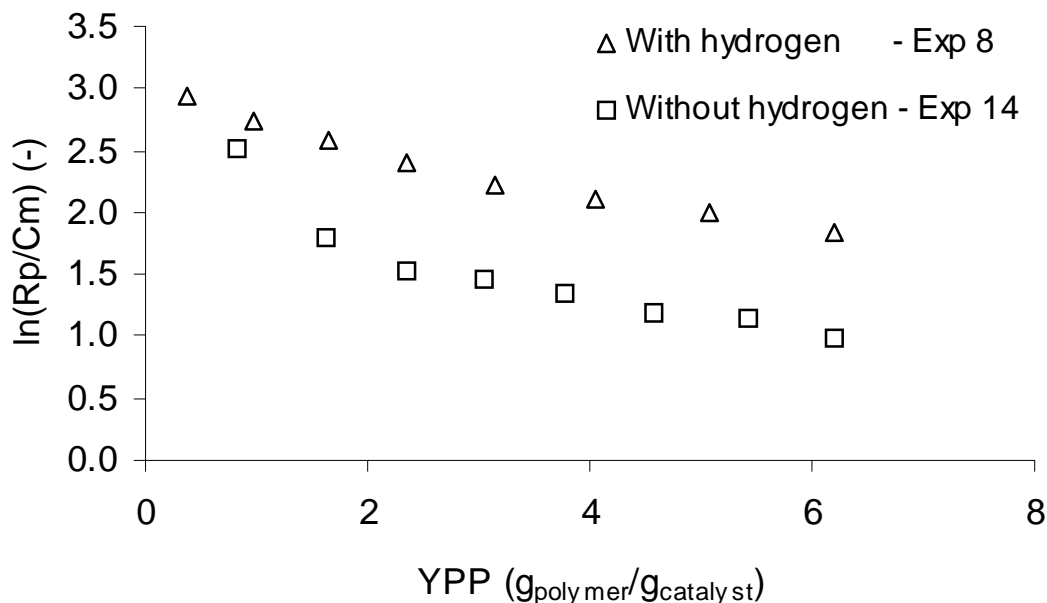


**Figure 5.12** Influence of hydrogen on activity and deactivation in the polymerization experiment. It can be seen that the decay in reaction rate is not changed by the introduction of the hydrogen.

Another explanation for the decrease in reaction rate in the early stage of the polymerization is the 'phase transition' that the growing particle undergoes during this period. Initially, the particles are made up essentially of support material, and only a small amount of polymer is present in the matrix. With increasing YPP, the particle is gradually transformed from a "support-dominated" material to a polymer particle with small amounts of catalyst. This significant change in morphology and the change of the kinetics seem to occur at the same time. To the best of our knowledge, no description of this behavior appears in the literature on catalytic olefin polymerization. This 'phase transition' could influence different factors in the polymerization process.

- The active site of the catalyst is formed by an interaction between the external electron donor, the cocatalyst and the catalyst itself. One could easily imagine that large amounts of polymer produced at this site could very well change this interaction, and with that, the kinetic behavior of the site. This diluting effect caused by the polymer could play a role in the decreasing reaction rates.
- Another factor that is changing with the 'phase transition' is the monomer concentration at the active site. If we assume that a fresh, initially active site is surrounded by hexane with a bulk monomer concentration, the concentration at the active site equals this bulk concentration. With progressing polymerization, the number of active sites surrounded by polymer is increasing. For the active sites surrounded by polymer, it holds that the concentration of monomer at the active site equals the monomer

concentration sorbed in the polymeric phase. So, with an increasing YPP, the number of active sites seeing a low monomer concentration is increasing and results in a decreasing reaction rate.

If the changes in morphology and in kinetics come together in the initial stage of polymerization, this effect should be present in all polymerization reactions with this type of catalyst. But as reaction rates are normally some orders of magnitude larger than the reaction rate used here, and almost all methods used to measure reaction rates are unreliable in the unstable initial stage of the experiment, this effect can not be observed there.

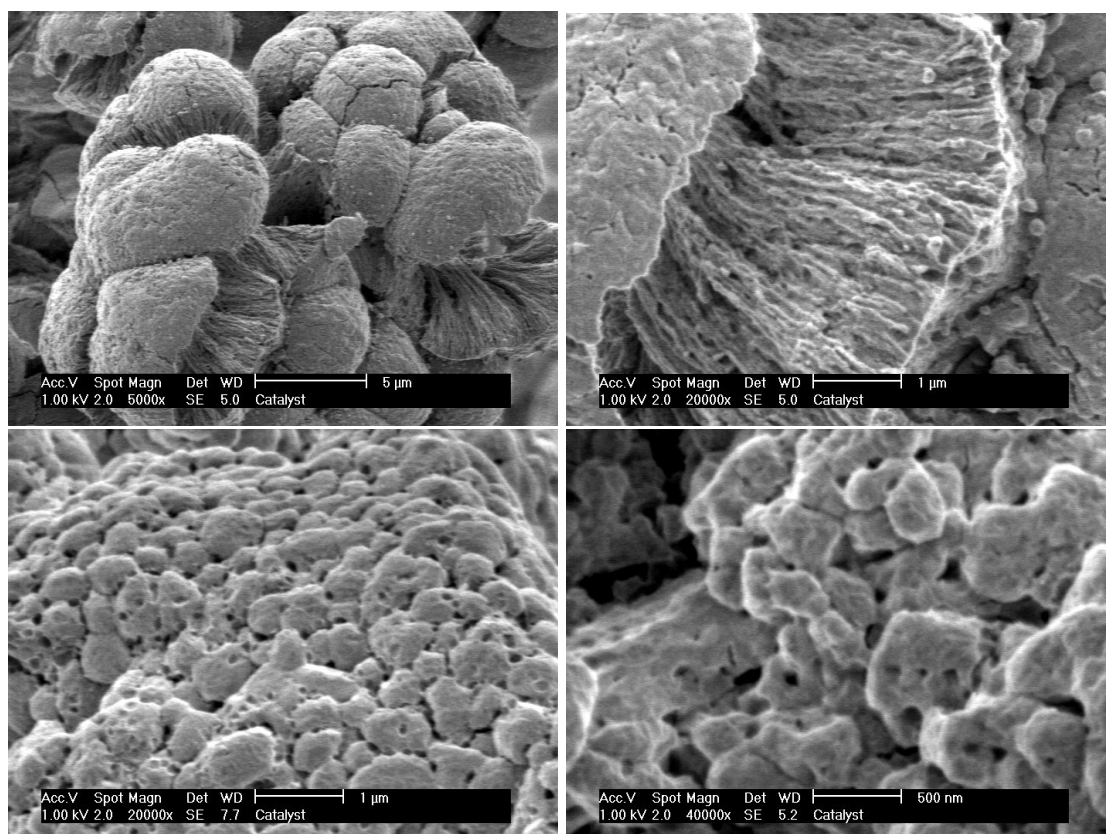


**Figure 5.13** These SEM pictures show the structure of the catalyst material used in the experiments.

#### 5.3.4 Morphology of polymer particles

The powders produced in the experiments presented above were analyzed with electron microscopy. SEM micrographs were made of the outer surface of the particles to show the developing shape of the particles, and to see the particle sizes. In addition, some particles were embedded in an epoxy resin and cut to allow imaging of the cross sectional surface of the polymer particles.

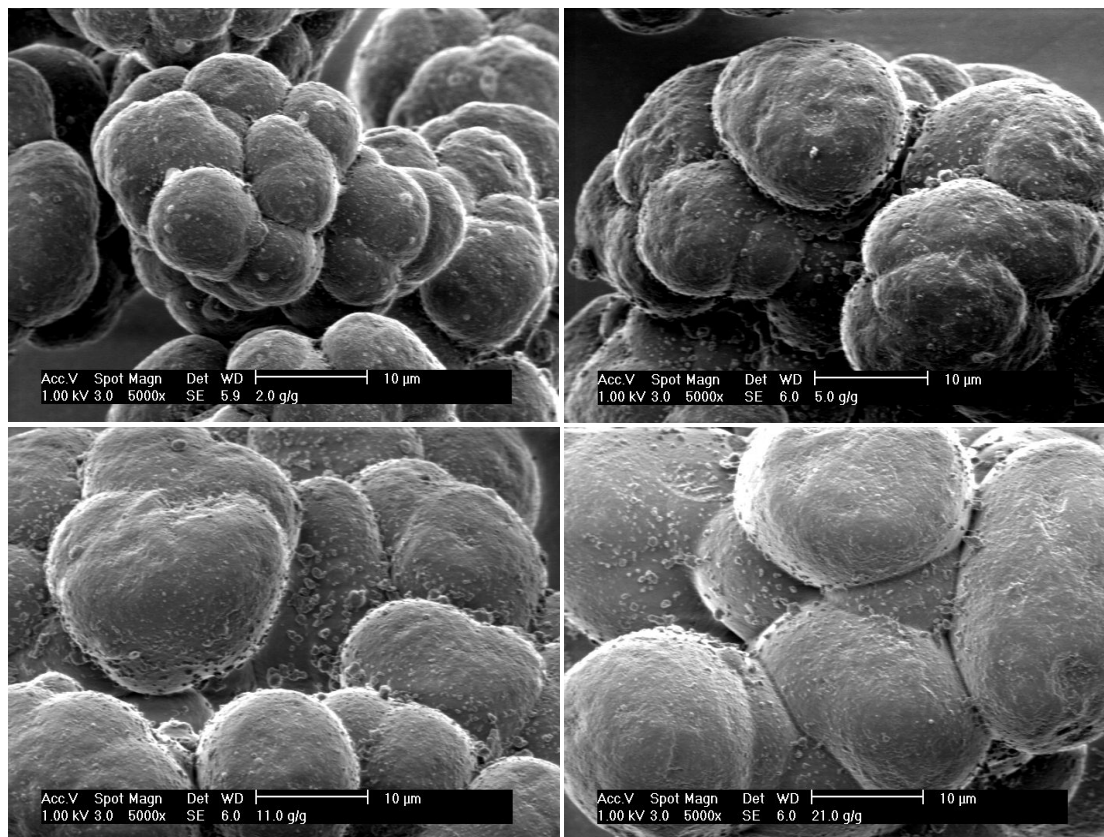


**Figure 5.14** SEM pictures of pre-polymerized catalyst particles, with respectively a yield of pre-polymerization of 2, 5, 11 and 21 g/g.

Figure 5.13 shows the SEM pictures of the catalyst material. The structure of the catalyst support can be easily seen. The material is very porous and the radial pores with diameters around 0.1 micron are clearly visible. The catalyst particles appear to be made up of 15 to 30 smaller spheres. The catalyst particles are around 25 microns in diameter, with the diameter of the smaller spheres on the order of 5-10 micron.

**Table 5.2** Development of theoretical particle size of the sub-particle with increasing YPP, based on  $\rho_{cat}=2.32$ ,  $\rho_{pol}=0.9$   $r_{part,0}=5$  micron and constant porosity.

YPP [g <sub>PP</sub> /g <sub>cat</sub> ]	Radius [micron]	Volume <sub>particle</sub> [micron <sup>3</sup> ]	Volume <sub>catalyst</sub> [micron <sup>3</sup> ]	Volume <sub>polymer</sub> [micron <sup>3</sup> ]
0	5.0	524	524	0
1	7.6	1873	524	1350
2	9.2	3223	524	2699
3	10.3	4573	524	4049
5	12.0	7272	524	6748
7	13.4	9971	524	9448
10	15.0	14020	524	13497
15	17.1	20769	524	20245
20	18.7	27517	524	26994
30	21.4	41014	524	40490
40	23.5	54511	524	53987
50	25.3	68008	524	67484



Figure 5.14 shows the particles after polymerization. The particle sizes obviously increase due to the accumulation of polymer. The four pictures in Figure 5.14 show particles with YPP values of 2, 5, 11 and 21 gram polymer per gram catalyst. There is a high degree of replication, as the shape of the polymer particles is almost identical to the shape of the initial catalyst particles. The smaller spheres from which the particle is made up can clearly be recognized. The size of the particles systematically increases with increasing YPP, as shown in Table 5.2.

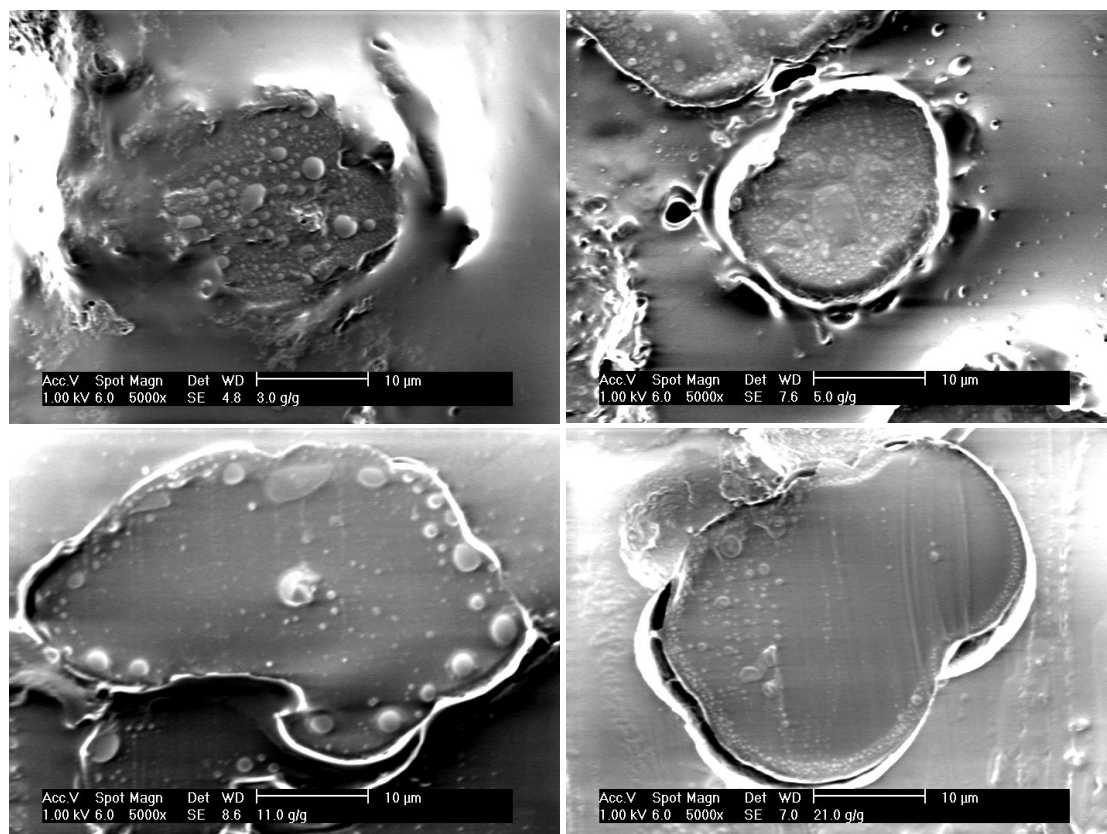


**Figure 5.15** Cross sectional SEM pictures of pre-polymerized catalyst particles with yield of pre-polymerization of respectively 3, 5, 11 and 21 g/g.

The SEM images in Figure 5.15 show the cross sectional surface of the polymer particle after cutting; the sphere shown on the picture of the cross sectional cut is one of the spheres of which the particle is composed.

Two phases can be recognized in the cut surfaces. The gray, continuous phase is assumed to be polymer material, the drop-like heterogeneous phase with the lighter color is believed to be support material. There are several arguments for this explanation. The ratio between the amount of homogeneous and heterogeneous phase is, within the possible accuracy of such 2-dimensional surface determination, in accordance with the values for YPP. Preliminary EDX tests also showed a high concentration of magnesium in the light colored areas and, when electron microscopy was performed in the presence of an oxygen-containing atmosphere, these areas changed color rapidly and a salty structure appeared in the light colored areas.

It can also be seen that the support fragments decrease in size with increasing YPP values. It seems as if fragmentation of the catalyst is continually progressing in the stage we visualized here. One thing that is remarkable is the place where the fragments are located in the growing particles. The fragments seem to drift to the outside of the particles. Although the part of the particle visualized here is not the same level that Cecchin et al.<sup>[11]</sup> show, the mechanism for the catalyst material convecting towards the surface of the particle seems to be the same. The process described by them for the subglobule seems to be present on a larger scale here. It would need TEM analysis of these samples to visualize the catalyst fragments after fragmentation (microparticles, in Cecchin's terms), to know where they are located.

Thus, in contrast to other fragmentation models described in literature by Ferrero and Chiovetta<sup>[1-5]</sup>, the fragmentation of the support used here does not proceed shell-by-shell from the outside of the particle towards the center. Rather, the particle seems to break into large fragments first, and subsequently with progressing polymerization the fragments increase in number and decrease in size. In later work related to this subject (Ferrero et al.<sup>[5]</sup>) an experimental study is shown with polymer powders with YPP values between 29 and 114 gram/gram, obtained in slurry polymerization in heptane. It is mentioned in their work that with the experimental data obtained it was not possible to confirm nor to disprove the sequential layer by layer type of fragmentation. We think that the fragmentation model can be disproved by the data shown here, at least for the catalyst and the reaction conditions used here.

Of course, one has to keep in mind that the pictures shown here are not pictures in a continuous series. The different experiments used to reach different YPP values differ from each other in monomer concentrations and therefore in reaction rates. One can imagine that fragmentation behavior depends on reaction rate. It is therefore hard to conclude that particles in, for example, low temperature liquid pool polymerization typical of industrial pre-polymerization conditions will look like the particles shown here. Reaction rates under those conditions are typically in the order of a few kilogram of polymer per gram catalyst and hour, so much higher than reaction rates used here. To be able to make an even more meaningful comparison, one should use a stopped flow method in liquid pool conditions, to be able to stop the polymerization reaction after seconds, and thus to produce particles with YPP values comparable to the ones shown here.

#### Formation of the wax-like material

In the pictures of the particles with low YPP values, below 3 g/g, a wax-like material can be observed on the surface of the particles. When this substance was observed, it was very difficult to cut the particles we embedded in resin for cross-sectional examination by SEM as the cut surface was always located within this wax-like layer, and not across the polymer particle. In experiments yielding in higher YPP values this problem was not present. An explanation for the formation of this material is given in

the monomer concentration. Because of the fact that monomer concentration is not constant during the polymerization experiments and polymer properties will depend on the monomer concentration during polymerization, it is hard to quantify the monomer concentration for a specific polymer product, for a specific YPP value. Here the average monomer concentration as defined by the formula in equation 5.14 is used to characterize the monomer concentration during the experiment. An experiment with a high initial monomer concentration after a large injection of monomer also has a rate curve with a low activity tail caused by low monomer concentration. Because the amount of polymer produced at a certain monomer concentration is important in order to understand the molecular weight, we used the 'yield average monomer concentration',  $C_{m,Yield}$ , as an indication of the "average" monomer concentration in a given experiment:

$$C_{m,Yield} = \frac{\sum (Yield_j * C_{m,j})}{\sum Yield_j} \quad (\text{eq. 5.14})$$

where  $Yield_j$  represents the amount of polymer produced in a certain interval at monomer concentration  $C_{m,j}$ . For the experiments shown here, the yield average monomer concentrations (YAMC) are shown in Table 5.3. It can be seen that in experiments designed to produce a final powder with low YPP values, the values for YAMC were much lower than the YAMC-values in experiments resulting in high YPP values.

**Table 5.3** Values for Yield average monomer concentration in experiments with shown SEM pictures, related to YPP values obtained in those experiments.

Exp. [-]	YPP [g/g]	Yield average monomer concentration [g/L]			
		Pulse 1	Pulse 2	Pulse 3	Pulse 4
9	2.0	0.24	-	-	-
10	4.9	0.17	0.32	0.45	-
11	11.3	0.31	0.60	0.58	0.86
12	20.9	0.28	0.54	0.60	0.60
13	3.0	0.57	-	-	-

These low values for YAMC might be the main cause for the formation of the waxy product with a poor stereospecificity. Figure 5.16 shows the DSC curves of the polymer products with low YPP values and that of polymer with a high YPP value. The additional peak at 115°C is expected to be caused by the atactic material, produced at the low monomer concentration in the experiments with low YPP-values.

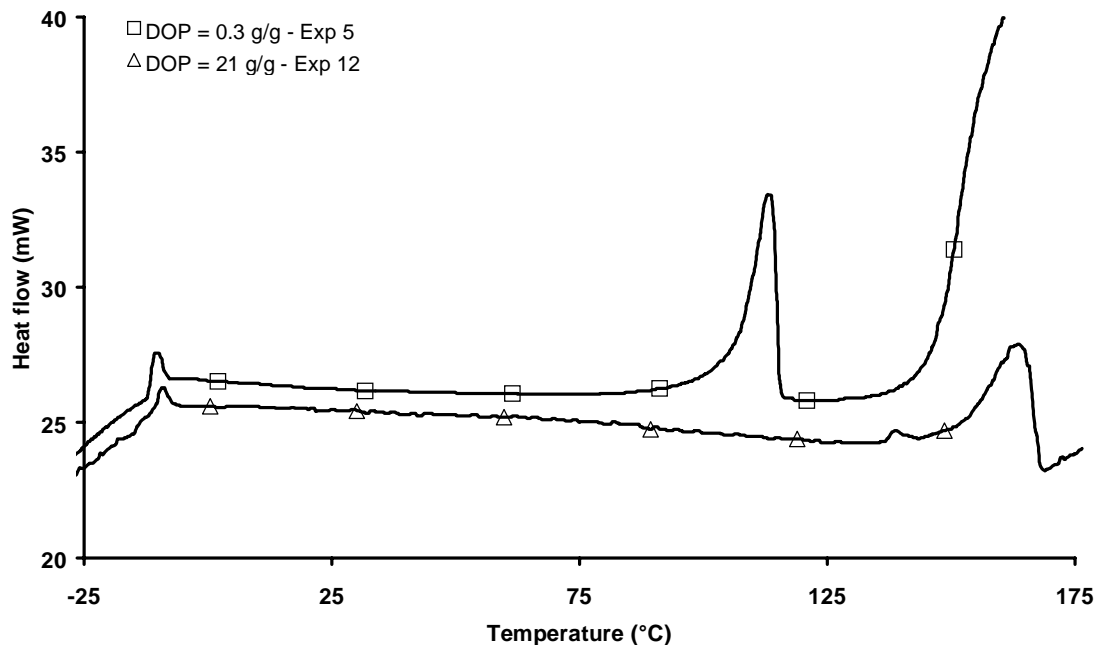


**Figure 5.16** DSC curves of polymer products with low and with high YPP values.

#### 5.4 Conclusions

The experimental method demonstrated in this paper has been shown to be a useful tool to investigate the processes implicated in the very early stage of catalyzed olefin polymerizations. The kinetics can be measured with a high reproducibility and, because of the good control of the polymerization rate, the reaction can be stopped at well defined, low yields. It is shown that in the very early stage of the polymerization of this type of catalyst, the reaction rates drop significantly with increasing yield of pre-polymerization (YPP). It is expected that this behavior is related with the changing morphology in this early stage and that it is present in all polymerizations with this type of catalyst. It is difficult to observe this type of behavior and to do this type of experiment with conventional polymerization equipment because of the extremely high reaction rates observed during typical polymerization procedures. In the experiments presented here, reaction rates become stable with increasing YPP after reaching a value of about 2 to 4 gram polymer per gram catalyst.

The SEM pictures of the cross sectional areas of the polymerized particles suggest that the "layer-by-layer" fragmentation models proposed in literature do not adequately describe fragmentation of the catalyst used in this work under our experimental conditions.

To be able to draw conclusions on fragmentation behavior at higher reaction rates, it is necessary to carry out stopped flow polymerizations in liquid propylene. The

powders obtained from such experiments should be investigated the same way as done here. It is not possible to measure kinetics in the initial stage of the polymerization that way, but it should clarify the reaction rate dependency of the fragmentation mechanism.

Acknowledgements - The work presented in this paper was carried out in corporation with The Dow Chemical Company, Freeport (TX), USA. I want to thank Dow for both the financial and the intellectual input. The aluminum alkyls used in the work were kindly donated by Witco GmbH, Bergkamen, Germany. This work would not have been completed without the experimental work carried out by Suzanne Huibers, Harriët Workel and Jantina de Waal. In addition, the technical assistance of Fred ter Borg, Karst van Bree and Geert Monnik of the High Pressure Laboratories is gratefully kindly acknowledged.

## Notations

$C^*$	Concentration of active sites	(mole/g)
$C_m$	Concentration of monomer	(g/L)
$C_{m,Yield}$	Yield average monomer concentration	(g/L)
$E_{a,p}$	Activation energy for the lumped propagation reactions	(J/mole)
$E_{a,d}$	Activation energy for the lumped deactivation reactions	(J/mole)
$H$	Henry's-law coefficient	(bar)
$k_d$	Deactivation rate constant	(hr <sup>-1</sup> )
$k_p$	Propagation rate constant	(L/mole· hr)
$m$	Mass	(g)
$n$	Order of propagation	-
$q$	Order of deactivation	-
$P$	Pressure	(bar)
$P^0$	Saturated vapor pressure	(bar)
$R$	Gas constant	(J/mole· K)
$R_p$	Reaction rate of polymerization	(g/g· hr)
$T$	Temperature	(K)
$t$	Time	(hr)
$x$	Mole fraction	-
Yield <sub>j</sub>	Amount of polymer produced in interval j, with $C_{m,j}$	(g)

### Subscripts:

$0$	Initial, at time = 0	<i>catalyst</i>	catalyst
<i>hex</i>	o hexane	$R$	Reactor
<i>ppy</i>	propylene		

*List of abbreviations*

D-donor	Di-cyclopentyl di-methoxy silane	SEM	Scanning Electron Microscopy
EDX	Energy dispersive x-ray	TEA	Tri ethyl aluminum
PP	Polypropylene	YAMC	Yield average $C_m$
PPY	Propylene	YPP	Yield of Pre-polymerization

**References**

- [1] Ferrero, M.A., & Chiovetta, M.G. (1987a). 'Catalyst Fragmentation during Propylene Polymerization: Part I. The Effects of Grain Size and Structure', *Polymerization Engineering Science*, **27**, 1436-1447.
- [2] Ferrero, M.A., & Chiovetta, M.G. (1987b). 'Catalyst Fragmentation during Propylene Polymerization: Part II. Microparticle Diffusion and Reaction Effects', *Polymerization Engineering Science*, **27**, 1448-1460.
- [3] Ferrero, M.A., & Chiovetta, M.G. (1991a). 'Effects of Catalyst Fragmentation during Propylene Polymerization. IV. Comparison between Gas Phase and Bulk Polymerization Processes', *Polymerization Engineering Science*, **31**, 904-911.
- [4] Ferrero, M.A., & Chiovetta, M.G. (1991b). Catalyst Fragmentation during Propylene Polymerization. III. Bulk Polymerization Process Simulation', *Polymerization Engineering Science*, **31** (12), 886-903
- [5] Ferrero, M.A., Koffi, E., Sommer, R., & Conner, W.C. (1992). 'Characterization of Changes in the Initial Morphology for  $MgCl_2$ -supported Ziegler-Natta Polymerization Catalysts', *Journal of Polymer Science: Part A. Polymer Chemistry*, **30**, 2131-2141.
- [6] Lawrence, R.L., Chiovetta, M.G., (1983). 'Heat and Mass Transfer during Olefin Polymerization from the Gas Phase", *Polymer Reaction Engineering*, edited by K. H. Reichert and W. Geiseler, 73-112, Hanser, Munich.
- [7] Kakugo, M., Sadatoshi, H., Yokoyama, M., & Kojima K. (1989). 'Transmission Electron Microscopic Observation of Nascent Polypropylene Particles using a New Staining Method. *Macromolecules*, **22**, 547-551.
- [8] Kakugo, M., Sadatoshi, H., Sakai, J., & Yokoyama, M. (1989). 'Growth of Polypropylene Particles in Heterogeneous Ziegler-Natta Polymerization', *Macromolecules*, **22**, 3172-3177.
- [9] Noristi, L., Marchetti, E., Baruzzi, G., & Sgarzi, P. (1994). 'Investigation on the Particle Growth Mechanism in Propylene Polymerization with  $MgCl_2$ -supported ZN Catalysts', *Journal of Polymer Science: Part A. Pol. Chem.*, **32**, 3047-3059.

- [10] Ferrero, M.A., Sommer, R., Spanne, P., Jones, K.W., & Conner, W.C. (1993). 'X-Ray Microtomography Studies of Nascent Polyolefin Particles Polymerized over Magnesium Chloride-supported Catalysts', *Journal of Polymer Science: Part A. Polymer Chemistry*, **31**, 2507-2512.
- [11] Cecchin, G., Marchetti, E., & Baruzzi, G. (2001). 'On the Mechanism of Polypropylene Growth over MgCl<sub>2</sub>/TiCl<sub>4</sub> Catalyst Systems', *Macromolecular Chemistry and Physics*, **202**, 1987-1994.
- [12] Weickert, G., Meier, G.B., Pater, J.T.M., & Westerterp, K.R. (1999). 'The Particle as Microreactor: Catalytic Propylene Polymerizations with Supported Metallocenes and ZN Catalysts.' *Chemical Engineering Science*, **54**, 3291-3296.
- [13] Moore, E.P. (1996). 'Polypropylene Handbook', Hanser Publishers, Munich Vienna New York, 11-14.
- [14] Meier, G.B. (2000). 'Fluidized Bed Reactor for Catalytic Olefin Polymerization', Ph.D. thesis at University of Twente, 5-35.
- [15] Samson, J.J.C., Weickert, G., Heerze, A.E., & Westerterp, K.R. (1998). 'Liquid-phase Polymerization of Propylene with a Highly Active Catalyst. *AIChE Journal*, **44** (6), 1424-1437.





## **CHAPTER 6**

**OPTICAL AND INFRARED IMAGING  
OF GROWING POLYMER PARTICLES  
IN THE HOMO AND COPOLYMERIZATION  
OF PROPYLENE AND ETHYLENE,  
USING A ZIEGLER-NATTA CATALYST**

## Abstract

*In typical systems used for studying catalytic olefin polymerization processes, only average overall values such as overall reaction rate and overall temperatures can be studied and it is not possible to study individual particles and their behavior. The present work describes a method that was developed to observe polymer particles during a polymerization reaction, using either an optical observation system or an infrared imaging system. The images obtained give good insight into catalyst-specific properties as shape replication, distribution of activity over different particles and distribution in time needed for activation of the particles. The advantage of this method is the possibility of studying different individual particles in the same conditions and in the same experiment, and to link the behavior the particle to some of its specific properties, for example initial particle size or shape. Images obtained with the optical system can be translated into reaction rates curves in time.*

*Here a typical fourth generation Ziegler-Natta catalyst was used with triethyl aluminum as cocatalyst and a dimethoxysilane as external electron donor. The relation between the reaction rate and temperature, pre-polymerization method, recipe and catalyst activation time was studied.*

*The infrared method was developed to measure surface temperatures of the growing polymer particles. Data obtained from this type of experiments can be an important experimental verification of the extensive modeling efforts that are made in this field. After thorough calibration efforts, it was possible to measure the surface temperatures as a function of time. The temperature – time curves did not fully agree with results obtained from the models presented in literature. In the experiments, maximum temperature was reached after some minutes, instead of after a few seconds. A simple model was used to describe this effect qualitatively. Maximum increase of the particle temperature was up to 20°C in copolymerization of propylene with ethylene at 70°C, and was shown, as expected, to depend strongly on reaction rate and particle size.*

*This chapter has been submitted for publication:  
J.T.M. Pater, G. Weickert and W.P.M. van Swaaij,  
'Optical and Infrared Imaging of Growing Polymer  
Particles in the Homo- and Copolymerization of  
Propylene and Ethylene, using a ZN catalyst', AIChE  
Journal (2001).*

## 6.1 Introduction

The expansion of polyolefins into the worldwide plastics markets has been huge over the past decades. The world market share of polyolefins was around 20% of the total thermoplastic market in the 1960s. These days, polypropylene and polyethylene count for almost 60% of the global plastic production with an annual increase of 7 to 8 %<sup>[1]</sup>. Developments in new catalysts are combined with developments in new process technologies, leading to new products with new properties. The success of these materials is a result of the combination between the excellent cost-performance balance and the environmentally friendly aspects of the processes used to make them, as well as of the products themselves. The advances in the catalyst materials and process technologies are the result of continued strong efforts in research and development and in improving the understanding in the mechanisms involved.

A characteristic of these investigations though, is the averaging of properties over a large number of particles. When looking into kinetics and/or morphology development of the growing particles, it is common to use batch experiments where an amount of catalyst material is introduced into a polymerization reactor. After the polymerization run, the product is evacuated from this reactor and analyzed on polymer properties - using methods like DSC, GPC, MFR - and on powder properties by using methods like electron microscopy, particle size analysis and porosity measurements. Average properties of the catalyst material, like metal concentrations and particle sizes, are related to average properties of the product, combined with the overall measured reactor conditions.

In addition, properties of the particles are, as already mentioned, measured after removing the product from the polymerization system. It is well known that evacuation of the product from the reactor, involving huge changes in pressure and temperature, can change some properties of the product, for example crystallinity, even before these properties are determined.

These two disadvantages would be overcome if individual particles were observed during the polymerization process. A polymerization cell with online and in-situ analysis and characterization methods would solve these difficulties. In this work, we will present a microreactor, composed of such a cell with a transparent lid. It comes in two different configurations:

- In the first system, an optical camera is connected to the set-up and optical images are obtained from the growing polypropylene particles. This application is used to study shape development of the particles and reaction kinetics.
- In the second application, the system is used for infrared observation of the growing particles. In this way, surface temperatures of the particles can be obtained in-situ, without disturbing the particles. This application will be of importance in supporting single particle modeling efforts.

### *6.1.1 Optical imaging in olefin polymerization reactions*

Different groups have used in situ measurements by micro-techniques on polymerizations before. The application of electron microscopy in combination with

growing particles in catalyzed olefin polymerization was shown in the 70's for the first time<sup>[2]</sup> and repeated after that by others<sup>[3]</sup>.

In 1996 the group of Reichert<sup>[4]</sup> showed application of the optical observation of growing polybutadiene particles at low pressures. After that, the method was further improved by Zoellner<sup>[5]</sup> and Bartke<sup>[6]</sup>.

More recently, also other groups have described<sup>[7-8]</sup> their work using similar techniques. Since 1998, our group has been performing investigations using a reaction cell with a transparent lid, to study the catalytic polymerization of propylene<sup>[9-10]</sup> at elevated pressures, up to 35 bars, which means for the first time at industrially relevant conditions.

### *6.1.2 Infrared imaging in Chemical Engineering*

The idea of infrared imaging is used in different applications, both within and outside chemical engineering. This powerful tool has been applied specially in studies on surface temperatures in catalysis research. The applicability of IR thermography in heterogeneous catalysis was demonstrated already in 1987<sup>[11]</sup>. The group of Luss published a number of papers on the use of IR thermography to study temperature profiles on surfaces of catalytic materials<sup>[12-17]</sup>. The same idea was used in the development of a catalyst screening method in the group of Reetz<sup>[18-21]</sup>. In that work, IR thermographic detection was used to identify catalytic activity in libraries of heterogeneous catalysts. The use of IR thermography as a screening method in a combinatorial way allows testing of large numbers of complexes in terms of their activity and selectivity.

The use of IR thermography in catalytic olefin polymerization has not been reported before, as the demands in this area were up to now incompatible with the technical possibilities. The dimensions of the catalyst particles are between 15 and 100 micron, requiring relatively strong magnification on the infrared camera system, which are not easy to obtain. Despite the fact that efforts were made to calculate particle temperatures during polymerization for decades, it was not possible to measure the real temperatures. Measuring bulk temperatures will not provide the particle temperatures and the use of direct contact in particle measurements would lead to disturbance of the particle's heat balance. Application of a new method to determine the particle temperature is therefore necessary. Infrared thermography seems to be promising to this aim based on literature results obtained in other areas as mentioned above.

### *6.1.3 This chapter*

The aim of the work presented in this chapter is to show the possibilities of direct observation methods in a system operating at industrially relevant conditions, respecting the circumstances needed in catalytic olefin polymerization: high pressure, high purity of the polymerization cell, highly purified starting chemicals and a reproducible procedure in catalyst preparation. Also, the applicability of this method for catalyst screening and for kinetic measurements will be tested.

This paper is organized as follows. First the experimental equipment and procedures are described. Then the results of optical observation of catalytic polymerization reactions are shown, followed by discussion of those results. Subsequently, the results of the infrared observation of the reacting system are presented. With the discussion of the temperature measurements, a simple model of mass- and heat-balances is used to qualitatively describe the particle temperatures during polymerization. Although only a restricted number of experiments are shown here, the results are indicative for the results observed in a large number of experimental tests.

## 6.2 Experimental

### 6.2.1 Chemicals

The catalyst used in this work is a commercially available Ziegler-Natta catalyst of the fourth generation, with  $\text{TiCl}_4$  on a  $\text{MgCl}_2$  support. As cocatalyst tri-ethyl aluminum was applied, kindly donated by AkzoNobel. As an external electron donor, di-cyclo pentyl di-methoxy silane (the so-called D-donor) was taken. To suspend the catalyst, hexane was used, of 'Pro Analsi' quality obtained from Merck. The propylene used was obtained from Indugas, with a purity  $>99.5\%$ , with propane as

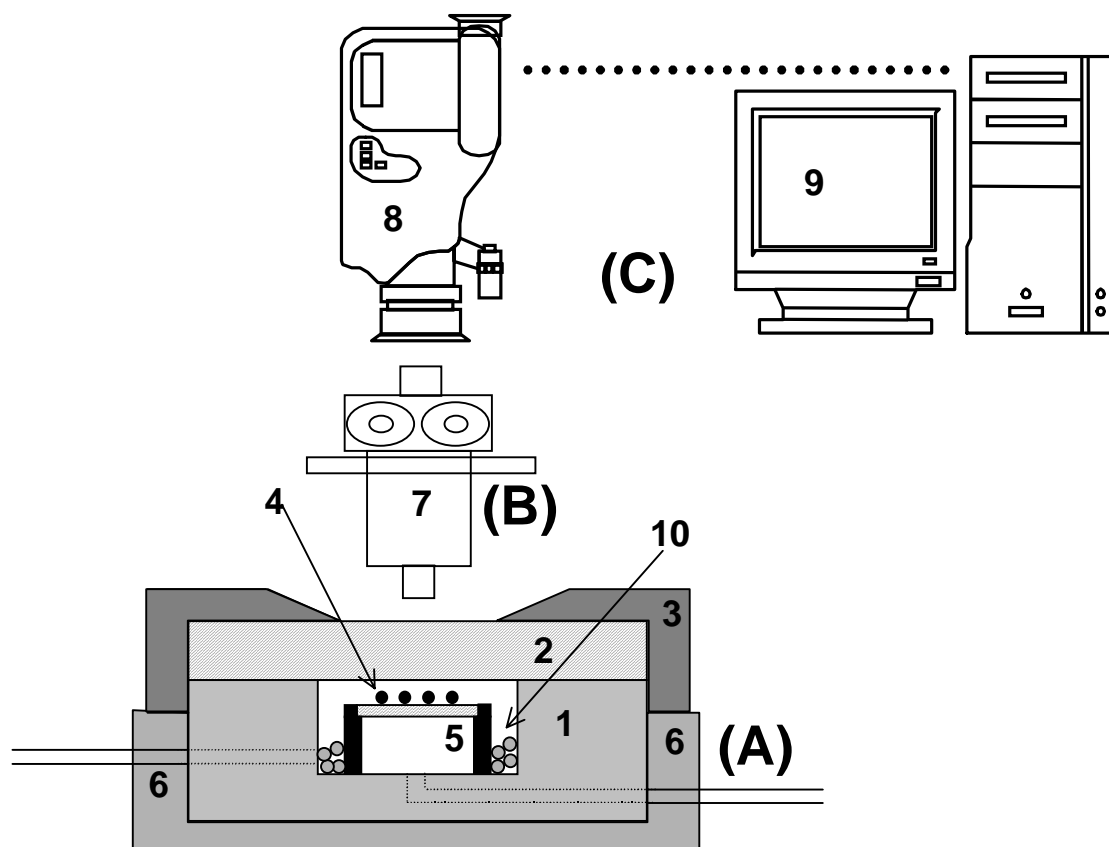


**Figure 6.1** Schematic representation of the microreactor set-up, with the body of the cell (1), the transparent lid (2), the metal lock for the lid (3), support material for particles (5), catalyst (4) and heating jacket (6). In the observations, a microscope (7) is used combined with the observation system (8). This camera is connected to the PC (9) for data acquisition. Polymer particles treated with TEA (10) are used for scavenging.

main impurity. The hydrogen and nitrogen used were of >99.999% purity. The hydrogen, nitrogen and hexane were extra purified by leading them over a reduced BTS copper catalyst and subsequent passing these gases over three different molecular sieve beds, with pore sizes of 13, 4 and 3 angstrom respectively. The BTS catalyst was obtained from BASF. The propylene was purified in the same way, after it was led over a bed of oxidized BTS copper catalyst.

### 6.2.2 Equipment

The micro-reactor set-up used here consists basically of two parts (Figure 6.1). The first part (A) is the polymerization cell in which the polymerization reactions are carried out. The second part (B+C) is the connected observation system with which information is collected on the growing polymer particles.

#### Polymerization cell

The polymerization reaction is carried out in a specially designed polymerization cell. The 6-ml stainless steel cell (1) has a transparent lid (2) to allow particle observation. The lid is mounted tight with a metal ring (3) to permit pressures up to 40 bar without leaking. Catalyst particles (4) are distributed on the support disk (5). The polymerization cell is placed in a thermostatic jacket (6) to ensure a constant temperature in the cell over time.

The cell has two inlets. The first inlet is used for evacuation of the cell and for introducing process gas in tangential direction. The second can be used as gas outlet, or for introduction of thermocouples. The tip of the thermocouple is located in the gas phase underneath the glass support disk.

**Table 6.1** *Properties of the three objectives used in the microscope of the optical microreactor system, with magnification, numerical aperture, resolution of lens and camera, depth of field, working distance, observable area and spherical aberration (at a lid thickness of 8 mm).*

Type	Mag	NA	Res <sub>len</sub> [μm]	Res <sub>cam</sub> [μm]	DOF [μm]	WD [mm]	OA [mm x mm]	SA [μm]
Epiplan 4x / 0.10	4	0.1	3.3	4.1	55	19.8	2.1 x 2.1	0.4
Epiplan 10x / 0.25	10	0.3	1.3	1.3	9	12.6	0.8 x 0.8	6.0
Epiplan 20x / 0.40	20	0.4	0.8	0.8	3	9.8	0.4 x 0.4	29

#### Optical observation

When the system is used for optical observation of the growing polymer particles, a *Pieper FK 7512-IQ* digital camera is connected to the *Carl Zeiss Axiotech Vario 25 HD* microscope (Part B in Figure 6.1). The microscope is equipped with different objectives, providing different features. Table 6.1 shows an overview of the different objectives used in the system. Next to the internal light source of the microscope a second, external light source is used to obtain good contrast of the polymer particles on their background. The digital camera is connected to a frame grabbing PC with imaging software. With a preset frequency images of the polymer particles are saved.

### Infrared observation

When the system is used for infrared observation, a *ThermaCAM PM 290* camera of Inframetrics is used with an *Inframetrics* microscope objective. This camera observes the infrared emission from the polymerization cell and determines the intensity of the radiation with a wavelength between 3.4 and 5.0  $\mu\text{m}$  with an update rate of 50 Hz. The camera uses a 256 x 256 platinum silicide focal plane array detector. An integrated closed-cycle cryogenic cooler maintains the low detector temperature of 77 K.

Using the mentioned microscope objective, one pixel in the infrared image equals 6.3 x 6.0  $\mu\text{m}$ . The average diameter of the catalyst particles used is around 25  $\mu\text{m}$ . Figure 6.2 shows a schematic distribution of the pixels over the initial catalyst particle.

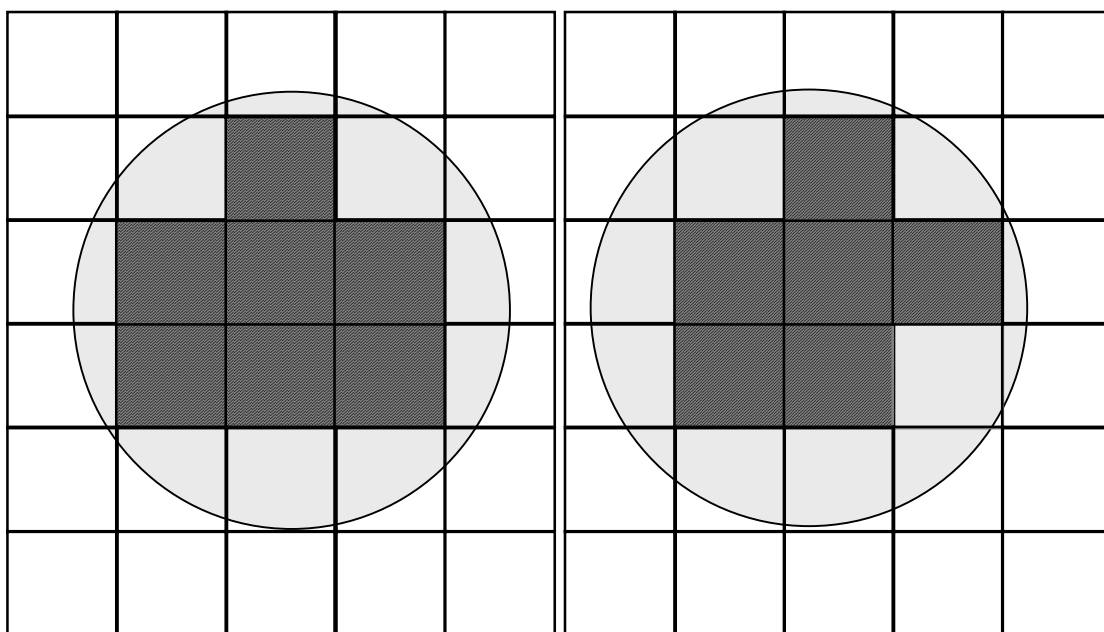


**Figure 6.2** Representation of image pixels on the 2-dimensional representation of a catalyst particle.

### *6.2.3 Procedures*

#### Preparation of the catalyst

The catalyst, suspended in a mineral oil, is weighed out in the glovebox under nitrogen atmosphere and subsequently hexane, a 4 mg/g TEA solution in hexane and a 2 mg/g donor solution in hexane are added to the catalyst to activate it. The suspension is gently shaken for 15 minutes at room temperature and next the liquid is removed from the catalyst after settling the solids. To be able to reproduce the amount of TEA remaining at the catalyst, the catalyst is washed with fresh hexane once, and after removal of the washing fluid it is dried at room temperature in vacuum. In this way, an activated, dry, free flowing catalyst powder is obtained.

The dry catalyst is dispersed on the background material, in this case a 25-mm diameter plate of a dark colored glass, in such a way that the observable area of the optical microscope will contain about 10 catalyst particles. Careful tapping with the

support glass will distribute the catalyst on the surface. Around the metal ring in the polymerization cell, a small amount of polyethylene powder is put, that was treated with a tri-ethyl aluminum alkyl solution in hexane (indicated with (10) in Figure 6.1). The polymer powder with active aluminum will scavenge impurities from the incoming gas, but due to the low vapor pressure of the alkyl, it will not show cocatalytic activity. The reaction cell is then closed in the glovebox, connected to the gas supply and camera system and brought to reaction conditions.

#### Polymerization Procedure

The cell is placed in the heated jacket to be brought to reaction temperature. Introducing the preheated and premixed process gas into the reactor starts the polymerization reaction. Typically this process gas will be the mixture of different monomers, in the present work being ethylene and propylene, a chain transfer agent being hydrogen and an inert gas being nitrogen. Just before the introduction of the process gas, the observation system - infrared or optical - is started. Normally the reaction is continued for 20 minutes; releasing the pressure will stop the reaction.

When applying one or two pre-polymerization steps in the experiment, the reactor is set to pre-polymerization temperature, typically 40°C. The process gas is introduced and after the pre-polymerization time, typically 2 minutes, the system is evacuated. When two pre-polymerization steps are used, this is repeated with another gas composition or at another polymerization temperature. After pre-polymerization steps, the reactor is brought to conditions of the main polymerization, typically 70°C and after reaching that temperature, the process gas is introduced. No monomer is therefore present during changing the temperature of the cell, and thus no reaction can take place.

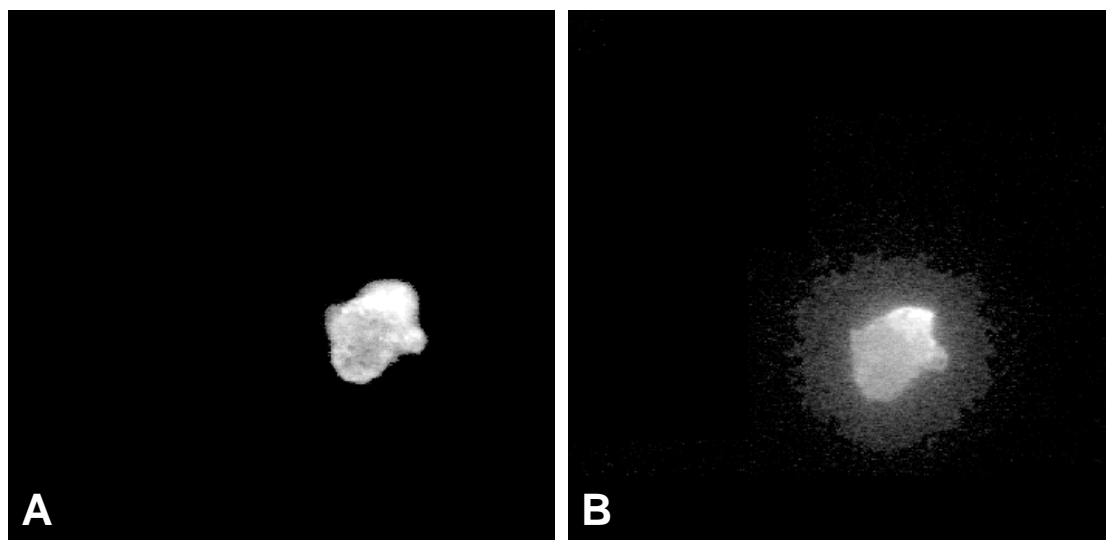


**Figure 6.3** *Effect of spherical aberration. A) Picture taken without transparent lid. B) Picture taken with the 8-mm thick lid, causing dispersion of the light.*



### 6.2.4 Determination of single particle polymerization rates

When the optical observations are used, a 2-dimensional image of the growing polymer particles is obtained. With a preset interval, here every 10 seconds, the optical image of the growing polymer particles is stored on the hard disk. After the experiment, imaging software is used to determine the size of the 2-dimensional representation of all the present catalyst/polymer particles in every picture. This is an important step in the data processing. Due to spherical aberration, blooming and background blurring, the boundary of the particle is often not easy to recognize. In every picture, an ‘intensity threshold’ has to be determined that indicates if a pixel belongs to the particle or to the background. Figure 6.3 illustrates these effects. Figure 6.3a shows a polymer particle without reactor lid, in Figure 6.3b the same particle is shown through an 8-mm glass window. The lid spreads the light from the particle, mainly due to spherical aberration the glass. With increasing magnification of the microscope objective, the spherical aberration will increase, or by reducing the thickness of the lid, this effect can be minimized. For example, the last column of Table 6.1 shows the measure of spherical aberration when using an 8-mm thick borate glass lid. By using a sapphire window, the thickness can be reduced without affecting the maximum allowable pressure in the cell. Here a 2-mm thick sapphire window was used, allowing maximum pressures of 27 bar.

After determination of the threshold, the 2-dimensional surface area can be calculated into a 3-dimensional particle volume. Here, the assumption is made that the particles do have a spherical shape. The increase of the particle volume is then transformed into a polymerization reaction rate, using the density and porosity of the polymer.

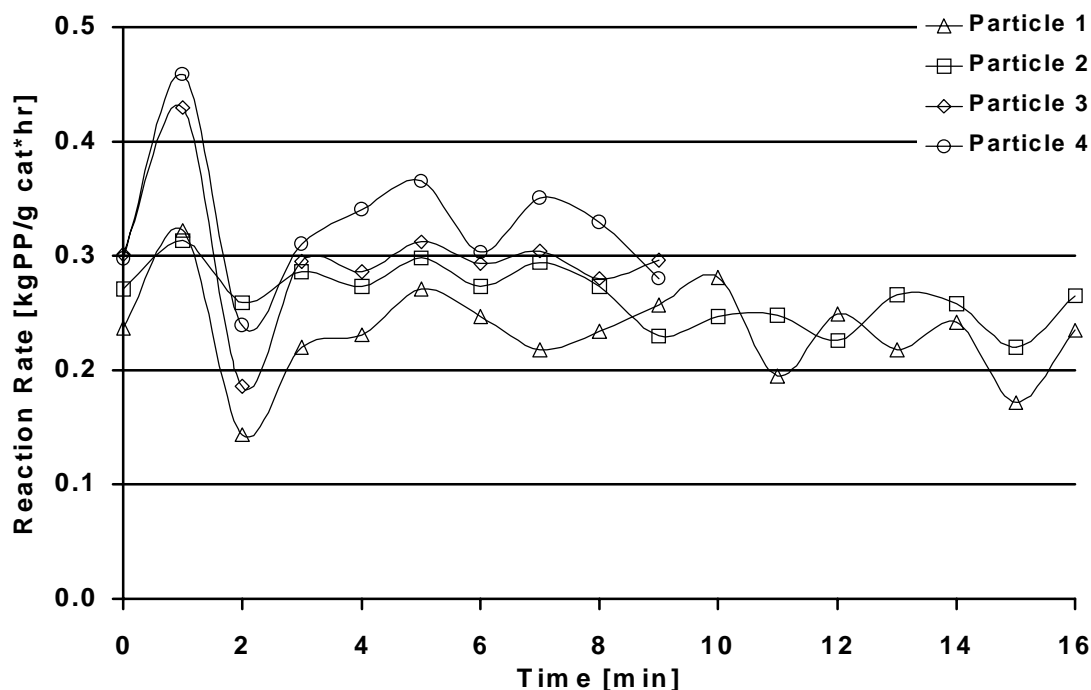


**Figure 6.4** Reaction rate in time for four different particles in the same polymerization experiment: homopolymerization of propylene at 70°C.

## 6.3 Results – Optical Observations

### 6.3.1 Reproducibility

Due to the fact that the amount of catalyst used is small and the surface of the reactor wall is relatively large, impurities will be an important issue in this system. Figure 6.4 shows a typical representation of the growth rate of different particles during the same polymerization experiment versus time, extracted from the 2D images, by using the method described before. The scattering that is shown in this figure is due to the poor contrast at the boundary of the polymer particle. As mentioned earlier, the lid of the cell causes spherical aberration. Therefore the edges of the polymer particles are not sharp on the black background, but rather show a fading contrast, and it is therefore hard to determine the exact edge of the particle. During determination of the surface of the 2-dimensional projection of the particle, pixels belonging to the background can be counted 'in' or particle pixels can be left out, resulting in a scattering reaction rate in time. The last column in Table 6.2 shows the bandwidth of the activities of different experiments at the same conditions.

It is seen that different particles in the same experiment show very similar behavior: they start growing at the same time and at the same reaction rate with respect to their initial volume. But in a comparison between different experiments reproducibility is poorer. It is hard to make a direct comparison, as measured reaction rates are scattering due to spherical aberration and background blurring. By increasing the number of experiments, fixed solid conclusions can be drawn from experimental results.

**Table 6.2** Overview of the recipes used in the experiments presented in this work.

	Catalyst Activation						prepol <sup>1)</sup> [-]	Main Polymerization						
	cat μmole	TEA μmole	donor μmole	T <sub>act</sub> [°C]	t <sub>act</sub> [min]	V <sub>act</sub> [ml]		T <sub>reac</sub> [°C]	C <sub>3</sub> <sup>=</sup> [bar]	C <sub>2</sub> <sup>=</sup> [bar]	H <sub>2</sub> [bar]	N <sub>2</sub> [bar]	R <sub>p</sub> [kg/g*hr]	Band [kg/g*hr]
1	6.5	260	130	20	15	10.7	none	40	8.7	-	0.5	1.1	0.27	0.22 - 0.33
2	6.5	260	130	20	15	10.7	none	50	9.1	-	0.5	1.1	0.35	0.29 - 0.40
3	6.5	260	130	20	15	10.7	none	60	9.3	-	0.5	1.1	0.47	0.41 - 0.53
4	6.5	260	130	20	15	10.7	none	70	9.3	-	0.5	1.1	0.72	0.60 - 0.85
5	6.5	260	130	20	1080	10.7	none	50	9.4	-	0.5	1.1	0.35	0.30 - 0.40
6	6.5	260	130	20	1	10.7	none	50	9.2	-	0.5	1.1	0.37	0.34 - 0.43
7	6.5	2600	1300	20	15	10.7	none	50	9.5	-	0.5	1.1	0.38	0.34 - 0.43
8	6.5	26	13	20	15	10.7	none	50	9.4	-	0.5	1.1	0.36	0.32 - 0.41
9	6.5	2600	1300	20	1080	10.7	none	50	9.1	-	0.5	1.1	0.35	0.29 - 0.40
10	6.5	26	13	20	1	10.7	none	50	9.3	-	0.5	1.1	0.37	0.33 - 0.42
11	6.5	260	130	20	15	10.7	meth.1	70	9.4	-	0.5	1.1	0.70	0.59 - 0.81
12	6.5	260	130	20	15	10.7	meth.2	50	9.0	-	0.5	1.1	0.85	0.70 - 1.00
13	6.5	260	130	20	15	10.7	meth.3	40	8.9	-	0.5	1.1	0.26	0.20 - 0.30
14	6.5	260	130	20	15	10.7	meth.1	40	8.4	1.0	0.5	1.1	0.43 <sup>2)</sup>	0.40 - 0.48
15	6.5	260	130	20	15	10.7	none	50	8.0	1.0	0.5	1.1	1.20	1.00 - 1.40
16	6.5	260	130	20	15	10.7	none	67	15.0	-	0.5	0.0	1.15	0.98 - 1.30

1) Prepolymerization methods are described in table 4

2) Reaction increased in 4 minutes to a final value of 0.43

### 6.3.2 Shape replication and induction period

As stated above, in modern polyolefin technologies shape development and the powder morphology of the product are important issues. With the present method it is possible to observe a large number of different particles in the same experiment. In Figure 6.5, images are shown of growing polymer particles at different moments during a copolymerization experiment. From Figure 6.5, it can be seen that the shape of the particles does not change with time. The shape of the catalyst particles is replicated, and is invariant during the reaction.

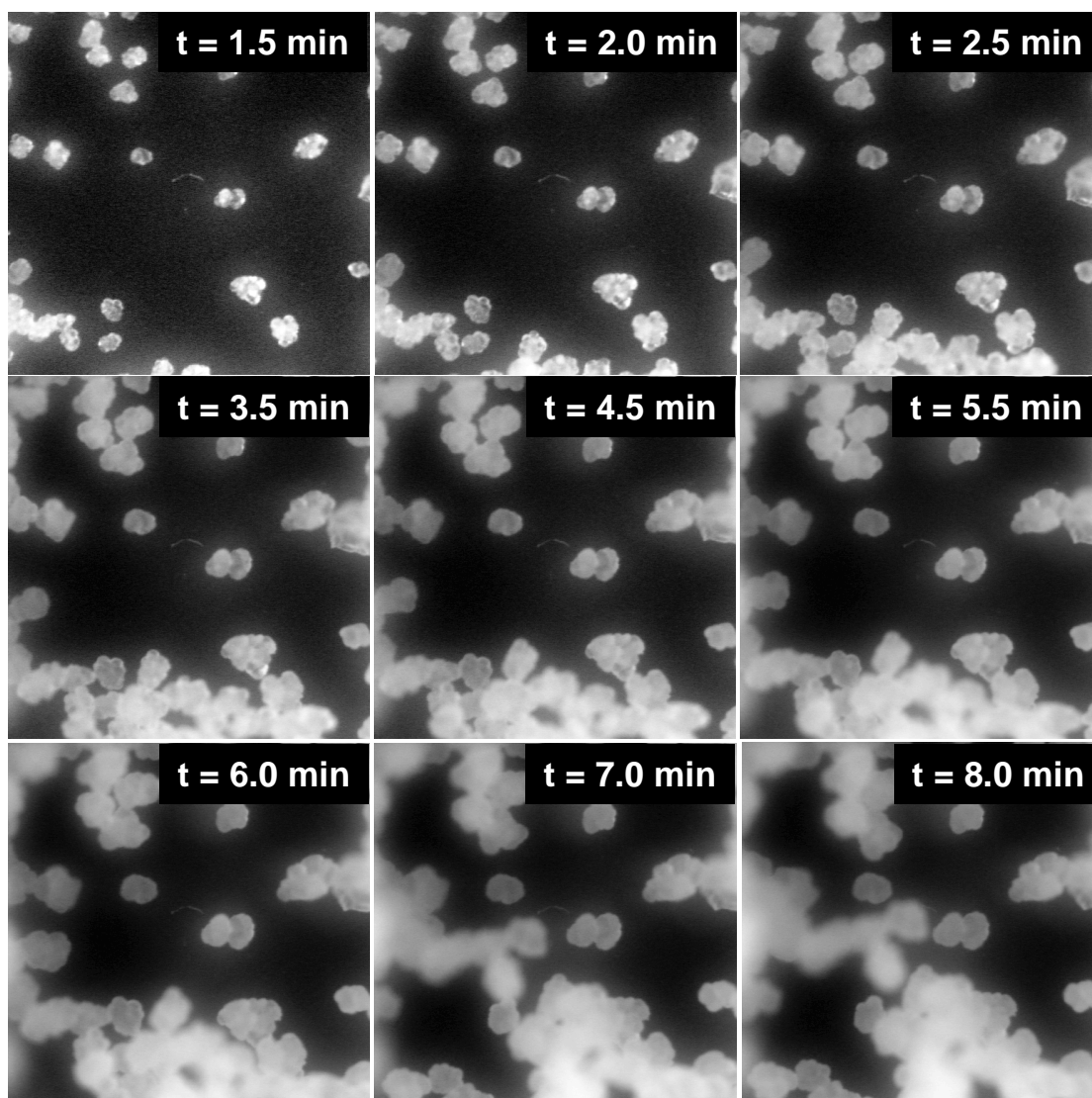


**Figure 6.5** Replication of shape in copolymerization experiment without a prepolymerization (indicated with experiment 15 in table 6.2). The pictures are taken after 1.5, 2.0, 2.5, 3.5, 4.5, 5.5, 6.0, 7.0 and 8.0 minutes.

It also seems as if all particles start growing at the same moment. In movies constructed from the pictures one sees that already in the first few images, passing

only 10 seconds, all the particles start growing (Example movies are shown on the research-group's homepage<sup>[22]</sup>).

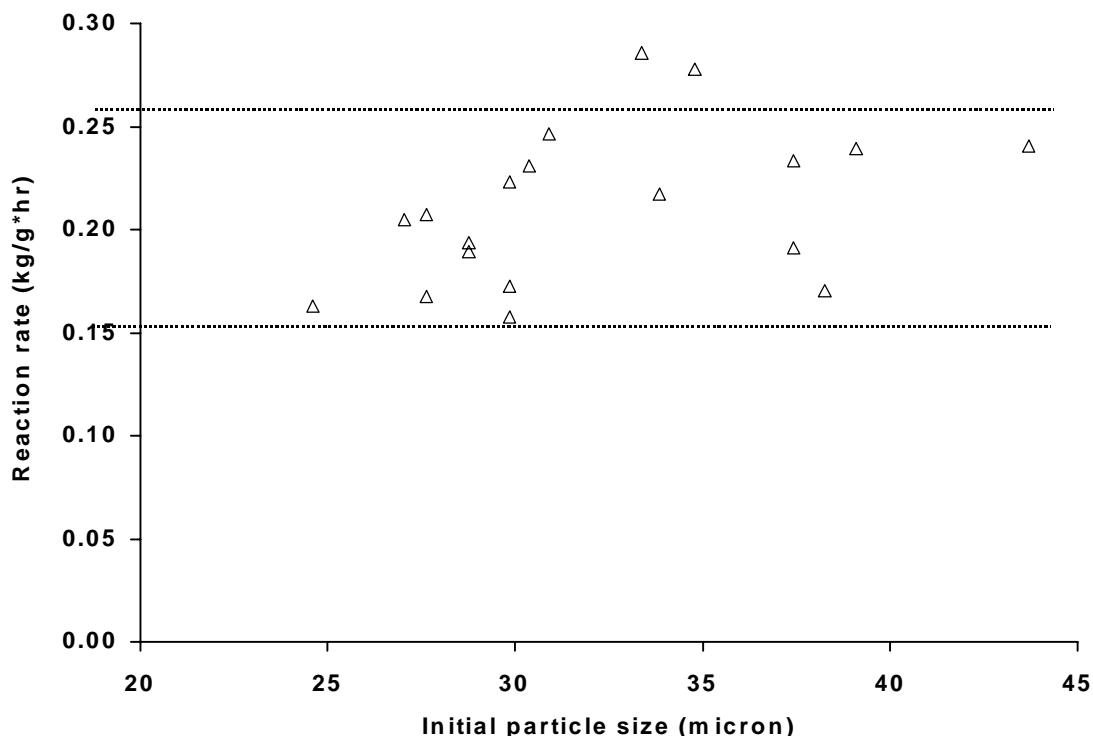


**Figure 6.6** Relation between initial size of catalyst particles and reaction rate in gas phase polymerization in microreactor, calculated from optical observation for 19 individual particles.

With imaging software the pictures, like the ones in Figure 6.5, can be interpreted. Figure 6.6 shows the relation between the initial particle size of the catalyst particle and its reaction rate in propylene polymerization. It is clear that when reaction rate is expressed per amount of catalyst, reaction rates do not depend on this initial particle size.

### 6.3.3. Influence of catalyst preparation

The influence of the duration of activation and of the concentrations of cocatalyst and electron donor during activation was tested in several series of experiments. In the first series, normal activation concentrations of D-donor and TEA were used, but activation time was varied strongly: 1 minute, 15 minutes and 1080 minutes. Table 6.2 shows that the single particle reaction rates calculated from these experiments were not influenced by this changing activation time.

In experiments where concentrations of D-donor and cocatalyst were varied strongly at constant activation times, the same constant reaction rates were observed. While maintaining a constant Al/Si mole ratio of 2, the Si/Ti mole ratio in the activation fluid was varied from 2, 20 and 200. In all these tests, no influence was seen on reaction rates.

To combine the most extreme cases with each other, the catalyst was activated for 1080 minutes at Si/Ti mole ratio of 200 and for 1 minute at Si/Ti mole ratio of 2. Even in these cases reaction rate was at the same value, as can be seen in Table 6.2.

### 6.3.4 Influence of temperature

The present method can be used to determine the kinetics of the individual particles. A series of experiments was carried out at different polymerization temperatures. In these tests, standard conditions were used as shown in Table 6.2. The polymerization temperature was varied from 40 to 70°C. The resulting reaction rates are listed in the same table as experiments 1 to 4. When taking the spread in activity of the different particles in the same experiment into account, one can determine from this plot an activation energy for the temperature dependence of the rate according to Arrhenius. Figure 6.7 shows the kinetics results from those tests indicated with the triangle-shaped markers, plotted as natural logarithm of the reaction rate versus the reciprocal temperature. It is obvious that reaction rates increase with increasing temperature and this relation seems to be linear. Activation energy determined in this plot is around 52 kJ/mole.

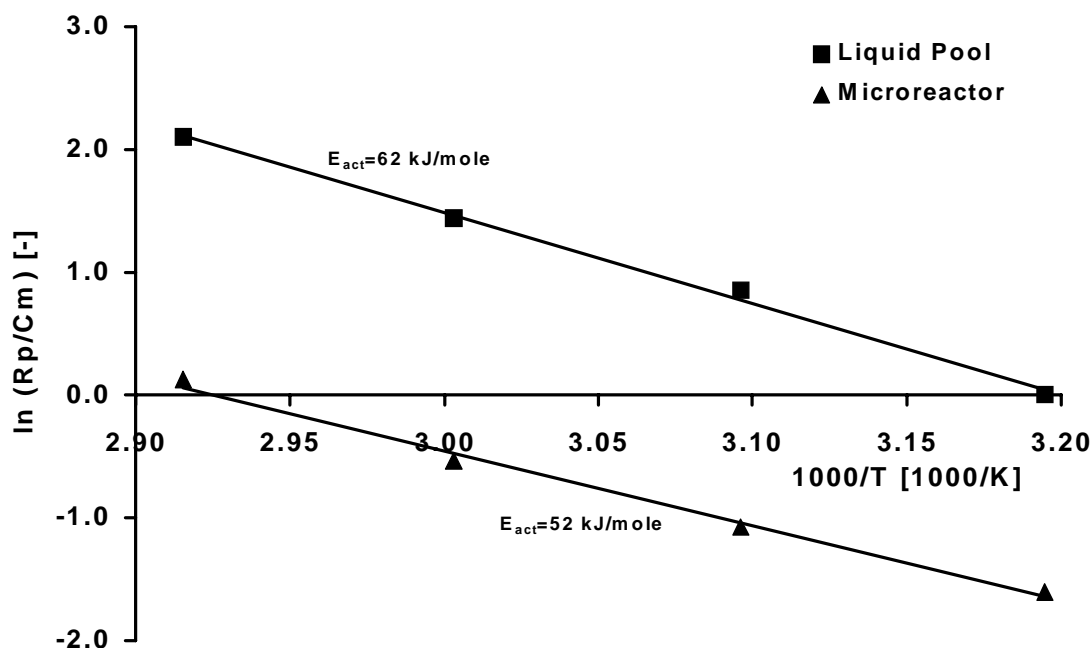


**Figure 6.7** Comparison between temperature dependency of reaction rate in gas phase polymerization (microreactor) and liquid pool polymerization, by taking into account the difference in monomer concentration at the active sites. In liquid pool polymerization  $C_m$  was calculated according to Meier, as described in 3.3.1

### 6.3.5 Pre- and Copolymerization

Above, the influence of temperature on polymerization kinetics is shown. To compare this influence with for example kinetics in liquid pool polymerization, as is discussed in chapter 3, it has to be kept in mind that there are experiment differences. One of the

differences in these two cases is the heat removal from the polymerizing particles. If reaction rates would be high in the initial stage of the gas phase polymerization, one could expect thermal runaway on particle scale due to too low heat removal capacity of the gas phase. A method to overcome this problem would be the use of a pre-polymerization step. In this pre-polymerization, the system is started up at a low polymerization temperature for a few minutes. The system is then evacuated to stop the polymerization, the cell is brought to the reaction temperature and the reaction is started up again. By doing this, the outer surface area of the particles would be enlarged by the pre-polymerization, possibly avoiding runaway during the main polymerization.

Experiment 11 in Table 6.2 shows that activity in experiments including a pre-polymerization step does not differ from activity in experiments without this pre-polymerization step (for example experiment 4 in the same table). From that, one can conclude that this thermal runaway does not reduce activity in a ‘normal’ gas phase experiment. In the second part of this work, we will go into more detail with respect to particle temperatures during polymerization, by using the infrared observation system.

**Table 6.3** *Three different methods for pre-polymerization of the catalyst, by changing gas composition during the first or second pre-polymerization step.*

Method	1 <sup>st</sup> prepolymerization						2 <sup>nd</sup> prepolymerization					
	T <sub>prepol</sub>	t <sub>prepol</sub>	C <sub>2</sub> <sup>=</sup>	C <sub>3</sub> <sup>=</sup>	H <sub>2</sub>	N <sub>2</sub>	T <sub>prepol</sub>	t <sub>prepol</sub>	C <sub>2</sub> <sup>=</sup>	C <sub>3</sub> <sup>=</sup>	H <sub>2</sub>	N <sub>2</sub>
	[°C]	[min]	[bar]	[bar]	[bar]	[bar]	[°C]	[min]	[bar]	[bar]	[bar]	[bar]
Prepol method 1	40	2	-	9.5	0.5	1.1	no 2 <sup>nd</sup> prepolymerization					
Prepol method 2	40	2	1.0	8.5	0.5	1.1	no 2 <sup>nd</sup> prepolymerization					
Prepol method 3	40	2	-	9.5	0.5	1.1	40	2	1.0	8.5	0.5	1.1

Because of the size of the polymerization cell, the system can be run very flexibly. A series of experiments were run using different pre-polymerization procedures, including pre-polymerization steps in the presence of ethylene. The accelerating effect of the presence of ethylene on the polymerization of propylene is well known in these systems but this effect is still not fully understood. Table 6.3 shows different pre-polymerization methods that were used in these experiments. In the second and the third method, the catalyst was pre-polymerized in different variations, in the presence of ethylene as comonomer. Experiments 11 to 13 in Table 6.2 show the influence of these pre-polymerizations on the reaction rate in the main polymerization with propylene. When defining the reaction rate in propylene main polymerization at 70°C as ‘normal’, one can see that reaction rate in this main polymerization reaches doubled activity when ethylene was present during the pre-polymerization step. Even when the system is evacuated after the pre-polymerization step and the presence of ‘free’ ethylene is unlikely, reaction rate in the main polymerization of propylene shows high activity. However, when the catalyst is pre-polymerized for two minutes

in propylene, subsequently in a co-pre-polymerization of ethylene and propylene, activity in the main polymerization has a normal value. In a main copolymerization after a propylene pre-polymerization, reaction rate increases in the course of about 4 minutes to the doubled value.

## 6.4 Discussion – Optical Observations

The possibilities of the present method are diverse, but in all the applications it is clear that the direct comparison between different particles, with different properties, for example particle size, in the same experiments under the same conditions, with the same history, is a big advantage of the method. It is not longer necessary to use average values for all the particles present in the experiment, but individual behavior of the particle can be studied.

### 6.4.1 *The experimental method*

It is clear from the results that the interval of values of the observed (or rather, calculated) reaction rates is relatively broad, and to obtain reliable information on polymerization kinetics it is necessary to repeat the tests several times to reduce errors. As said, these errors are mainly due to the deviations that occur in the determination of the 2-dimensional surface. These errors are magnified because of the 2D-3D translation. Another method for measuring single particle kinetics is the application of a thermobalance, as used by Garmatter<sup>[23]</sup>. This method does not have these problems, and would be more suitable for determination of single particle kinetics only, but lacks the other possibilities of the optical method.

### 6.4.2 *Tool for catalyst screening*

In the development of new catalysts a number of different important issues can be distinguished.

#### Activity in polymerization

This is probably the most obvious issue. The catalyst should show enough activity in polymerization, at the desired process conditions. Although ‘conventional’ lab-scale batch reactors (for example as Meier<sup>[24-25]</sup> described) are maybe more suited for the overall determination of kinetic behavior of a catalyst in gas phase polymerization, the present method can be used to determine the kinetics of the individual particles, enabling to relate these to properties of those individual particles, like initial particle size. Moreover, different catalyst systems, for example catalyst activated in a different way, can directly be compared in the same polymerization test.

#### Induction period

Besides the activity, the presence of an induction period is of importance. An induction period can have negative effects on the application of the catalyst in existing technologies, for instance quick blowout of catalyst particles that are too small in a fluidized bed reactor. But on the other hand, it can also have positive effects like the prevention of thermal runaway, inherent in the largest

catalyst particles in the initial stage of the polymerization, without the application of a pre-polymerization step. Although in conventional kinetic reactors this induction behavior can be observed, it is not possible to compare the individual particles, and to relate the start-up behavior to particle properties.

#### Replication of particle shape

To obtain a final product with a predictable powder morphology, it is of importance that the shape of the catalyst particle be replicated in the growth of the polymer particle. With this method we can compare not only the starting and final material, but can also study the development of the particle shape throughout the entire reaction.

#### Distribution of active material

To learn about the distribution of the active metal in the catalyst, one could analyze cross-cuts of the particles using an EDX-type of analyses. However, one can not be sure that all present potential active metal will really be activated. In the screening of the catalyst it is therefore important to make a comparison between the different catalyst particles to find the spread in behavior

### *6.4.3 The currently used catalyst*

From information on shape replication and particle size influence on single particle kinetics shown here, we can conclude directly that in this catalyst the active sites are homogeneously distributed over the different catalyst particles. All particles start to grow at the same moment, immediately after introduction of monomer to the system, all particles replicate the initial shape of the catalyst particle, and the polymerization rate expressed per volume of catalyst does not depend on the initial particle size.

### *6.4.4 Comparing gas phase polymerization with bulk polymerization*

When comparing the results of experiments carried out in this system to other experimental work with the same catalyst in the bulk polymerization of propylene, one has to keep in mind that catalyst preparation often differs significantly.

The results of the recipe variations described in 6.3.3 show the activation of this catalyst to be a very fast process. Assuming that  $Ti^{2+}$  is not active in propylene polymerization (as commonly accepted in literature), it can be concluded that deactivation of the catalyst by overreduction of the titanium due to excessive concentrations of the aluminum alkyl does not occur at the levels used here, not even at extremely long contact times. From the tests with varied activation procedure we can conclude that during interpretation of experimental results in the present work, the activation step does not need to be taken into account. (This does not necessarily mean that  $R_p(t=0)=R_{p,max}$ ! Other effects than activation of the sites can influence the reaction rate in the initial stage.)

As said, the same catalyst was also used in liquid pool polymerization of propylene. Those experiments were carried out in the procedure and set-up as described by



Samson et al.<sup>[26]</sup> and Shimizu et al.<sup>[27]</sup>. In principle, when the difference in monomer concentration is taken into account, the reaction rates observed in microreactor gas phase polymerization should show the same values as liquid pool polymerization with the same catalyst. When assuming a first order dependency of the reaction rate in monomer concentration, the reaction rates of the experiments can be compared. Meier<sup>[24]</sup> proposed a method to calculate monomer concentration at the active site, in the amorphous part of the polymer, using the Flory-Huggins equation:

$$\ln\left(\frac{P}{P^0}\right) = \ln(\phi) + (1-\phi) + \chi(1-\phi)^2 \quad (-) \quad (\text{eq. 6.1})$$

Table 6.4 shows the values for the interaction parameters as reported by Meier et al. The concentration of monomer in the amorphous part of the polymer is calculated using these values and the density of the liquid monomer. When assuming a first order dependency of the reaction rate in monomer concentration, the reaction rates in gas phase and in bulk can directly be compared. Figure 6.7 shows the temperature dependent reaction rates for both cases (bulk and gas phase) corrected for the monomer concentration at the active site. It is shown that reaction rates in the microreactor are a factor 5-7 smaller than expected from liquid pool polymerization, despite the correction for the monomer concentration. The fact that temperature dependency is in both cases well described with Arrhenius, and yielding in very comparable activation energies, one could conclude that this ‘correction’ can not cope with the differences.

**Table 6.4** Comparison of monomer concentration and reaction rate in liquid pool (LP) and microreactor (MR) polymerization of propylene (PPY).

Temperature	[K]	313	323	333	343
Rho PPY	[mole/l]	11.31	10.81	10.26	9.59
Chi	[-]	0.833	0.760	0.692	0.629
Phi 1	[-]	0.440	0.514	0.600	0.702
Phi 2	[-]	0.118	0.095	0.079	0.066
C <sub>m,LP</sub>	[mole/l]	4.972	5.553	6.159	6.733
C <sub>m, 9 bar</sub>	[mole/l]	1.336	1.026	0.806	0.636
R <sub>p,LP</sub>	[kg/g*hr]	5	13	26	55
R <sub>p,MR</sub>	[kg/g*hr]	0.27	0.35	0.47	0.72
R <sub>p,LP</sub> /C <sub>m,liq</sub>	[kg*/g <sub>cat</sub> *hr*mole]	1.006	2.341	4.222	8.168
R <sub>p,micro</sub> /C <sub>m,gas</sub>	[kg*/g <sub>cat</sub> *hr*mole]	0.202	0.341	0.583	1.132
Ratio	[-]	5.0	6.9	7.2	7.2

The principle explanation for this difference can be found in the different preparation of the catalyst system. Earlier we concluded that the activation has shown to be a fast process that is not very sensitive to TEA concentrations and contact time. But in addition to the difference in the preparation of the catalyst, the concentrations of donor and cocatalyst during polymerization can be different. In liquid pool conditions,

D-donor and cocatalyst are injected into the liquid monomer and are available for the catalyst during the entire experiment. In microreactor experiments, the catalyst is activated, washed and dried, probably resulting in lower donor and cocatalyst concentrations on the catalyst surface compared to liquid pool conditions. Therefore the difference in activity, in our opinion, should be ascribed to the difference in cocatalyst and donor concentration during the polymerization reaction. A series of experiments in liquid pool at various temperatures, using a catalyst that was treated the same way as in the present experiments, would give insight in this effect.

#### *6.4.5 The effect of ethylene addition*

From the pre- and copolymerization experiments, the picture emerges that the first monomer that the catalyst is in contact with is important in the development of the system. Even after only a short pre-polymerization in the presence of ethylene (experiment 12 in Table 6.2) the reaction rate of the propylene homopolymerization is permanently increased. We can think of different explanations for this effect.

It is possible that, just like hydrogen, the ethylene has the ability to activate certain catalyst sites. The presence of ethylene would increase the number of active sites, and with that the activity. When the catalyst is pre-polymerized with propylene, the ethylene is not able to reach the potentially active sites, because of hindrance by the polymer.

Another explanation would be different concentrations of monomer at the active sites of the catalyst, resulting in different reaction rates. In a copolymerization, a highly amorphous product is produced. One could imagine that solubility and diffusivity of monomers in this polymer is different from that in the homopolymer.

A third option would be that at the active site, the ethylene would take part in activation of the titanium. An active site that has the presence of the ethylene molecule in the complex is showing a larger ability to propagate the polymerization of propylene.

The enhancement of the propylene polymerization rate by the presence of ethylene is described in literature before. To discriminate between the different mechanisms that could play a role in this effect, it would be necessary to perform a series of experiments with systematically varied types of comonomer to vary the rate of incorporation of both the monomers and its possible function in the complexation at the active site.

## **6.5 Results – Infrared Measurements**

### *6.5.1 Particle temperature during polymerization*

When starting to observe surface temperatures of reacting particles, it is important to realize that the measured surface temperature is the maximum temperature in the particle. It is pointed out often in literature (for example Floyd et al.<sup>[28-30]</sup>) that heat transfer problems - being large temperature rises in and around the particle - can be important in gas phase reactions, especially at high activities and small catalyst particles. But at the present low reaction rates – at a maximum of  $2 \text{ kg}_{\text{polymer}}/\text{g}_{\text{cat}} \cdot \text{hr}$ ,

compared to normal gas phase polymerization reaction rates up to  $10 \text{ kg}_{\text{polymer}}/\text{g}_{\text{cat}} \cdot \text{hr}$  - temperature gradients will not exist inside the particle, maybe only at the very initial stage of the polymerization. In the present case, a small temperature gradient might occur due to non-symmetric heat removal from the particle by the underlying glass disk. The relatively large heat conductivity of the polymer material will ensure though that the temperature at the point observed by the infrared camera will be close to the average particle temperature.



**Figure 6.8** *Infrared image of a well thermostated coin, at 25°C. The difference in emissivity of different places on the coin causes apparent temperature differences. (The color image was for printing purpose converted to grayscale.)*

### Calibration

Infrared radiation detected by the infrared camera can be used to determine the surface temperature of the objects in the observed area. The amount of infrared radiation coming from the objects is not only determined by the surface temperature of the object, but also by surface orientation and nature of the material, as indicated by:

$$Q_{rad} = \sigma F_{\epsilon} F_a A (T_1^4 - T_2^4) \quad (\text{eq. 6.2})$$

Figure 6.8 shows an infrared image of a coin that is well thermostated. Although one can be sure that temperature gradients in the material are negligible, the infrared image shows us differences of 20°C. The influence of the orientation of the surface complicates the interpretation of the image. The product of the material factor  $F_{\epsilon}$  and the surface orientation factor  $F_a$  is called the emissivity factor  $\epsilon$ . The  $\sigma$  in this equation

is the Stefan-Boltzman constant. Typically, the software of infrared cameras use one emissivity factor for the interpretation of the complete observed area.

To be able to measure real particle temperatures, the emissivity of the materials used and the background radiation in the present set-up were determined. First, deactivated particles were placed on electrical tape stuck to a heated plate. The emissivity of the particles was determined outside the polymerization cell. Once these emissivity values were known, particles were placed in the reactor and the background temperature for the system was determined. The results of the calibration are shown in Table 6.5.

**Table 6.5** Typical emissivity factors for components present in the microreactor system during the polymerization of propylene.

Material	Size [micron]	Emissivity [-]
Polypropylene particles, rough surface structure	500	0.69
Polypropylene particles, smooth surface structure	500	0.87
Polypropylene particles produced in micro reactor	200	0.77
Ethylene-Propylene-Rubber particles from micro reactor	200	0.79
Ziegler-Natta catalyst, activated	25	0.79

In the experiments, an emissivity factor of 0.77 is used for interpretation of the infrared data, as the calibration experiments showed that this is the most common value for the powders. The maximum theoretical uncertainty of the temperature measurements executed at 70°C is  $\pm 4.9^\circ\text{C}$ . Experiments and calibration tests show that a realistic estimation of the error made by the system is  $\pm 1.0^\circ\text{C}$ .

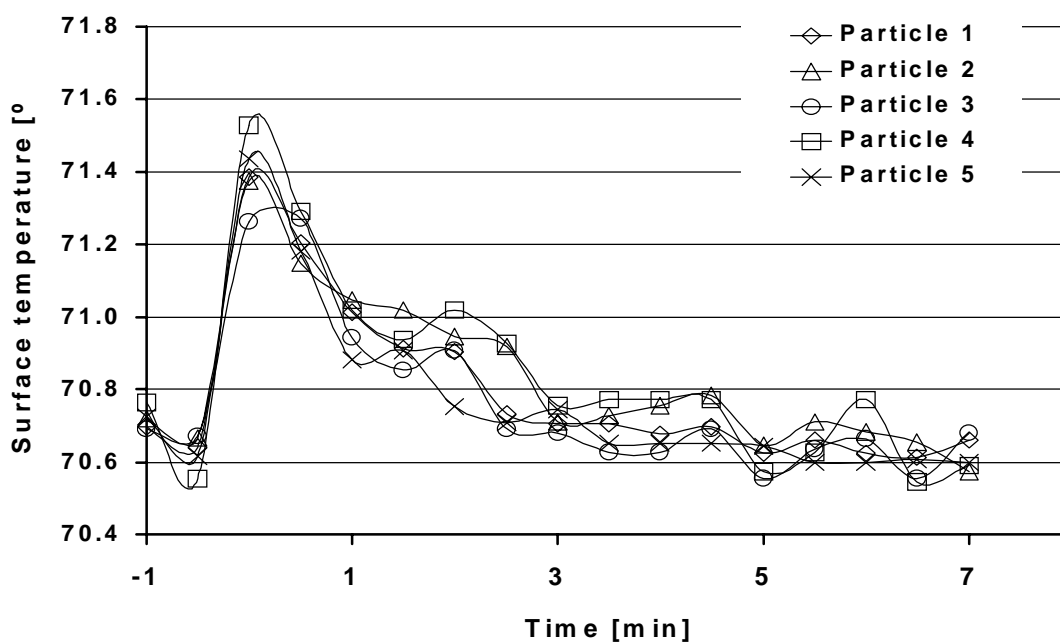


**Figure 6.9** Observed surface temperatures of 5 individual deactivated particles. The increase in temperature is caused by the introduction of monomer gas to the polymerization cell.

### No chemical reaction

To be able to interpret results from polymerization experiments, tests were done using deactivated catalyst particles and deactivated polymer particles in the course of a typical experimental procedure. Figure 6.9 shows the observed temperature of 5 deactivated catalyst particles. It is interesting to see that directly after injection of monomer the surface temperature of the particles seems to increase with about 0.8°C. There are two possible explanations for this. When the temperature of the gases introduced into the system is slightly higher than the reactor temperature, this reactor temperature will increase when injecting the gas. Beside that, compression of the gas in the reactor, from 1 to for example 10 bar will increase gas temperature caused by the well-known Joule-Thomson effect. For propylene the adiabatic temperature rise for propylene from 1 to 10 bar would be about 7°C. Of course the system used here is far from adiabatic for the incoming gas. With interpretation of the measured temperatures in presence of chemical reaction, one should keep this effect in mind. The plots shown below were not corrected for this temperature difference; temperature increase in those plots caused by reaction might therefore be slightly smaller in the first two minutes.

### Homopolymerization of propylene

The technique described before, using the infrared imaging camera was applied in the homopolymerization of propylene, indicated as experiment 16 in Table 6.2. The reaction rate of this polymerization was around 1.15 kg/g· hr. The temperature profiles of different particles in that same experiment, presented in Figure 6.10, show a uniform behavior. The measurement is using the same value for the emissivity for the

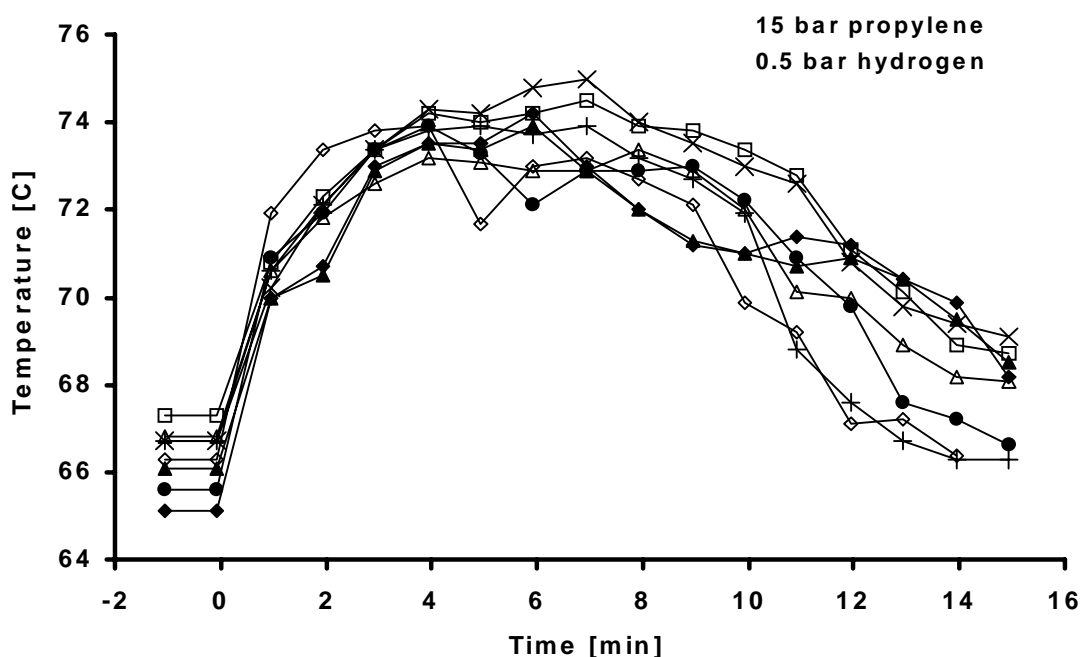


**Figure 6.10** Observed surface temperatures of 6 individual particles in the same experiment (homopolymerization of propylene).

complete picture, the value being obtained in calibration tests. This means that only the temperature value obtained from the center of the 2-dimensional representation of the polymer can be trusted, as discussed in paragraph 6.6 'Discussion, infrared observations'.

In the homopolymerization, starting at a temperature around 66°C, the temperature climbs to a maximum of 74°C on the surface of the particles as measured in the center of the circular 2D representation of the particle. The maximum is reached 7 minutes after the start of the polymerization. In the next 10 minutes the temperature falls to the reactor temperature, probably due to the increase of the heat-exchanging surface of the particle.

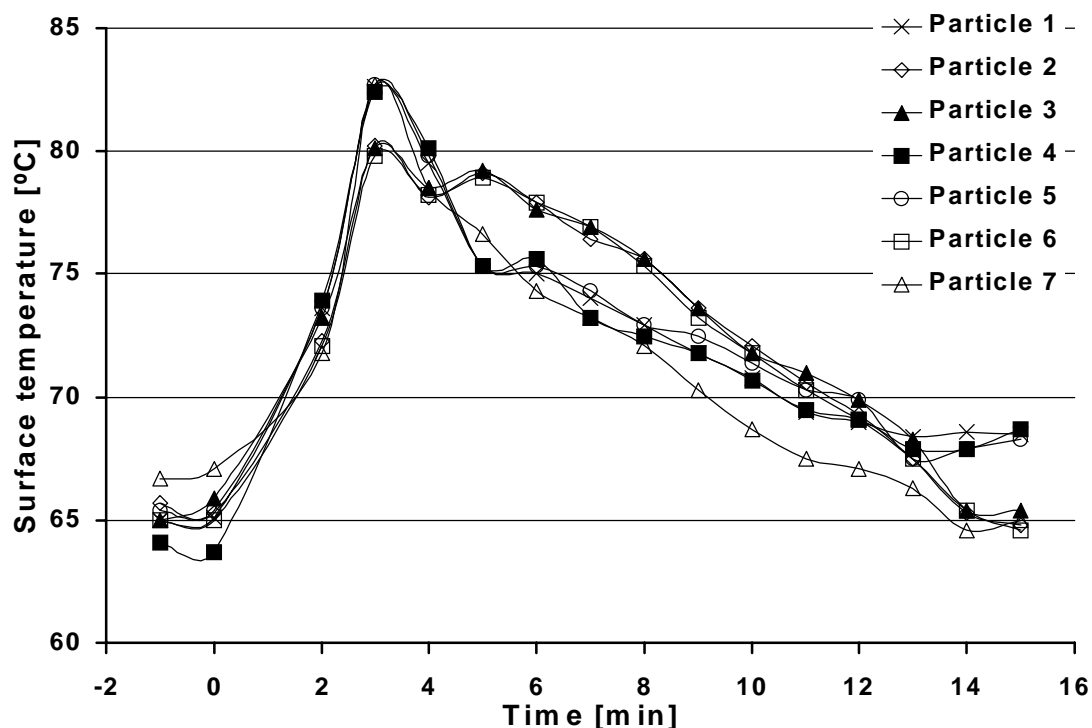
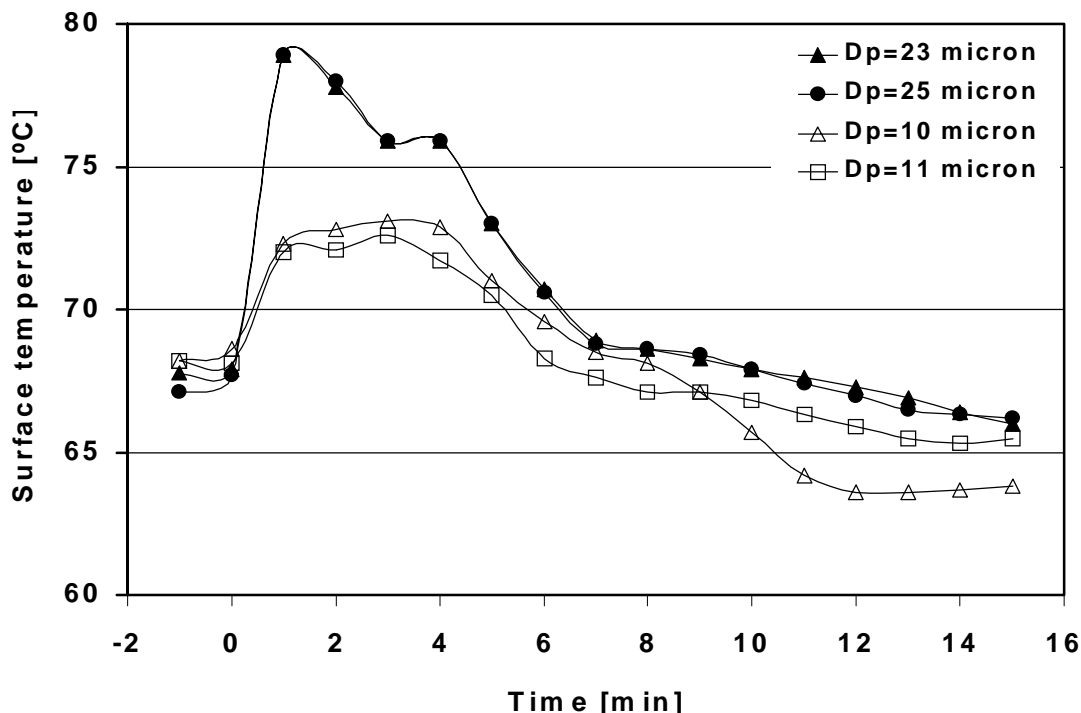


Figure 6.11 Surface temperature in time of 7 different particles in the same copolymerization experiment.

#### Copolymerization of ethylene and propylene

Figure 6.11 shows the surface temperature over time for different particles in the same copolymerization experiment of propylene and ethylene. As can be seen, the maximum temperatures are significantly higher than in the homopolymerization of propylene, due to the higher reaction rates. The maximum temperature is reached after 3 minutes and reaches a value of 83°C. After this maximum, the temperature decreases within 10 to 15 minutes to values close to the initial temperature. From optical measurements we know that the decrease in temperature is not due to a decrease in reaction rate, as deactivation is small in these experiments. The decrease in particle temperature is therefore ascribed to the increasing heat removal, rather than the decreasing heat production.



**Figure 6.12** Influence of initial particle size on the particle's surface temperature over time, in the copolymerization of propylene with ethylene. The larger particles show significant more overheating than the smaller ones, especially in the initial stage.

### Influence of initial particle size on particle temperature

The method shown here allows us to make a direct comparison between different particles within the same polymerization experiments. It is not necessary to use the average value of all the particles within the experiment, one can directly observe individual temperatures. In this experiment, we recorded temperatures of smaller and larger particles within the same experiment. Figure 6.12 shows the temperature of the different particles over time, in the copolymerization of ethylene and propylene. As expected, larger particles having a larger volume to surface ratio, show larger temperature rises than the smaller particles. Here, the power of the method proposed here, i.e. the ability to compare individual catalyst particles in exactly the same conditions, without having to worry about experimental reproducibility, becomes clear.

## 6.6 Discussion - Infrared observations

### 6.6.1 Observation method

It has shown to be possible, to observe growing polymer particles with an infrared camera and measure its temperature this way with the hardware presented here. The resolution of the camera used is not optimal, but to our knowledge the best possibility available at this moment, for an acceptable price.

Another disadvantage of the proposed method is the presence of an underlying surface. Because of the significant contact with the underlying glass, it is hard to

translate the measured results to particle temperature for free particles. A further complication of this matter is the fact that particles are laying in a stagnant gas. Convective cooling, at Nusselt numbers larger than the theoretical value of 2 for the ‘conduction only’ situation will change the particle’s heat balance, especially for the larger particles. Applying a moving gas in the polymerization cell would improve this situation.

The temperatures that were measured in the polymerization experiments do, at some points, not agree with the expectations obtained from classical single particle models. The maximum temperature is reached after a much longer period of time than predicted. One of the reasons for this, we believe, is the underlying material that is heated up by the particle during polymerization. To try to quantify this influence, a simple calculation was made, presented below.

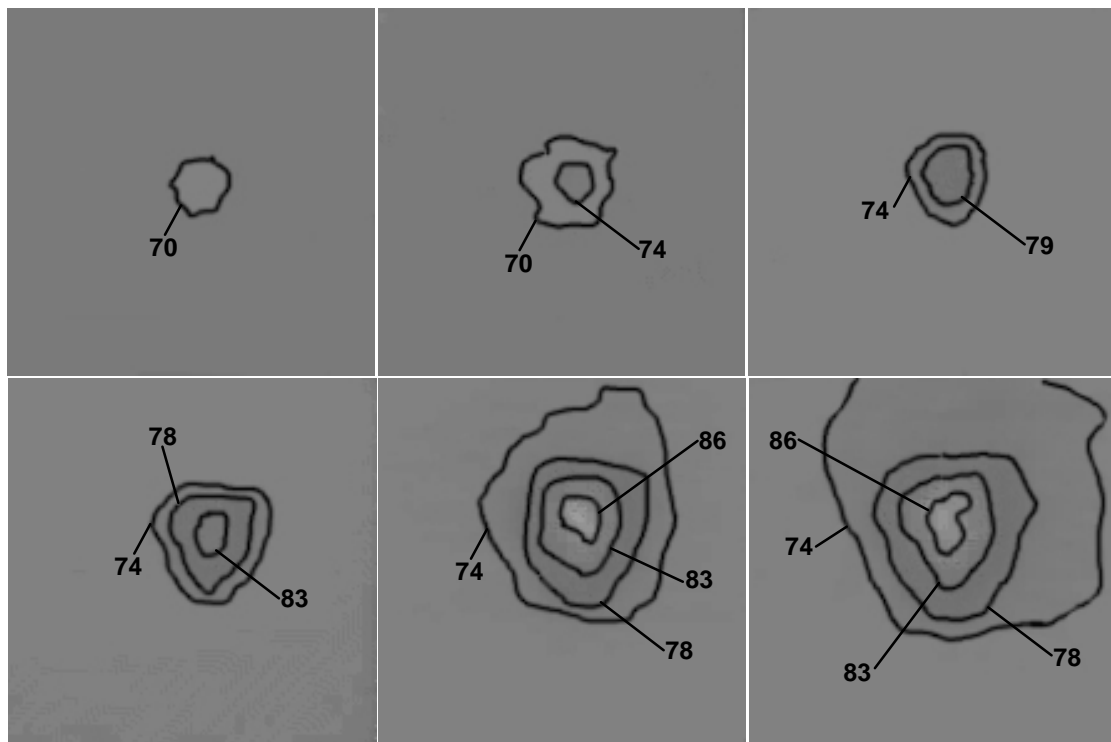


**Figure 6.13** *Infrared images of a growing particle during polymerization, all with  $\varepsilon=0.77$ . (Color images for printing purpose converted to grayscale images.)*

### 6.6.2 Curved surfaces

With interpretation of the results, we should take into account that the surfaces of the particles are curved. In Figure 6.13 it can be seen that an apparent temperature gradient exists over the particle, even when the particle is free of real temperature gradients. Due to the curved surface, radiation density seems to be higher at the outer side of the 2 dimensional representation. This effect is shown in Figure 6.14. This means that in the case of a real temperature gradient, it is hard to measure real radial temperature gradients with the methodology used here. In the results shown in the present chapter, the center of the 2-dimensional representation is used to measure the particle’s surface temperature.



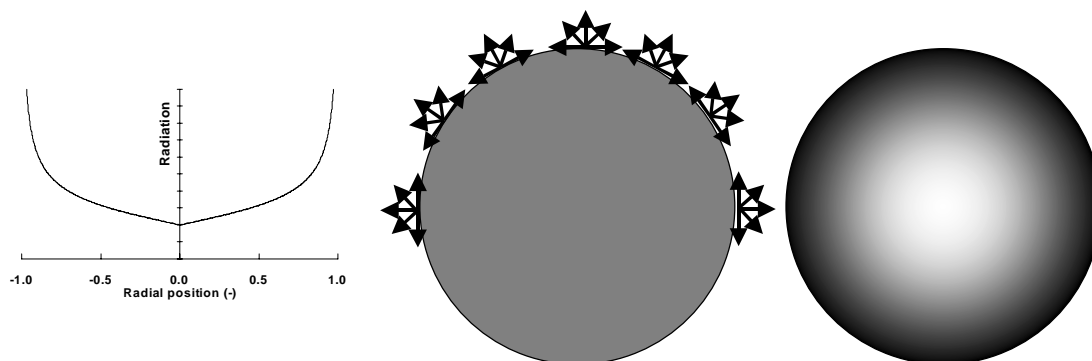


**Figure 6.14** Influence of surface orientation. A) Indication of the amount of radiation from particle surface. B) Distribution of point-sources on the surface. C) Apparent temperature gradient on particle surface due to surface orientation.

### 6.6.3 Relation between reaction rate and temperature rise

It is possible to relate the temperature increase of the particles with the reaction rate, for the present polymerization cell. Variations of the reaction rate have been made by changing gas composition in the reactor - homopolymerization versus copolymerization - and with that, of course also the heat-exchanging properties of the gas were changed to some extent. Of these experiments, Table 6.6 shows the temperature rise at three different reaction rates. It is clear that the temperature rise increases with reaction rate, and is dependent on the particle size.

To improve this correlation, one could modify the current polymerization cell in such a way that optical and infrared observations are allowed at the same moment. This facilitates determination of single particle kinetic behavior and determination of the single particle temperature at the same particle, at the same moment.

**Table 6.6** Temperature rises of the polymerizing particles, depending on the polymerization rate.

T <sub>reaction</sub> [°C]	Reaction conditions				Reaction rate [kg <sub>polymer</sub> /g <sub>cat</sub> *hr]	Temperature rise [K]
	C <sub>3</sub> <sup>=</sup> [bar]	C <sub>2</sub> <sup>=</sup> [bar]	N <sub>2</sub> [bar]	H <sub>2</sub> [bar]		
66	10	0	0	0.5	0.8	2
66	15	0	0	0.5	1.2	8
65	14	1	0	0.5	3	15-20

## 6.7 Modeling of particle temperature

The measured rate of increase of the particle temperature, and the moment in time of the maximum value for the temperature is different from calculated results in single particle modeling work done before, for example by Floyd<sup>[28-29]</sup>. Calculations show a maximum temperature after very short time (within a few seconds, or below), while here a maximum temperature is reached after a few minutes. The most probable explanation for this shift in time of the maximum particle temperature is the heating of the underlying surface. McKenna et al.<sup>[31]</sup> showed in their CFD-work the importance of the direct solid-solid contact in the heat transfer of the polymer particle in a fluid bed situation, especially for the smallest particles.

Here, a model with significant simplifications was worked out to investigate in a qualitative way the effect of the heating of the underlying surface by the growing polymer particles. In this calculation, it was assumed that about 100 particles are present on the surface in this experiment. Some very simplifying assumptions were:

- No temperature gradients within the particle, the bulk or the glass plate
- Heat transfer between particle and surrounding can be described as heat transfer of a sphere in stationary gas phase; the convective contribution to heat transfer is neglected
- All particles are perfectly spherical, and have the same size
- Particle growth consists completely of polymer and internal morphology is not changing (no swelling, no change in particle porosity)
- A quasi steady state is assumed:  $dR_p/dt=0$  ;  $dC_p/dT=0$  ;  $dp/dT=0$
- Constant gas phase bulk temperature is assumed

#### Mass and heat balances

The following equation is used to describe the mass balance of the growing particle:

$$\frac{(1 - \varepsilon_{part})}{m_{cat}} \cdot \frac{d(\rho_{PP} V_{part})}{dt} = \frac{R_p(t)}{3600} \quad (\text{kg/g} \cdot \text{s}) \quad (\text{eq. 6.3})$$

with  $R_p$  being the reaction rate in  $\text{kg}_{PP}/\text{g}_{cat} \cdot \text{hr}$ .

Equation 6.4 is a representation of the heat balance of the polymer particle, with heat accumulation in the left hand term, and production, transfer to the gas and transfer to the glass disk respectively in the right hand term:

$$C_{p,part} \cdot (1 - \varepsilon_{part}) \frac{d(T_{part} \rho_{PP} V_{part})}{dt} = \frac{-R_p m_{cat} \Delta H_r}{3600} - A_{pg}(t) U_{pg}(t) [T_{part}(t) - T_{gas}] - A_{pd}(t) U_{pd}(t) [T_{part}(t) - T_{disk}(t)] \quad (\text{W}) \quad (\text{eq. 6.4})$$

The values for the different parameters as used in the calculation are shown below.

**Table 6.7** Values for the parameters used in calculation of particle temperature.

$d_{part}$	25 (micron)	$C_{p,disk}$	800 (J/kg· K)	$\lambda_{gas}$	0.017 (W/m· K)
$R_p$	1 ( $\text{kg}_{PP}/\text{g}_{cat} \cdot \text{hr}$ )	$\rho_{cat}$	2300 ( $\text{kg}/\text{m}^3$ )	$\lambda_{PP}$	0.12 (W/m· K)
$n$	1000 -	$\rho_{PP}$	900 ( $\text{kg}/\text{m}^3$ )	$\lambda_{disk}$	0.93 (W/m· K)
$\Delta H_r$	2470 (kJ/kg)	$\rho_{PPY}^{1)}$	16.37 ( $\text{kg}/\text{m}^3$ )	$Nu$	2 (-)
$V_{reactor}$	6 (ml)	$C_{p,PP}$	2250 (J/kg· K)	$x$	1 (micron)
$r_{disk}$	9 (mm)	$C_{p,cat}$	803 (J/kg· K)	$T_{gas}$	343 (K)
$y_{disk}$	2 (mm)	$C_{p,PPY}^{1)}$	1667 (J/kg· K)	$T_0$	340 (K)
$\rho_{disk}$	2500 ( $\text{kg}/\text{m}^3$ )	$\varepsilon_{part}$	0.4 (-)		

<sup>1)</sup> Properties of the gaseous propylene, at 70°C and 10 bar

Density and heat capacity of the particle

The values for heat capacity and density of the particle are taken as fractionally weighed average values of the values for the pure components. Of course this is only of interest in the initial stage of the calculation, as the fraction of polymer quick tends to one.

Heat transfer coefficient from particle to gas

The heat transfer coefficient for the particle in the gas mixture will be described with the well-known relation for the Nusselt number:

$$Nu = \frac{U_{pg}(t)d_{part}(t)}{\lambda_{gas}} \quad (-) \quad (eq. 6.5)$$

Here Nu can be estimated with the empirical relation to the Reynolds and Prandl number:

$$Nu = A + B(Re^a Pr^b) \quad (-) \quad (eq. 6.6)$$

where various values for the constants A, B, a and b are mentioned in literature, with A always being 2. This correlation was developed for particles with characteristic lengths in the order of millimeters or tenths of millimeters, and not for the tens of micrometers dealt with here<sup>[32]</sup>. Nevertheless, this relation was used for these calculations, and when assuming a stagnant gas in the reactor, Nusselt becomes equal to 2.

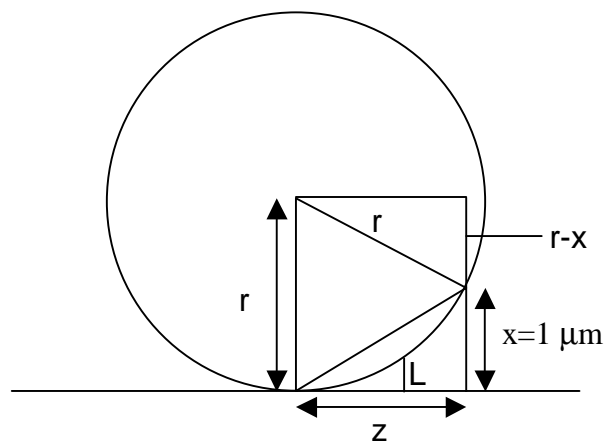


**Figure 6.15** Schematic representation of the contact area between the spherical particle and the underlying surface. The area with a distance smaller than  $x$  is considered as contact area.

Heat transfer coefficient from particle to disk

To define a contact area between the underlying surface and the particle, which theoretically would be infinitely small in case of a perfect spherical particle, all surface where the distance between particle and underlying material is smaller than  $x$  micron is considered as being contact area. In Figure 6.15 this would mean  $A_{pd}=\pi z^2$ , or more complete:

$$A_{pd} = \pi(r^2 - (r - x)^2) \quad (\text{m}^2) \quad (\text{eq. 6.7})$$

The heat flux from the particle to the disk can be described as:

$$Q = \left( \frac{\lambda_{\text{gas}}}{L} \right) A_{pd} (T_{\text{part}} - T_{\text{disk}}) \quad (\text{W}) \quad (\text{eq. 6.8})$$

where the contact area between particle and disk  $A_{pd}$  is calculated using relation 6.7 with 1 micron as critical distance  $x$ . The parameter  $L$ , the characteristic length scale for this heat transfer is variable, as the particle is spherically shaped, is set equal to the average distance between particle and disk for the region with  $x < 1$  (see Figure 6.15). For the heat transfer coefficient between particle and disk we now find:

$$U_{pd} = \frac{\lambda_{\text{gas}}}{L} \quad (\text{W/m}^2 \cdot \text{K}) \quad (\text{eq. 6.9})$$

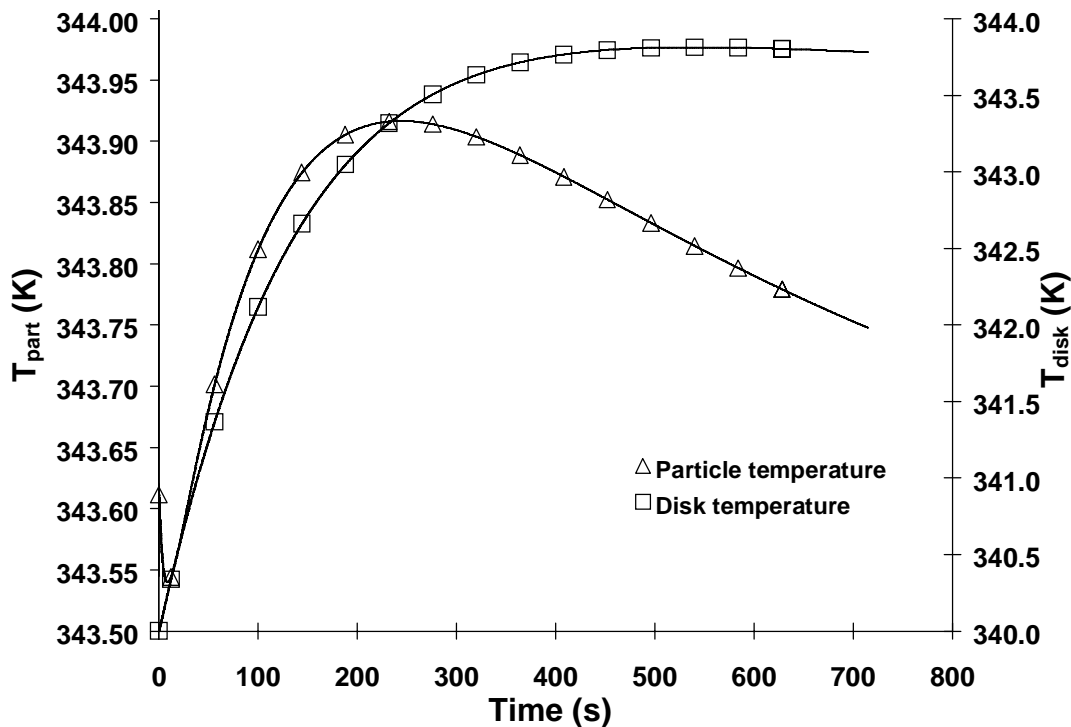


**Figure 6.16** Result of calculation of particle and disk temperature as function of time, with taking into account heat transfer to gas and to underlying surface.

Figure 6.16 shows the result of calculation of the particle and disk temperature as a function of time, when heat transfer from particle to gas and glass are both taken into account. One can see that the particle temperature is predicted to rise during the initial phase of the reaction until the maximum is reached, in this case after about 5 minutes, and to decrease after that. The heat absorbed by the glass disk leads to a temperature increase, in this example of about 4K. (When doing the same calculation without heat transfer to the gas, the disk temperature increases about 23K.)

Calculations show that the predicted temperatures are relatively sensitive to the number of particles that are put on the reactor plate, as this determines how much the glass plate heats up, and sensitive to the initial gas temperature, as this determines the heat transfer to the gas. Despite the fact that the model is a rough estimation of orders of magnitude, it qualitatively explains the shift in time of the measured maximum particle temperature.

## 6.8 Conclusions

### 6.8.1 *Optical and infrared application*

A new microreactor system was developed that allows in-situ observations of growing polymer particles, at industrial relevant conditions, using optical and infrared camera systems. The huge advantage of the present system is the ability to link kinetic information of individual particles to properties of these particles, rather than being obliged to settle for average values for all particles. High reproducibility in reaction rates was reached between different particles in the same experiment, but deviation in the results of different experiments was larger. Reaction rate curves showed some scatter due to blooming and background blurring. The method proved to be a good tool for catalyst screening, as it is possible to directly compare different catalyst particles and different catalyst systems in the same experiment, even relating results to particle properties like initial size.

Nevertheless, the present system showed some drawbacks. First, the gas in the system is stagnant. To allow a more direct comparison between particles in the present system and particles in a fluidized bed system, a convective flow should be present in the system. In addition, the contact between the particle and the underlying surface is significantly influencing the particle's heat balance. The heat exchange between the particle and the underlying surface should be significantly minimized (either through reducing contact area or through reducing heat exchange coefficient).

### 6.8.2 *Current catalyst system*

The currently used catalyst showed a very good shape replication and did not show any significant induction period. Activation energy of the system was about 52 kJ/mole. The concentrations of donor and cocatalyst during the activation step did not change its activity in polymerization, nor did the activation time.

When comparing activity of the catalyst system in the gas phase to polymerization rate in liquid propylene, a decrease of a factor of 5 was found. This is ascribed to the absence of cocatalyst and electron donor during polymerization in gas phase.

A short pre-polymerization in the presence of some ethylene (as a copolymerization) showed a remarkable and persisting effect of increasing the reaction rate in the main homopolymerization of the catalyst. A more systematic view into copolymerization and accelerating effects of comonomers is necessary to be able to explain this.

The infrared observations demonstrated that it is possible to measure particle temperature during polymerization. Observed temperature rises strongly correlated, as expected, strongly with catalyst particle size and polymerization rate. With the catalyst used here, temperature rise was up to 20 degrees at a reaction rate of about  $3 \text{ kg}_{\text{polymer}}/\text{g}_{\text{cat}} \cdot \text{hr}$  at  $70^\circ\text{C}$ . The temperature – time profiles measured on the current system did not agree with expectations from single particle models. The main reason mentioned to explain this discrepancy is the presence of the underlying surface of the particle. Temperatures are not constant in the glass plate, resulting in a drift in the heat exchange between the particle and its surroundings, as was shown in a qualitative model.

Acknowledgements - The work presented in this paper was carried out in co-operation with The Dow Chemical Company, Freeport (TX), USA. The authors wish to thank Dow for both the financial and the intellectual input. The aluminum alkyls used in the work were kindly donated by AkzoNobel. The technical assistance of Gert Banis, Fred ter Borg, Karst van Bree, Geert Monnick is well appreciated. The work could not have been completed without the experimental work carried out by Ronald Capel, Frank de Nobel and Petra Meulman. The importance of their contribution is highly acknowledged.

## Notations

A	surface area	( $\text{m}^2$ )
$C_p$	specific heat	( $\text{J}/\text{kg} \cdot \text{K}$ )
d	diameter	(m)
$F_a$	surface orientation factor	(-)
$F_s$	material factor	(-)
L	characteristic length scale	(m)
M	molecular weight	(g/mole)
m	mass	(g)
Nu	Nusselt number	(-)
P	pressure	(bar)
$P^0$	pressure at saturation	(bar)
$Q_{\text{rad}}$	radiation	(W)
r	radius	(m)
$R_p$	rate of polymerization	( $\text{kg}_{\text{PP}}/\text{g}_{\text{cat}} \cdot \text{hr}$ )
t	time	(s)
T	temperature	(K)
U	heat transfer coefficient	( $\text{W}/\text{m}^2 \cdot \text{K}$ )
V	volume	( $\text{m}^3$ )
x	critical distance for contact heat transfer	(m)
y	thickness	(m)
$\Delta H_r$	heat of polymerization	( $\text{J}/\text{kg}$ )

*Greek*

$\varepsilon$	porosity	(-)
$\lambda$	heat conductivity	(W/m· K)
$\rho$	density	(kg/m <sup>3</sup> )
$\sigma$	Stefan-Boltzmann constant	(W/m <sup>2</sup> · K <sup>4</sup> )
$\varphi$	monomer volume fraction	(-)
$\chi$	Flory-Huggins interaction parameter	(-)

*Subscripts*

0	initial condition	LP	liquid pool	PP	polypropylene
act	activation	MR	microreactor	PPY	propylene
cat	catalyst	part	particle	prepol	prepolymerization
disk	disk	pd	particle-disk	reac	reaction
gas	gas phase	pg	particle-gas		

*List of abbreviations*

D-donor	dicyclopentyl dimethoxy silane	MFR	melt flow rate
DSC	differential scanning calorimetry	Nu	Nusselt number
GPC	Gel permeation chromatography	TEA	triethylaluminum
IR	infrared	ZN	Ziegler-Natta

**References**

- [1] Galli, P.(1995). ‘Forty Years of Industrial Developments in the Field of Isotactic Polyolefins’, *Macromolecular Symposia*, **89**, 13.
- [2] Baker, R.T.K., Harris, P.S. & Waite, R.J. (1973). ‘Continuous Electron Microscopic Observation of the Behavior of Ziegler-Natta Catalysts’, *Polymerization Letters*, **11**, 45.
- [3] Corradini, P., Busico, V. & Guerra, G. (1988). ‘Possible Models for the Steric Control in the Heterogeneous High-Yield and Homogeneous Ziegler-Natta Polymerizations of 1-alkenes’, in: *Transition Metals and Organometallics as Catalysts for Olefin Polymerization*, W. Kaminsky, H. Sinn, Eds., Springer-Verlag, Berlin, 337
- [4] Eberstein, C., Garmatter, B. Reichert, K.-H. & Sylvester, G. (1996). ‘Gasphasenpolymerisation von Butadien’, *Chemie Ingenieur Technik*, **68** (7), 820.
- [5] Zoellner, K., & Reichert, K.-H. (2001) ‘Gas Phase Polymerization of Butadiene. Kinetics, Particle Size Distribution and Modeling’, *Chemical Engineering Science*, **56**, 4099-4106.

- [6] Bartke, M., Wartmann, A. & Reichert, K.-H., 'Gas Phase Polymerization of Butadiene. Data Acquisition using Minireactor Technology and Particle Modeling', *Journal of Applied Polymer Science*, submitted October 2000.
- [7] Kaneko Y., (2000). 'Particle Behavior and Reaction in Gas Phase Olefin Polymerization Reactors', Ph.D. thesis, Tokyo University of Agri. & Tech., Japan.
- [8] Oleshko, V.P., Crozier, P.A. Cantrell, R.D. & Westwood, A.D. (2001). 'In-situ and Ex-Situ Microscopy Study of Gas Phase Propylene Polymerization over a High Activity TiCl<sub>4</sub>-MgCl<sub>2</sub> Heterogeneous Ziegler-Natta Catalyst', *Macromolecular Rapid Communications*, **22**, 34.
- [9] Weickert, G., Meier, G.B. Pater, J.T.M. & Westerterp, K.R. (1999). 'The Particle as Microreactor: catalytic propylene polymerizations with supported metallocenes and Ziegler-Natta catalysts', *Chemical Engineering Science*, **54**, 3291.
- [10] Pater J.T.M., Weickert, G. & van Swaaij, W.P.M. (2001). 'New Method for Online Observation of Growing Polyolefin Particles', *Chimia*, **55**, 231-233.
- [11] Pawlicki P.C., & Schmitz, R.A. (1987). *Chem. Eng. Progr.*, **2**, 350.
- [12] Annamalai J., Ballandis, C. , Somani, M. , Liauw, M.A. & Luss, D. (1997). 'Effects of Reactant Composition and Non-uniformities on Temperature Fronts', *Journal of Chemistry and Physics*, **107** (6), 1896.
- [13] Annamalai J., Liauw, M.A., & Luss, D., (1999). 'Temperature Patterns on a Hollow Cylindrical Catalytic Pallet', *Chaos*, **9** (1), 36.
- [14] Liauw M.A., Somani, M., Annamalai, J., & Luss, D. (1997). 'Oscillating Temperature Pulses During CO and Oxidation on a Pd/Al<sub>2</sub>O<sub>3</sub> Ring', *AIChE Journal*, **43** (6), 1519.
- [15] Lobban, L., Philippou, G. & Luss, D. (1989). 'Standing Temperature Waves on Electrically Heated Catalytic Ribbons', *Journal of Physical Chemistry*, **93**, 733.
- [16] Moates, F.C., Somani, M. , Annamalai, J., Richardson, J.T., Luss, D. & Willson, R.C. (1996). 'Infrared Thermographic Screening of Combinatorial Libraries of Heterogeneous Catalysts', *Industrial and Engineering Chemistry Research*, **35**, 4801-4803.



- [17] Somani M., Liauw, M.A. & Luss, D. (1997). 'Evolution and Impact of Temperature Patterns during Hydrogen Oxidation on a Ni Ring', *Chemical Engineering Science*, **52** (14), 2331.
- [18] Reetz, T.M., Becker, M.H., Klein, H-W. & Stöckigt, D. (1998). 'A Method for High-Throughput Screening of Enantioselective Catalysts' *Angewandte Chemie International Edition*, **38** (12), 1758.
- [19] Reetz, T.M., Becker, M.H., Kühling, K.M. & Holzwarth, A. (1998). 'Time-Resolved IR-Thermographic Detection and Screening of Enantioselectivity in Catalytic Reactions', *Angewandte Chemie Internat. Edition*, **37** (19), 2647.
- [20] Reetz, T.M., Becker, M.H., Liebl, M. & Fürstner, A. (2000). 'IR-Thermographic screening of Thermoneutral or Endothermic Transformations: The Ring-Closing Olefin Metathesis Reaction', *Angewandte Chemie International Edition*, **39** (7), 1236.
- [21] Holzwarth A., Schmidt, H-W. & Maier, W.F. (1998). 'Detection of Catalytic Activity in Combinatorial Libraries of Heterogeneous Catalysts by IR Thermography', *Angewandte Chemie International Edition*, **37** (19), 2644.
- [22] Link 'Industrial Polymerization Processes' group at <http://www.ct.utwente.nl>
- [23] Garmatter, B. (1999). 'Anwendung der Mikrogravimetrie zur Erfassung kinetischer und stofftransportspezifischer Daten von Polymerisation aus der Gasphase', Ph.D. thesis at Technical University of Berlin.
- [24] Meier G.B., Weickert, G. & van Swaaij, W.P.M. (2001). 'Comparison of Gas and Liquid Phase Polymerization of Propylene with a Heterogeneous Metallocene Catalyst', *Journal of Applied Polymer Science*, **81**, 1193-1206.
- [25] Meier G.B., Weickert, G. & van Swaaij, W.P.M. (2001). 'Gas-Phase Polymerization of Propylene: Reaction Kinetics and Molecular Weight Distribution', *Journal of Polymer Science: Part A. Polym. Chem.*, **39** (4), 500.
- [26] Samson, J.J.C., Weickert, G., Heerze, A.E. & Westerterp, K.R. (1998). 'Liquid-Phase Polymerization of Propylene with a Highly Active Catalyst', *AIChE Journal*, **44**(6), 1424.
- [27] Shimizu, F., Pater, J.T.M., Weickert, G. & van Swaaij, W.P.M. (2001). 'Three-site Mechanism and Molecular Weight: Time Dependency in Liquid

Propylene Batch Polymerization Using a  $\text{MgCl}_2$ -supported Ziegler-Natta Catalyst', *Journal of Applied Polymer Science*, **81**, 1035-1047.

- [28] Floyd S., Choi, K.Y., Taylor, T.W. & Ray, W.H. (1986). 'Polymerization of Olefins Through Heterogeneous Catalysis: III. Polymer Particle Modeling – Analysis of Intraparticle Heat and Mass Transfer Effects', *Journal of Applied Polymer Science*, **32**, 2935.
- [29] Floyd S., Choi, K.Y., Taylor, T.W. & Ray, W.H. (1986). 'Polymerization of Olefins Through Heterogeneous Catalysis: IV. Modeling of Mass and Heat Transfer Resistance in the Polymer Particle Boundary Layer', *Journal of Applied Polymer Science*, **31**, 2231.
- [30] Floyd, S., Heiskanen, T., Taylor, T.W., Mann, G.E. & Ray W.H. (1987). 'Polymerization of Olefins Through Heterogeneous Catalysis: VI. Effect of Particle Heat and Mass Transfer on Polymerization Behavior and Polymer Properties', *Journal of Applied Polymer Science*, **33**, 1021.
- [31] McKenna, T.F., Spitz, R., & Cokljat, D. (1999). 'Heat Transfer from Catalyst with Computational Fluid Dynamics', *AIChE Journal*, **45** (11), 2392.
- [32] McKenna, T.F., Dupuy, J. & Spitz, R. (1995). 'Modeling of Transfer Phenomena on Heterogeneous Ziegler Catalysts: Differences between Theory and Experiment in Olefin Polymerization (An Introduction)', *Journal of Applied Polymer Science*, **57**, 371.

## Samenvatting

Door ontwikkelingen in de katalyse en het gebruik van verbeterde en specifiekere katalysatoren in de moderne polymerisatie processen, is de diversiteit in grades van polypropyleen (en daarmee de verscheidenheid van de toepassingen) snel gegroeid in de afgelopen 40 jaar. Die ontwikkeling, gecombineerd met de lage kostprijs van de polyolefinen, heeft geleid tot een enorme groei in de wereldwijde productiecapaciteit van deze polymeren.

De modernere processen maken vrijwel altijd gebruik van meerdere polymerisatiereactoren in serie, vaak een combinatie van een of meerdere vloeistoffase reactoren en een of meerdere gas fase reactoren. Tegelijkertijd vragen de ontwikkelingen om een verbeterde beheersing van de poeder morfologie. Een betere morfologie zal de hoeveelheid fijne deeltjes verminderen, het zal de kans op agglomeratie in de gas fase reactoren verkleinen en het transport van het poeder zal vergemakkelijkt worden. Daarnaast zal in de productie van polypropyleen met een grote slagvastheid de beheersing van de interne morfologie van het poeder het mogelijk maken de rubberfase beter te verdelen over de homopolymeer matrix.

In dit proefschrift is een Ziegler-Natta katalysator gebruikt van de vierde generatie. De katalysator bestaat uit  $\text{TiCl}_4$  op een  $\text{MgCl}_2$  drager, waarbij triethylaluminium gebruikt is als cokatalysator en di-cyclopentyl di-methoxysilaan als externe elektrondonor.

### Experimentele hulpmiddelen voor onderzoek naar morfologieontwikkeling

In dit proefschrift worden twee nieuwe hulpmiddelen beschreven die gebruikt kunnen worden bij onderzoek naar de morfologische eigenschappen van polymeerdeeltjes. In de eerste plaats is dat de zogenaamde microreactor. Een 6 ml gasfase cel met een transparant deksel maakt het mogelijk om deeltjes te observeren tijdens het polymerisatieproces. In de eerste toepassing is het systeem uitgerust met een optische camera, in combinatie met een microscoop. Het is aangetoond dat dit systeem een zinvolle aanvulling kan zijn in de screening van nieuwe katalysatoren. Bij zo een screening zijn eigenschappen als de ontwikkeling van de vorm van het deeltje en het activatie- en deactivatiegedrag van de katalysator van groot belang. Met dit systeem kunnen deze karakteristieken bestudeerd worden voor de individuele deeltjes, wat het mogelijk maakt om die eigenschappen te correleren met eigenschappen van de betreffende deeltjes, zoals initiële deeltjesgrootte.

In de tweede toepassing van de microreactor, is een infraroodcamera gebruikt, die het mogelijk maakt om oppervlaktetemperaturen van de deeltjes tijdens de polymerisatie te meten. Een direct vergelijk tussen deeltjes in de microreactor en deeltjes in een gefluidiseerd bed reactor is natuurlijk gewaagd, omdat het gas in de microreactor stagnant is, maar niettemin is het belangrijk om de deeltjestemperatuur in laboratoriumtesten nauwkeurig te weten. Het is gebleken dat bij polymerisatiesnelheden rond  $3 \text{ kg}_{\text{PP}}/\text{g}_{\text{cat}} \cdot \text{uur}$ , de deeltjes tot  $20^\circ\text{C}$  warmer kunnen zijn dan de

omgeving. In tegenstelling tot veel dat eerder gepubliceerd werd, worden de maximale temperaturen vaak na enkele minuten bereikt, in plaats van na enkele seconden of korter.

Het tweede hulpmiddel dat ontwikkeld is in het hier gepresenteerde werk, is een reactor voor polymerisatie in slurry-fase bij extreem lage polymerisatiesnelheden. Door gebruik te maken van dit systeem waren we in staat de polymerisatie stop te zetten bij een goed gedefinieerde opbrengst en zo deeltjes te bestuderen in verschillende fases van het fragmentatieproces. Nadat de prepolymerdeeltjes in een epoxyhars waren ingebed, werden SEM foto's van de doorsneden gemaakt, om zo de fragmentatie van de drager te kunnen volgen. EDX technieken zijn gebruikt om de herkomst van de materialen op de foto's te kunnen bewijzen.

#### Katalysator fragmentatie

Het fragmentatiegedrag van de hier gebruikte katalysator is bestudeerd in een polymerisatie in de slurryfase bij extreem lage polymerisatiesnelheden. Met doorsnede SEM foto's is aangetoond dat de fragmentatie niet laagsgewijs plaatsvindt vanaf de rand van het deeltje naar het centrum toe. In plaats daarvan brak de drager homogeen verdeeld over het partikel in relatief grote fragmenten, die vervolgens zelf afnamen in grootte door verdere fragmentatie.

De verandering in de deeltjesmorfologie valt samen met een scherpe verandering in de polymerisatiekinetiek. Reactiesnelheden lieten een snelle daling zien met toenemende opbrengst, tussen 0 en 5 gram polymeer per gram katalysator, die niet afhankelijk was van de polymerisatietijd en polymerisatiesnelheid. Deze afname wordt toegeschreven aan de veranderingen van de interne deeltjes morfologie in de vroege fase van de polymerisatie. Een magnesiumdichloride deeltje met weinig polymeer verandert in een polymeer deeltje met weinig katalysator materiaal.

#### Damp-vloeistof evenwicht van het waterstof-propyleen systeem

Om het molgewicht van het polymeer te sturen wordt normaal gesproken waterstof gebruikt om het molgewicht te beperken. Het is daarom noodzakelijk om de vloeistof- en dampstamstelling te kennen in het evenwicht tussen het vloeibare propyleen en het waterstof.

Een aantal toestandvergelijkingen zijn getest in hun vermogen om experimentele data van dit evenwicht te beschrijven. Er is gebleken dat de Peng-Robinson en de Sour-Soive-Redlich-Kwong toestandvergelijkingen het best presteerden, hoewel er nog steeds significant onderscheid te zien was tussen de berekende en de gemeten gegevens. Een temperatuurafhankelijke interactieparameter voor de Peng-Robinson toestandvergelijking is vervolgens geïntroduceerd, waarmee de beschrijvende prestaties van het model sterk verbeterd werden.

Daarnaast werd getoond dat de aanwezigheid van variabele hoeveelheden hexaan en stikstof in het systeem het waterstof-propyleen niet significant beïnvloeden. Dit is van belang, omdat deze factoren in de polymerisatie testen niet perfect werden beheerst.

### Polymerisatiekinetiek in vloeibaar propyleen

Als gevolg van de grote gevoeligheid van de moderne katalysatoren voor kleine hoeveelheden verontreinigingen, en de hoge polymerisatiesnelheden van dergelijke katalysatoren, die resulteren in een grote warmteproductie in een uiterst brandbaar medium, bij een relatief hoge druk, is het publiek onderzoek naar de polymerisatie van vloeibaar propyleen erg beperkt. Door gebruik te maken van een calorimetrische meetmethode, waarbij de reactor isotherm wordt bedreven en een constante warmteoverdracht coëfficiënt naar de mantel wordt gegarandeerd, kan het temperatuurverschil tussen de reactorinhoud en de koelmantel gebruikt worden als een maat voor de reactiesnelheid. Met deze methode kan in één enkele polymerisatietest een volledige reactiesnelheid-tijd curve gemeten worden.

In dit werk is de kinetiek gemeten van de polymerisatie van vloeibaar propyleen met een vierde generatie Ziegler-Natta katalysator, als een functie van temperatuur, prepolymerisatiemethode en de waterstof en monomeer concentraties.

Het effect van de polymerisatietemperatuur op de reactiesnelheid en het deactivatiegedrag is beschreven als een Arrhenius relatie. De methode die gebruikt wordt voor het bepalen van de monomeerconcentratie op de actieve plaats beïnvloedt de lineariteit van de Arrhenius plots nauwelijks, maar heeft wel invloed op de berekende activeringsenergieën. De waarden van de activeringsenergieën variëren van 38 tot 91 kJ/mol in de afwezigheid van waterstof en van 60 tot 104 kJ/mol in de aanwezigheid van waterstof.

Bij de hoogste gemeten temperaturen, tussen 70 en 80°C, lijkt de polymerisatiesnelheid een plateau te bereiken: de reactiesnelheid neemt daar niet meer toe met toenemende temperatuur. Dit effect verdwijnt nadat een prepolymerisatie is uitgevoerd en daarom wordt het toegeschreven aan oververhitting van de grootste katalysatordeeltjes.

Het effect van de waterstofconcentratie is in detail bestudeerd bij 60 en 70°C. Het blijkt dat bij lage waterstofconcentraties ( $X_{H_2}$  onder 0.0025) de reactiesnelheden scherp toenemen met een toenemende waterstofconcentratie. Bij hogere waterstofconcentraties werd de toename minder sterk, tot een plateau in de reactiesnelheid bereikt werd. Deze waterstof afhankelijkheid wordt verklaard door het ontstaan van 'slapende actieve plaatsen' die door mis-inserties van het monomeer reversibel geblokkeerd zijn. De relatief grote methylgroep van het monomeer blokkeert de toegang tot de actieve plaats. Waterstof kan de slapende polymeerketen van de katalysator afkoppelen, zodat de actieve plaats vrij wordt voor polymerisatie.

Verder is gebleken dat als de monomeerconcentratie geleidelijk wordt verlaagd door hexaan aan het vloeibare propyleen toe te voegen, de reactiesnelheid tussen concentraties van 500 en 200 g/L slechts minimaal daalde. Als de monomeerconcentratie beneden 200 g/L wordt verlaagd, daalt de reactiesnelheid scherp met dalende concentratie.

Tenslotte blijkt er een duidelijke relatie te zijn tussen de reactiesnelheid in een polymerisatie en het deactivatiegedrag. Bij lagere reactiesnelheden, onafhankelijk of die veroorzaakt wordt door lage temperatuur of lage waterstof concentratie wordt een kleine deactivatie waargenomen. Met toenemende reactiesnelheid zal ook de deactivatie groter worden.

#### Poeder morfologie

De morfologie van de poeders geproduceerd in de polymerisatie van vloeibaar monomeer zijn kwalitatief bestudeerd met elektron microscopie en kwantitatief met stortdichtheid metingen, als functie van procescondities zoals monomeerconcentratie, waterstofconcentratie, polymerisatietemperatuur en prepolymerisatiemethode. Het is gebleken dat er voor deze katalysator een sterke relatie bestaat tussen de initiële reactiesnelheid en de morfologie van het geproduceerde polymeer poeder.

Als de initiële reactiesnelheid laag genoeg is, typisch onder  $35 \text{ kg}_{\text{PP}}/\text{g}_{\text{cat}} \cdot \text{uur}$ , dan is de stortdichtheid van het product hoog, zo rond  $450 \text{ g/L}$ , de porositeit van het poeder is laag en de vorm van de deeltjes is een perfect replicatie van de vorm van de katalysatordeeltjes. Dit effect is niet afhankelijk van de reden voor de verlaagde reactiesnelheid: lage temperatuur of lage waterstofconcentratie.

Een geleidelijke verandering van de vorm en de structuur van de deeltjes is waargenomen als de polymerisatietemperatuur veranderd wordt. Bij lage temperaturen, bijvoorbeeld  $40^\circ\text{C}$ , worden zoals vermeld massieve deeltjes gevormd met een regelmatige oppervlakte structuur. Bij verhoging van de polymerisatietemperatuur wordt het oppervlak onregelmatiger, de deeltjes krijgen een grotere porositeit, resulterend in verlaagde stortdichtheden. Bij polymerisatietemperaturen van  $70^\circ\text{C}$  of hoger, worden de laagste stortdichtheden gemeten, zo rond  $250 \text{ g/L}$ .

Het is aangetoond dat na een korte prepolymerisatie van bijvoorbeeld 10 minuten op een lage temperatuur van bijvoorbeeld  $40^\circ\text{C}$ , de morfologie van het verkregen poeder blijvend veranderd is. Na zo een prepolymerisatie zal het deeltje zijn regelmatige structuur en vorm behouden, onafhankelijk van de omstandigheden in de hoofdpolymerisatie. Zelfs als er een hele korte prepolymerisatie wordt gebruikt bij een snel oplopende polymerisatietemperatuur, ook dan ontstaat er een poeder-morfologie die past bij de deeltjes die bij lage temperaturen geproduceerd zijn. Het gebruik van deze zogenaamde niet-isotherme prepolymerisatie is volledig voldoende om een poeder te verkrijgen met een hoge stortdichtheid, zelfs als de reactor binnen enkele minuten wordt opgewarmd naar  $70^\circ\text{C}$ .

Deze korte prepolymerisatie staat het gebruik van een continu bedreven buisreactor toe voor prepolymerisatiedoeleinden. Naast het voordeel van de smalle verblijftijdspread is dan ook een snelle controle op de activiteit van het systeem mogelijk door middel van temperatuur metingen.

## Dankwoord

Ik wist het allemaal nog niet, wat ik met mijn toekomst moest gaan doen, toen ik in januari 1998 begon aan een project binnen een 1-jarige samenwerking tussen vakgroep IPP en Mitsubishi Chemical Company. Maar in de loop van dat jaar zag ik het licht. Günter Weickert en Roel Westerterp deden me inzien wat onderzoek in polyolefinen technologie betekende. Westerterp bracht me in contact met Dow en al snel werd duidelijk dat ik er drie jaar aan zou vastknopen. Drie jaar werden er vier, doordat ik in de tussentijd me ook een beetje ben gaan bezighouden met organisatorische zaken, en daar sta ik nu. Erg veel ervaring rijker. Dank jullie wel, Günter en Roel, voor jullie inzet in die fase.

I would like to thank the members of the commission for the time and interest that they have showed in my work, and for the stimulating and interesting discussions. In particular thanks to Tim for the inciting remarks and the efforts in improving my English.

Wim en Günter, hartelijke dank voor de inspanningen rond de publicaties en het proefschrift en voor het geduld dat soms nodig was door mijn chaotische planningsen.

Hoewel de voor mijn werk belangrijkste hardware al grotendeels draaide toen ik in de groep kwam, was het noodzakelijk een aantal andere zaken vanaf de grond op te bouwen. Dat had nooit gekund zonder de hulp van vaardige en meedenkende HDL-technici. Karst, Fred, Geert, Arie en in de laatste periode ook Johan: bedankt voor jullie hulp!

Vooraf nadat ik staf lid werd heb ik vaak nauw samengewerkt met Gert Banis. Hem wil ik danken voor de prettige manier waarop we dat deden en de heldere blik op een aantal goede dingen in het leven die hij ook belangrijk vindt: een goede sigaar en een goed glas rode wijn.

Heel erg veel werk waarover ik geschreven heb is tot stand gekomen in nauwe samenwerking met 'team Pater', zoals de groep afstudeerders in dit project zich op een gegeven moment doopten. Eigenlijk waren het meerdere kleinere teams, ingedeeld naar de aard van het werk dat ze deden: Eelko Bos, Marlies Kopmels, Tom Cellissen, Jeroen Crouzen en Roxane van Arneman maakten serieuze hoeveelheden polymeer op de liquid pool reactor in box 2.

'Een beetje minder kwantiteit, maar des te meer kwaliteit'. Dat was de insteek van de mensen die van de microreactor een voor IPP belangrijke research-tool hebben gemaakt: Ronald Capel, Frank de Nobel en Petra Meulman.

Op een gegeven moment hadden we het gezien: we zouden stoppen met het proberen reproduceerbare resultaten te verkrijgen op de low-yield slurry prepolymerisatie opstelling. Maar door de inzet van het damesteam Suzanne Huibers, Harriët Workel en Jantina de Waal kregen we de zaak wel aan de praat en schreef ik er zelfs een mooie publicatie over.

Twee mensen vielen niet echt binnen de subteams, omdat zij gewoon beter waren dan de rest: ze hielden zich bezig met zaken waar de anderen geen verstand van hadden. Inge van Putten ontwikkelde de HPVEE software voor box 2, waar dagelijks nog gebruik van wordt gemaakt en Jorina Verhoog liet zien wat de kracht is van een stopped-flow reactor. Helaas heb ik niet genoeg tijd gehad om de veelbelovende zaken die we daar deden volledig uit te werken.

Ik wil alle teamgenoten hartelijk dank voor het meedenken, de discussies, de inzet ze toonden, maar vooral ook voor de gezelligheid. Dank!

Ik wil de 'externe leden' van de D-commissies van mijn afstudeerders hartelijk danken voor de tijd die ze investeerden en voor de interessante discussies die we gevoerd hebben: Seshan, Reinoudt Gaymans, Jan van Ommen, Ben Betlem, Mark Hempenius en Dirk Grijpma, bedankt voor jullie bijdragen.

Het proefschrift dat voor u ligt is het resultaat van een driejarige samenwerking met de Dow Chemical Company. Officieel met Dow Benelux, maar ook een aantal mensen in Freeport en Midland waren nauw betrokken bij het project. Allereerst zou ik Johan Thoen willen bedanken voor zijn inzet om dit project op te starten in samenwerking met Prof. Westerterp en Weickert. Next to that JobJan and Ravi who were most closely involved in the project from Dow side. Thank you both for the pleasant and effective co-operation. Next to that, thanks to the other Dow people: Patricia, Roger, Giel, Bernie, Flip and the others, thank you all for your efforts!

Omdat de vakgroep Industriële Polymerisatie Processen de afgelopen jaren volop in de opbouwfase zat, hebben we veel moeten investeren. Gelukkig heeft de faculteit CT ook mensen die je helpen van je geld af te komen. Hartelijke dank aan de mensen van de afdeling inkoop: Wim, Nellie, Jan en Ineke. Daarnaast een grote dank voor de whizzkids van SGA, Jan, Joachim, Gilbert en Mark Hulshof voor het weer vlottrekken van vastgelopen computersystemen.

Een groot deel van mijn plezier in de IPP-groep is te danken geweest aan mijn collega's. Ontelbare malen naar de Casper voor krentenbollen en een frikandellenbroodje met Gerben, Bart, Michiel, Hans-Pieter en Parasu. Ze mogen dan misschien niet zoveel verstand hebben van voetbal, perfecte collega's en goede vrienden zijn het. Ook de andere mensen uit de IPP-groep wil ik hartelijk danken voor prima tijd die ik heb gehad.

In het bijzonder zou ik Gerben Meier nog willen noemen. De ontelbare discussies over kinetiek en reactoren, over MWD's en waterstof vormden een grote stimulans, om van de wereldhit 'Polypropyleen olee-olee' (wijze 'Twente Enschede') nog maar te zwijgen. Ik hoop en denk dat het feit dat we nu concurrenten zijn, het goede contact ook in de toekomst niet in de weg zal staan.



De afgelopen 5 en een half jaar heb ik steeds nauwer samengewerkt met Günter Weickert. Ongelofelijk veel blijvende zaken heb ik van hem geleerd. Naast een hele grote vakkennis en het leren denken als een engineer, werkt zijn grote enthousiasme aanstekelijk en zorgt zijn enorme creativiteit ervoor de zaken steeds weer op een nieuwe manier te kunnen zien. Günter, dank je wel voor je hulp, de prima samenwerking, en niet te vergeten de goeie reizen, zoals die naar San Diego en naar Japan. Ik hoop dat we nog een lange tijd, in welke hoedanigheid dan ook, kunnen samenwerken.

De paranimfen Mic 'TCD' Bergstra en Eelko 'Plofkop' Bos hartelijke dank voor jullie hulp in de voorbereiding, jullie interesse in de schrijfactiviteiten en jullie steun op D-day. Mic, dank voor je energie in het intensief naspeuren van het proefschrift op onvolkomenheden.

En dan wil ik graag mijn ouders bedanken voor de niet aflatende interesse en steun die ik de afgelopen jaren van hen heb mogen ontvangen. Ik ben er van overtuigd dat de eerlijkheid, de werklust en de positieve kijk op zaken die jullie Sander, Sjoerd en mij hebben bijgebracht de basis zijn geweest voor het feit dat het ons nu goed gaat. Dank jullie wel!

Tenslotte wil ik Mariska bedanken voor haar hulp en geduld in de afgelopen periode, en dan met name in de laatste maanden. Voor je begrip tijdens mijn pogingen je uit te leggen waarom een buisreactor een goede keuze kan zijn als prepol-reactor.

Dank je wel dat je er bent.

Jochem  
Oktober 2001



## Curriculum Vitae

Jochem Pater was born on the 6<sup>th</sup> of January 1972, in Anna Paulowna. After his primary education at the R.K. Spoorbuurtschool, it took 6 years to finish secondary school at the Rijks Scholen Gemeenschap in Schagen, where he got the diploma in June 1990.

Subsequently he started his studies Chemical Engineering at the University of Twente (UT). In December 1996 he finished his studies by defending his master thesis entitled 'Polymerization of Ethylene in Slurry-Phase with Heterogeneous Metallocene Catalysts - a kinetic study'.

In January 1997 Jochem started as a research fellow at the Industrial Polymerization Processes group of the UT in a yearlong research co-operation between the Mitsubishi Chemical Company and the UT. Within his assignment the kinetics of the polymerization of liquid propylene using a 4<sup>th</sup> generation Ziegler-Natta catalyst were investigated.

Subsequently, he started in January 1998 as a Ph.D. student in the group of professor Westerterp (after Westerterp's superannuation lead by professor van Swaaij) and professor Weickert, the research group Industrial Polymerization Processes. His assignment was formulated within a co-operation between the UT and the Dow Chemical Company. In September 1999, he also became a member of the scientific staff of the IPP research group.

As from December the 1<sup>st</sup> 2001, Jochem is working at the Centre Recherche et Technologie of BP Chemical in Lavéra, France.



## List of Publications

Pater J.T.M., Roos P., Weickert G., Westerterp K.R., Shimizu F., and Ko G., (1998). "Integral Research Aspects of Gas Phase Olefin Polymerization: Kinetics, Absorption and Fluidization", *6<sup>th</sup> International Workshop on Polymer Reaction Engineering*, Berlin, 5-7 October 1998, **134**, 103-114.

Weickert G., Meier G.B., Pater J.T.M., and Westerterp K.R., (1999). "The Particle as Microreactor: Catalytic Propylene Polymerizations with Supported Metallocene and Ziegler-Natta Catalysts", *Chemical Engineering Science*, **54**, 15-16, 3291-3296.

Shimizu F., Pater J.T.M., and Weickert G., (2001). "Three-site Mechanism and Molecular Weight: Time Dependency in Liquid Propylene Batch Polymerization Using a MgCl<sub>2</sub>-Supported Ziegler-Natta Catalyst", *Journal of Applied Polymer Science*, **81** (4), 1035-1047.

Pater J.T.M., Weickert G., and van Swaaij W.P.M., (2001). "New Method for Online Observation of Growing Polyolefin Particles", *Chimia*, **55** (3), 231-233.

Pater J.T.M., Weickert G., Loos J., and van Swaaij W.P.M., (2001). "High Precision Prepolymerization of Propylene at Extremely Low Reaction Rates - Kinetics and Morphology", *Chemical Engineering Science*, **56**, 4107-4120.

Shimizu F., Pater J.T.M., van Swaaij W.P.M., and Weickert G. (2001). "Kinetic Study of a Highly Active MgCl<sub>2</sub>-supported Ziegler-Natta Catalyst in Liquid Pool Propylene Polymerization II. The Influence of Alkyl Aluminum and Alkoxysilane on Catalyst Activation and Deactivation", *accepted for publication by Journal of Applied Polymer Science*.

Pater J.T.M., Weickert G., and van Swaaij W.P.M., (2001). "Effect of Prepolymerization on Kinetics and Morphology in Polymerization of Propylene with a Ziegler-Natta Catalyst", *Proceedings of 7<sup>th</sup> International Workshop on Polymer Reaction Engineering*, Hamburg, 8-10 October 2001.

Shimizu F., Pater J.T.M., and Weickert G., (2001). "Kinetics Study of a Highly Active MgCl<sub>2</sub>-supported Ziegler-Natta Catalyst in Liquid Pool Propylene Polymerization I. The Effect of Temperature", *submitted to Journal of Applied Polymer Science*.

Pater J.T.M., Weickert G., and van Swaaij W.P.M., (2001). "Optical and Infrared Imaging of Growing Polymer Particles in the Homo- and CoPolymerization of Propylene and Ethylene, using a Ziegler-Natta Catalyst", *submitted to AIChE Journal*.

Pater J.T.M., Weickert G., and van Swaaij W.P.M., (2001). "Polymerization of Liquid Propylene with a  $\text{TiCl}_4/\text{MgCl}_2$  catalyst –Temperature and Prepolymerization influence on kinetics and VLE of the  $\text{H}_2$ -propylene system", *submitted to AIChE Journal*.

Pater J.T.M., Weickert G., and van Swaaij W.P.M., (2001). "Polymerization of Liquid Propylene with a 4<sup>th</sup> Generation Ziegler-Natta Catalyst - Influence of Temperature, Hydrogen and Monomer Concentration and Prepolymerization Method on Polymerization Kinetics", *submitted to Chemical Engineering Science*.

Pater J.T.M., Weickert G., and van Swaaij W.P.M., (2001). "Polymerization of Liquid Propylene with a 4<sup>th</sup> Generation Ziegler-Natta Catalyst - Influence of Temperature, Hydrogen, Monomer concentration and Prepolymerization Method on Powder Morphology", *submitted to Journal of Applied Polymer Science*.













